Quantitative electron probe microanalysis of boron in binary borides

for Physical Chemistry

University of Technology
Eindhoven

Quantitative Electron probe Microanalysis of Boron in Binary Borides

University of Technology Eindhoven
Laboratory for Physical Chemistry
P.O.Box 513, 5600 MB Eindhoven
The Netherlands

ISBN 90-3860-898-5

Dr.ir. G.F. Bastin and ir. H.J.M. Heijligers

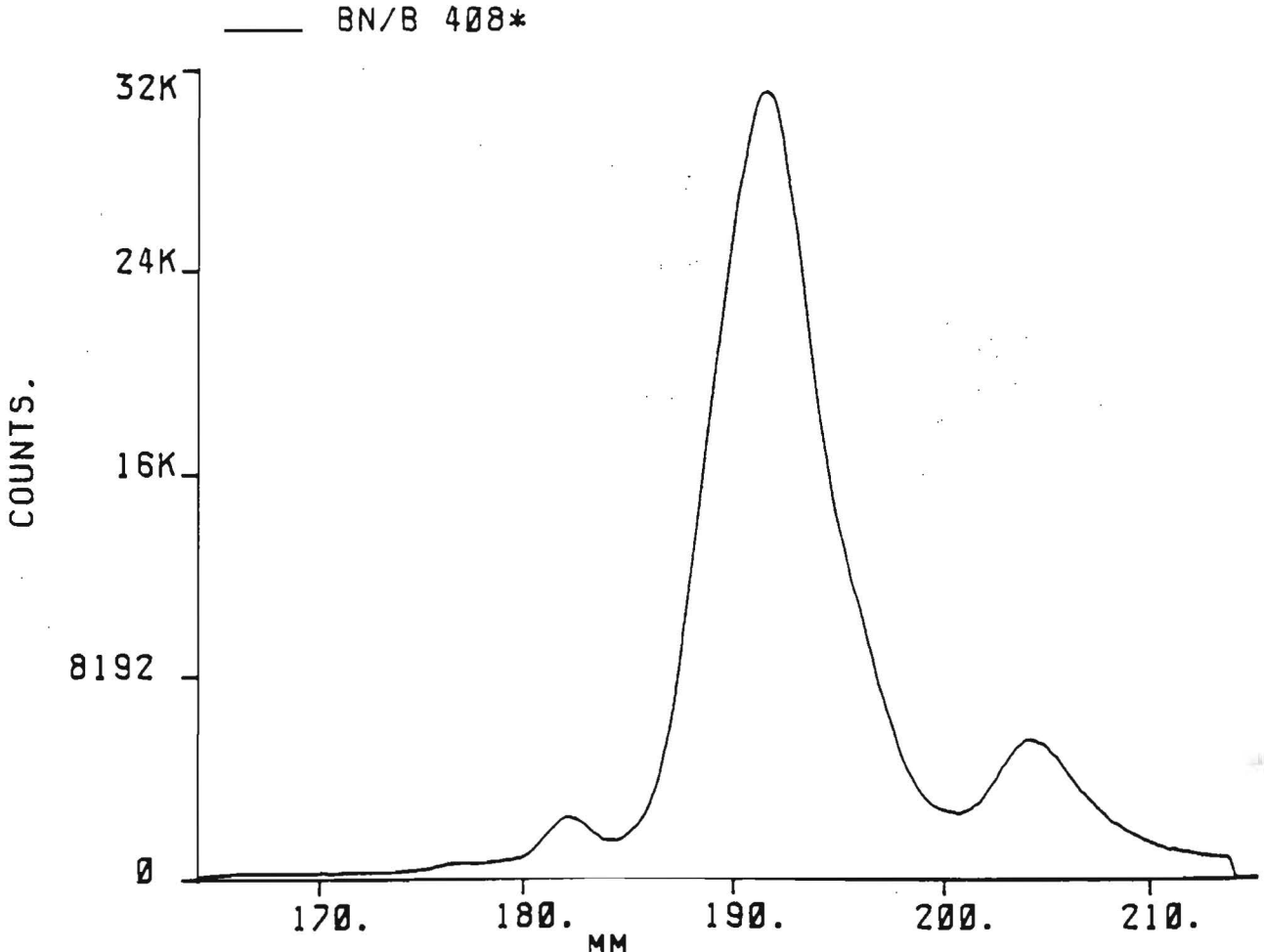

QUANTITATIVE ELECTRON PROBE MICROANALYSIS OF BORON IN BINARY BORIDES

Dr.Ir. G.F. Bastin and Ir. H.J.M. Heijligers
Laboratory for Solid State Chemistry and Materials Science
P.O. Box 513, NL-5600 MB EINDHOVEN
The Netherlands

First Edition : March 1st 1986.
Second Revised Edition : January 1st 1997.

CIP-DATA LIBRARY TECHNISCHE UNIVERSITEIT EINDHOVEN

Bastin, G.F.

Quantitative electron probe microanalysis of boron in binary borides /
by G.F. Bastin and H.J.M. Heijligers. -2nd rev. ed.-Eindhoven :
Technische Universiteit Eindhoven, 1997.- 1e dr. :1986.
ISBN 90-3860-898-5
NUGI 841
Trefw. : elektron probe micro-analyse / borium
Subject headings : electron probe microanalysis / boron

Laboratory for Solid State Chemistry and Materials Science
P.O. Box 513, NL-5600 MB Eindhoven
The Netherlands

ISBN 90-3860-898-5

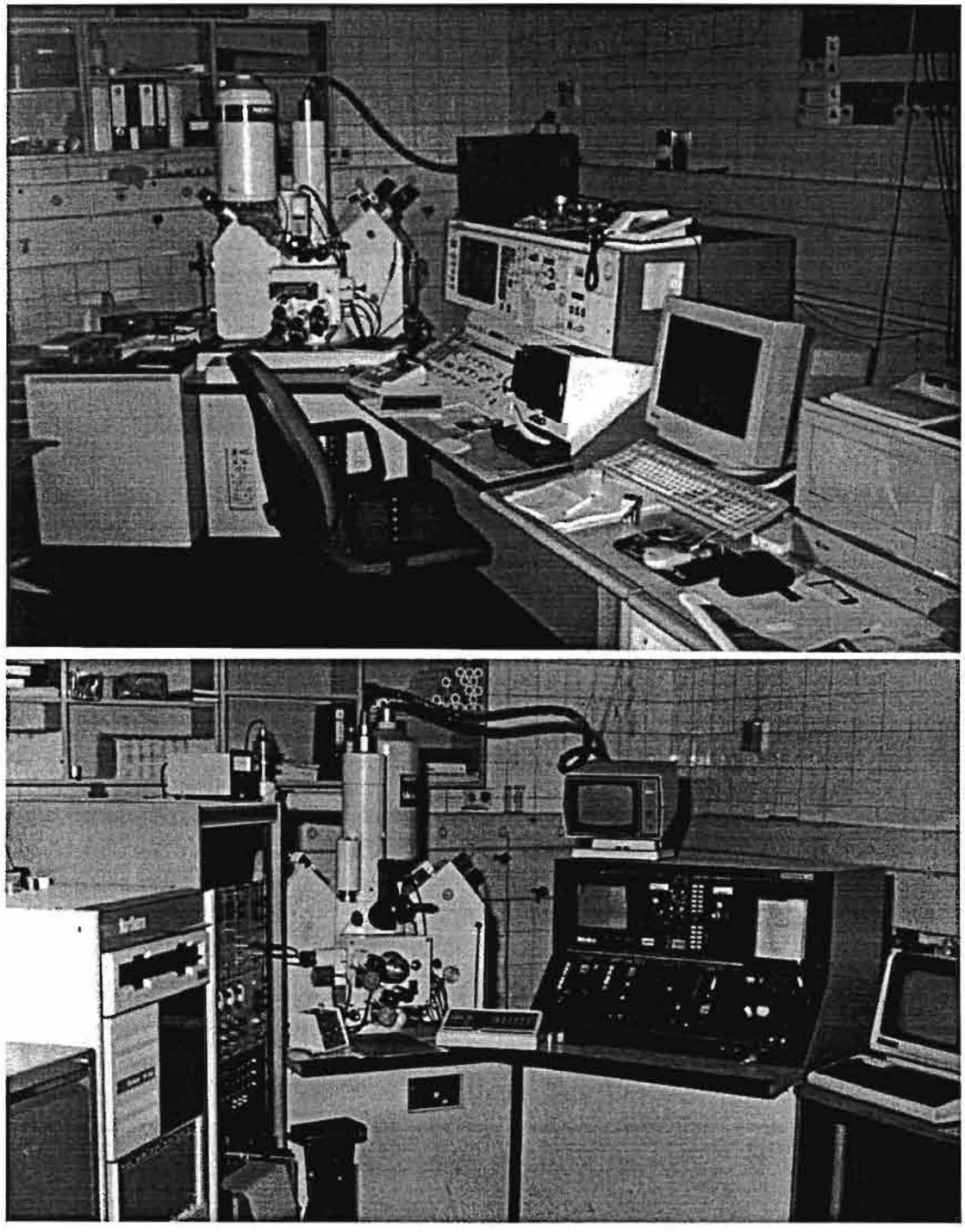

Overview of the equipment used in the present work. The top picture shows the JEOL 733 Superprobe with Tracor Northern (TN 2000) automation system on which the Boron measurements were originally performed. The bottom picture shows the present JEOL 8600 microprobe with NORAN Voyager automation system.

CONTENTS

PREFACE TO THE SECOND EDITION

Now, more than 10 years after the first publication of our internal report on Electron Probe Microanalysis of Boron, we felt that it was about time to carry out a major revision of the original report, for a number of reasons :

1) Many of the correction programs discussed in the original report (including our own program at that time) are now completely obsolete. In the past decade a number of new high-performance programs have emerged : **"PAP"** (Pouchou and Pichoir, Double Parabolic $\varphi(\rho z)$), **"XPP"** (Pouchou and Pichoir, Double exponential $\varphi(\rho z)$), **SELOS91** (Love and Scott, "Quadrilateral model, improved), **"Merlet"** (Double Gaussian $\varphi(\rho z)$), **"PROZA"** (one of our own later correction models, based on a surface-centred Gaussian $\varphi(\rho z)$ approach), and **"PROZA96"** (our most recent correction program, based on a Double Gaussian $\varphi(\rho z)$ approach). It seemed worthwile to re-evaluate the results that can be obtained with all these newer programs in order to find out where we stand today.
2) The measurements we collected in the original report are, of course, still the same. However, in one case (Hexagonal BN, with its problems of non-conductivity) we replaced the measurements by a new, more consistent and more reliable set (on sufficiently conductive) Cubic BN. In addition, we were able to add a set of measurements (4-30 kV) on B_6O to our data base, which now contains 192 Boron analyses.
3) Since the publication of our first edition we acquired a number of synthetic multilayer crystals. One of these (OVH, Mo/B_4C) has been specifically designed for the analysis of Boron. We were fortunate enough, for some time, to have both this crystal as well as the original Pb-Stearate crystal on the same microprobe. This gave us an unique opportunity to compare the performances of both crystals simultaneously on the same specimen. In particular, we were able to compare the effects of peak shape alterations with both crystals in dependence of the crystallographic orientation of the specimen with respect to the spectrometer. All the findings we accumulated with this new crystal have been added to the material presented in this new report.
4) Last, but not least, the word-processing as well as the graphical capabilities of PC's have evolved tremendously, which enables us to present the material in a much better lay-out and shape than we could in 1986.

It is our special pleasure to report that for each of the reports on EPMA of Boron, Carbon, Nitrogen, and Oxygen between 100 and 200 copies have been distributed throughout the world, and we still receive requests regularly. This goes to show that there is a vivid interest in this (rather specialistic) field. It has also given us great pleasure to see that our data bases of measurements on ultra-light element radiations have been used extensively in setting up and/or testing new correction procedures.

Eindhoven, January 1997.

G.F.Bastin and H.J.M. Heijligers.
Laboratory for Solid State Chemistry and Materials Science,
University of Technology, P.O. Box 513, NL-5600 MB Eindhoven, The Netherlands.

SUMMARY

Quantitative electron probe microanalysis has been performed in 28 binary borides in the range of 4-30 kV, both for the metals as well as for Boron. The procedures along which accurate intensity measurements for B-K_α must be carried out are discussed in detail. It is shown that, similar to the analysis of Carbon, intensity measurements can only be performed in an integral fashion. Apart from peak shifts and peak shape alterations, however, there is an additional problem in the analysis of Boron and that concerns the fact that peak positions and peak shapes may be dependent also on the crystallographic orientation of the specimen with respect to electron beam and position of the spectrometer used. Approximately 50% of the borides were found to exhibit such an effect. This implies that the approach proposed earlier, i.e., the use of a fixed Area/Peak Factor to deal with peak shape alterations, can be applied only in 50% of the cases in a straight-forward manner. In the remaining cases, where the crystallographic orientation of the specimen also plays a role, the variation of APF with peak position (or wavelength) has to be established experimentally.

The present work has resulted in a total of 196 k-ratios with respect to elemental standards for the metal X-ray lines and 192 k-ratios for B-K_α relative to elemental Boron. These data have been used to test our recently introduced improved $\varphi(\rho z)$ matrix correction program "PROZA96", which is based on a Double Gaussian $\varphi(\rho z)$ procedure. This new program was next compared to a number of other current correction programs. At the same occasion the available sets of mass absorption coefficients for Boron were tested on their consistency and better values suggested where necessary. Finally, it is shown that our latest matrix correction program ("PROZA96") is highly successful in the analysis of Boron : a relative root-mean-square value of 3.31 % was obtained, in combination with a mean k'/k value of 1.0022. This demonstrates that even for an ultra-light element such as Boron an experimental accuracy can be achieved that hitherto was considered normal for the analysis of much heavier elements. This is, of course, only possible if due care is exercised in the measurements and if the correct procedures are followed.

I. INTRODUCTION

In a number of publications[1-3] we have reported on our systematic work on quantitative electron probe microanalysis of Carbon in binary carbides. It has been demonstrated that quantitative analysis of an ultra-light element such as Carbon is indeed possible with unexpected high accuracy, provided that proper care is exercised in the measurements and that a suitable matrix correction program is used in conjunction with a consistent set of mass absorption coefficients (mac's).

The work on Carbon was, in fact, part of a much wider research effort aimed at exploring the possibilities for quantitative analysis of elements like Boron, Carbon, Nitrogen and Oxygen; elements which enjoy a growing interest in fields like high temperature materials and special ceramics. It must be expected, therefore, that there will be a rapidly growing demand for quantitative analysis of these elements in the future, especially for **local** microanalysis for which the electron probe microanalyzer still appears to be the most powerful tool. The object of this long-term investigation, which was initiated in January 1983, was not only to explore the feasibility of light-element analysis but also to supply (for the first time) large data bases of systematic and accurate measurements for each of these elements, on which present and future matrix correction programs can be tested. As far as the latter purpose is concerned it is our firm conviction that it is absolutely no use to test programs on a few isolated analyses, as has been done frequently in the past. Only consistent sets of measurements taken over widely varying conditions and systems can provide the necessary information on both the performance of programs as well as on the consistency of published sets of mac's. It must be emphasized that the latter are often of equal importance as the programs themselves[3] . These considerations are the reason for the sometimes extreme conditions (4-30 kV accelerating voltage) under which we perform our measurements and the large number of systems (10-30) on which they are performed. The philosophy on which our work is based is perhaps best described as: "Correction programs may come and go in the future but accurate measurements will retain their value almost indefinitely".

It is the object of the present work to report on our efforts concerning the quantitative analysis of Boron in 28 binary borides. As far as we know it is for the first time that a systematic investigation on this subject is carried out. Apart from its intrinsic relevance the analysis of Boron is very interesting because, being almost the lightest element that can be measured in an electron probe microanalyzer, it must be anticipated that it will provide the most testing conditions for any matrix correction program.

II. PRACTICAL PROBLEMS in the ANALYSIS of ULTRA-LIGHT ELEMENTS

II.1. General problems

The practical problems which have to be faced during the analysis of the ultra-light elements B, C, N or O, have already been discussed in detail[1-4] and will only briefly be recalled here.

1. Low yield of X-rays (especially for N-K_α X-rays), coupled with a relatively inefficient detection system. For B-K_α X-rays the situation is not particularly bad because in general the count rates which can be obtained are quite acceptable and Peak-to-Background ratios rather favourable. Moreover, in the past decade very promising new synthetic multilayer crystals have become commercially available for the analysis of ultra-light elements Not only can they provide tens of times higher peak intensities for B-K_α than the conventional Lead-stearate crystal, they can occasionally also suppress higher-order metal reflections, which are frequently a nuisance in the analysis of ultra-light elements. Since the first edition of this report we gained some experiences with a synthetic multilayer crystal ("OVH"), Mo/B_4C, 2d-spacing 147 Å (supplied by "Ovonix Corporation", Troy, Michigan, U,S,A.), which was specifically optimized for the analysis of B-K_α and Be-K_α. On pure elemental Boron we observed Peak count rates on OVH which were 50 times higher than on the conventional Lead-stearate Crystal. Obviously, these new crystals hold great promises for the future.

2. Dead-time-problems for the metal lines if these are to be measured simultaneously with the light element and **pulse shift problems** for the light element itself. These problems are a direct consequence of the use of very high beam currents which are frequently necessary and of the sometimes very high differences in count rates between standard (e.g. elemental Boron) and specimen. That the latter problem is not merely of academic interest is demonstrated in Fig. II.1 where the shape of the Boron-K_α pulse is shown as a function of the beam current. It is evident that an increase of a factor of 3 in the beam current produces a shift of -0.1 Volt in the location of the pulse maximum. Taking into account that differences in count rates between (elemental) standards and specimens may well exceed two orders of magnitude it is obvious that pulse shifts of several tenths of a Volt may occur. This may, in turn, lead to appreciable errors in the intensity measurements if a narrow window (sharp discrimination) is applied in the Pulse-Height-Analyzer. The best practical solution to these problems would be to adjust the beam current between measurements on standard and specimen in order to maintain approximately the same peak count rates.

3. Interference of higher-order metal lines with the light-element line can be quite a nuisance, mainly in the analysis of Carbon, Nitrogen and Oxygen (see e.g. Ref. 1). Fortunately, for the present case of Boron these problems are much less pronounced due to the fact that in this wavelength range (~67 Ångstroms) the higher orders of metal lines have gradually faded away. The use of a new synthetic multilayer crystal might provide improvements here too. However, in some cases new problems can turn up, e.g. in combinations with the elements Nb and Mo where the 1st order M-ζ lines of these metals show up very close to the B-K_α line in comparable

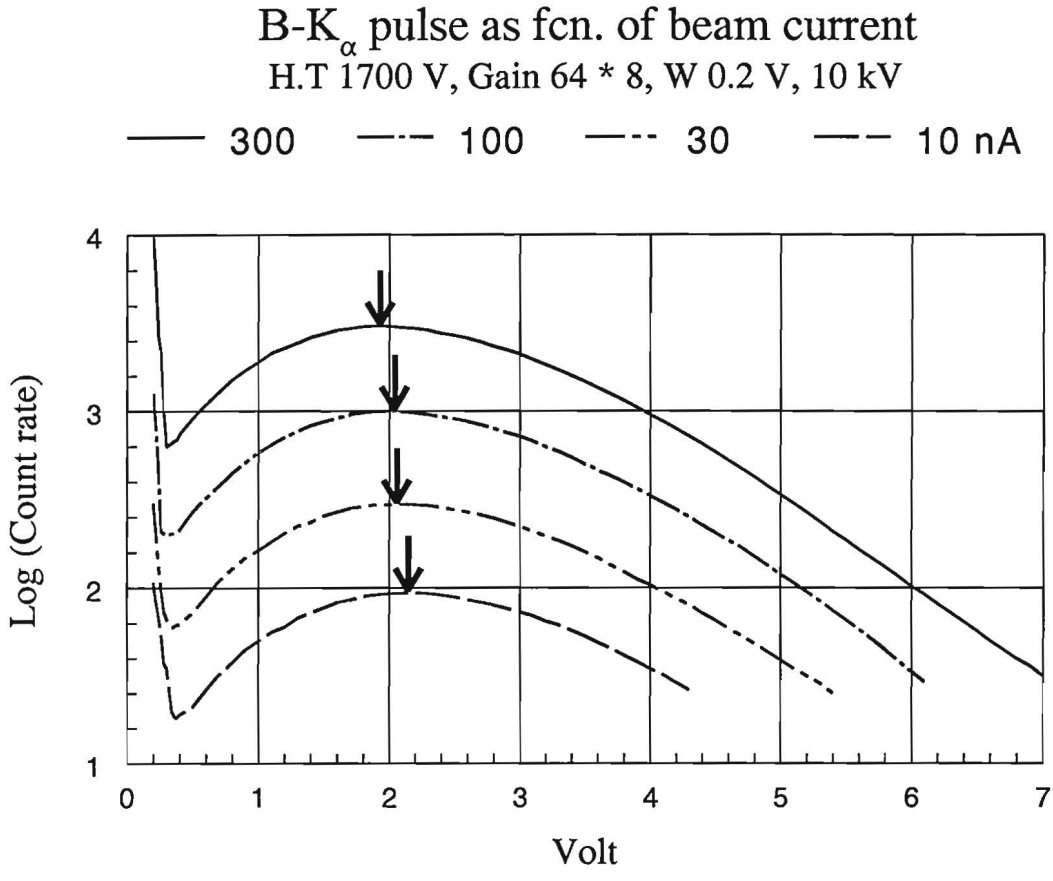

Fig. II.1 Shift of the B-K_α pulse with count rate at 10 kV. JEOL 733; Pb-Stearate crystal; Gas flow counter (Ar-10 % methane); High tension 1700 V, Gain 64 x 8, Ortec counting electronics; window 0.2 Volt. Variation in beam current between 10 and 300 nA on elemental Boron.

intensities. Whereas in these cases the STE crystal is able to resolve the M-ζ from the B-K_α line the OVH crystal is not, due to a poorer spectral resolution. Examples of these effects and solutions to these problems will be presented later on.

4. Background and **contamination** problems, which play a very important role in the analysis of Carbon (and sometimes also for Oxygen), are not prominent in the analysis of Boron, with an exception for the cases mentioned under 3.
However, due to the extremely shallow X-ray emission for B-K_α X-rays it is still advisable to use some kind of anti-contamination device (preferably an air-jet[1]) during the measurements, especially during the time-consuming integral measurements[1-3] where a lot of time has to be spent on the same location on the specimen (see also 8).

5. The choice of a standard, which was a real problem in Carbon analysis and, to a lesser extent, also in the analysis of Nitrogen and Oxygen, is not much of a problem in the analysis of Boron because an unambiguous Boron standard is readily available in the form of crystalline elemental Boron. In fact, for reasons which will be discussed in II.2 we are almost forced to use this standard, which, by the way, makes the problems mentioned under 2. all the more real.

6. The knowledge of the **mass absorption coefficients** is an extremely vital issue. It has been pointed out[1-3] that as a rule of thumb an uncertainty of 1% in these values produces an uncertainty of 1% in the calculated concentrations Now, it seems highly unlikely that the published sets of mac's for ultra-light elements are anywhere near within 1%. As a matter of

Table II.1

Mass Absorption Coefficients for Boron-K_α X-rays according to various sources.

Absorber	Henke (74)[7]	Henke (82)[8]	Henke (93)[9]	Present Work
B	3353	3350	3350	3350
C	6456	6350	6400	6450
N	10570	11200	10900	10400
O	16530	16500	18500	16500
Al	65170	64000	77300	64000
Si	74180	84000	86100	81400
Ti	15280	15300	16800	15100
V	16710	16700	19900	18250
Cr	20670	20700	22400	20200
Fe	25780	27600	31000	27000 (?)
Co	28340	30900	30900	33000 (?)
Ni	33090	35700	39600	41500 (?)
Zr	38410*	8270	7240	4330
Nb	4417	6560	5470	4600
Mo	4717	5610	5710	4400
La	3826	3730	3400	2900
Ta	20820	20800	20800	21800 (?)
W	19660	19700	19400	20400 (?)
U	2247	9020	9600	8000 (?)

*Value obviously extrapolated over M-5 Absorption Edge.

fact, published mac values for ultra-light element X-rays may differ by as much as 100%![1]
As one of the results of our work on Carbon we proposed a new and consistent set of mac's for Carbon which were found to produce significant improvements in all recent (since 1980) correction programs[3,5,6] .Obviously, it is possible to produce "better", or at least more consistent, mac's through EPMA procedures using good sets of measurements in combination with reliable matrix correction procedures.

Considering the fact that the coefficients for Carbon range from 2,500 to 40,000 and those for Boron[7-9] from 3,300 to 84,000 (see Table II.1) it must be anticipated that the uncertainties in the latter values play an even more drastic role than in the case of Carbon. There appears, however, to be no obvious reason to expect higher accuracies in the mac values for B-K_α from literature. The opposite is probably true. At present three independent (i.e. not generated through EPMA procedures) sets of mac's are available[7-9] (Table II.1). It will be clear, that the doubts expressed in this Table will have a large impact on the results calculated by any matrix correction program. For comparison we also give the most consistent set which results from our current correction program when applied to our own measurements. It must be mentioned here that in the past decade considerable convergence has taken place between the most recent and probably most reliable matrix correction programs in the sense that they all show their best performance with mac values within a few % of the values we show here.
Anyway, it is our firm belief that an independent judgement of the performance of a particular correction program is impossible as long as the mac's are not available with an accuracy better than 1% relative. Until then (if this time will ever come) we shall simply have to satisfy ourselves with statements about the performance of a specific correction program made in conjunction with the particular (and consistent) set of mac's used in the test.
In those cases where the mac's we propose are marked with (?) they are **not consistent** with the measured relative B-K_α intensities; according to these measurements **substantially lower** values are more appropriate. (See paragraph on relative emitted intensities).

7. The choice of a matrix correction program.
For many years it has been common practice to discuss the matrix correction procedure, which is necessary in order to convert the measured intensity ratio between specimen and standard (k-ratio) into concentration, in terms of Z, A and F factors.
The Z-factor stands for the ratio between the amount of X-rays **generated** in standard and specimen, respectively. The **emitted** intensity, which is of course the vital issue, is obtained by applying an absorption correction, which is usually expressed by $F(\chi)$, with $\chi = \mu/\rho$ .cosec θ (μ/ρ = mac; θ = X-ray take-off angle).
The quantity $F(\chi)$ is simply the fraction of generated X-rays, which is actually emitted from standard or specimen. The F-factor, finally, accounts for the fact that sometimes additional, non-electron beam generated, X-rays can be produced by primary X-radiations of other elements in the specimen. The concentration C is now related to the intensity ratio k by the following relationship:

$$C = k * Z * A * F$$

or:

$$C = \frac{I_{spec}}{I_{std}} * \frac{Z_{std}}{Z_{spec}} * \frac{F(\chi)_{std}}{F(\chi)_{spec}} * F$$

Due to the straight-forward proportionality of the concentration to all three factors Z, A and F it is obvious that in principle they are of equal importance. However, fluorescence effects are usually small and for ultra-light elements they can commonly be neglected; this leaves only the Z and A factors to be considered.
The atomic number correction (Z) for medium-to-heavy elements (Z>11) is usually less than 30% from unity; the absorption correction, on the other hand, can be much larger: A-factors of more than 10 are not uncommon in unfavourable cases[10]. As a result the absorption correction has rightfully received the most attention in the past.

In our opinion it is doubtful if this is still appropriate for cases of ultra-light elements. Our experiences with a number of current correction programs for the analysis of Boron (or Carbon) show that the differences in atomic number corrections produced by these programs (of the order of 20%) might, in themselves, already account for the discrepancies between calculated and nominal concentrations. What it all comes down to is that the same product (Z times A) can be produced by a variety of Z and A factors and that in cases of ultra-light elements nobody is at present able to establish what the correct distribution over Z and A factors should be.
This is an obvious consequence of a total lack of measured φ(ρz) (ionisation, φ-vs-mass depth, ρz) data for ultra-light elements. Hence, it follows that all separate atomic number corrections, which are currently in use, must be regarded as more or less blind extrapolations towards very light elements.
The φ(ρz)-based correction programs[3,5,10,11] may suffer from the same uncertainties, of course. The calculated φ(ρz) curves on which the corrections are based can only be compared to actually measured φ(ρz) data for medium-to-heavy elements, for which they are usually highly successful[10]. In many respects it is somewhat uncertain whether the equations used in the φ(ρz) approaches can safely be extrapolated to conditions which are common in ultra-light element analysis. Monte Carlo simulation procedures[12] can be a great help in these circumstances.
The main problem in quantitative electron probe microanalysis is that one is always discussing **ratios** between quantities; the intensity (or φ(ρz) curve) of the standard is compared to that of the specimen. In many respects it is possible that large errors are present in both the numerator and the denominator and that still the (k-)ratio is correct. As a consequence it is often very difficult to obtain evidence about the correctness of absolute values.
A further discussion on this subject will be given in Chapter V, where the numerical results of the boron-analyses will be evaluated.

8. Peak Shifts and Peak Shape Alterations.

We have shown[1-3] before that the intensity measurements for ultra-light element radiations can be seriously influenced by:

- **Peak shifts** and
- **Peak Shape Alterations**

which can occur simultaneously in the light-element-K_α emission spectrum when moving from standard to specimen. While the first problem can easily be dealt with by retuning the spectrometer the second problem is much more difficult to tackle.
The direct consequence of peak shape alterations is that the net **peak** intensity, which is usually measured in day-to-day practice, is no longer a correct measure for the emitted intensity. In fact, this routine practice is based on the tacit assumption that the **peak** intensity is proportional to the **integral** intensity emitted by the specimen. Fortunately this is true in the vast majority of cases, like all medium-to-heavy element K-, L- and M-lines
Due to the sometimes extreme variations in peak shapes in ultra-light element K_α -lines, however, this assumption no longer holds. As a result it is **imperative** to perform **integral** measurements which is not a very attractive option, certainly not, of course, for a Wavelength-Dispersive-Spectrometer (WDS).

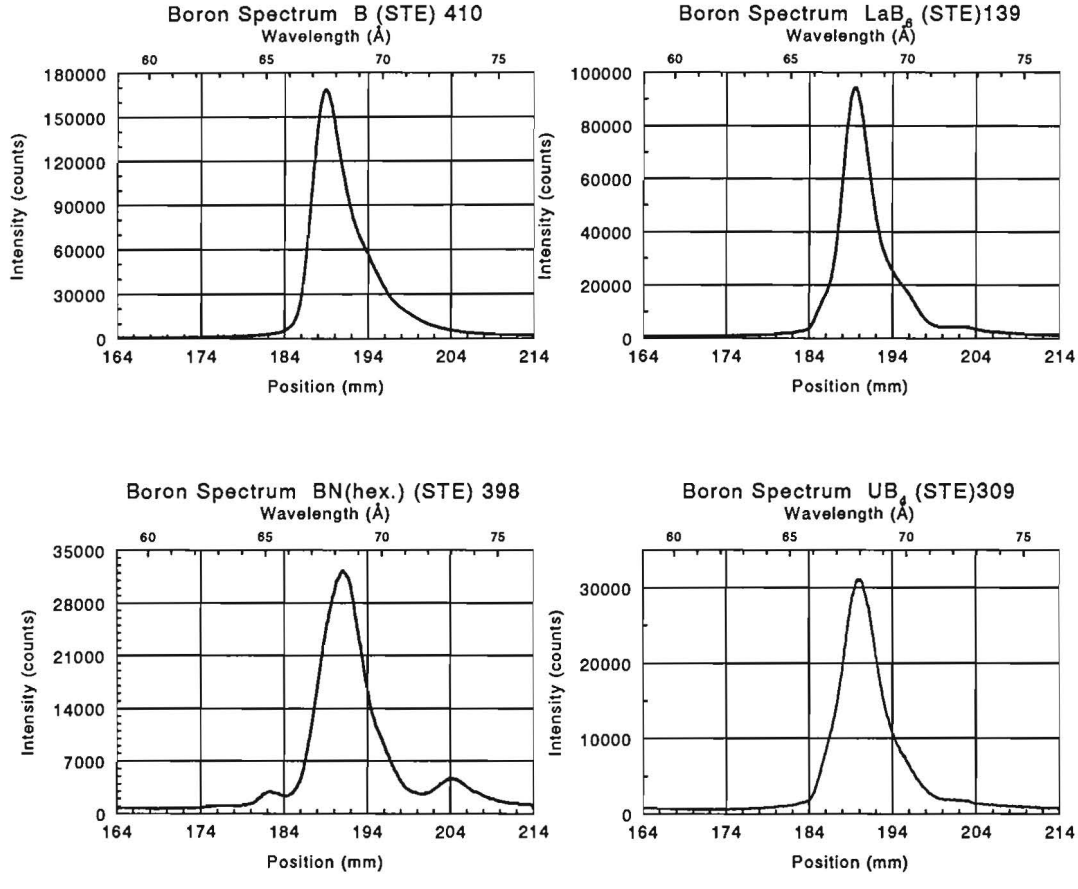

Fig. II.2. Typical B-K_α emission spectra from three binary borides as compared to that from elemental Boron. Note the peak shifts and the pronounced peak shape alterations. Pb-Stearate crystal; 10 kV, 300 nA.

We have shown before[1-3] that a considerable reduction in effort can be obtained by the introduction of so-called Area-Peak Factors (APF's). This APF has been defined as the ratio between the correct **Integral (Area)** k-ratio and the **Peak** k-ratio. Of course, this factor is only valid for a given compound with respect to a given standard and for a given spectrometer. Once an APF is known, subsequent measurements can simply be carried out on the peak again and multiplication of the peak k-ratio by the APF will simply yield the correct integral k-ratio.

From our work on Carbon in binary carbides it was obvious that the APF was essentially independent of accelerating voltage and that individual values (relative to Fe_3C as a standard) could range from 0.72 (TiC) to 1.05 (B_4C). If Vitreous Carbon would be chosen as a standard then the deviations would be even more extreme: down to 0.5 for TiC; which clearly demonstrates the need for integral measurements.

Considering the fact that Boron is even lighter than Carbon we must expect to run at least into similar problems for the B-K_α emission spectra. That this is indeed the case is demonstrated in Fig. II.2 where four B-K_α emission bands are shown. Apart from the differences in peak positions the variations in peak shapes are very prominent indeed. Quite frequently two or three separate contributions can be distinguished in the spectra, even to the extent that two completely distinct and well-separated additional contributions are present in (hexagonal) BN. It will be clear that in the latter case the additional contributions would go unnoticed in a peak intensity measurement, demonstrating once more the necessity of integral measurements.

From a chemical point of view these spectra are also interesting because they must contain a lot of information on the occupation of electron energy levels. In combination with XPS measurements perhaps valuable information on the nature of the chemical bond could be extracted. This is, however, clearly beyond the scope of the present work.

Unfortunately the problems in Boron analysis are not restricted to peak shifts and peak shape alterations alone, as we will see in the next section.

II.2 Specific Problems in the Analysis of Boron.

Our first experiences with integral measurements in borides were made on needle-shaped TiB-crystals (orthorhombic crystal structure), grown in a Ti-matrix. These measurements (using a STE crystal) were carried out relative to elemental Boron as a standard and the results were at first astonishing. From the work on Carbon we were used to APF's with reproducibilities of better than 2%; now we were suddenly facing data which showed variations of up to 30%. The explanation of these peculiar phenomena was eventually found in the observation that the peak position was no longer a constant but showed variations from one TiB-crystal to another.

Stranger still, the peak shape was found to vary in a completely synchronous way with the peak position: the lowest APF, i.e. the highest peak intensity in combination with the narrowest peak, was always found at the lowest peak position (shortest wavelength). Reversely, the highest APF was found at the highest peak position (longest wavelength). Fig. II.3 shows the two extremes in the Boron spectra emitted by TiB. Apparently each individual TiB-crystal can emit its own specific Boron-K_α peak, both in shape as well as in peak position.

It was further found that each individual crystal could be made to emit peak shapes between the two extremes in Fig. II.3, merely by rotating the specimen in a plane perpendicular to the electron beam. This must be taken as an indication that it is not so much the position of the specimen with respect to the electron beam that matters, but rather the position of the specimen with respect to the Pb-Stearate analyzer crystal. In extreme cases a rotation of 90 deg. was enough to shift the B-K_α peak over 1 mm (0.358 Å on the STE crystal) from the maximum to the minimum position. A further rotation of 90 deg. brought it back to the original position and so on. These observations strongly reminded us of the effects observed when examining a non-cubic specimen under an optical microscope with crossed Nicoll's prisms. A literature research revealed that the observed effects were indeed due to polarization effects in the emitted X-radiation and that the phenomenon itself has been known since 1969[13] . It can be expected[14,15]

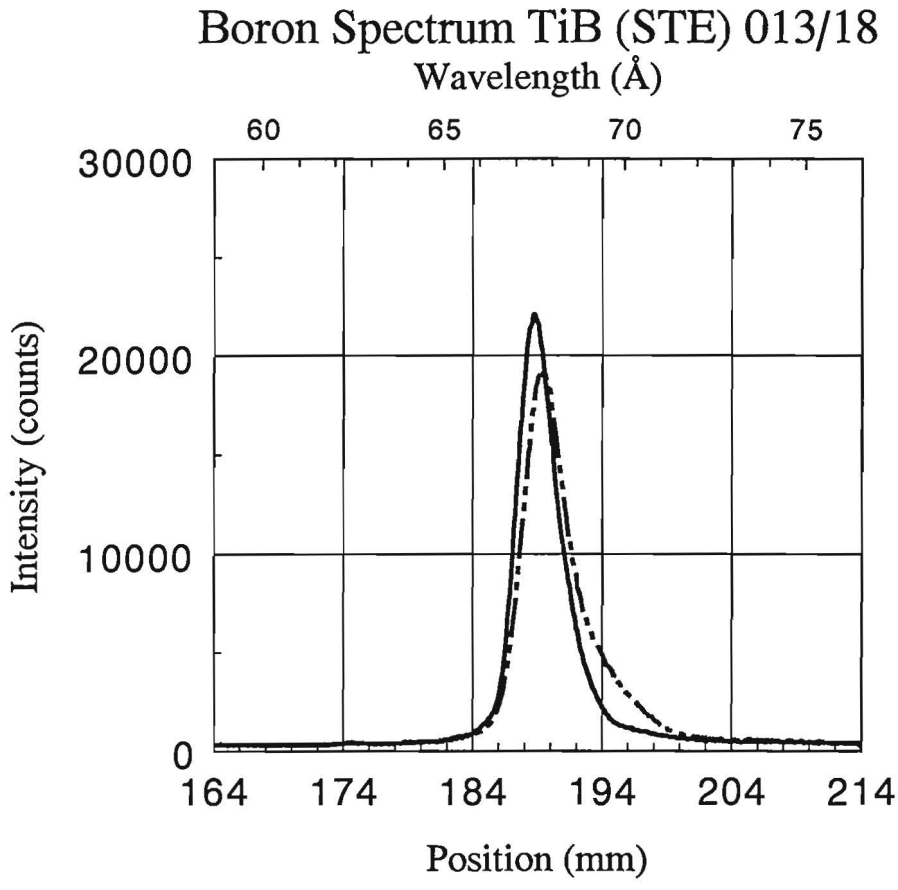

Fig. II.3. The two extremes that can be observed in the shape of the B-K_α peak emitted by various TiB crystals, or within the same crystal upon rotation of the specimen in a plane perpendicular to the electron beam.

in all compounds with a crystal symmetry lower than cubic and higher than triclinic. Polarization takes place (Fig. II.4) in two mutually perpendicular planes, which are aligned along the principal crystallographic directions of the crystal lattice. Unfortunately for quantitative analysis, the analyzer crystal can assume the function of a polarization filter and its action as such is optimal when the angle of incidence of the X-rays on the crystal is 45 deg.
For our specific crystal spectrometer (JEOL Superprobe 733) with a Pb-stearate crystal ($2d$ = 100.15 Å) the relation between wavelength (λ, in Å) and linear position (L, in mm) of the crystal is given by:

$$n\,\lambda = 2d\,\frac{L}{2R} = 2d\,\sin(\theta)$$

in which θ is the Bragg angle, n is the order of the reflection and R (mm) is the radius of the Rowland circle (140 mm).
It follows that for the wavelength of the B-K_α peak (67.6 Å), which is detected at 189.0 mm with our STE crystal, the corresponding Bragg angle θ is equal to 42.5 deg. This coincidence explains a great deal of the exciting and interesting phenomena observed.

The most pronounced effects have, so far, been found in hexagonal compounds like TiB_2 and ZrB_2, with up to 40% variation in APF (rel. to elemental Boron) and shifts of approx. 1 mm

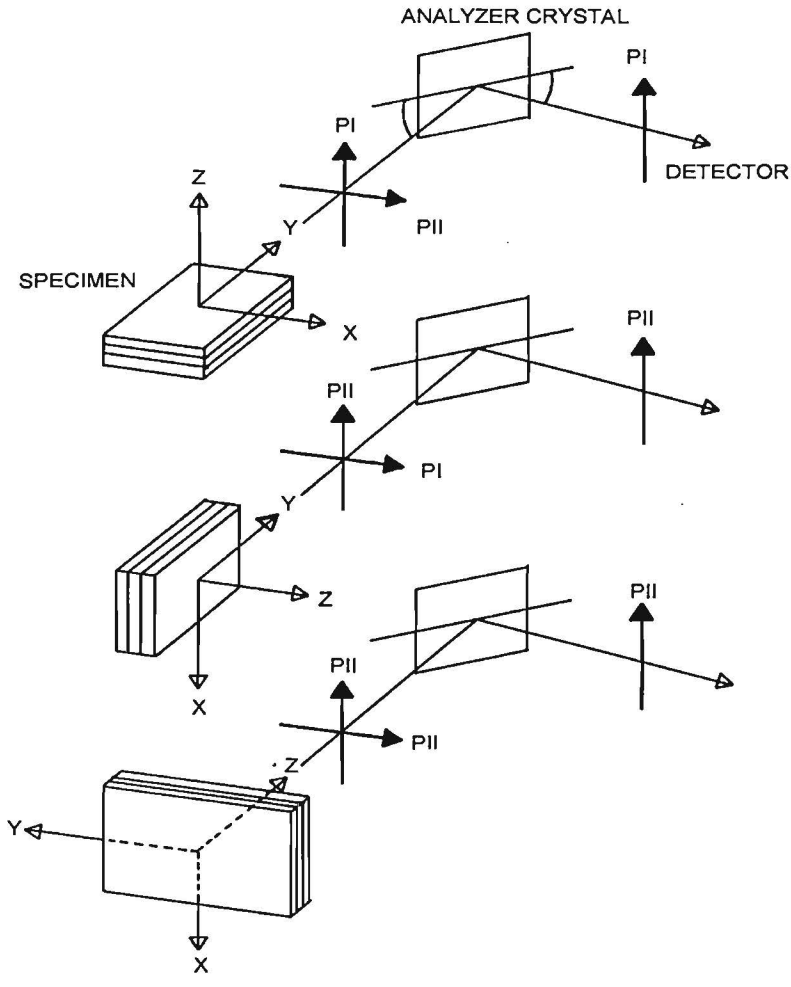

Fig. II.4. Schematic drawing showing the interaction of the analyzer crystal with the polarizedcomponents in the emitted B-K_α radiation. P1 and P11 are the main polarization directions which are aligned along the principal crystallographic directions in the crystal lattice of the specimen. The electron beam is considered to hit the specimen in the origin of the coordinate system X, Y, Z. (After Wiech[15]).

(0.358 Å) . As was to be expected the very few cubic borides like LaB_6 did not show these effect and could thus be considered as potential complex standards. Unfortunately, due to the low mac for B-K_α in these compounds (see Table II.1), the emitted intensity is already 30-50% of that from pure Boron; so, there is little to be gained. Crystalline Boron does not show these polarization phenomena, although its rhombohedral crystal structure would in principle allow this, so we were ultimately forced to adopt crystalline elemental Boron as our Boron- standard.

An immediate implication of these polarization phenomena is that anyone who is unaware of these effects could make large errors in the intensity measurements; even if these measurements were performed with the same compound as a standard and if the spectrometer would be retuned for each individual measurement. One could easily come to the conclusion that the Boron content in compounds like TiB_2 and ZrB_2 showed variations of 25%, whereas they actually have very limited homogeneity ranges.

It goes without saying that for quantitative analysis these effects are very much of a nuisance because one is forced **either** to measure all intensities in an **integral** fashion, **or** to determine first the **variation of the APF with the observed peak position** for each non-cubic compound.

We have done the latter for all orientation-sensitive binary borides and the general results are that although the Peak k-ratios and the APF's sometimes show a remarkable variation (20-30 %) with Peak position (or wavelength) the Area (Integral) intensities showed only a relatively small variation (approx. ± 4%) relative to the mean values. At present it is almost impossible to say whether there is a small residual effect of crystallographic orientation or that the remaining variation in Integral intensity must be attributed to small variations in composition. After all, the residual variation of the order of 4 % relative is getting dangerously close to the experimental accuracy.

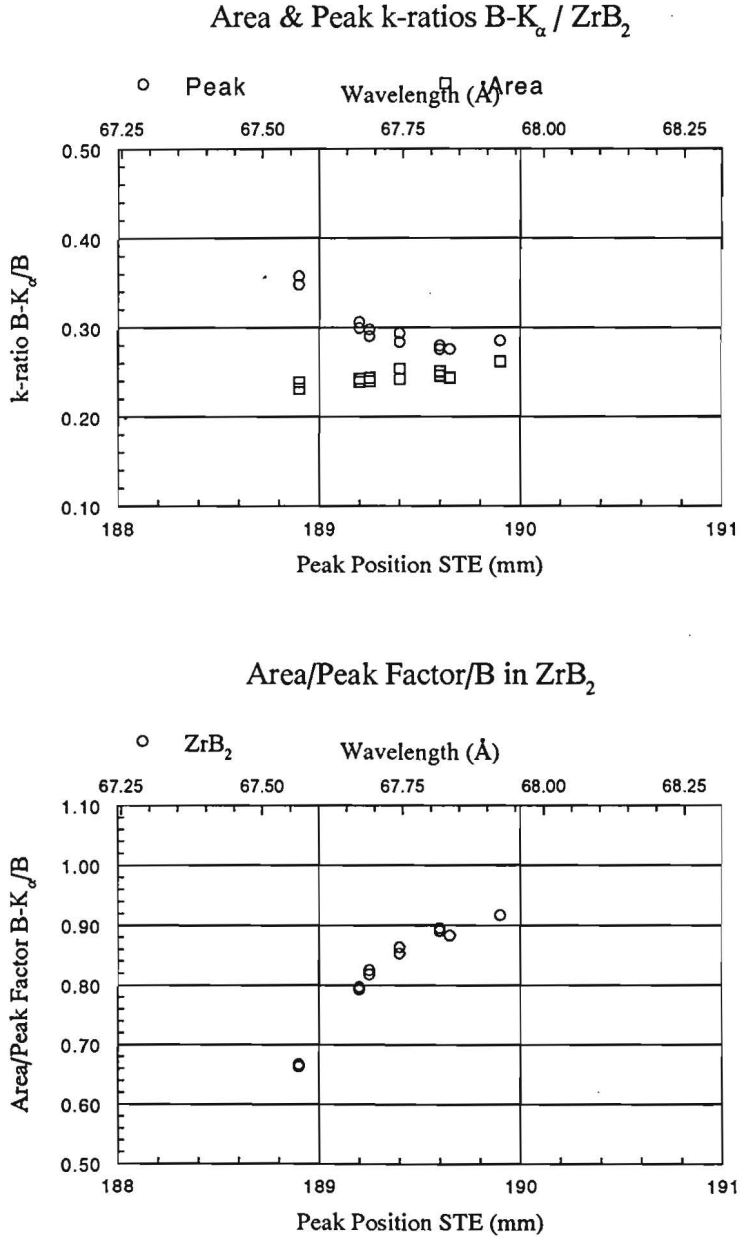

Fig. II.5. Variation of Area (Integral) and Peak k-ratio for B-K_α (top) and Area/Peak factor (bottom) with detected peak position on Pb-Stearate in ZrB_2 (Hexagonal) as a typical representative of the non-cubic borides.

Fig. II.5 shows the results of the measurements on ZrB_2, which must be regarded as a typical representative of non-cubic borides. Note the very strong variation in Peak k-ratio as compared to the slight variation in Area k-ratio.
The resulting APF for ZrB_2 shows almost 40% variation. In Fig. II.6 the B-K_α emission spectra corresponding to the two extremes are represented.
The detailed results of the APF measurements for the other borides will be discussed later on.

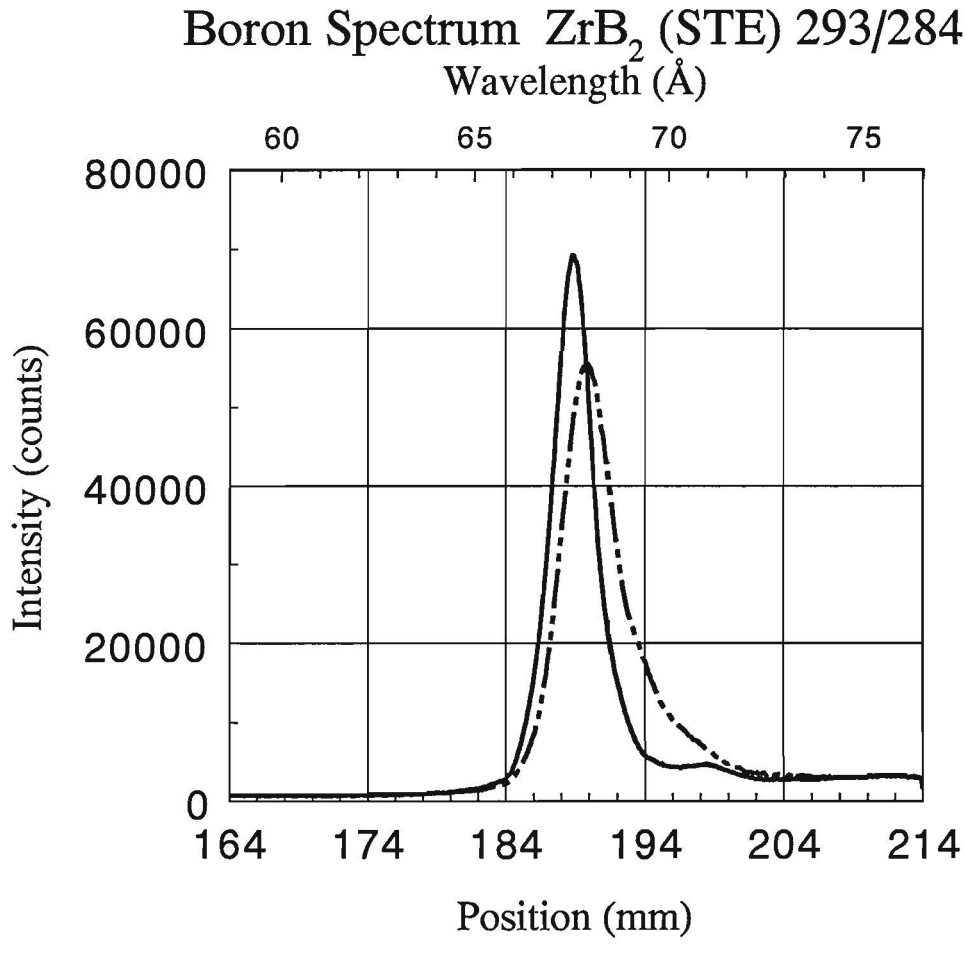

Fig. II.6. The two extremes that can be observed in the shape of the B-K_α peak emitted by ZrB_2. The corresponding values for peak and area k-ratio, as well as APF, can be found in Fig. II.5.

III EXPERIMENTAL PROCEDURES

For the purpose of the present work it is, in principle, required to have boride specimens with 100% density and accurately known compositions. Like we experienced in the case of Carbon already such specimens can hardly be obtained commercially. It was, therefore, decided to prepare them in our own laboratory. Only 5 out of 29 borides were obtained from outside our laboratory; these were a specimen of hexagonal BN (kindly supplied to us by Mr. G. Verspui; C.F.T. Philips, Eindhoven, The Netherlands), a specimen of cubic BN, (supplied by Mr. R. de Vries, Gen. Electric Company, U.S.A.), a specimen of B_6O (supplied by Dr. P. Karduck, G. f. E, RWTH Aachen, Germany), an UB_4 specimen (single crystal, supplied by Dr. Menovsky, Univ. of Amsterdam, The Netherlands) and a LaB_6 specimen (single crystal, supplied by Prof. L. Swanson, Field Electron and Ion Sources Company, Mc Minville, Oregon, U.S.A.).

III.1 Preparation and characterization of binary borides

The vast majority of boride specimens (Table III.1) were prepared by repeated Argon-Arc melting techniques. Mixtures of elemental Boron and metal powders (purity both better than 99.8%) were first pressed into pellets and subsequently melted in an Argon plasma (20 cm Hg) on a water-cooled copper plate. After repeated melting (3-5 times) with intermediate turning-over of the buttons, the specimens were sectioned and polished using conventional polishing techniques for very hard materials.

Optical microscopy was used to get a first impression of the quality of the specimens, as far as presence of second and/or third phases, presence of unreacted starting materials, grain size (using polarized light) etc. are concerned.

In some cases (e.g. BN) X-ray diffraction procedures were used to identify the compounds. Microprobe analysis of the metal component was used to check such vital items as homogeneity, identity of second phases and the compositions of the specimens. Special emphasis was hereby laid on the consistency of the results obtained in cases where 2 or 3 representatives of the same system (e.g. Ni_3B, Ni_2B, NiB) were available. This was, by the way, the reason that we preferred to have more than one compound in the same binary system.

During melting it was frequently observed that small pieces of Boron splashed away from the plasma, due to the often very high melting points of many borides. On the other hand it was sometimes observed that evaporation of the metal took place. As a result it must be expected that the nominal (real) compositions of the specimens (Table. III. 1) may differ significantly from the weighed-in compositions. In the majority of cases the changes in compositions led to the production of second and third phases, which, in turn, made an independent chemical analysis impossible and meaningless. However, precisely the presence of second phases, like traces of Fe at the grain boundaries of Fe_2B, and the observations made during melting, led us to adopt the final nominal compositions in Table III.1. In cases where we observed second phases richer in metal we have assumed that the Boron content of our boride specimen corresponds to the metal rich boundary according to the latest phasediagram[16]. On the rare occasions where second phases richer in Boron were found we assumed that the Boron-rich limit of the homogeneity region was attained. Fortunately most borides have rather high Boron-contents

and in general the homogeneity regions are rather restricted. The estimated accuracy of the nominal compositions in Table III.1 is therefore better than 5% relative.

In the following we will give a brief description of the preparation of the specimens, together with some remarks relevant to their compositions.

Table III.1

Survey of the binary borides used in the present work, with their nominal compositions and crystal lattices. (S) indicates stoichiometric composition, (L) line compound

Compound	Comp.(wt % B)	Structure
B	99.80	Rhombohedral
B_4C	79.81	Rhombohedral
BN	43.48 (S) (L)	Hexagonal
BN	43.48 (S) (L)	Cubic
B_6O	80.20 (S) (L)	Rhombohedral
AlB_2	44.49 (S) (L)	Hexagonal
AlB_{12}	82.78 (S) (L)	?
SiB_3	53.59 (S)	Rhombohedral
SiB_6	69.78 (S)	Orthorhombic
TiB	16.78	Orthorhombic
TiB_2	30.07	Hexagonal
VB_2	28.40	Hexagonal
CrB	16.80	Orthorhombic
CrB_2	27.31 (Lim)	Hexagonal
Fe_2B	8.82 (S) (L)	Tetragonal
FeB	16.22 (S) (L)	Orthorhombic
Co_2B	8.40 (S) (L)	Tetragonal
CoB	15.50 (S) (L)	Orthorhombic
Ni_3B	5.78 (S) (L)	Orthorhombic
Ni_2B	8.43 (S) (L)	Tetragonal
NiB	14.40	Orthorhombic
ZrB_2	17.89	Hexagonal
NbB	10.42 (S)	Orthorhombic
NbB_2	17.15	Hexagonal
MoB	10.13 (S)	Orthorh. (HT)/Tetragonal (LT)
LaB_6	31.83 (S)	Cubic
TaB	5.64 (S)	Orthorhombic
TaB_2	9.23 (S)	Hexagonal
WB	5.55 (S)	Orthorh./Tetragonal
UB_4	15.37 (S)	Tetragonal

Preparation and metallographic characteristics of boride specimens

– B_4C Arc-melted; no special remarks.
Weighed-in: 79.81 w/o B. Nominal : 79.81 w/o B.

– BN Chemical Vapour Deposited layer of **hexagonal BN**.
Extremely fine-grained structure (X-ray diffraction).
Line Compound. Nominal : 43.48 w/o B.
Special remark : Extremely poor electrical conductivity, efforts to obtain meaningful EPMA measurements eventually abandoned !! Measurements removed from data file.

– BN "Borazon" Process. (General Electric Company). **Cubic BN**.
Faceted crystals up to 100 μm, black and yellow (different procedures)
Sufficient electrical conductivity for meaningful EPMA measurements. Measurements included in data file.
Line Compound. Nominal : 43.48 w/o B.

– B_6O Sintered product of finely-grained B_6O matrix, occasionally containing crystals large enough for reliable EPMA measurements. Nominal : 80.20 w/o B.

– AlB_2 R.F.melted; slowly cooled down overnight into two-phase region AlB_2/AlB_{12}.
– AlB_{12} Gold-coloured (strongly polarizing) crystals of AlB_2 (few) + grey AlB_{12} crystals in Al-matrix.
Line compounds. Nominal : 44.49 w/o B.
82.78 w/o B.

– SiB_3 Arc-melted (Si-30 w/o B) alloy, rapidly cooled.
– SiB_6 SiB_3 crystals (light in backscattered image) + SiB_6 crystals (dark) in Si-matrix.
Non-equilibrium situation. Nominal : 53.59 w/o B.
69.78 w/o B.

– TiB Arc-melted Ti (2-10 w/o B) alloys, slowly cooled.
Primary Ti-rich TiB-needles in Ti-matrix. Nominal : 16.78 w/o B.

– TiB_2 Arc-melted, very large grains; traces of second phases at grain boundaries and near edges of specimen (evaporation of Ti; m.pt. of TiB_2 3225 °C). Splashing of Boron.
Weighed-in: 31.10 w/o B. Nominal: 30.07 w/o B.

– VB_2 Arc-melted; splashing of Boron, resulting in second and third phases (V-richer).
Weighed-in : 29.80 w/o B. Nominal : 28.40 w/o B.

– CrB Arc-melted; splashing of Boron, resulting in presence of fine lamellae of Cr-richer phase.
Weighed-in : 17.21 w/o B. Nominal : 16.80 w/o B.

– CrB_2 Arc-melted; splashing of Boron, resulting in traces of Cr-richer phases. Weighed-in : 29.37 w/o B. Nominal : 27.31 w/o B.

– Fe_2B Arc-melted; presence of eutectic Fe/Fe_2B at grain boundaries. Line compound. Weighed-in : 8.82 w/o B. Nominal : 8.82 w/o B.

– FeB Arc-melted; presence of Fe_2B at grain boundaries. Weighed-in : 16.22 w/o B. Nominal : 16.22 w/o B. Line compound.

– Co_2B Arc-melted; presence of Co at grain boundaries. Weighed-in : 8.40 w/o B. Nominal : 8.40 w/o B. Line compound.

– CoB Arc-melted; presence of Co_2B at grain boundaries. Weighed-in : 15.50 w/o B. Nominal : 15.50 w/o B. Line compound.

–Ni_3B Arc-melted; two-phase mixture of Ni_3B + Ni. Weighed-in : 5.78 w/o B. Nominal : 5.78 w/o B. Line compound.

– Ni_2B Arc-melted; two-phase mixture of Ni_2B + Ni_3B. Weighed-in : 8.43 w/o B. Nominal : 8.43 w/o B. Line compound.

– NiB Arc-melted; traces of (unreacted?) Boron. Weighed-in : 15.55 w/o B. Nominal : 14.40 w/o B.

– ZrB_2 Arc-melted; splashing of Boron + evaporation of Zr possible (m.pt of ZrB_2 3245 °C); very large (>> 100 μm) grains. Presence of Zr at grain boundaries (locally). Weighed-in : 19.16 w/o B. Nominal : 17.89 w/o B.

– NbB Arc-melted. Weighed-in : 10.42 w/o B. Nominal : 10.42 w/o B.

– NbB_2 Arc-melted; splashing of Boron; traces of Nb-richer compound very locally. Weighed-in : 18.88 w/o B. Nominal : 17.15 w/o B.

– MoB Arc-melted, very large (>> 100 μm) grains; Single-phased. Weighed-in : 10.13 w/o B. Nominal : 10.13 w/o B.

– LaB_6 Sintered bar, converted into single-crystalline rod (approx. 1.5 mm diameter) through triple-arc floating zone technique. Nominal : 31.83 w/o B.

– TaB — Arc-melted, large elongated grains; presence of Ta-richer phase at grain boundaries.
Weighed-in : 5.64 w/o B. Nominal : 5.64 w/o B.

– TaB_2 — Arc-melted, very large grains (>> 100 μm); presence of Ta-richer phase at grain boundaries.
Weighed-in : 10.67 w/o B. Nominal : 9.23 w/o B.

– WB — Arc-melted, very large grains. Traces of unidentified second phase only at the edges of the specimen.
Weighed-in : 5.55 w/o B. Nominal : 5.55 w/o B.

– UB_4 — Arc-melted and drawn from the melt using triple-arc technique.
Nominal : 15.37 w/o B.

III.2 Mounting, polishing and cleaning procedures

Each of the boride specimens, lumps of crystalline boron (used as standards) and pieces of the pure metals were mounted and polished separately. This was done in order to avoid polishing problems with materials with extreme differences in hardness. The specimens were mounted in copper-filled resin and very carefully polished. Diamond abrasive discs were used for the coarse stages (70, 30, 15 μm); final polishing was done on a nylon cloth with diamond (3-1 μm). When a satisfactory polish was obtained the specimens were cut out again in small cubes of mounting material containing the specimen after which all edges were carefully rounded off. Next the specimens were turned upside down to be remounted groupwise (e.g. TiB, TiB_2, B and Ti) with the polished sides facing the carefully cleaned bottom side of the mould. This procedure was found to guarantee perfectly plane and parallel top and bottom planes of the mount which is extremely important in view of the correctness of the take-off angle in light element work. Superficial contaminants were removed from the polished faces by a brief polishing treatment on a soft cloth using 0.05 μm γ-Alumina. Final cleaning was done ultrasonically using alcohol.

III.3 Some details on the equipment used

All measurements were performed on an automated JEOL 733 Superprobe, equipped with 3 wavelength-dispersive spectrometers (later 4) and an energy-dispersive system (Tracor Northern, TN2000). The automation system was also supplied by Tracor Northern (TN-1310). The first spectrometer, specifically for light elements, was equipped with a lead-stearate crystal which was used for the boron measurements, and a TAP crystal. The counter was of the Gas-flow Proportional type, counter gas Argon-10% methane. The other two spectrometers each contained a PET and an LIF crystal while the counters were of the sealed Xenon-type.

On a previous occasion[1] we have already described the tests on the operating conditions of the microprobe (accelerating voltage, beam current stability, stability of beam position) which were found highly satisfactory. Besides, our instrument is fitted with an automated beam current detector and count rates are automatically corrected for any drift that might occur.

During all Boron-measurements an air-jet[1] was used to prevent carbon contamination of the spot to be analyzed. This was necessary in view of the often very long (up to 3 hrs) measuring times on the same location during integral measurements. It must be expected that without anti-contamination device the B-K_α count rate would gradually deteriorate due to carbon build-up as the result of the presence of an oil-diffusion pump. At present this has been replaced by a turbo-molecular pump.

As mentioned before, we acquired a synthetic multilayer crystal, "OVH" (Mo/B_4C, 2-d spacing ≅147 Å) some years after the publication of the first edition of this report. Since then we have been able to repeat some of the more vital tests and experiments with this crystal, which appears to be eminently suited for the analysis of Boron. For some time we had both the conventional STE as well as the new OVH crystal mounted on the same microprobe, which gave us a unique possibility to compare the performances of both crystals. We were greatly impressed by the huge increase in peak count rates for Boron : up to 50 times more than STE. Further on, we will refer to this new crystal when appropriate.

III.4 Measurements of Area/Peak Factors (APF's)

The APF's for B-K_α radiation were measured by recording and comparing the integral emission profiles from the boron standard and each of the boride specimens. The spectrometer was hereby scanned in steps of 0.05 mm (0.01788 Å) over the range 164-214 mm (58.66-76.54 Å). In each of the 1000 intervals the B-K_α intensity was measured during 10 seconds after which the counts were transferred to successive channels of the multichannel-analyzer and displayed on the CRT of the TN-2000 system. After completion of the spectrum the data were automatically stored on floppy disk and the procedure repeated on a different location of the specimen. The beam current was measured at the beginning and the end of each measurement and stored in the first and last channel, respectively. The measurements were typically carried out in the following alternating sequence: Boron standard, 3 times a boride specimen, Boron standard etc. All integral measurements were carried out over night and in the weekends, so, full advantage of the automation system was taken.

All together approximately 500 spectra have been accumulated. In a first run the global variation of APF with peak position was established (See chapter IV). In a second run certain gaps in the graphs (missing crystallographic orientations) were filled in by rotating the specimen mount with respect to the first run. In principle each location was chosen to represent a different grain in the specimen. In general this could easily be accomplished using the backscattered image in which different grains could be distinguished by their differences in greytones.

The vast majority of APF measurements were carried out at the same accelerating voltage of 10 kV. We have shown before[1-3] that the APFs for Carbon-K_α were essentially independent of accelerating voltage and there is no reason to expect that it would be different in the case of Boron-K_α. The beam current was usually 300 nA.

The Pulse Height Analyzer (Ortec) conditions were chosen to produce a pulse of 2.0 Volt (Counter High Tension 1700 Volt; Gain 64 x 8). The lower level (threshold) was set at 0.6 Volt and the window at 3.5 Volt. These settings (see Fig.II.1) were selected in order to cut off the continuous noise level and at the same time to accept as much of the pulse as possible, thus allowing for possible shifts.

The stored spectra were processed to obtain the net integral (area) and peak intensities from standard and specimen by subtracting the linearly interpolated background over the relevant region of interest. In cases of spectral interference like the Nb- and Mo-borides, where a relatively strong M-ζ peak interferes with the B-K_α peak (see Chapter IV) a special procedure has been used to strip the M-ζ peak from the spectrum. This will be discussed in Chapter IV.

The accuracy of the APF's is, of course, strongly dependent on the system analyzed: individual measurements in TiB_2 have an estimated accuracy of better than ± 3 % relative. In a heavily absorbing boride like Ni_2B this probably deteriorates to ± 8 %, mainly because of the uncertainty in the peak count rates which drop to ± 100 cps. On the basis of the large number of measurements performed we expect that the final APF's quoted have an accuracy of ± 1.5 % for the "easy" specimens and ± 3 % for the "difficult" ones.

III.5 Measurements of Peak k-ratios between 4 and 15 (30 kV)

The APF-concept has been introduced to facilitate accurate integral measurements with a considerable reduction in time. Once the APF for a certain system is known, or like in the present case the variation of APF with peak position, the measurements can simply be carried out again on the peak. Subsequent multiplication of the peak k-ratio with the APF for the appropriate peak position will simply yield the correct integral k-ratio. In order to appreciate the reduction in time it must be realized that when using the conditions applied by us only 4 boride spectra can be recorded (apart from the standard) during one night. If the range 4-30 kV has to be measured at 9 different accelerating voltages then two weeks would be necessary for each boride specimen and still the statistics would be very poor with only 4 integral k-ratios for each accelerating voltage. Using the APF-concept this full range can be measured in much less than a day and with very much improved statistics as we will see later on.

With a few exceptions (La, U), where no suitable elemental standards are available, the k-ratios of the metals have also been measured over the range 4-30 kV. Where possible more than one X-ray line has been measured (e.g. W-L_α and M_α) in order to supply complementary evidence to the boron measurements. In view of the very high beam currents necessary for Boron-K_α, which would cause dead-time problems for the metal lines, it has been decided to measure the latter separately. The procedure for the metal lines was the following : In a preliminary survey 10 suitable areas for analysis were selected. These locations were stored in computer memory. In each area 5 measurements were taken and the automation system was instructed to move the specimen over a specified distance in a specified direction. In this way 50 measurements were performed for each specimen and for each accelerating voltage. The beam current was usually adjusted as to ensure a maximum count rate in the order of 3000 cps to avoid significant dead-time corrections. A total number of 196 metal k-ratios were thus collected. Backgrounds were measured on either side of the peak and interpolated. The standard deviations in the final k-ratios are usually better than 1%.

For the Boron measurements a slightly different procedure was followed. Here the airjet was used and the 10 areas were selected each to represent a different grain and, consequently, probably a different crystallographic orientation. Care was taken that all 5 consecutive measurements were all inside the same grain. For each new area a very slow peak search procedure was used to ensure that the measurements would be performed at the correct peak position. Backgrounds were usually measured at ± 25 mm (± 8.94 Å), except where spectral

interference occurred (Ta, W, see Fig.IV.1). The peak k-ratios for each area were next multiplied by the APF appropriate for the observed peak position. In this way a total number of 192 k-ratios were obtained. In some cases, with not too heavy absorption and/or high boron contents (B_4C, AlB_{12}, TiB_2 etc) the measurements were performed in the range 4-30 kV; in heavier cases of absorption the measurements had to be broken off at 15 kV. Beyond that value the observed count rates (on STE) simply became too low.

IV. RESULTS

IV.1 Boron-K_α emission spectra

Fig.IV.1 gives a survey of the B-K_α spectra emitted by the various borides at 10 kV. Originally, these spectra were recorded with the STE crystal with a beam current of 300 nA (500 steps of 0.10 mm; 20 seconds counting time per step). Several years later we had the opportunity to record similar spectra with the OVH crystal (also at 10 kV), under the following conditions : Beam current 10 nA, 500 steps of 0.07 mm, 5 seconds counting time per step.

Upon inspection of these spectra (notably on STE) some features become immediately obvious:

- In the first place there is a very large variation in peak shapes possible from one boride to another. Some spectra appear to contain only one single-valued Boron-component (TiB, TiB_2, ZrB_2 as far as the short-wavelength extremes are concerned), while others clearly contain at least 2 components (e.g. LaB_6, CoB, NiB).
  In several cases even three components can be distinguished. Examples are B, SiB_3, SiB_6, AlB_{12} and B_4C. The most extreme example is Hexagonal BN where two clearly distinct and well-separated small peaks are visible which genuinely belong to the B-K_α emission spectrum.

- In the second place it is apparent that shifts in the peak position of up to 1 mm (0.358Å) relative to elemental Boron can occur; not only from one boride to another, but also within the same boride from one crystallographic orientation to another.

  Where this has been observed the extremes in the spectra have been represented in Fig.IV.1 (solid vs. dotted lines). It must be emphasized that apart from the shifts in peak positions also pronounced peak shape alterations, due to the filtering of polarized components from the B-K_α emission spectrum by the action of the analyzer crystal, take place (see also II.2). On theoretical grounds[13-15] the presence of polarized components can only be expected in non-cubic compounds. That explains why the only cubic boride in the present investigation (LaB_6) does not show these effects. As it turns out, however, 14 out of the 28 borides do not show the variations in peak positions and shapes, although their crystal structures would allow this. Among these is elemental Boron itself and this has been the reason why we adopted this as the Boron-standard. The only other possible candidates would be LaB_6 or AlB_{12}, considering the magnitudes of mac's in all other cases (Table II.1).

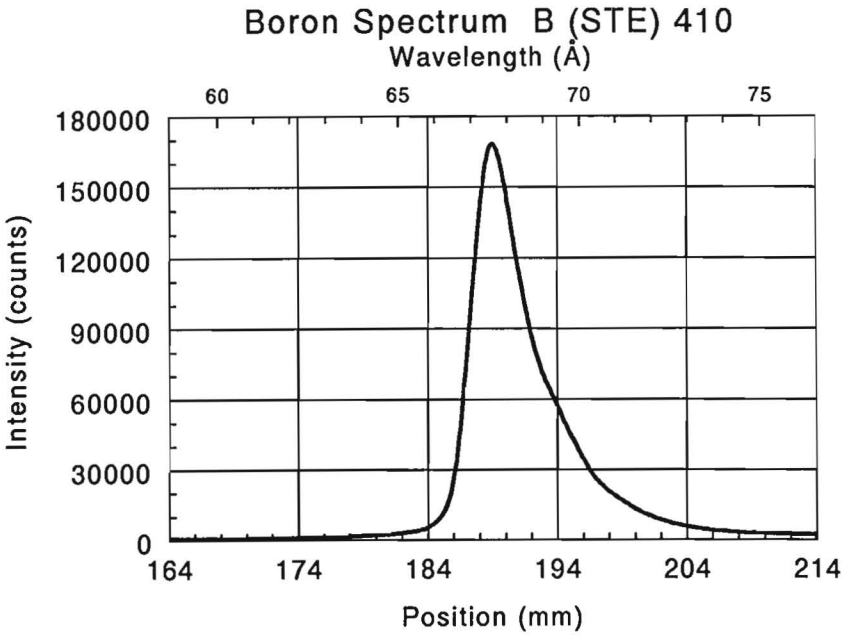

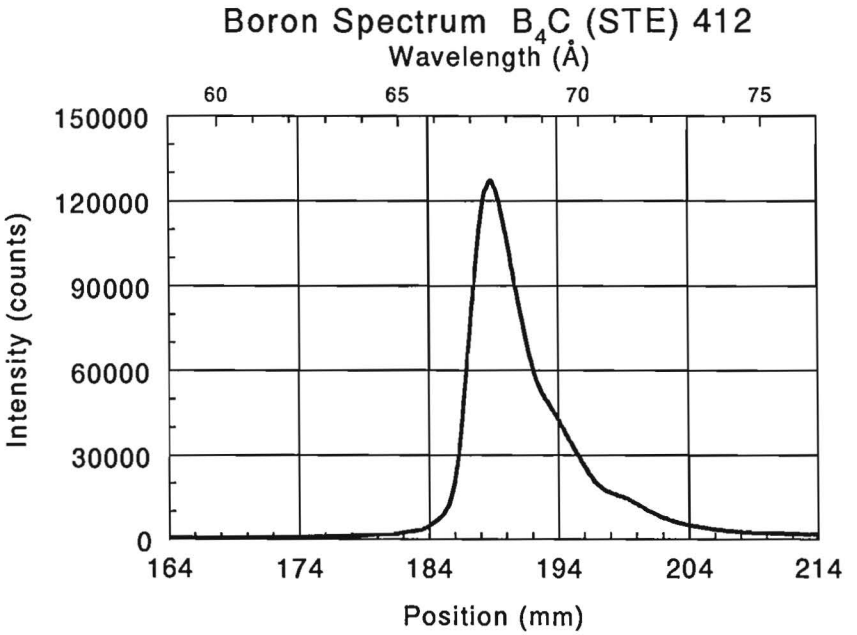

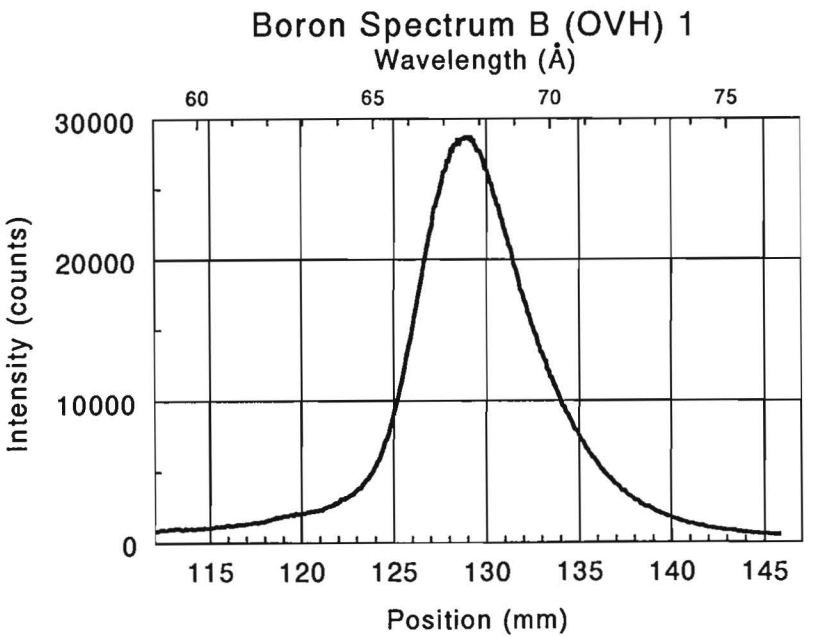

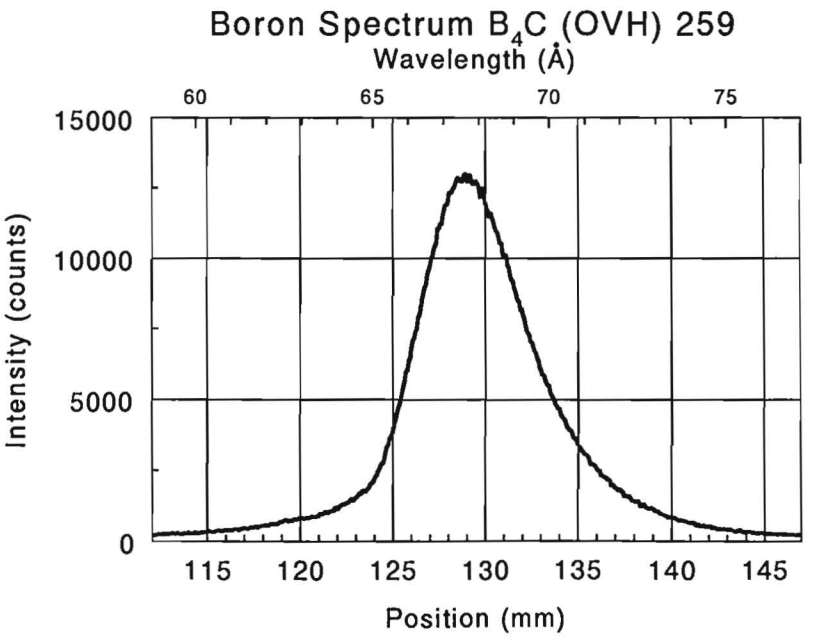

Fig. IV.1.a. B-K_α spectra recorded with STE (top) and OVH (bottom) of B and B_4C.

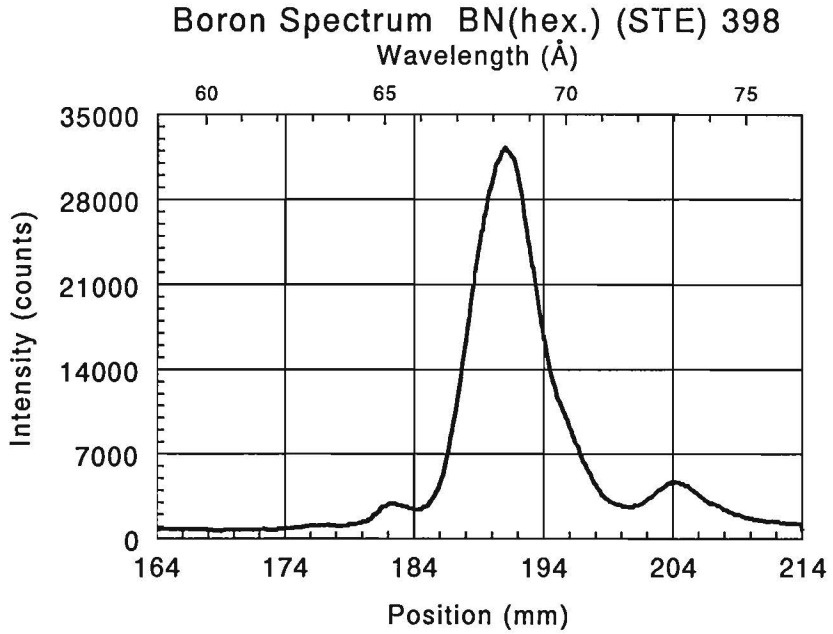

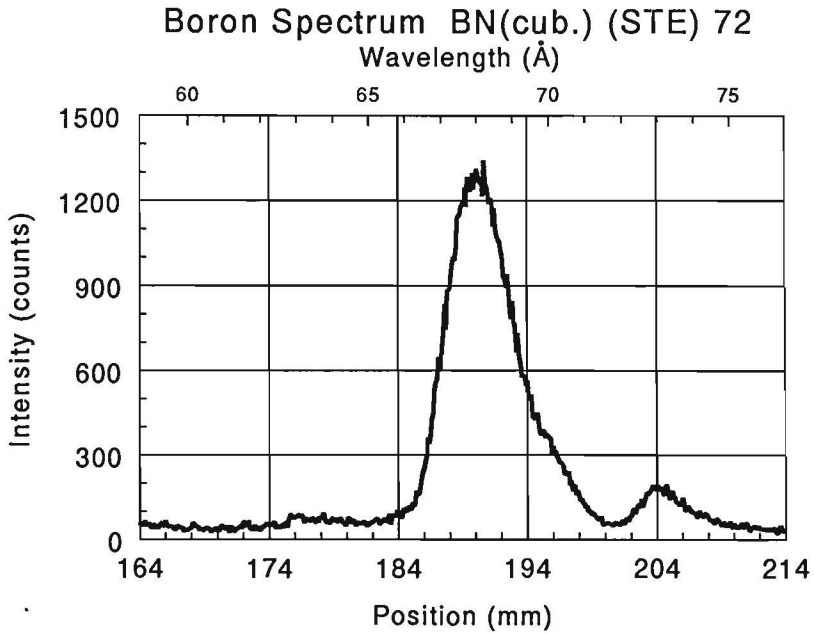

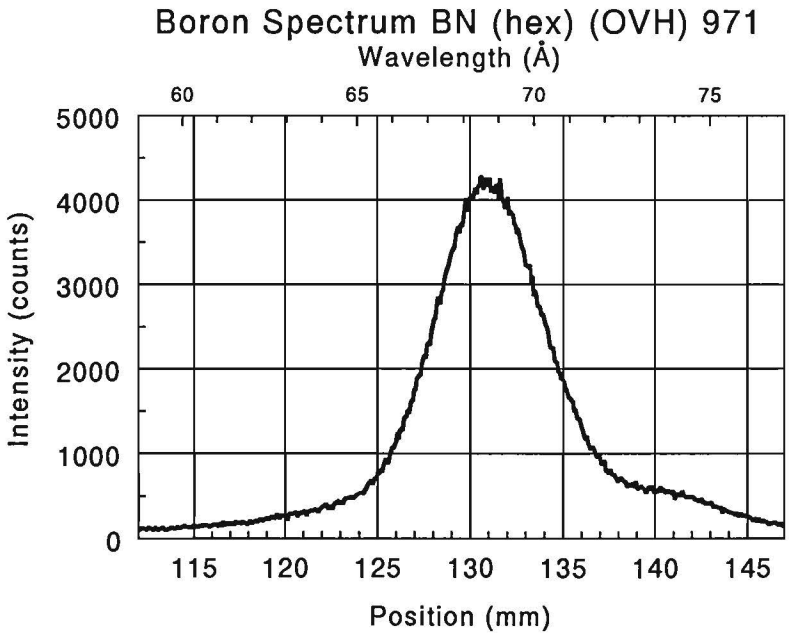

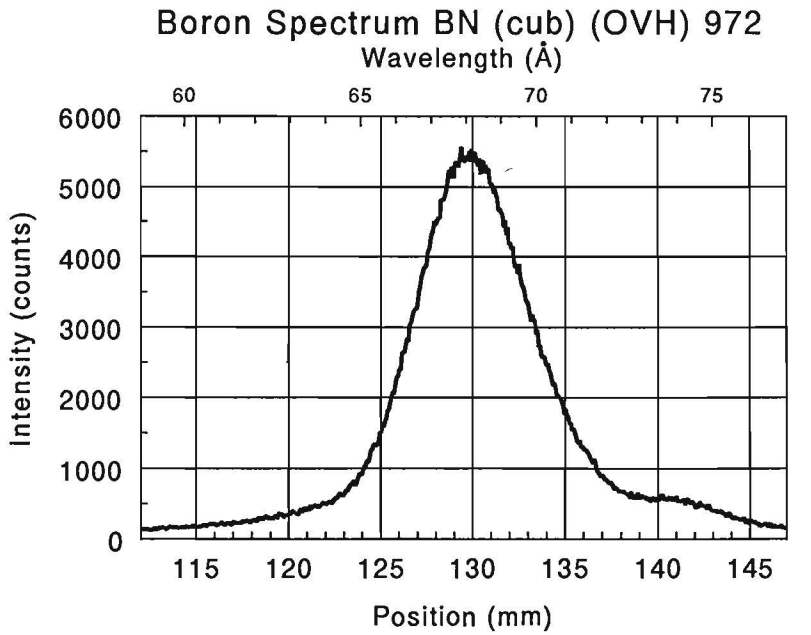

Fig. IV.1.b. B-K_α spectra recorded with STE (top) and OVH (bottom) of Hexagonal and Cubic BN.

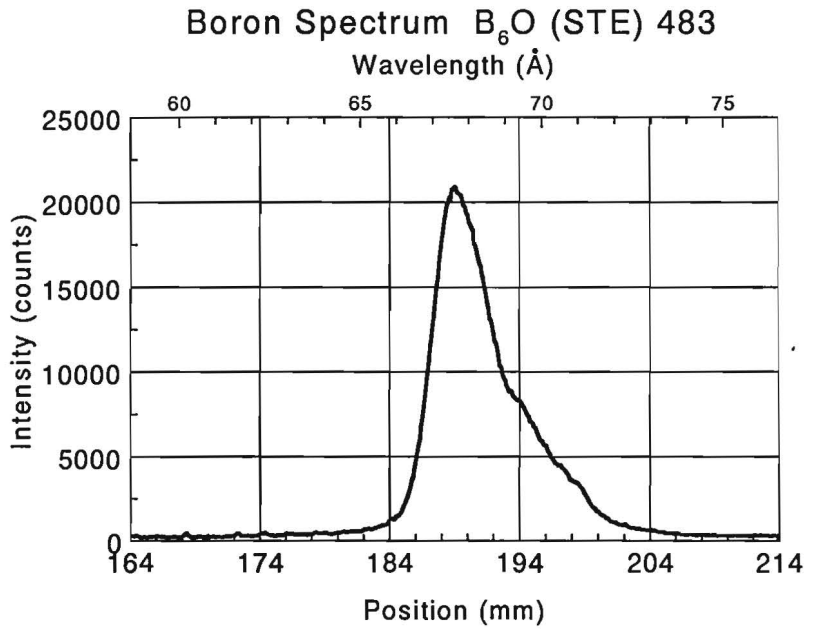

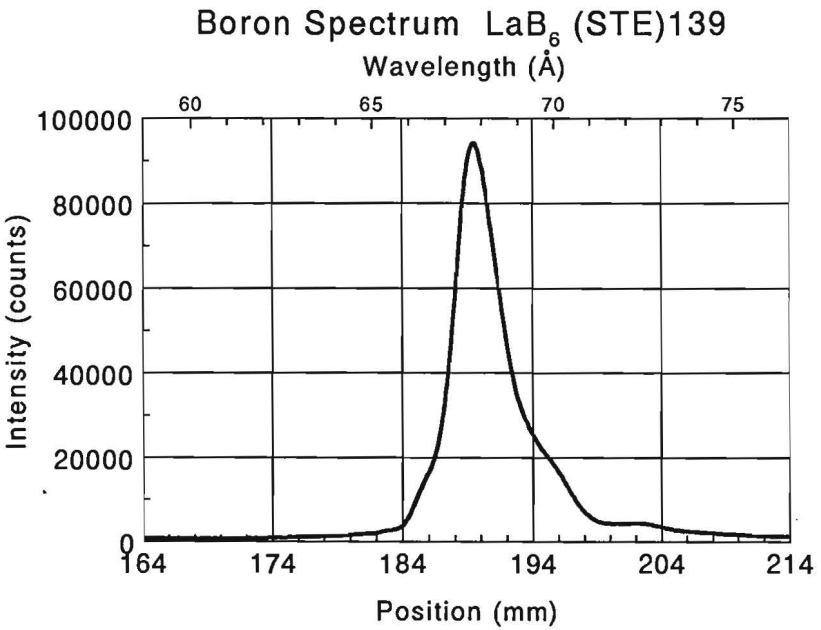

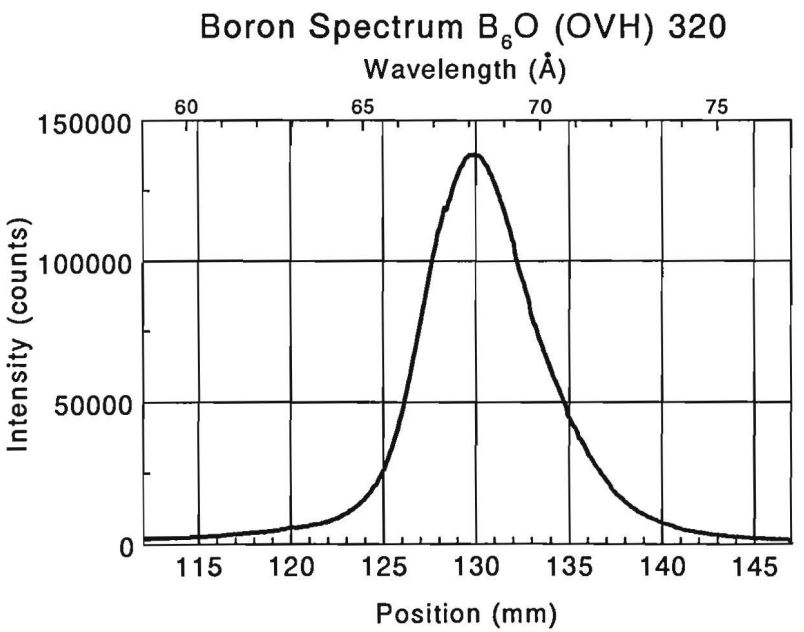

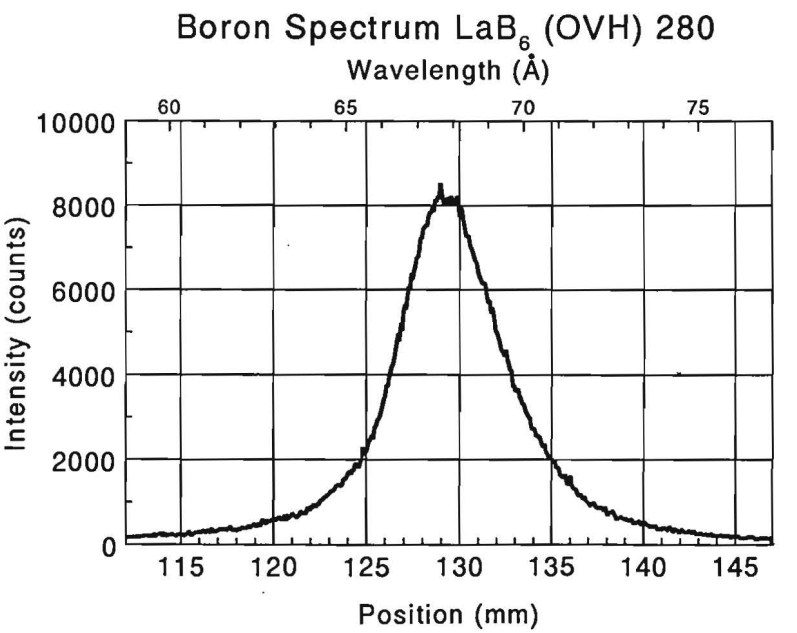

Fig. IV.1.c. B-K_α spectra recorded with STE (top) and OVH (bottom) of B_6O and LaB_6.

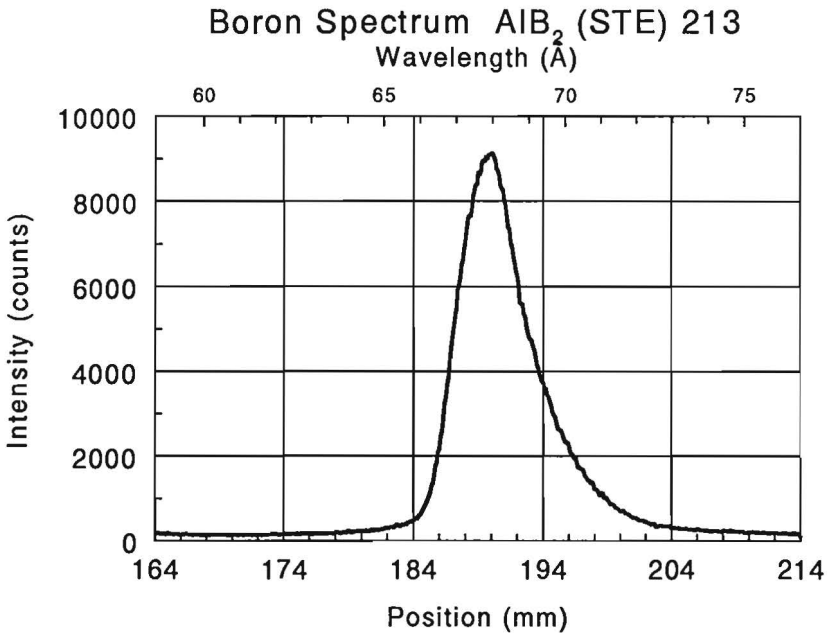

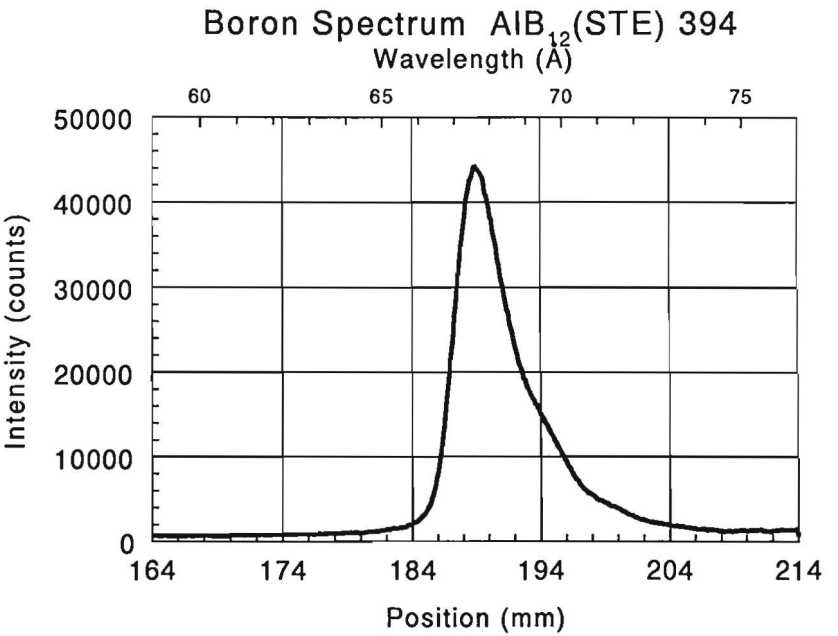

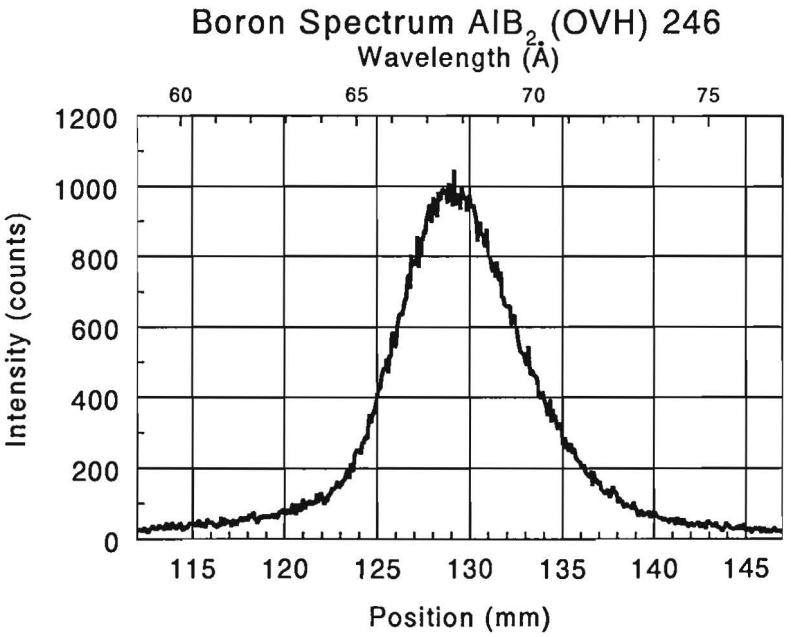

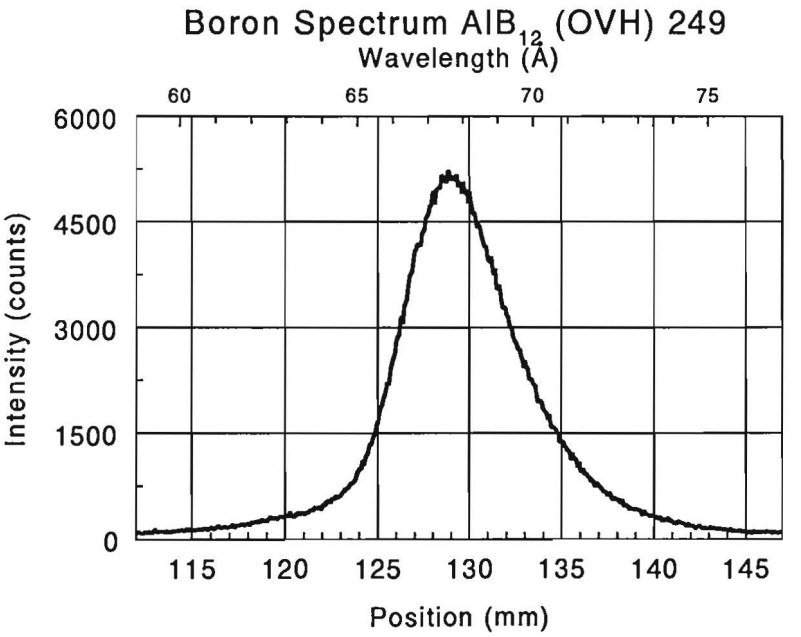

Fig. IV.1.d. B-K_α spectra recorded with STE (top) and OVH (bottom) of AlB_2 and AlB_{12}.

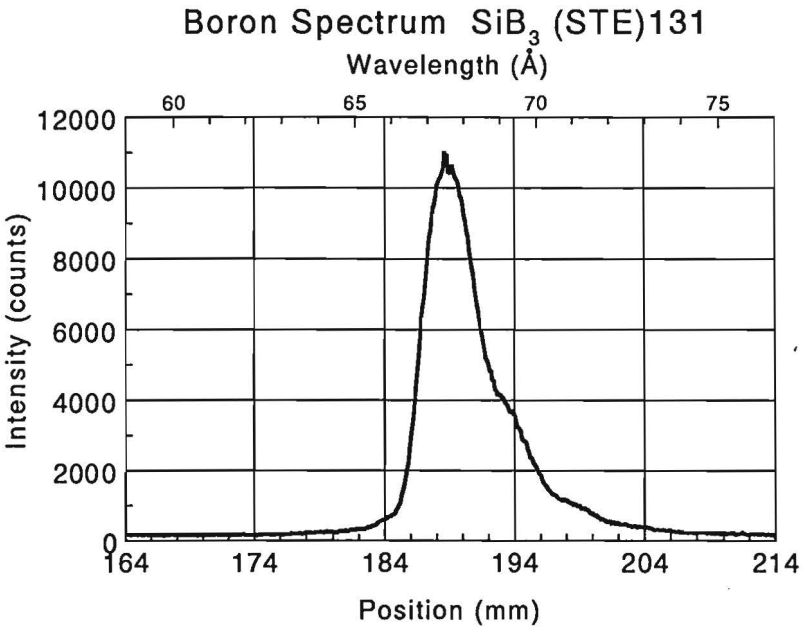

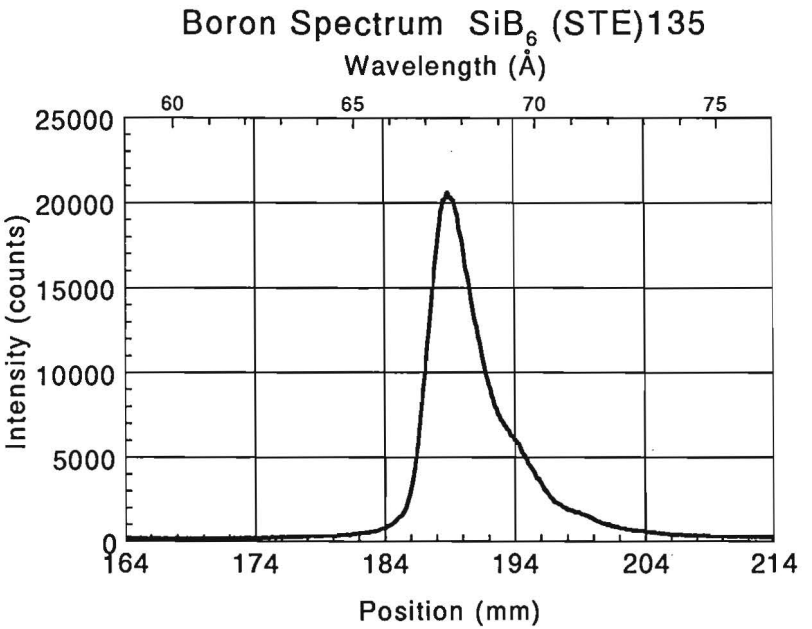

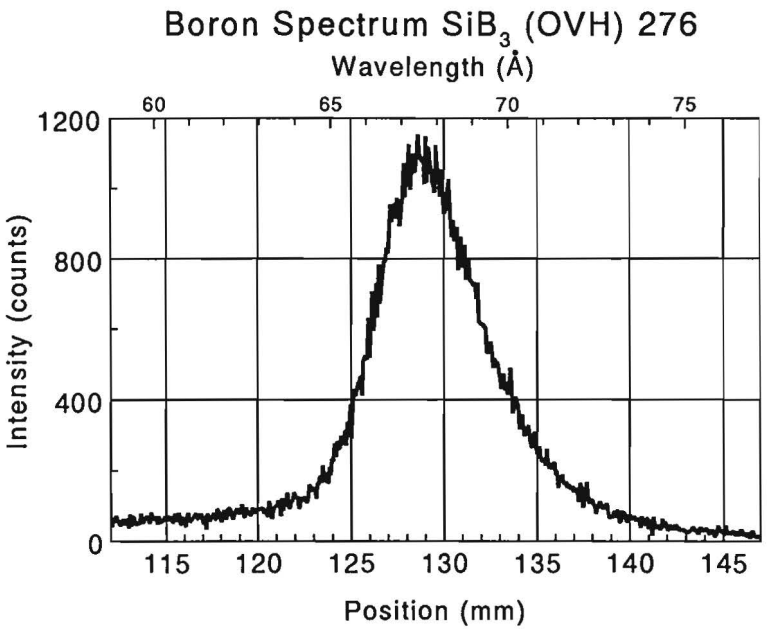

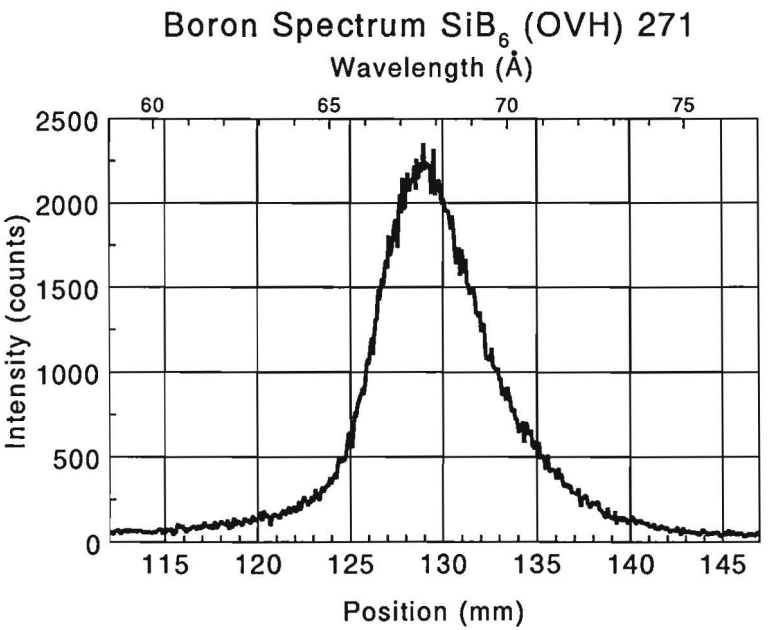

Fig. IV.1.e. B-K_α spectra recorded with STE (top) and OVH (bottom) of SiB_3 and SiB_6.

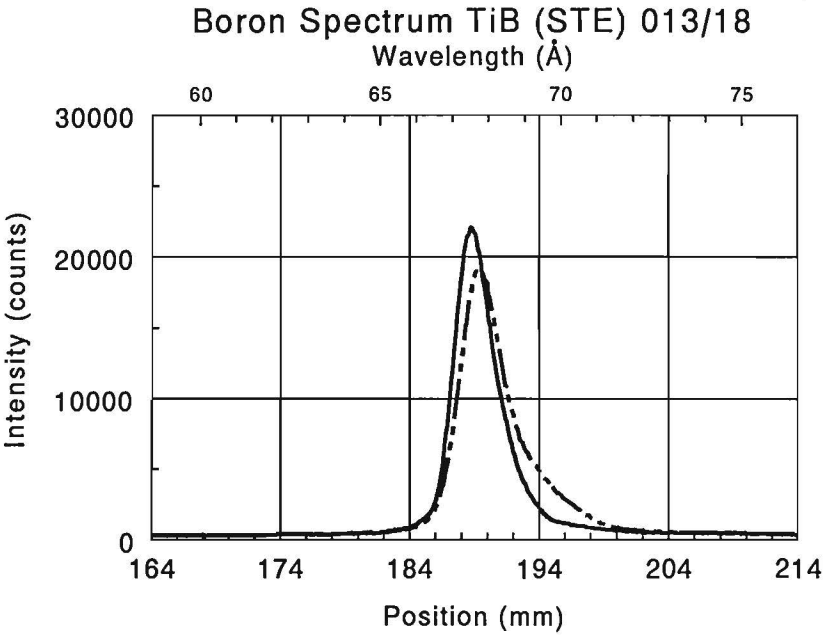

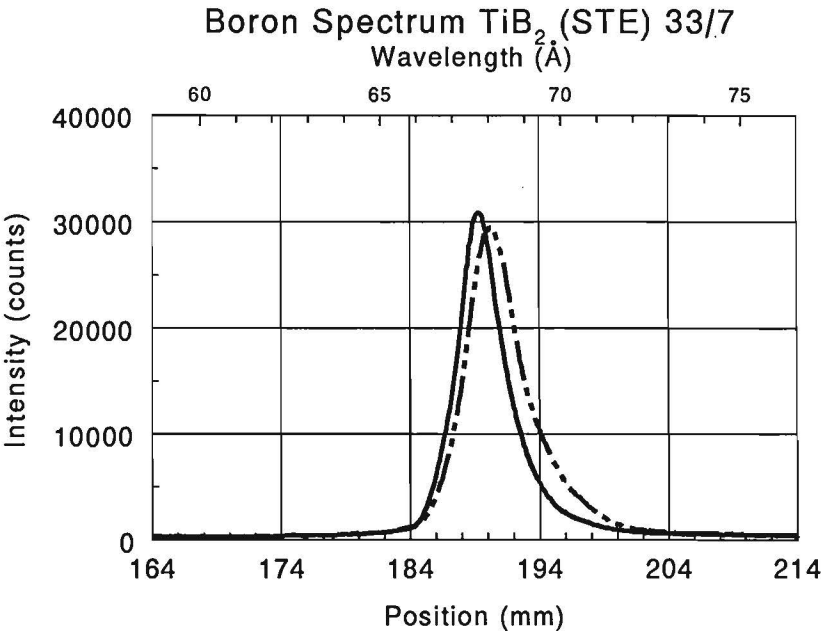

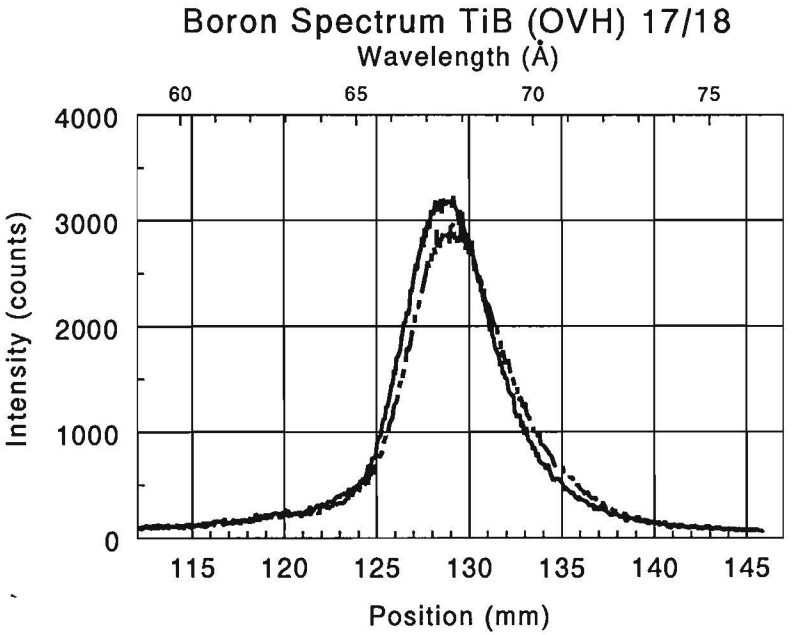

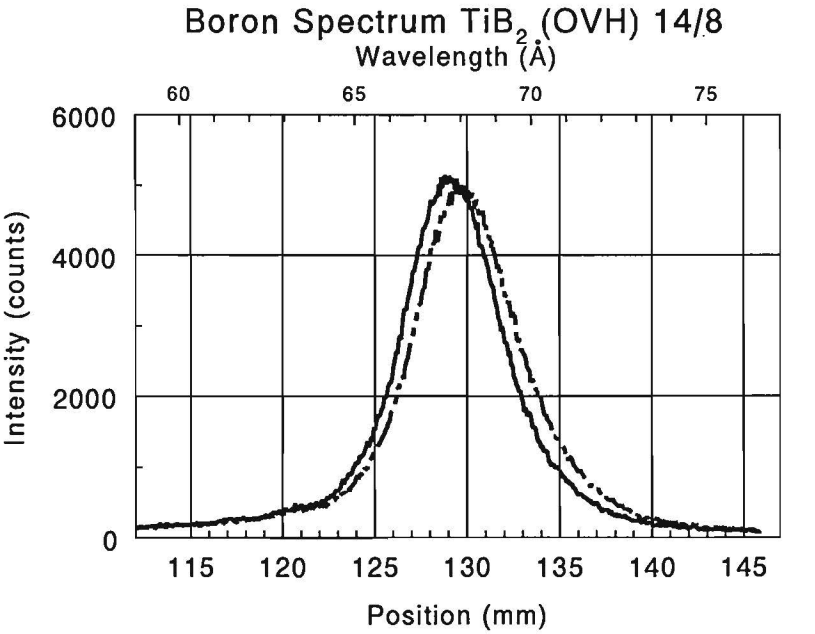

Fig. IV.1.f. B-K_α spectra recorded with STE (top) and OVH (bottom) of TiB and TiB_2.

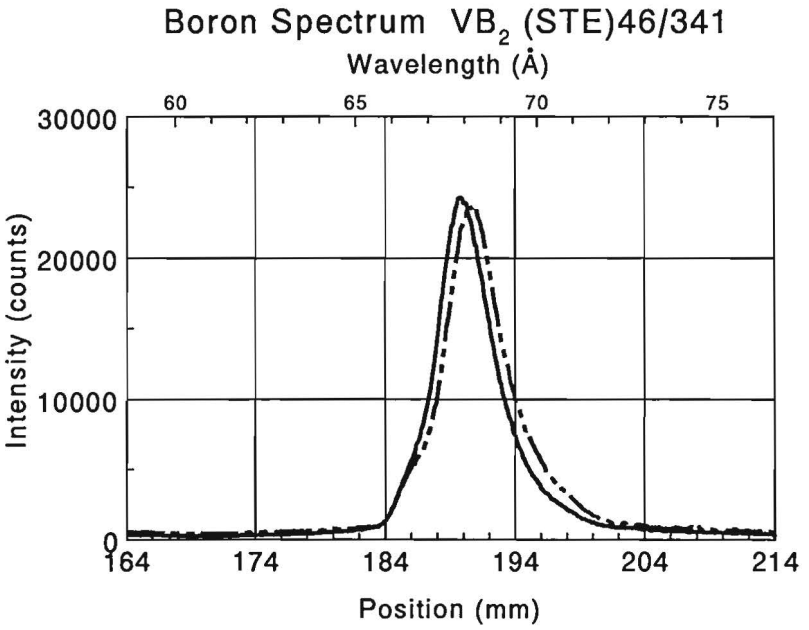

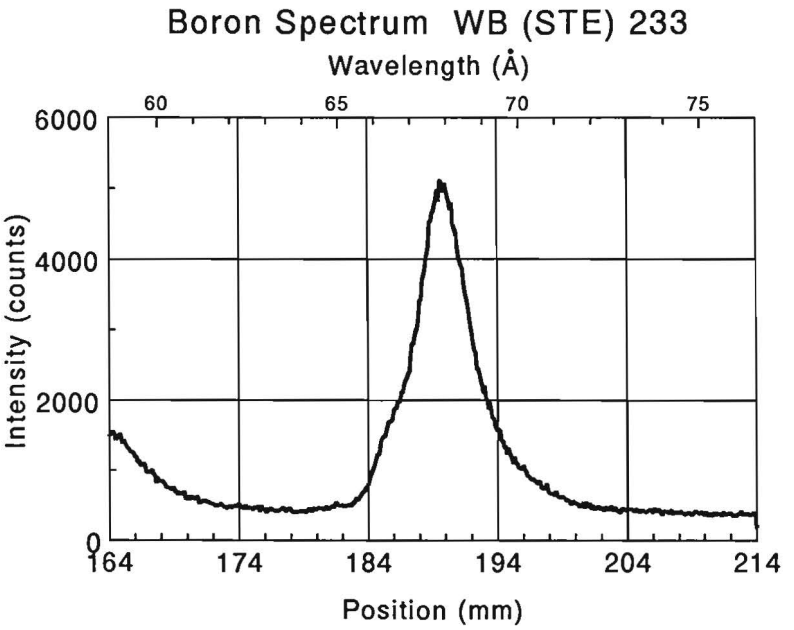

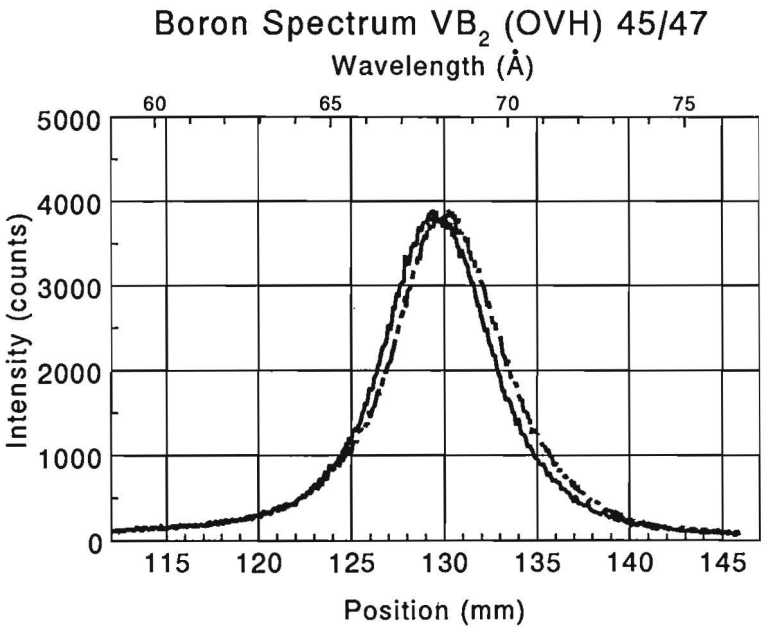

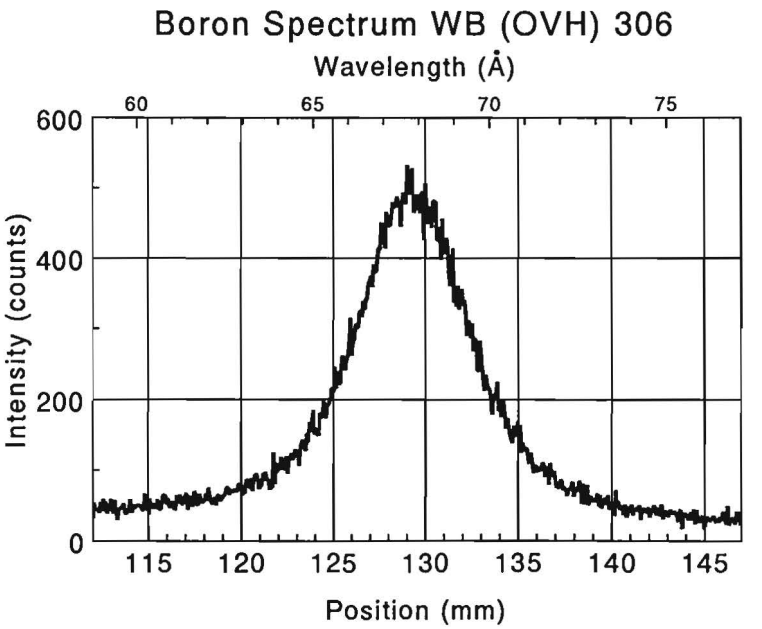

Fig. IV.1.g. B-K_α spectra recorded with STE (top) and OVH (bottom) of VB_2 and WB.

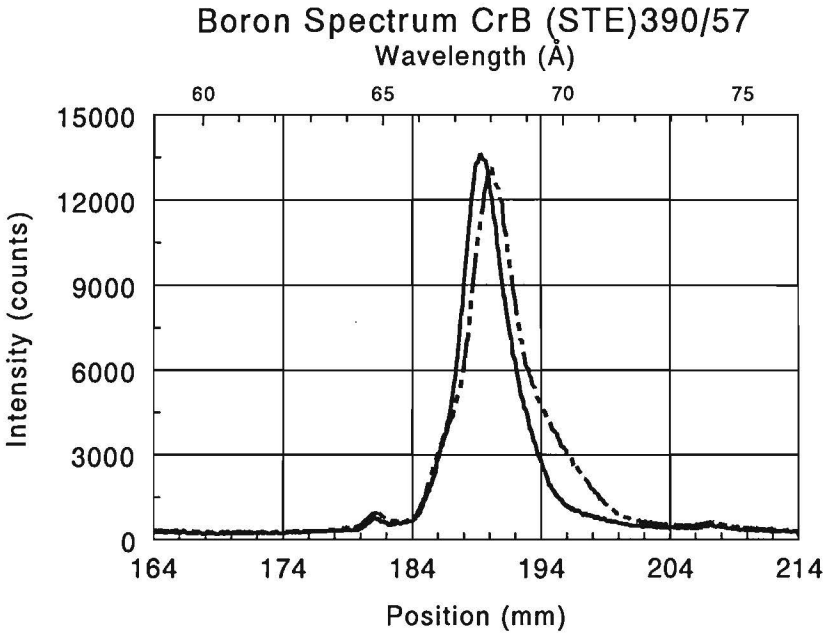

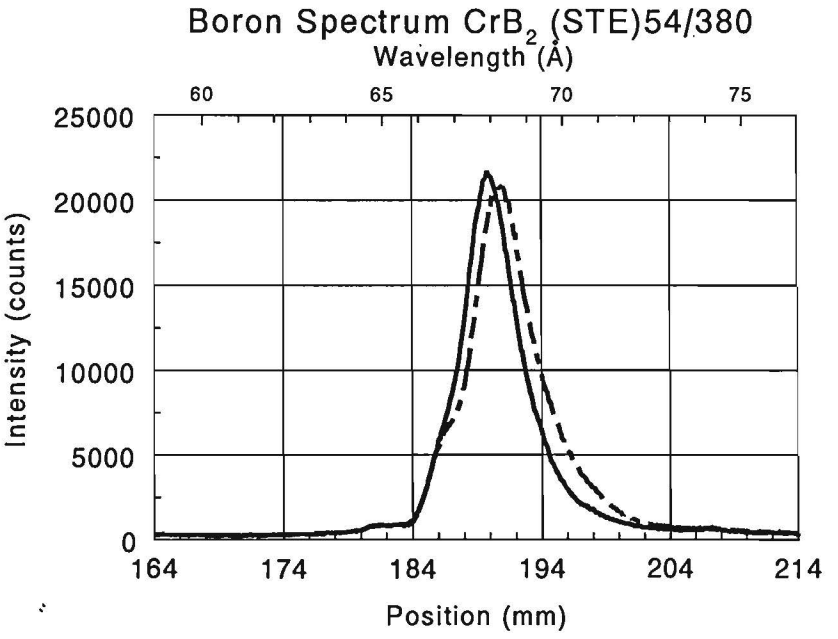

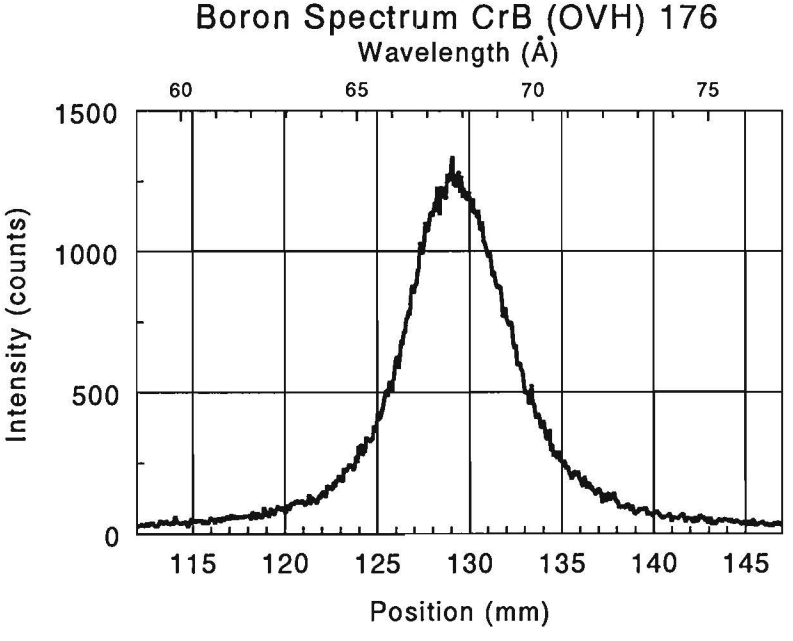

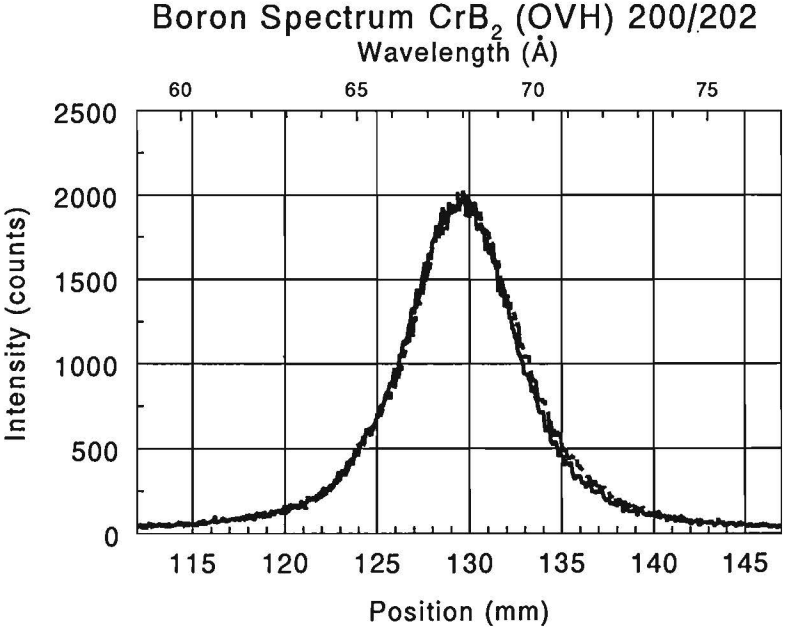

Fig. IV.1.h. B-K_α spectra recorded with STE (top) and OVH (bottom) of CrB and CrB_2.

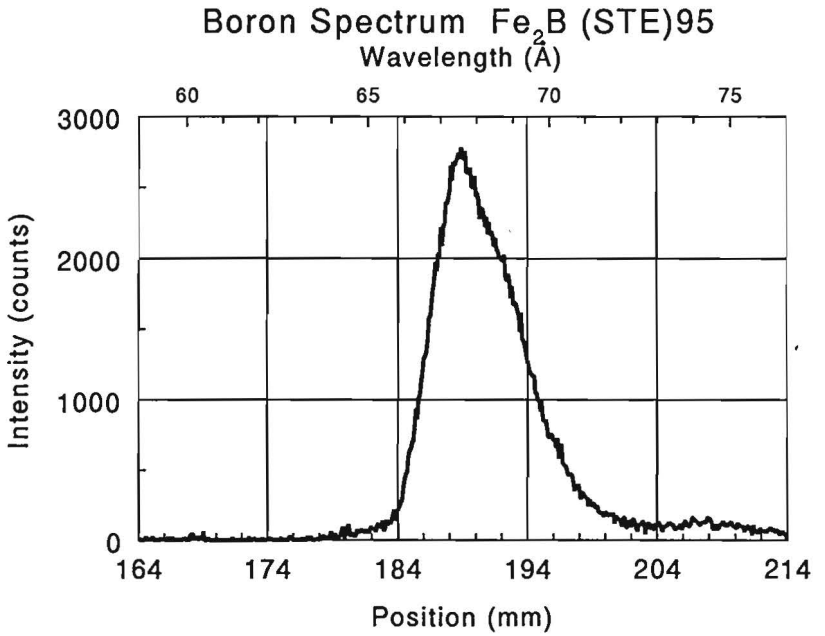

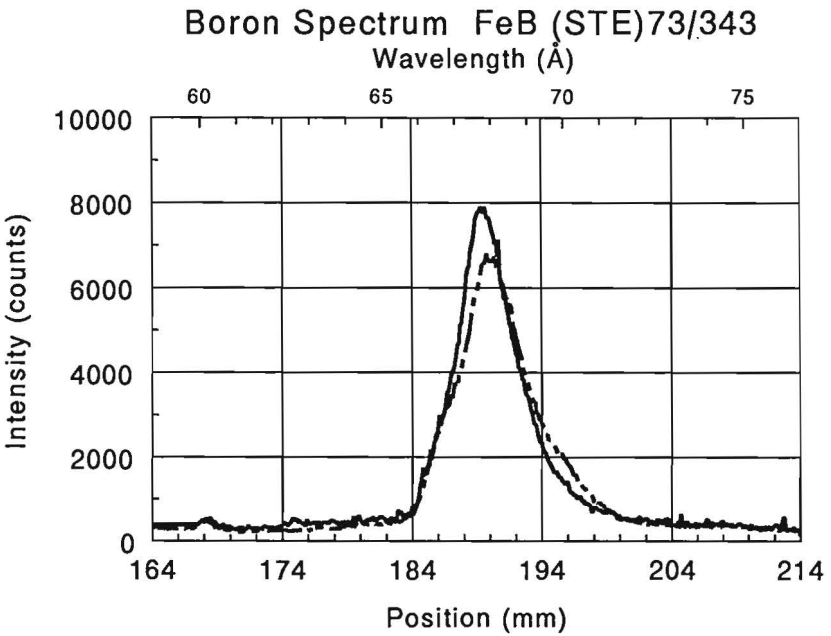

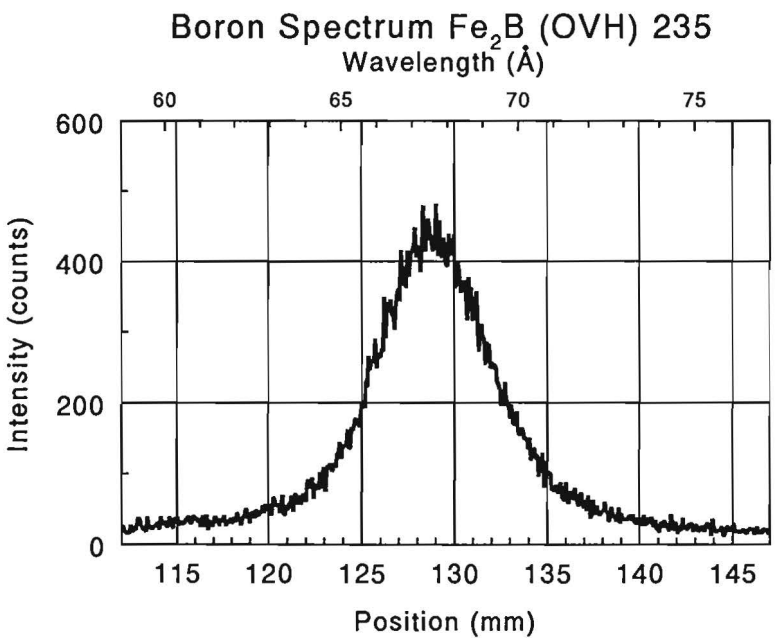

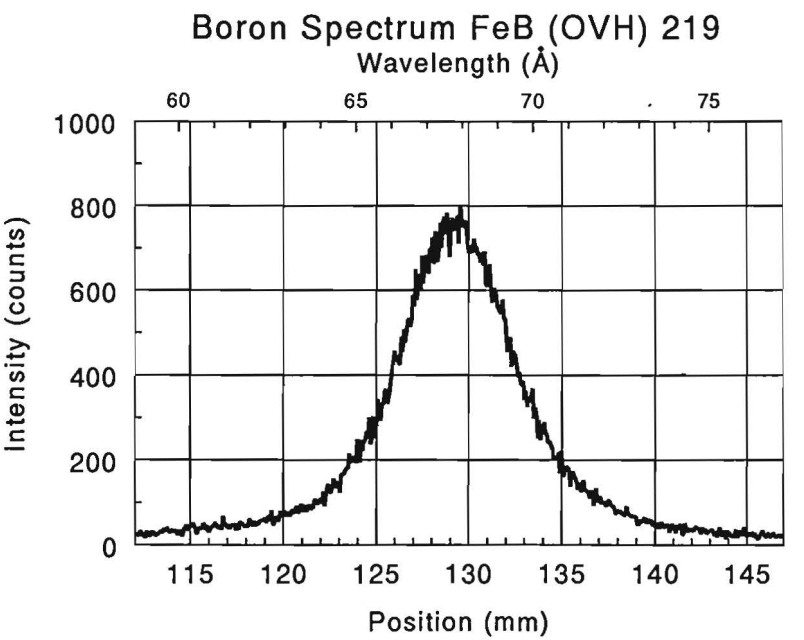

Fig. IV.1.i. B-K_α spectra recorded with STE (top) and OVH (bottom) of Fe_2B and FeB.

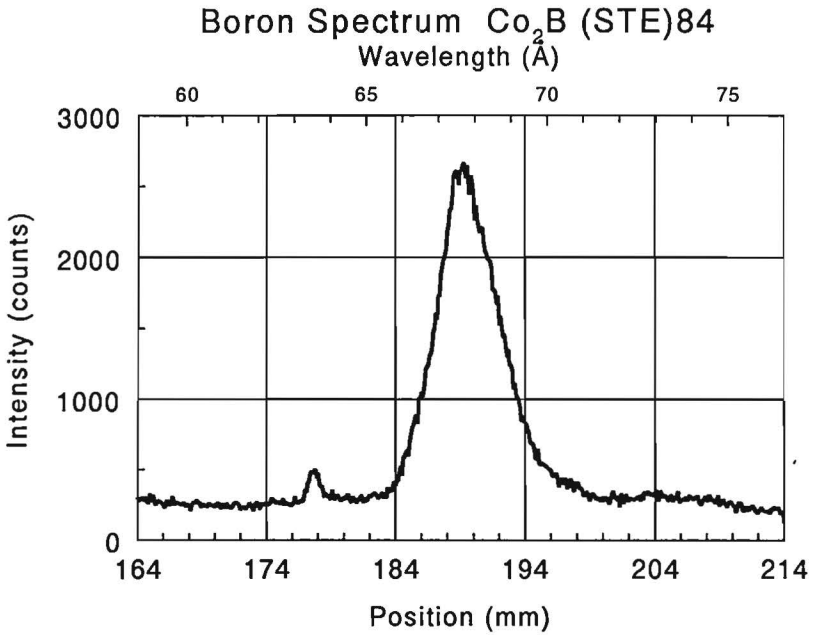

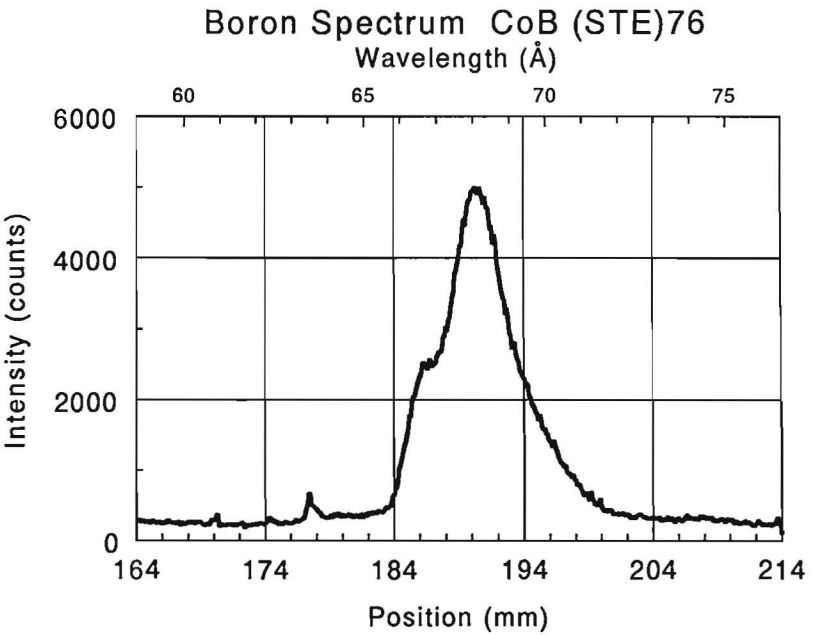

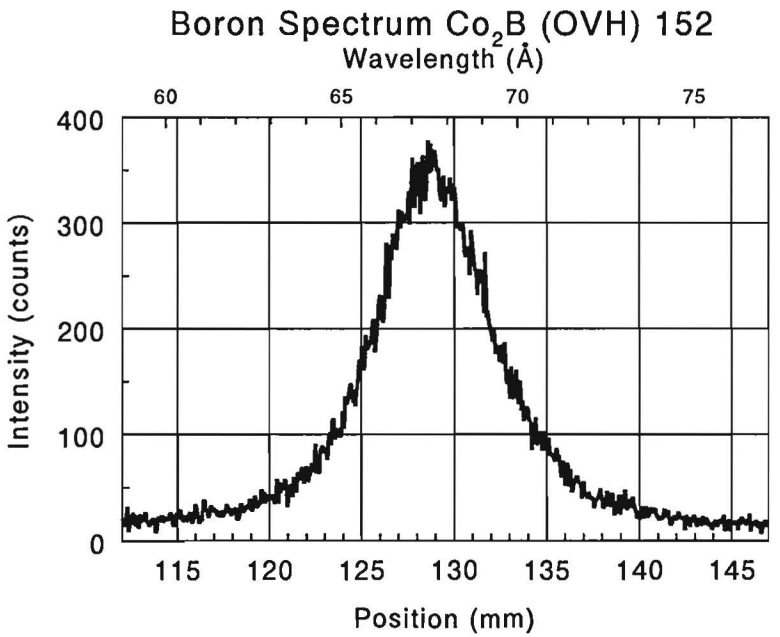

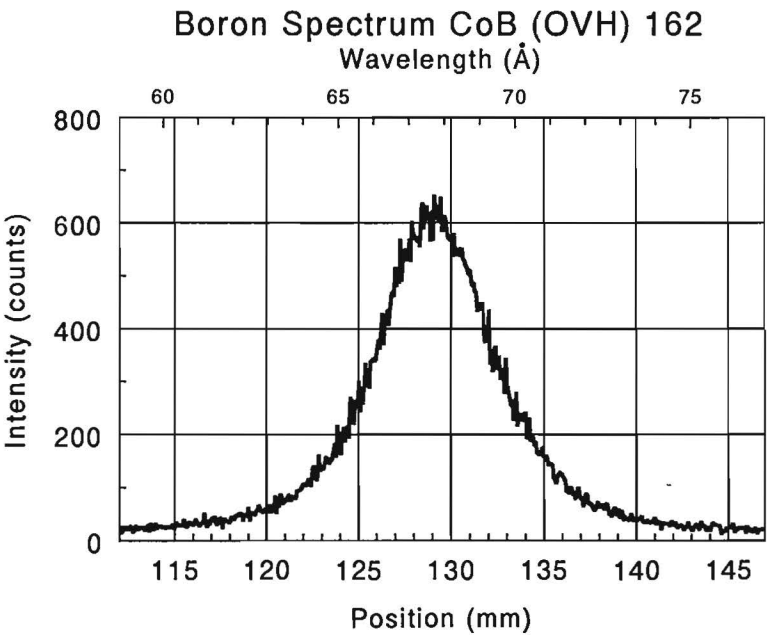

Fig. IV.1.j. B-K_α spectra recorded with STE (top) and OVH (bottom) of Co_2B and CoB.

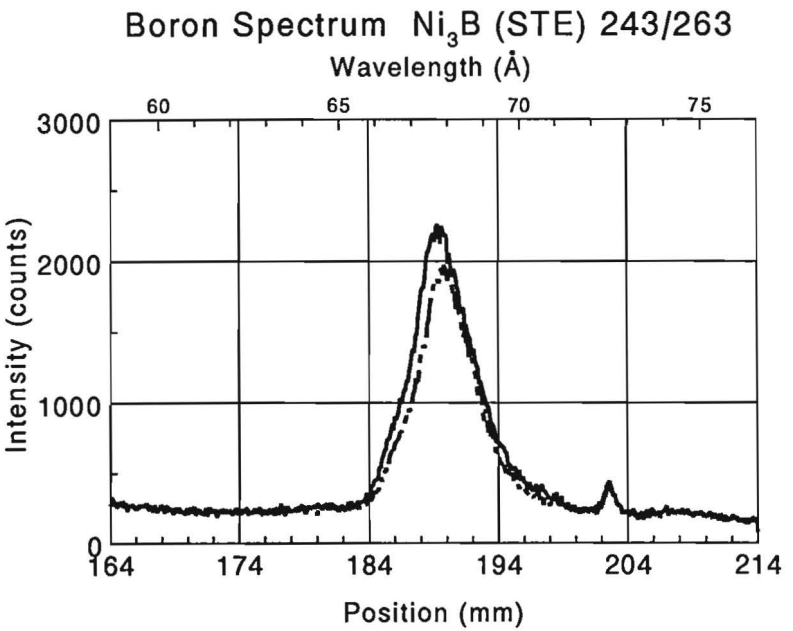

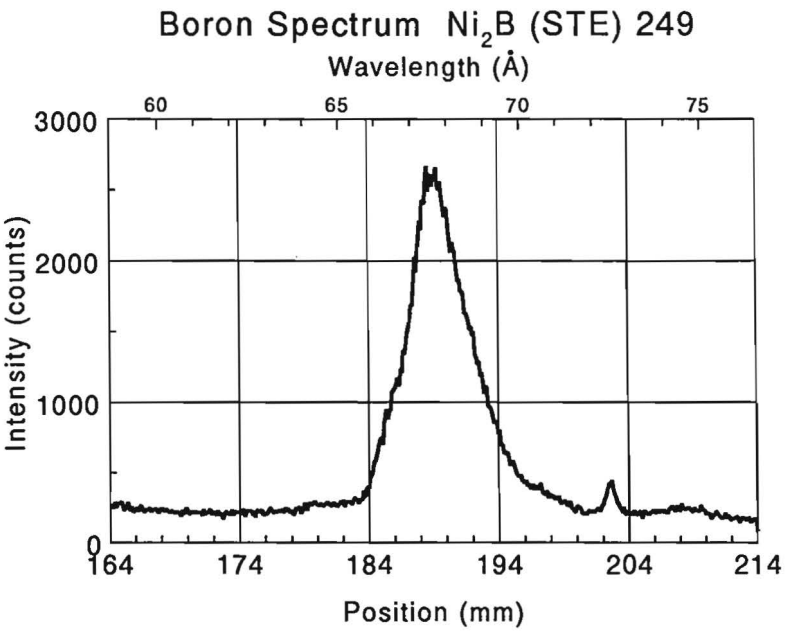

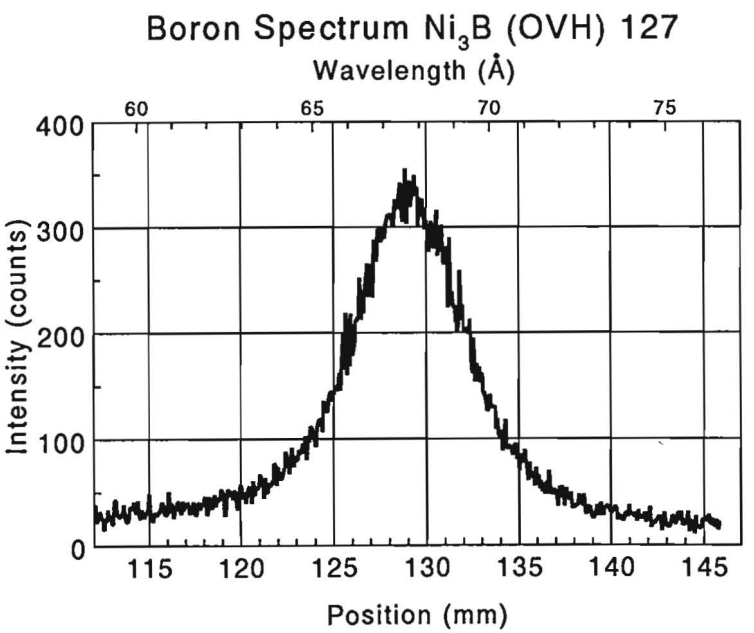

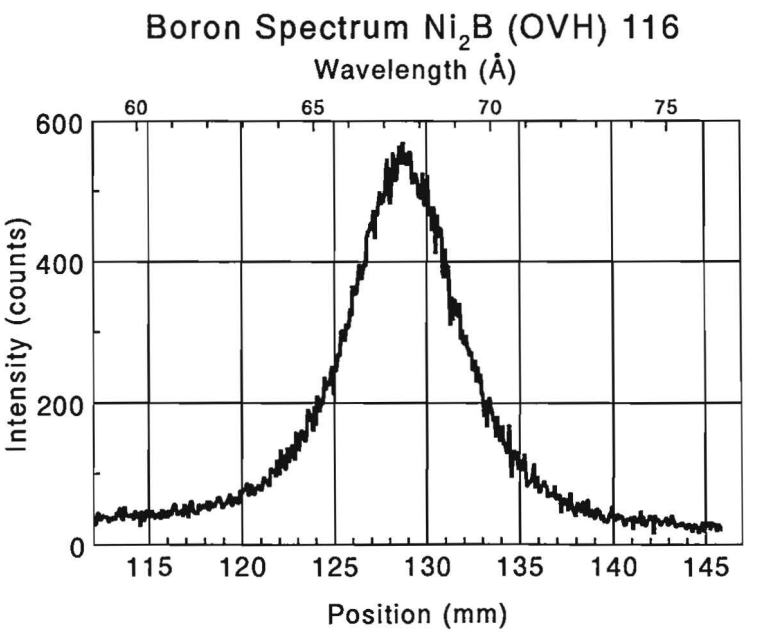

Fig. IV.1.k. B-K_α spectra recorded with STE (top) and OVH (bottom) of Ni_3B and Ni_2B.

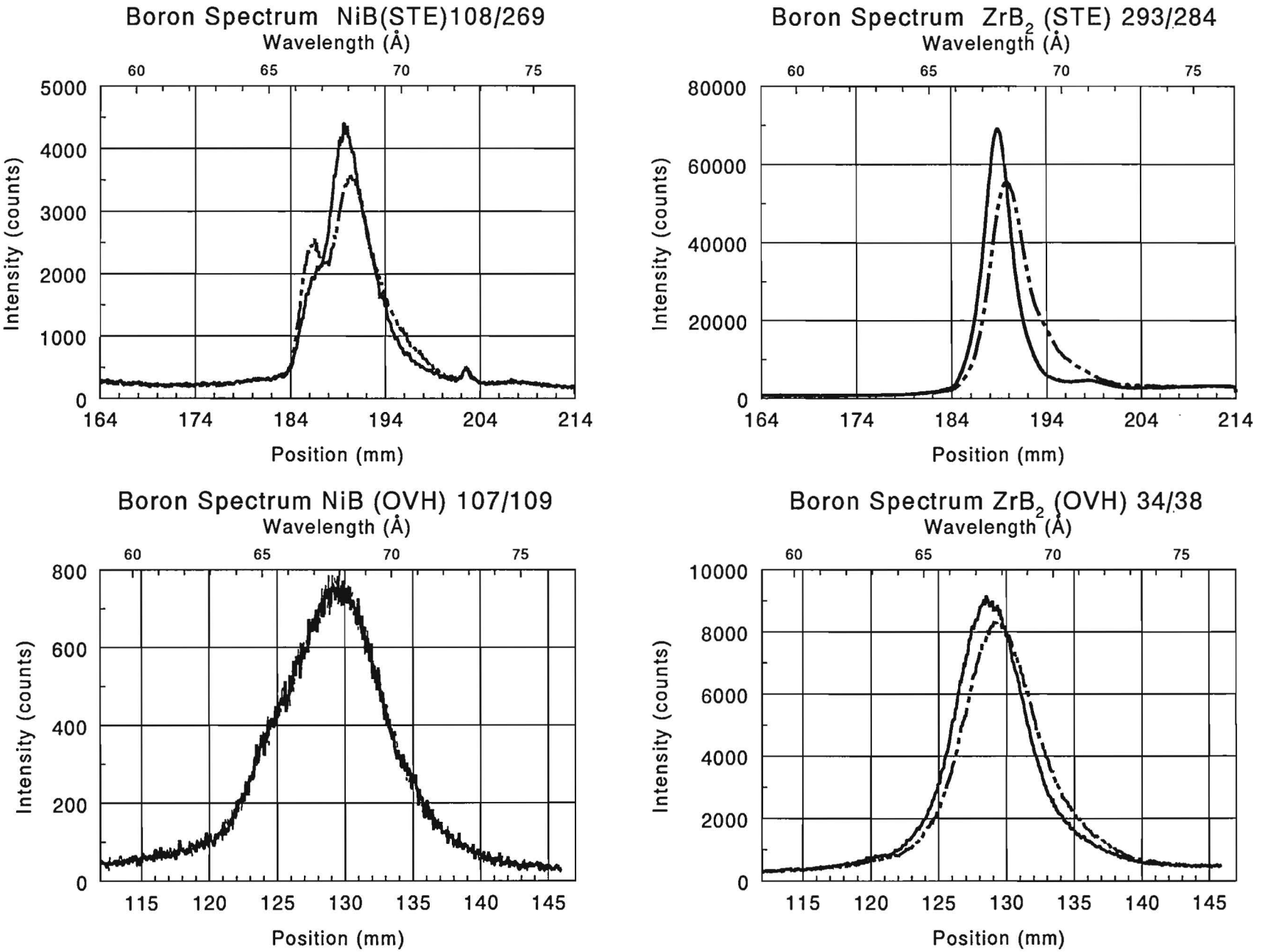

Fig. IV.1.1. B-K_α spectra recorded with STE (top) and OVH (bottom) of NiB and ZrB_2.

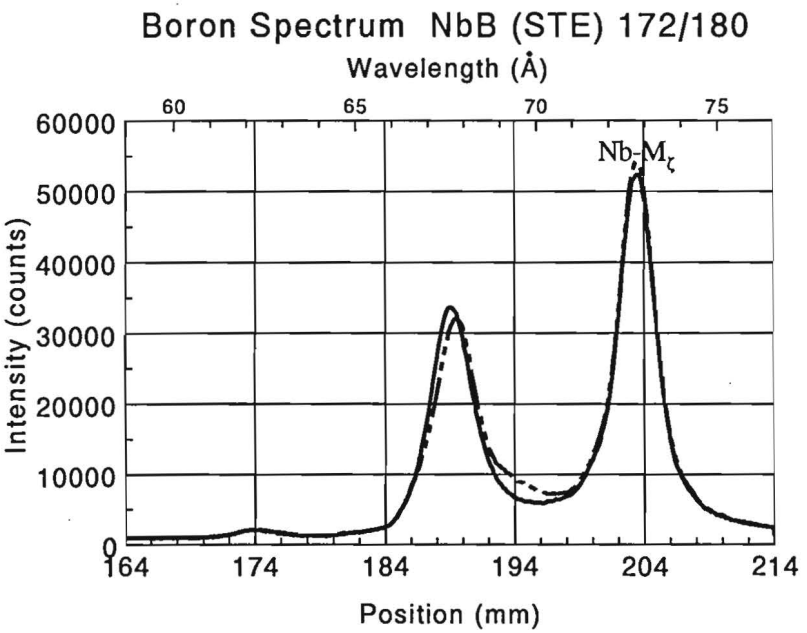

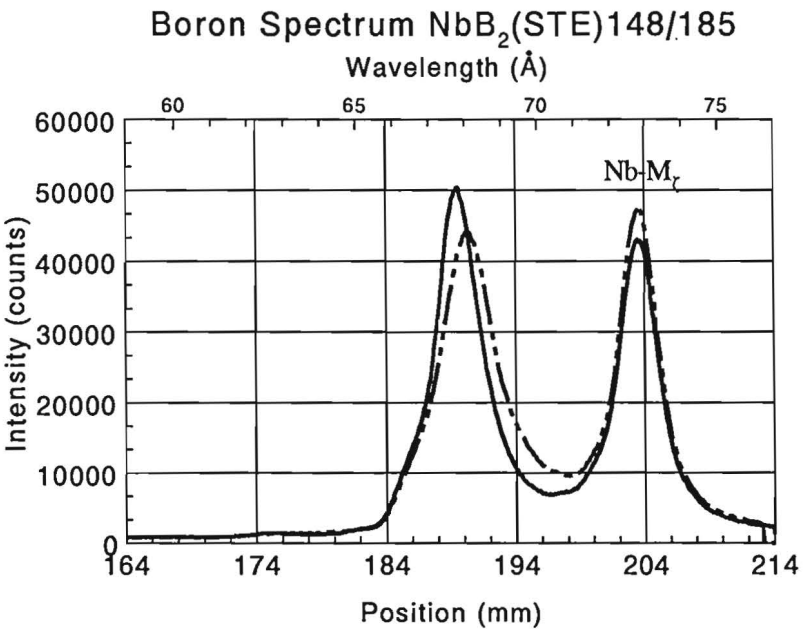

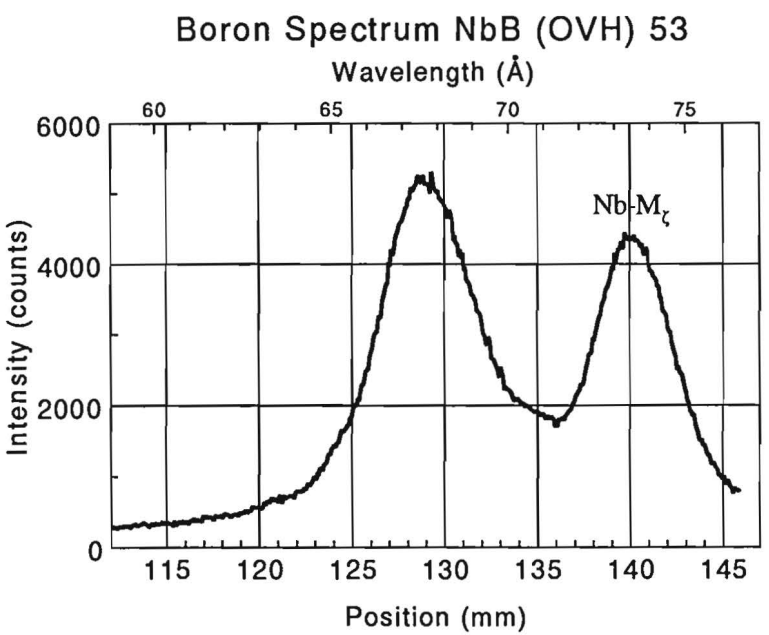

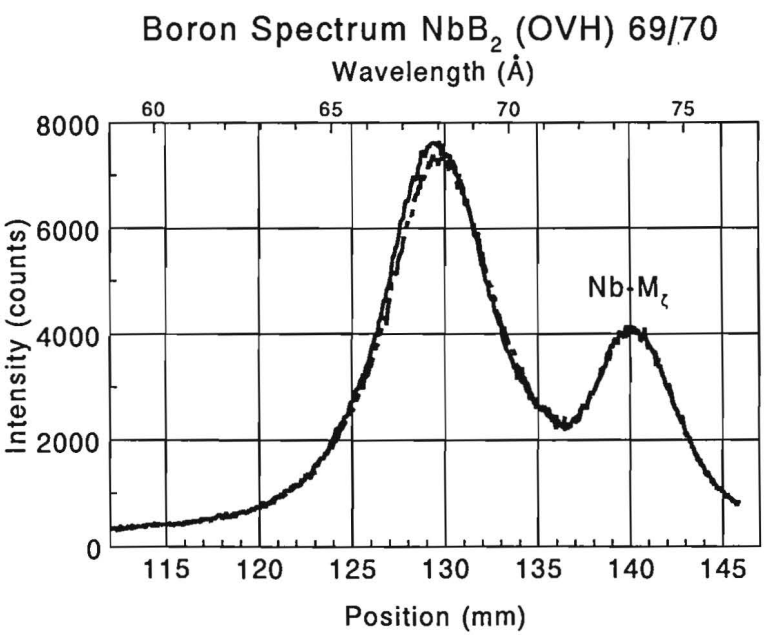

Fig. IV.1.m. B-K_α spectra recorded with STE (top) and OVH (bottom) of NbB and NbB_2.

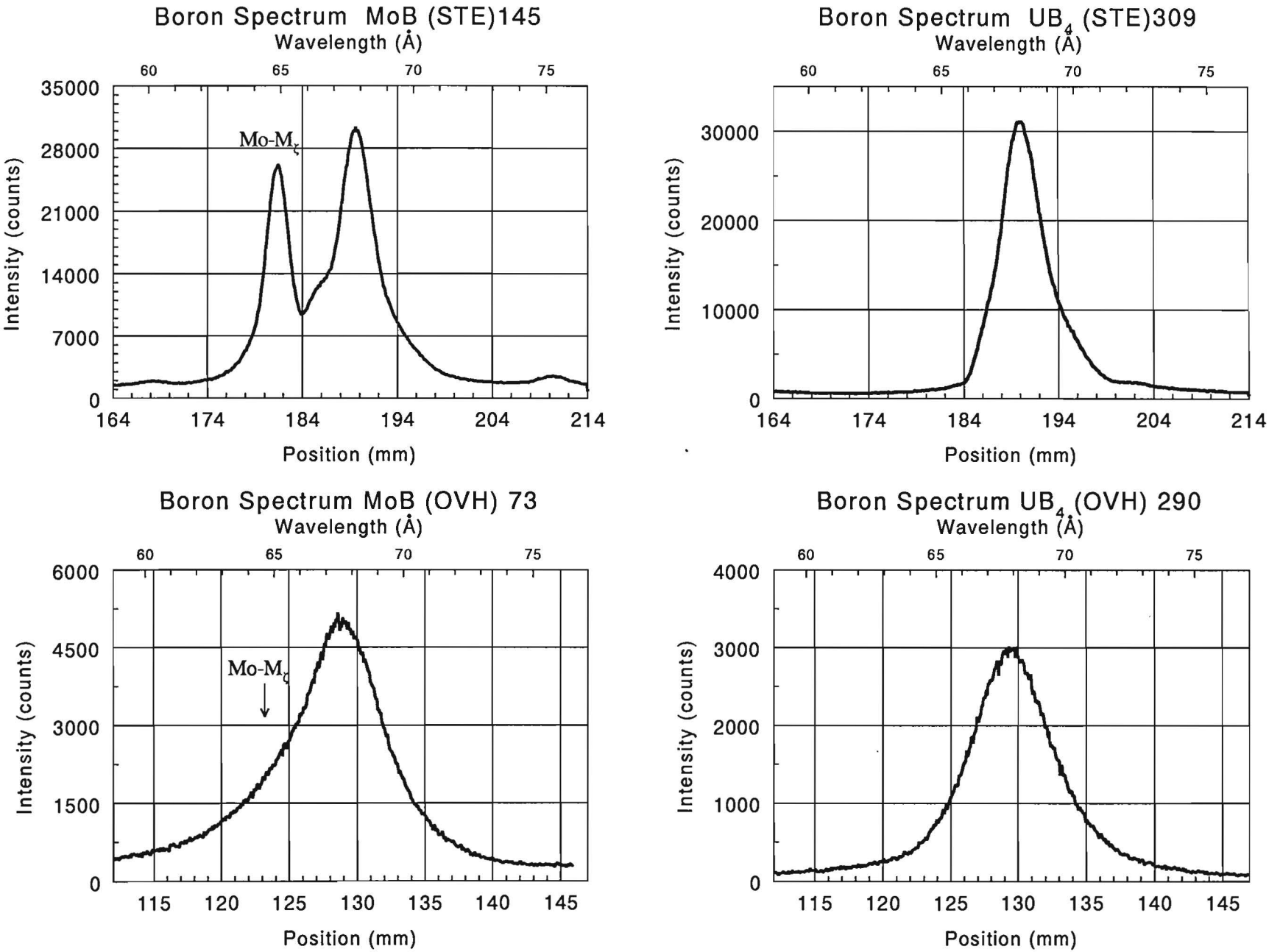

Fig. IV.1.n. B-K_α spectra recorded with STE (top) and OVH (bottom) of MoB and UB_4.

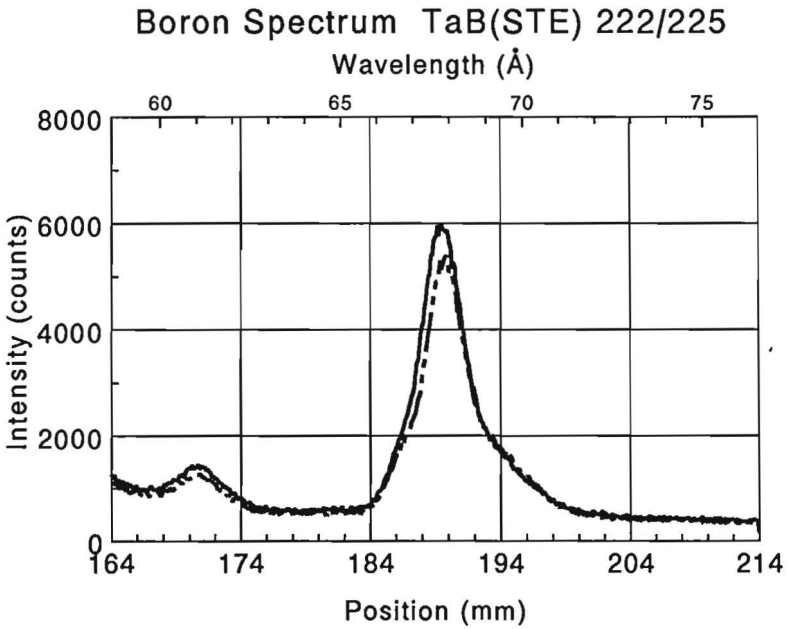

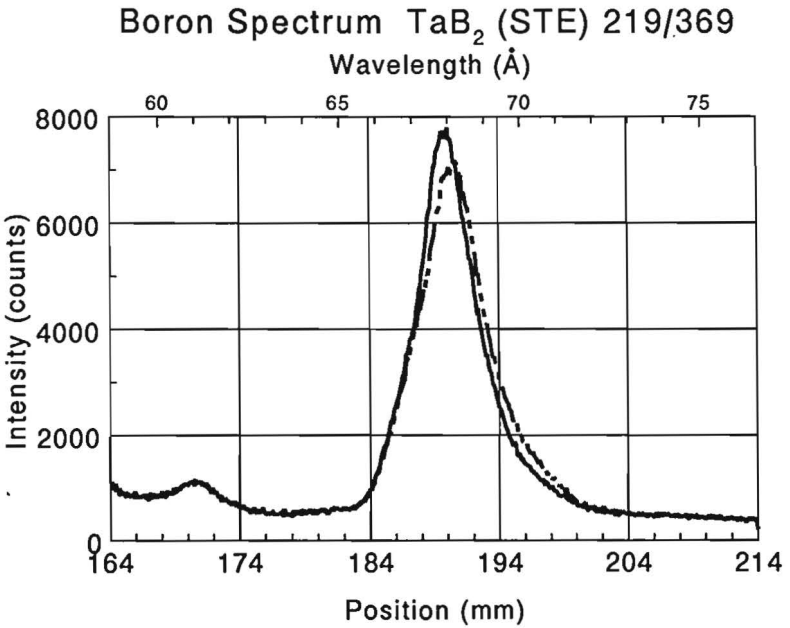

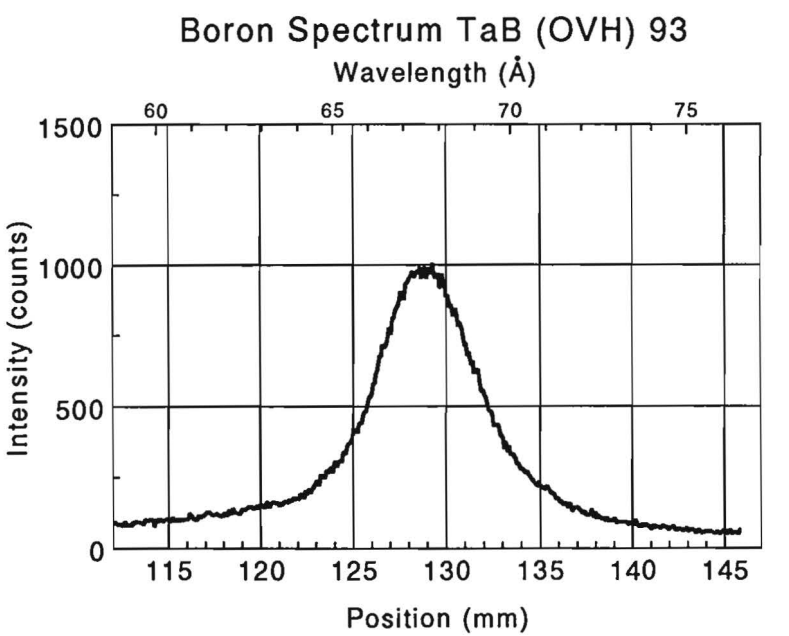

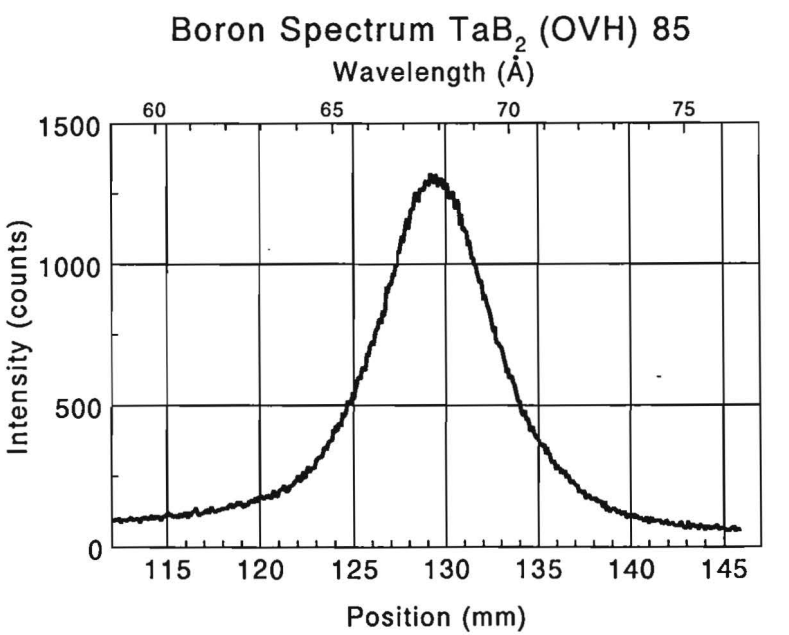

Fig. IV.1.o. B-K_α spectra recorded with STE (top) and OVH (bottom) of TaB and TaB_2.

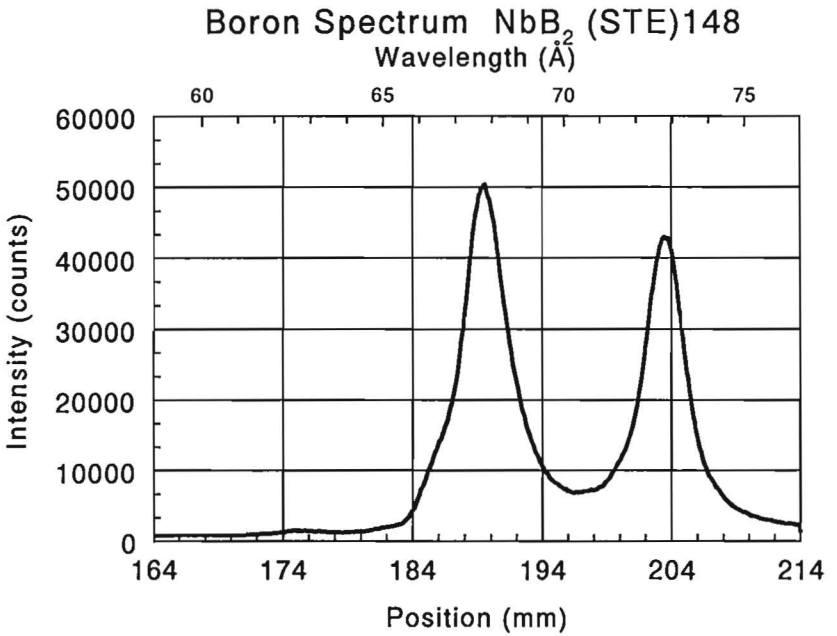

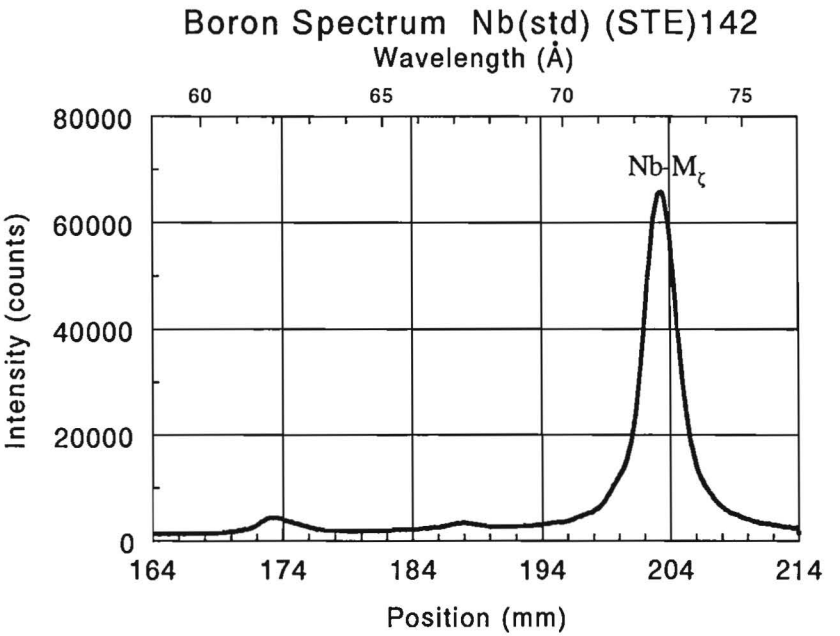

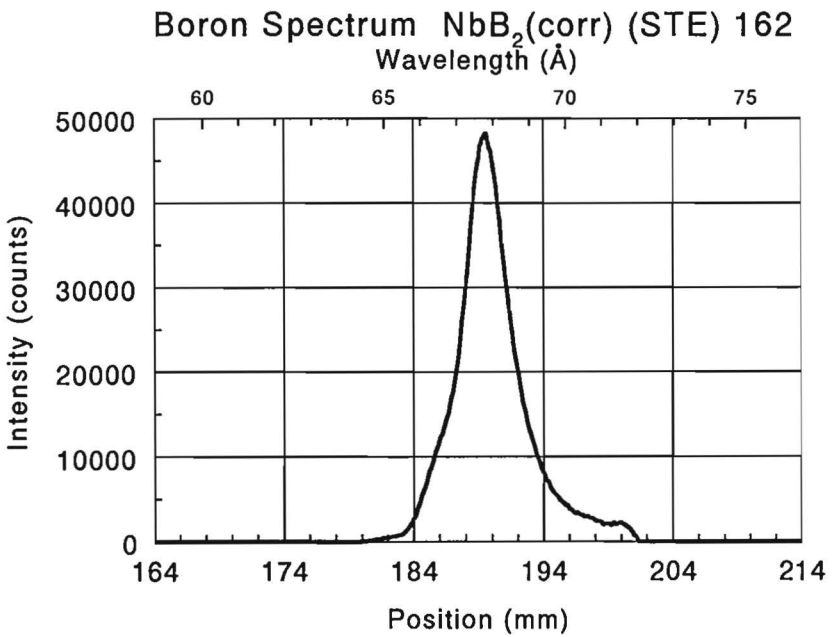

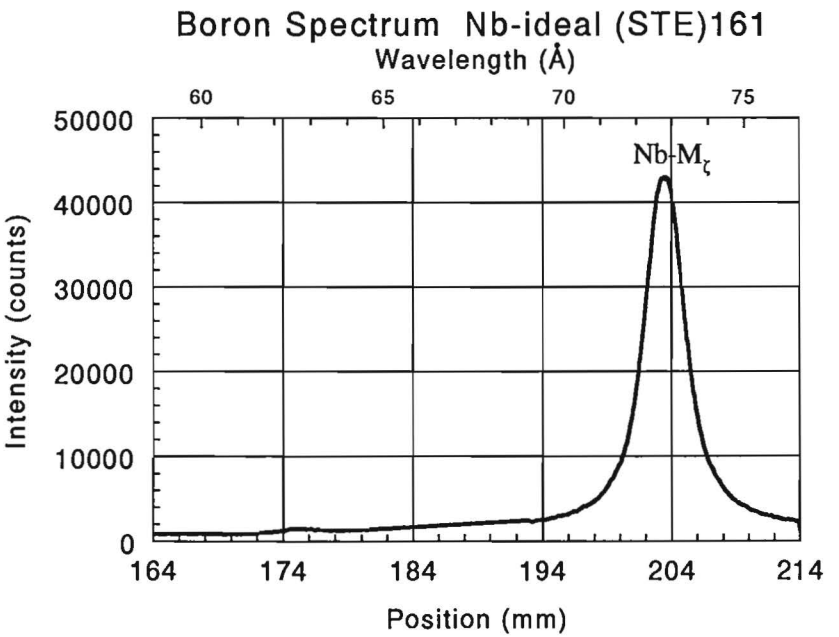

Fig. IV.1.p. Correction procedure for the elimination of the Nb-Mζ line from B-K_α spectra of the Nb-borides (STE crystal).

The borides of Nb and Mo (Fig. IV.1) give rise to a special problem due to the presence of the M-ζ lines of the metals in (unexpectedly) high intensities very close to the B-K_α peak. In the former case the Nb-M-ζ line is at the right hand side of the B-K_α peak; in the latter case at the left hand side. Several procedures have been tried in order to strip the M-ζ lines from the Boron spectra.
Efforts to multiply the spectrum from pure Nb (upper right-hand side) by the calculated k-ratio for the Nb-M-ζ line and to strip this from the NbB_2 spectrum failed, due to small shifts in the peak position of the M-ζ line. As a result areas with negative count rates appeared in the resulting spectrum. The following procedure was more successful : It was observed that the M-ζ peak in the Nb-standard (Fig. IV.1.p, top right) was highly symmetrical and that the right-hand side of the M-ζ peak in the NbB_2 spectrum (upper left-hand corner) is probably not influenced by the B-K_α peak. Symmetrizing the right-hand half of the peak (approx. 203-214 mm) and connecting the new left-hand end through linear interpolation to the background at approx. 180 mm yielded the so-called "idealized" Nb-M-ζ spectrum in NbB_2 (lower right-hand corner). This was finally stripped from the NbB_2 spectrum to yield the corrected NbB_2-spectrum. The result is shown in the lower left-hand corner of Fig.IV.1.p. Apart from a very small artifact at 200 mm the stripped spectrum has a quite reliable appearance, when compared to e.g. WB, UB4, VB_2, or CrB_2, which gives us confidence in the correctness of the procedure.
In MoB the left-hand side of the Mo-M-ζ peak was used for symmetrizing and the right-hand end of the symmetrized M-ζ peak connected to the background at approx. 200 mm.

Considering all the variations in peak positions and certainly those in peak shapes it is clear that intensity measurements made on the peak will have to fail for ultra-light elements. Errors of 20-30% can easily be made. Even if the spectrometer is retuned for each measurement in a certain compound, and if the measurements are performed relative to the same compound as a standard, substantial errors are still likely, due to the variations in peak shapes.
As we have stated before these effects can all be accounted for by using the appropriate APF. The only alternative is to record the full integral emission spectrum for each measurement, which is evidently not a very attractive option for a wavelength-dispersive spectrometer.

IV.2 Area/Peak Factors for B-K_α relative to elemental Boron

It lies at hand to draw a parallel to the case of Carbon[1-3] where we have shown that strong shape alterations but no dependence on crystallographic orientation of the specimen occur. In addition, we have found a strong dependence of APF on the atomic number of the metal partner in the carbide, giving rise to a conspicuous saw-tooth like variation of APF in the periodic system.
In Table IV.1 the APF's for B-K_α are represented numerically, together with the observed peak positions. A single value for the APF indicates that no dependence of peak shape on crystallographic orientation has been observed. The results of the individual Area/Peak measurements graphically displayed for each boride as a function of detected peak position are given in Appendix A where an impression can be obtained on the accuracy and the reproducibility of the measurements. From Table IV.1 it is evident that both substantial narrowing of the Boron-peak with respect to elemental Boron, as well as broadening can occur.

Table IV.1

Area/Peak Factors for B-K_α radiation relative to Boron. The figures in parentheses are the number of measurements on which the data are based (see also Appendix A).
Lead-Stearate Crystal

Boride	APF		Peak. pos. (mm)	Wavelength (Å)
B	1.000	(def.)	189.00	67.60
B_4C	1.014	(27)	189.00	67.60
BN (Hex)	1.198	(9)	191.05-191.60	68.33-68.53
BN (Cub)	1.192	(14)	190.10	67.99
B_6O	1.145	(8)	188.74	67.51
AlB_2	1.152-1.095	(7)	189.50-189.90	67.78-67.92
AlB_{12}	1.008	(9)	189.03	67.61
SiB_3	1.003	(5)	188.85	67.55
SiB_6	0.922	(5)	189.00	67.60
TiB	0.690-0.835	(12)	188.80-189.45	67.53-67.76
TiB_2	0.799-0.945	(12)	189.35-190.25	67.73-68.05
VB_2	0.950-1.045	(9)	189.85-190.70	67.91-68.21
CrB	0.825-1.000	(19)	189.25-190.25	67.69-68.05
CrB_2	0.950-1.090	(10)	189.90-190.90	67.92-68.28
Fe_2B	1.242	(6)	188.90	67.57
FeB	0.985-1.160	(11)	189.55-190.00	67.80-67.96
Co_2B	1.015	(5)	189.10	67.64
CoB	1.186	(5)	190.40	68.10
Ni_3B	1.020-0.935	(7)	189.40-189.85	67.74-67.91
Ni_2B	1.059	(14)	189.10	67.64
NiB	1.060-1.310	(18)	189.80-190.45	67.89-68.12
ZrB_2	0.665-0.915	(13)	188.90-189.90	67.57-67.92
NbB	0.775-0.855	(7)	189.05-189.55	67.62-67.80
NbB_2	0.810-1.025	(9)	189.50-190.55	67.78-68.16
MoB	0.936	(4)	189.70	67.85
LaB_6	0.898	(6)	189.55	67.80
TaB	0.853-0.881	(5)	189.55-189.85	67.80-67.91
TaB_2	0.990-1.120	(8)	189.95-190.60	67.94-68.17
WB	0.978	(5)	189.80	67.89
UB_4	1.028	(6)	189.95	67.94

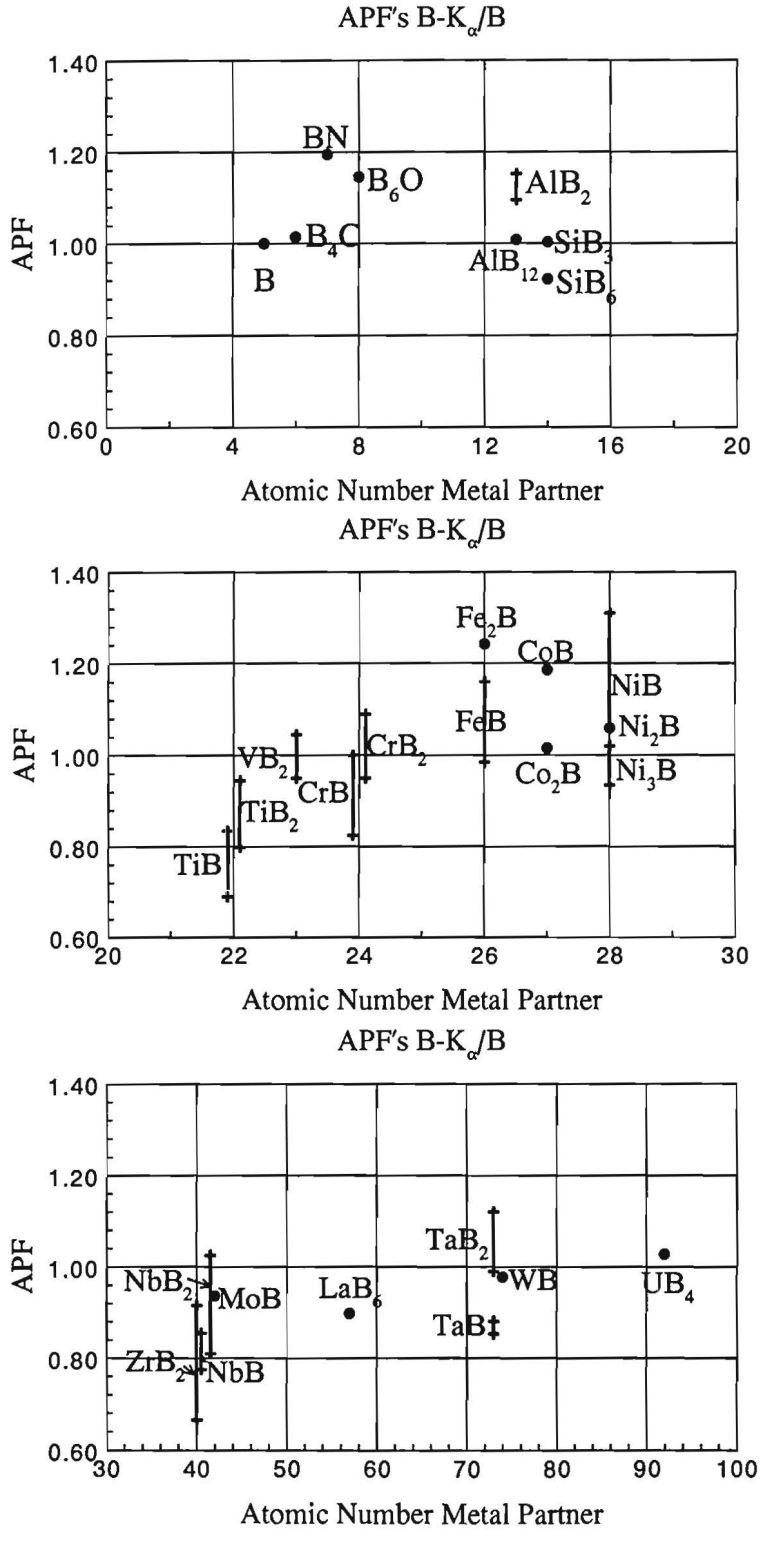

Fig. IV.2. Area/Peak Factor for STE, relative to elemental Boron, as a function of the atomic number of the metal partner for 28 binary borides. Dots indicate fixed APF values; bars indicate the variation that can be observed in dependence of the crystallographic orientation of the specimen.

This is reflected in the variation of the APF which can assume values as low as 0.665 in ZrB_2 or as high as 1.31 in NiB.

A very peculiar observation was made on hexagonal BN (Carbon coated). This specimen was a hollow cylinder of CVD-deposited BN, cut and polished in a plane perpendicular to the cylindrical axis. The APF measurements were performed in a sequential way, covering approx. ¾ of the circumference. The position of the B-K_α peak was thereby found to behave in a most peculiar way: At the starting position it was found to have a minimum value (191.05 mm), 90 deg. further the maximum value (191.60 mm) was found; almost the minimum value (191.20 mm) was found again in a position opposite to the starting point etc. Strange enough no peak shape alterations could be detected from one location to another.

As only a very weak texture was found and the grain size was extremely fine, as established from X-ray diffraction photographs, an influence of crystallographic orientation can probably be ruled out. Perhaps some process of electrical charging of the specimen, causing a shift away from the Rowland circle, may account for these phenomena.

An equally peculiar observation was made on cubic BN, which is sufficiently conductive for EPMA. Here, we measured the same APF-value of 1.19-1.20 as on hexagonal BN. However, at a much lower linear position (190.10 mm as compared to 191-191.60 mm), or shorter wavelength (67.99 as compared to 68.33-68.53 for hexagonal BN).

All these effects, strange as they may be, have to be kept in mind during the analysis of Boron, because on each **new location** a **new peak search** should be conducted; if not, catastrophic errors can be made.

When the APF's in Table IV.1 are plotted as a function of atomic number of the metal partner (Fig. IV.2) then the parallel to the carbides becomes obvious. In spite of the sometime large variation in APF within the same specimen a similar saw-tooth-like variation as found in the carbides is visible. Again, strong boride-formers like Ti and Zr, which have highly stable borides with very high melting points, hold the minimum APF values whereas the reverse applies to elements such as Fe, Co and Ni. Again, discontinuities appear at the beginning of new periods in the periodic system. Besides, as it was the case for the carbides, the magnitude of the variation of APF with atomic number is decreasing with increasing atomic number, resulting in APF's close to unity for very heavy metals such as W and U.

It is interesting to note further that in the sequence TiB, CrB, FeB, NiB both the minimum as well as the maximum APF show an almost linear variation with atomic number, with CoB being an exception.

From a chemical point of view the variations in APF in Fig.IV.2 and the parallel that can be drawn with the carbides gives a strong feeling of consistency which, in turn, gives confidence in the obtained results. Most probably the B-K_α emission spectra contain a lot of valuable information on the chemical bond and, in conjunction with XPS and related techniques, it is perhaps possible to gain more insight into the Density of States. This is, however, beyond the scope of the present work, which is on quantitative analysis.

A matter which is highly relevant to the latter issue is the question whether the X-ray fluorescence yield can be considered as a constant throughout all borides. It is a well-known fact that the X-ray fluorescence yield is only of the order of 1% for ultra-light elements. The competitive Auger-effect takes 99%: i.e. 99 out of every 100 K-shell ionizations result in the emission of an Auger-electron. Only 1% is left for X-ray production. Even very small variations

(of the order of 0.1%) in the Auger yield would produce relatively large (of the order of 10%) variations in the X-ray fluorescence yield. To our knowledge this problem has never been discussed in papers on microprobe analysis. It is clear, however, that if such fluctuations would occur in the Auger yield they would cause inconsistencies in the results calculated by any matrix correction program; simply because none of the programs takes such effects into account.

A last point of concern is the question whether peak shape alterations, due to the polarization phenomena, can be avoided. One possibility is, of course, the use of a grating[13,14] instead of a diffracting crystal because gratings do not filter polarized components. We did not have such a grating at our disposal, unfortunately. Another possibility is to use a crystal with a much larger 2 d-spacing, in order to shift the B-K_α peak to much smaller Bragg-angles, away from the present dangerous position with an X-ray incidence angle of almost 45 deg.
This is possible, nowadays, with the use of Layered Synthetic Microstructure analyzer crystals (sequences of heavy element ,e.g., W and ultra-light element, e.g., C layers), which can be tailored to exhibit a variety of 2 d-spacings. At the moment such a crystal (W-Si layers) is available in our new 4th spectrometer; however, this particular crystal is optimized for Nitrogen, Oxygen and Fluorine. In our original report we indicated already that efforts were being undertaken to acquire a crystal with a 2 d-spacing suitable for the detection of Boron (at the desired new position) and Beryllium. In the meantime we actually purchased two of such crystals (designated OVH), both of the type Mo/B_4C; the first with 2 d =144.8 Å, the second with 2 d=147 Å. Since the angle of incidence of the B-K_α x-rays on these crystals is now ~27 degrees instead of 42.5 (for the STE crystal), it was very interesting to repeat some of the APF-measurements on a number of our borides and also to investigate the orientation-dependency of the shape of the B-K_α emission profile. Table IV 2 shows some preliminary results of the APF-measurements.

Table IV.2

Area/Peak Factors for B-K_α radiation relative to elemental Boron. Comparison between Pb-Stearate (STE) and OVH (Mo/B_4C) crystal

Boride	STE	OVH
B_4C	1.014	1.061
AlB_2	1.152-1.095	1.054
TiB	0.690-0.835	0.855-0.915
TiB_2	0.799-0.945	0.922-0.965
Fe_2B	1.242	1.085
ZrB_2	0.665-0.915	0.904-0.948
LaB_6	0.898	0.951

These results show that the OVH crystal is indeed less sensitive to shape alterations than the STE crystal, because :

1) The ranges in APF are smaller.
2) The numerical APF values are (usually) closer to unity.

Still, for quantitative EPMA of Boron the effects of peak shape alterations have to be taken into account, also with the OVH crystal.

In order to gain more insight into the peculiar relationship between crystallographic orientation of the specimen and the shape of the B-K_α peak we did some interesting experiments with needle-shaped crystals of TiB in which the needle axis most likely represents a major crystallographic direction. The emission spectra were recorded once with the needle axis pointing in the direction of the spectrometer and once in a direction perpendicular to it, for both the STE as well as the OVH crystal, simultaneously on the same TiB needle. The results (Fig. IV.3) indicate that the shape alterations on both crystals, apart from their magnitude, are quite similar. In both cases the highest peak intensity, in combination with the narrowest peak at the shortest wavelength, is obtained when the TiB needle axis points in the direction of the spectrometer, whereas the reverse applies in a direction perpendicular to it.

The performance of the OVH crystal has been compared (Fig. IV.1) to that of the STE on a number of our binary boride specimens, with the following global conclusions :

1) OVH gives a **hughe increase in peak count rates** (30-50 times higher).
2) OVH is **less sensitive** to **peak shape alterations** and crystallographic orientation. This must (partly) be attributed to a **poorer spectral resolution** of the OVH crystal. This is particularly evident in MoB where the Mo-Mζ peak can no longer be resolved from the B-K_α peak. Furthermore, it is noticeable from the B-K_α spectra in BN, where the two additional contributions can no longer be resolved.
3) There is evidence that **OVH suppresses higher-order reflections** in the wavelength range of B-K_α The latter observation can contribute considerably in obtaining "cleaner" backgrounds.

Further advantages of synthetic multilayer crystals are that :

1) They are sturdy, mechanically stable, and, presumably, have a very long life.
2) The 2 d-spacing can be tailored to meet specific demands.

The disadvantage may be that one needs more than one crystal to do the best possible job on each of the ultra-light elements.

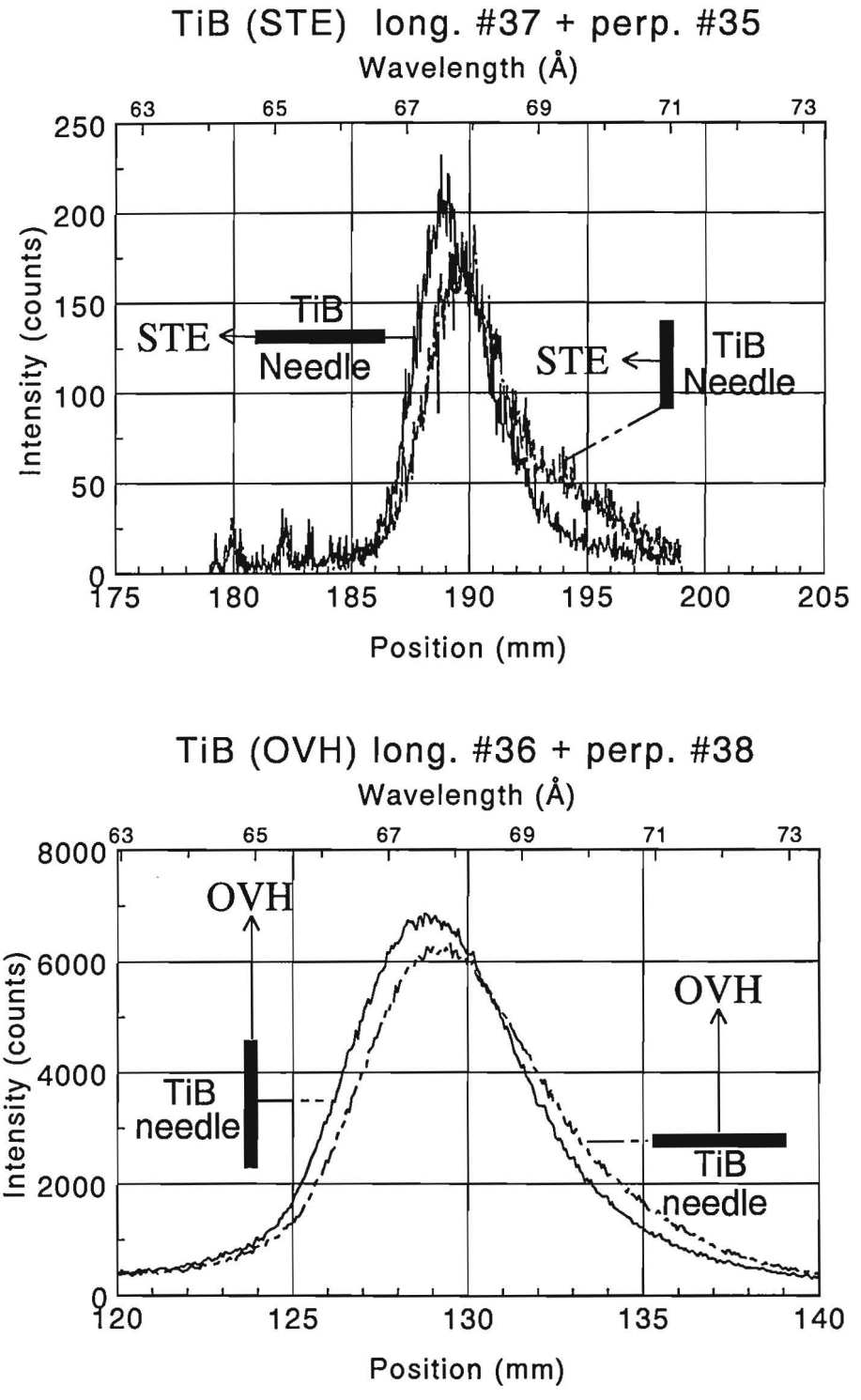

Fig. IV.3. Peak shape alterations in dependence on the crystallographic orientation of a needle-shaped TiB crystal, simultaneously recorded on STE (top) and OVH (bottom). In both cases the spectra have been recorded, once with the TiB needle pointing in the direction of the spectrometer and once in a direction perpendicular to it. The highest peak intensity (at the shortest wavelength) is always found when the needle points in the direction of the spectrometer. Accelerating voltage 10 kV, beam current 100 nA, counting time 1 sec./channel. Also note the huge difference in count rate between the STE and OVH crystals.

IV.3 Intensity ratios for metals and boron

The peak k-ratios for the metal lines have been measured in the range from 4 up to 30 kV: at 4, 6, 8, 10, 12, 15, 20, 25 and 30 kV. All the X-ray lines that could be excited have been measured. This has been done with the purpose of supplying additional evidence to the Boron measurements. Such data can always be used, not only to test correction programs, but also to test consistencies of calculated results and to perform cross-checks, especially where more than one boride in a binary system is available.

The procedure for the Boron-measurements has been described before (III.5). In eight cases the measurements have been performed over the full range 4-30 kV; in the remaining 20 cases this range has been restricted: 4-15 kV. The absolute intensities and all relevant numerical data on the measurements are given in Appendix B.

The measured integral k-ratios for B-K_α are presented in Fig. IV.4, together with the predictions of our latest correction program "PROZA96", using the mac's (Table II.1) indicated.

An inspection of the results immediately reveals two facts:

- In the first place it is apparent that the variation of k-ratio for Boron with accelerating voltage is basically the same in all borides: After an initial, more or less rapid, decrease we see a kind of saturation (usually at 10-15 kV), followed by a slow increase again. This is, of course, closely connected to the way the relative emitted intensities in Boron standard and boride specimens behave a function of accelerating voltage. This, in turn, is an immediate result of the fact that the B-K_α intensity emitted from pure Boron decreases much more rapidly beyond a specific accelerating voltage than that emitted from borides containing heavier elements, as a result of the much higher surface ionization in the latter comounds.
- In the second place it must be concluded that accurate and highly consistent intensity measurements are indeed possible for an extremely light element like Boron. Needless to say that this is a prerequisite for an accurate determination of Boron; without accurate sets of measurements it is no use bothering about matrix correction procedures which will be the subject of the next chapter.

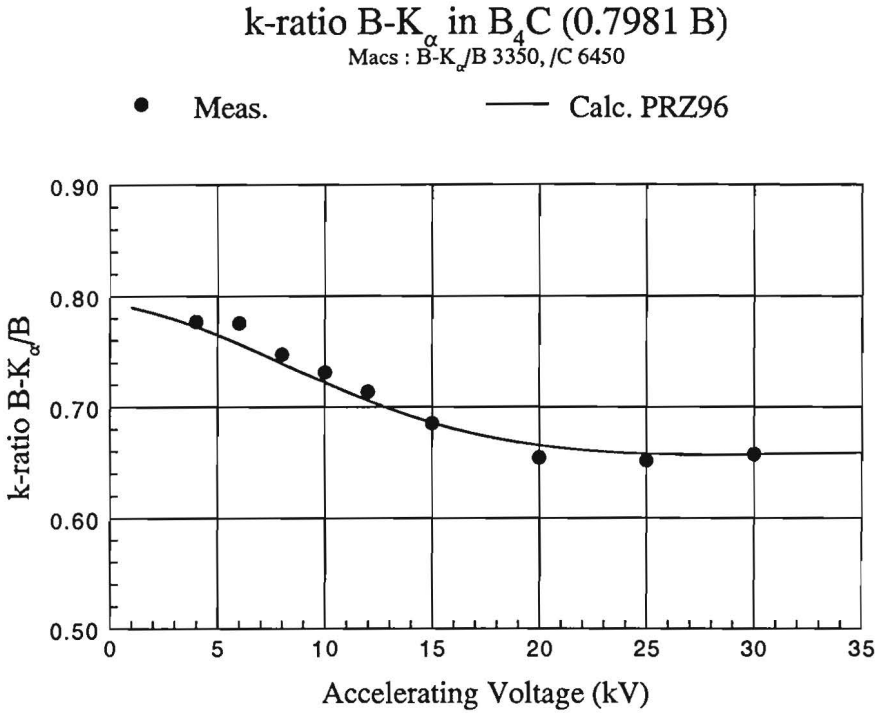

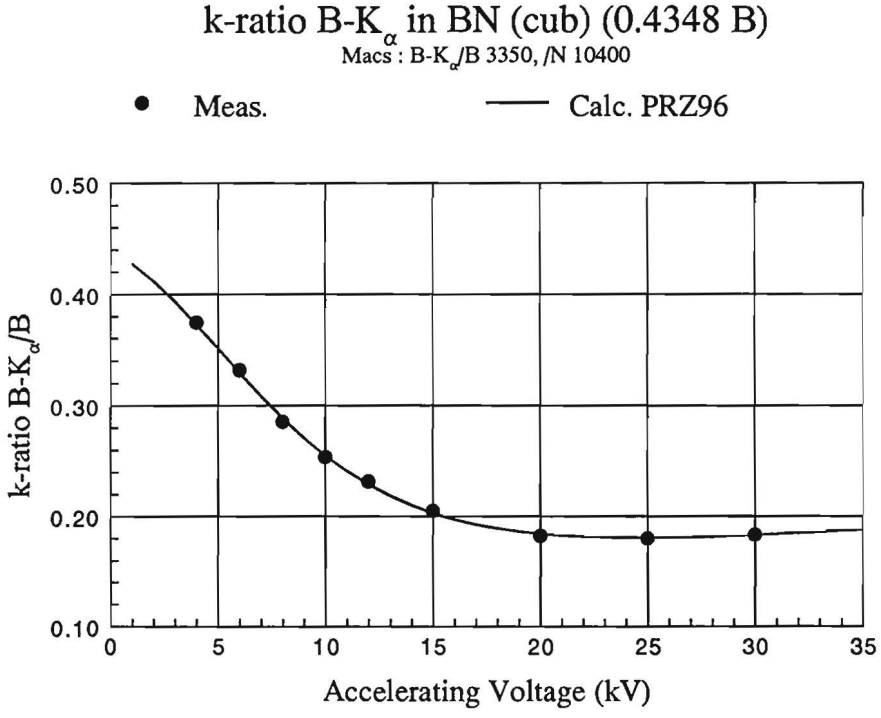

Fig. IV.4.a. Intensity ratios for Boron-K_α (integral) as a function of accelerating voltage for B_4C (top) and cubic BN (bottom). Dots represent our measurements and the curve the predictions of our PROZA96 correction program, using the mac's indicated.

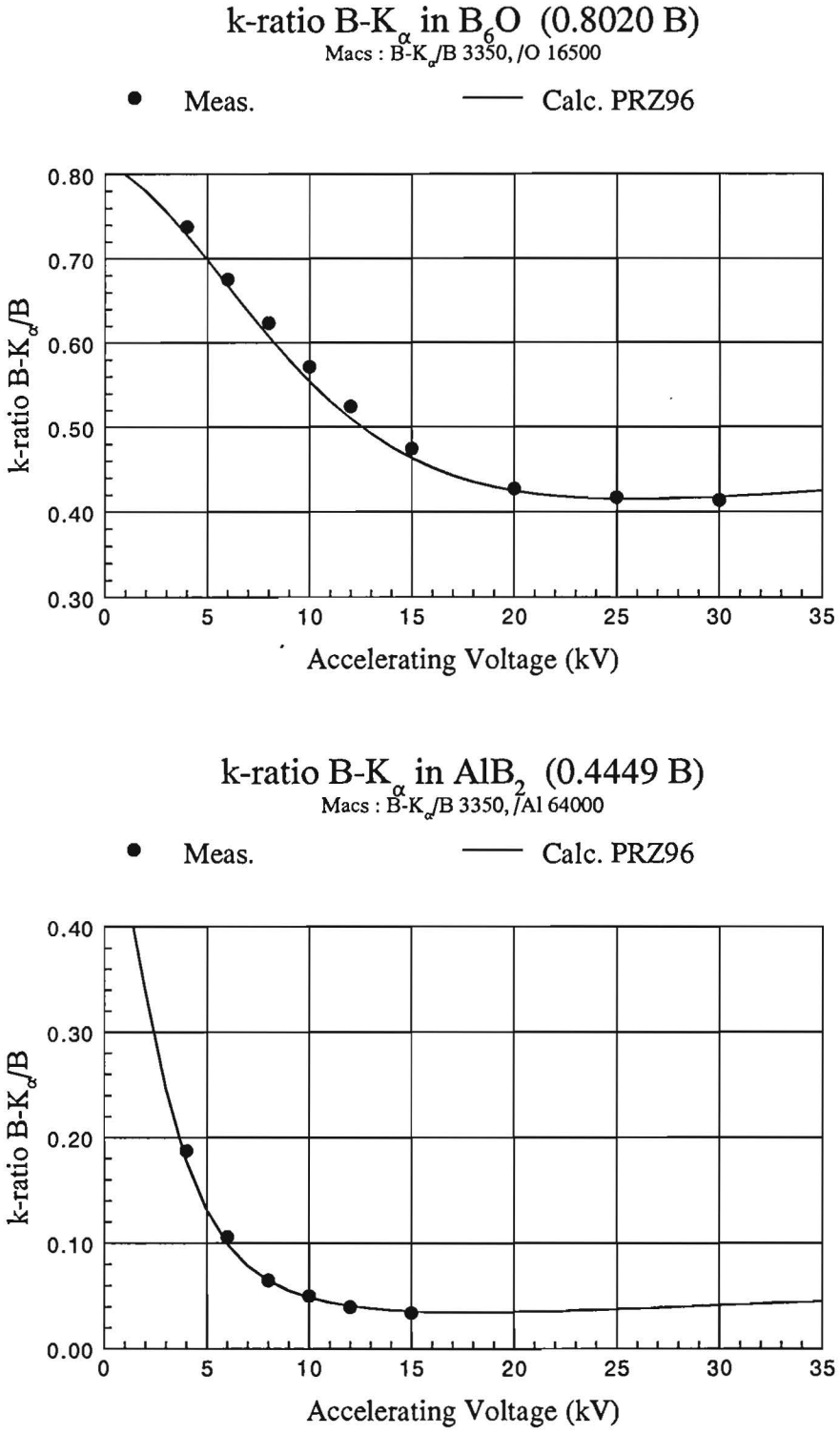

Fig. IV.4.b. Intensity ratios for Boron-K_α (integral) as a function of accelerating voltage for B_6O (top) and AlB_2 (bottom). Dots represent our measurements and the curve the predictions of our PROZA96 correction program, using the mac's indicated.

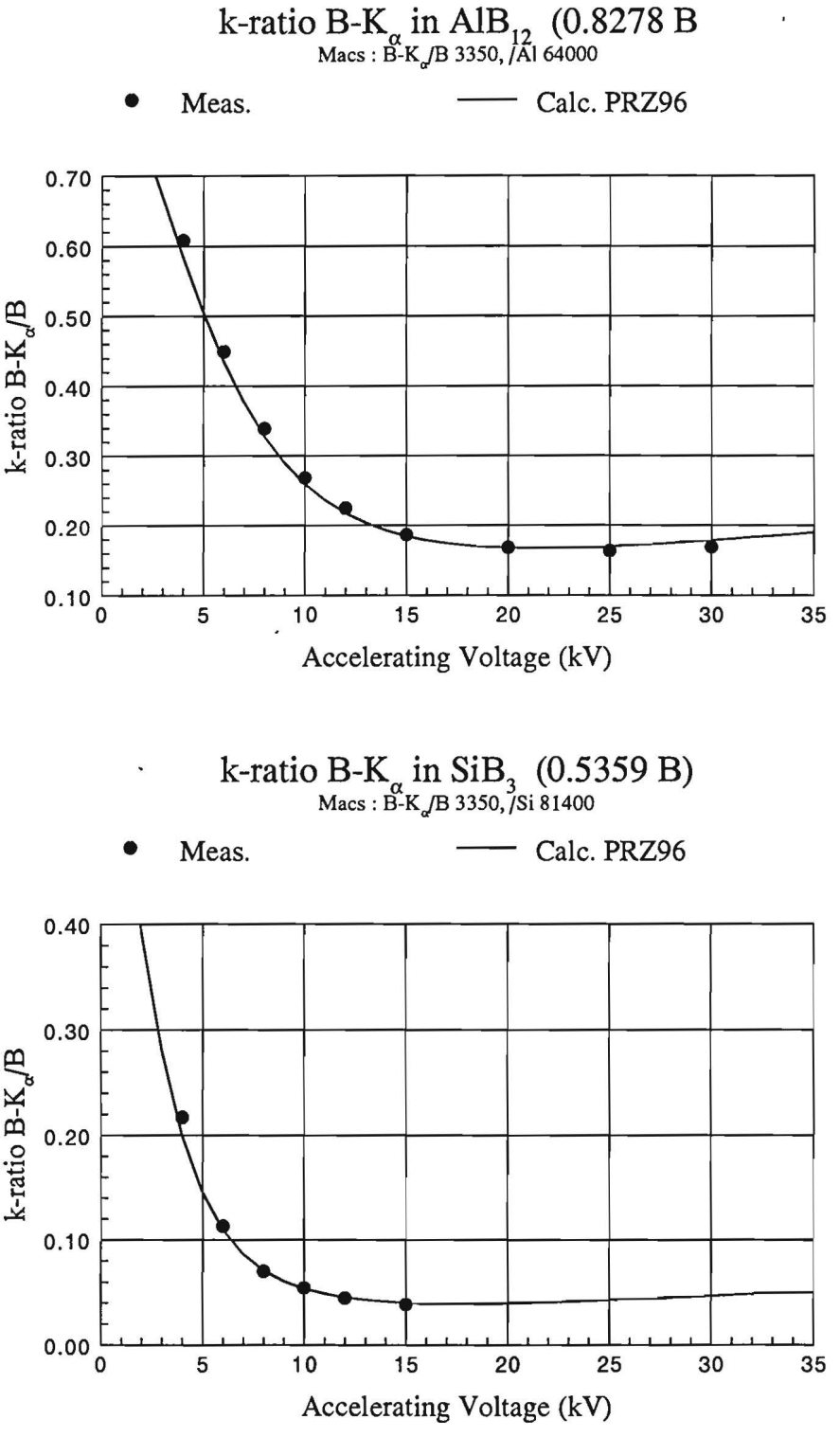

Fig. IV.4.c. Intensity ratios for Boron-K_α (integral) as a function of accelerating voltage for AlB_{12} (top) and SiB_3 (bottom). Dots represent our measurements and the curve the predictions of our PROZA96 correction program, using the mac's indicated.

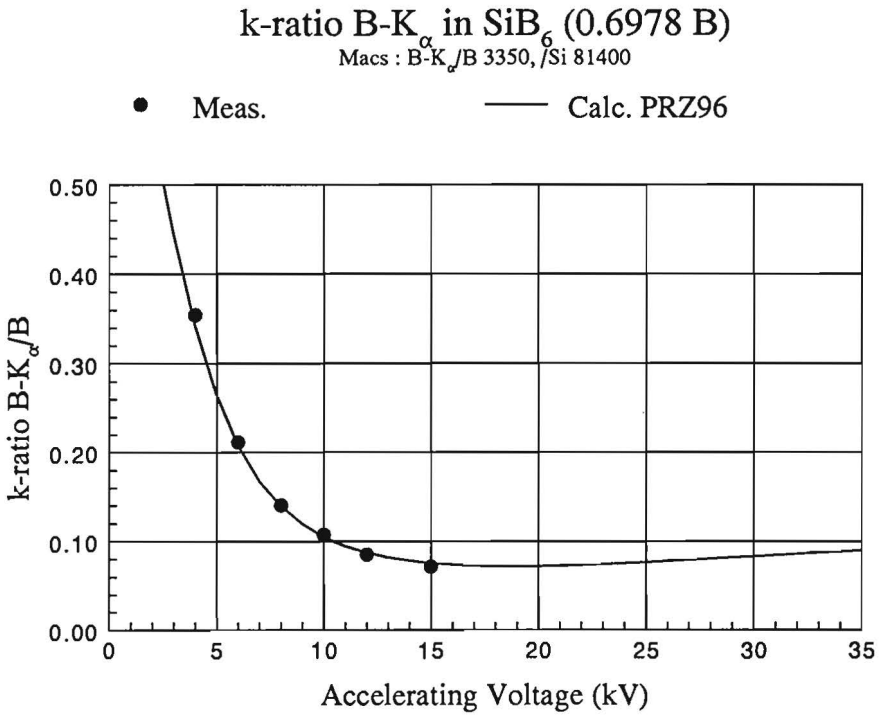

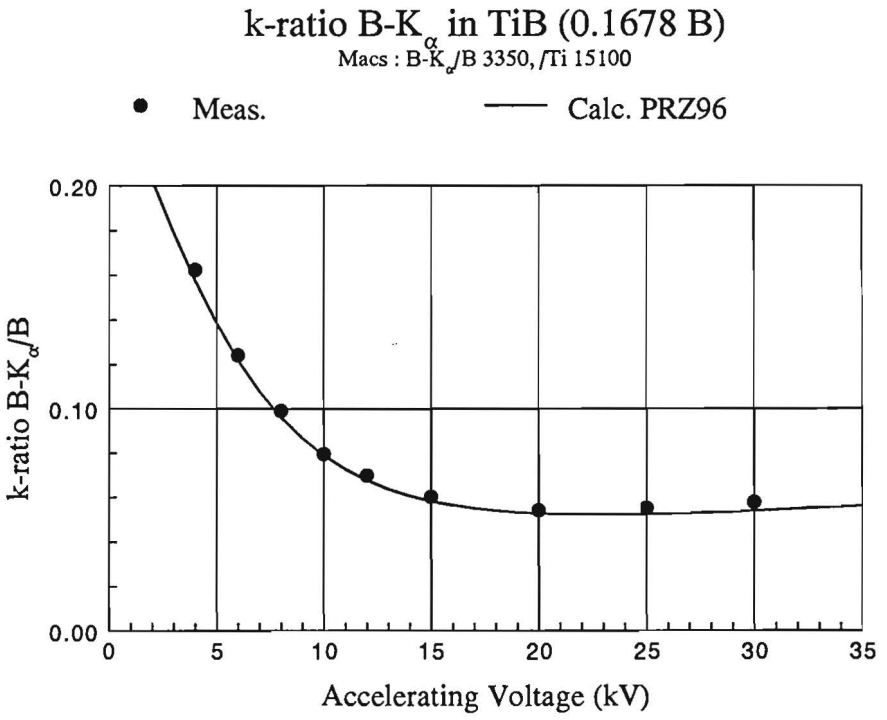

Fig. IV.4.d. Intensity ratios for Boron-K_α (integral) as a function of accelerating voltage for SiB_6 (top) and TiB (bottom). Dots represent our measurements and the curve the predictions of our PROZA96 correction program, using the mac's indicated.

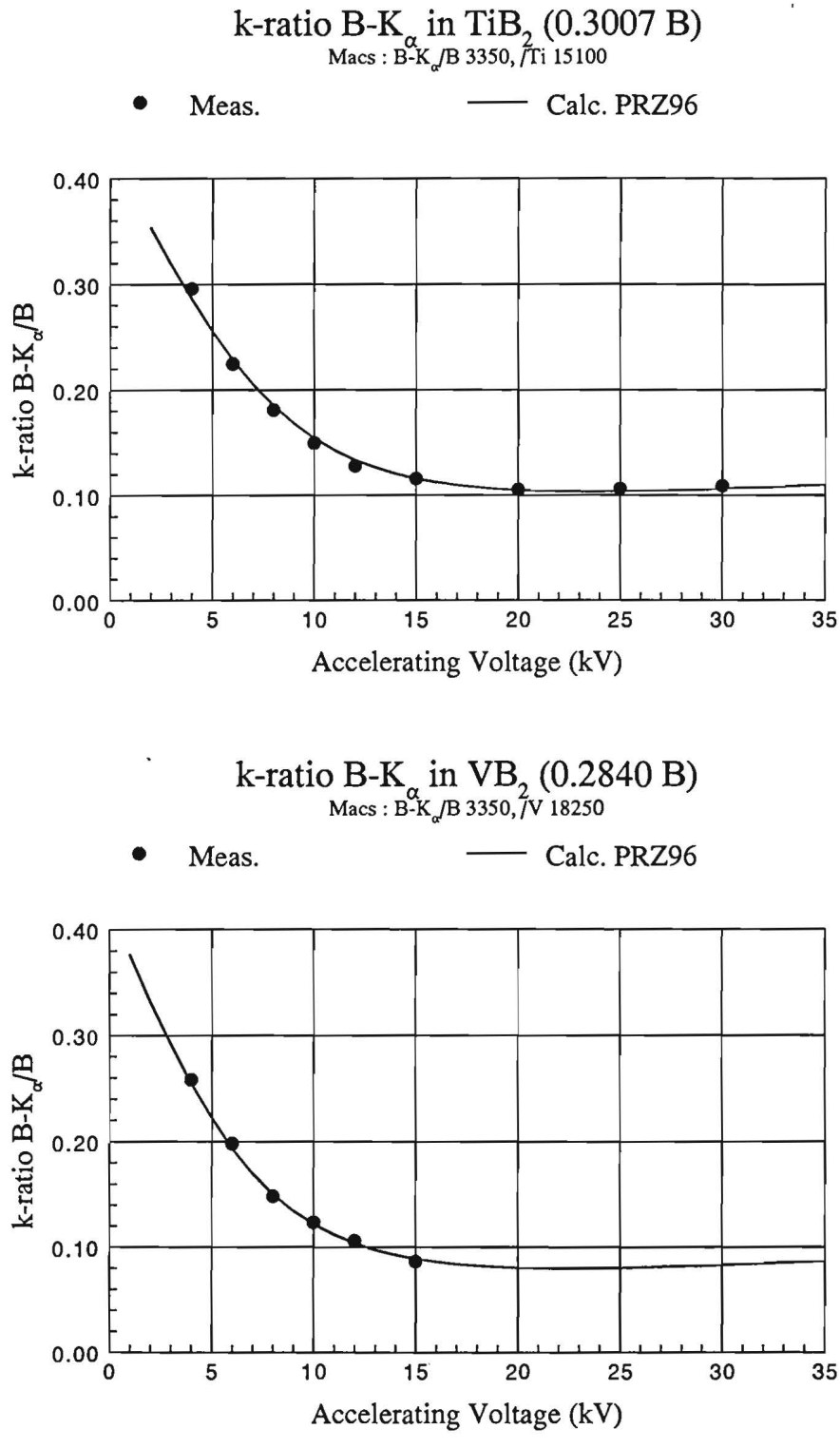

Fig. IV.4.e. Intensity ratios for Boron-K_α (integral) as a function of accelerating voltage for TiB_2 (top) and VB_2 (bottom). Dots represent our measurements and the curve the predictions of our PROZA96 correction program, using the mac's indicated.

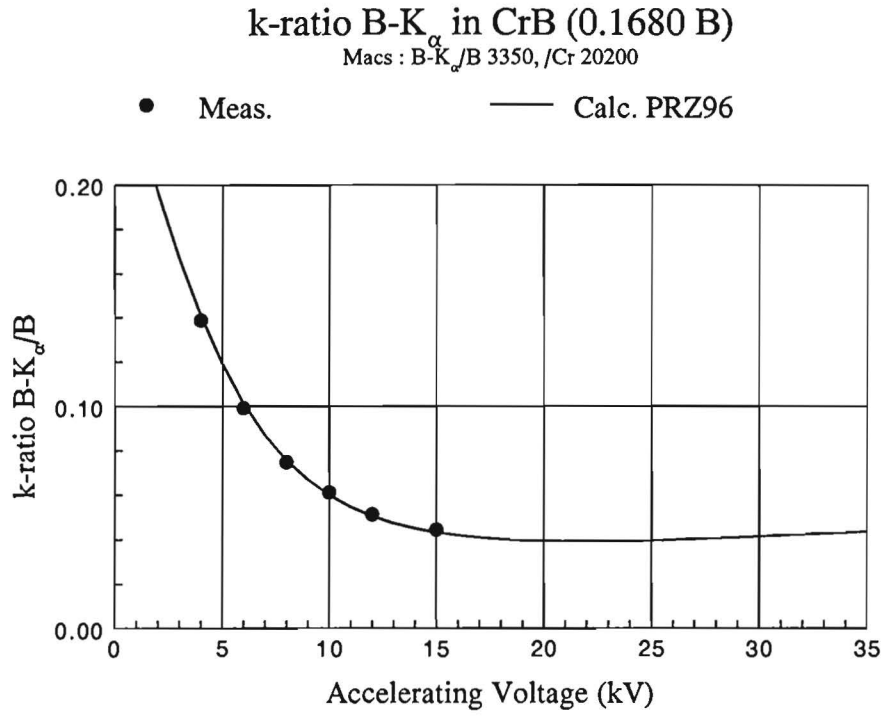

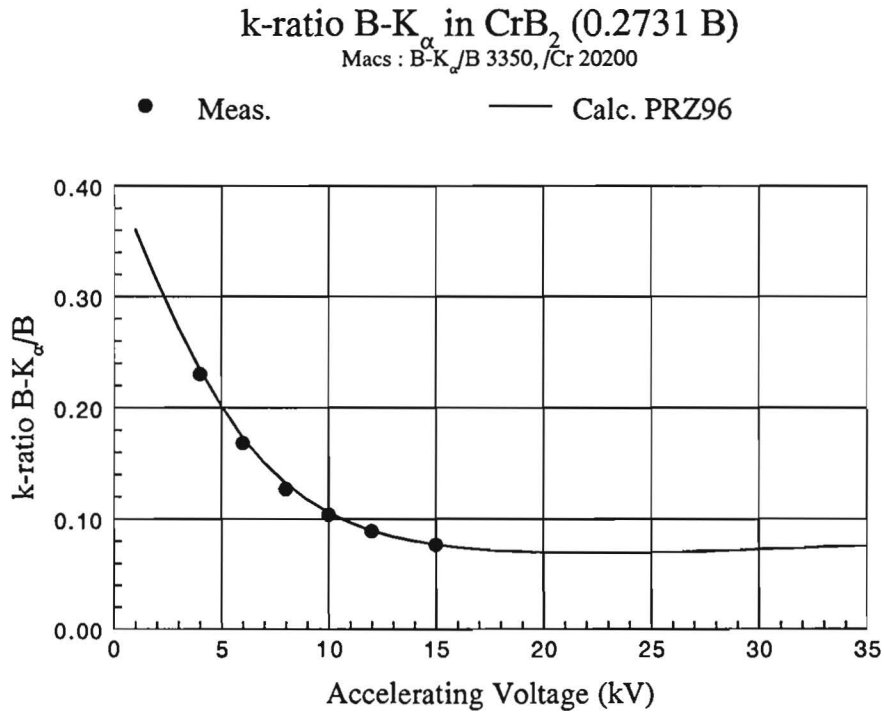

Fig. IV.4.f. Intensity ratios for Boron-K_α (integral) as a function of accelerating voltage for CrB (top) and CrB_2 (bottom). Dots represent our measurements and the curve the predictions of our PROZA96 correction program, using the mac's indicated.

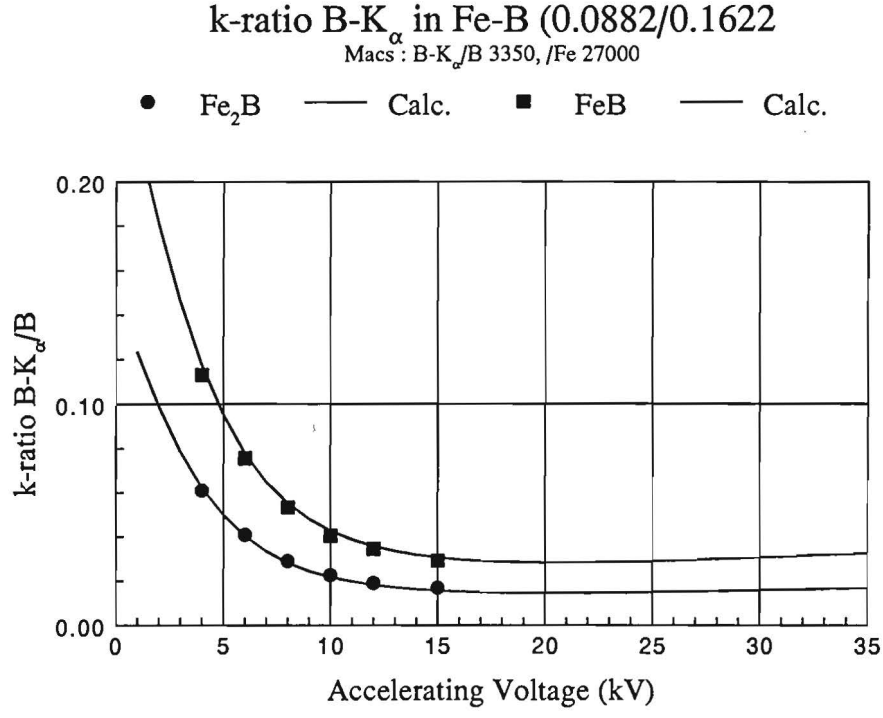

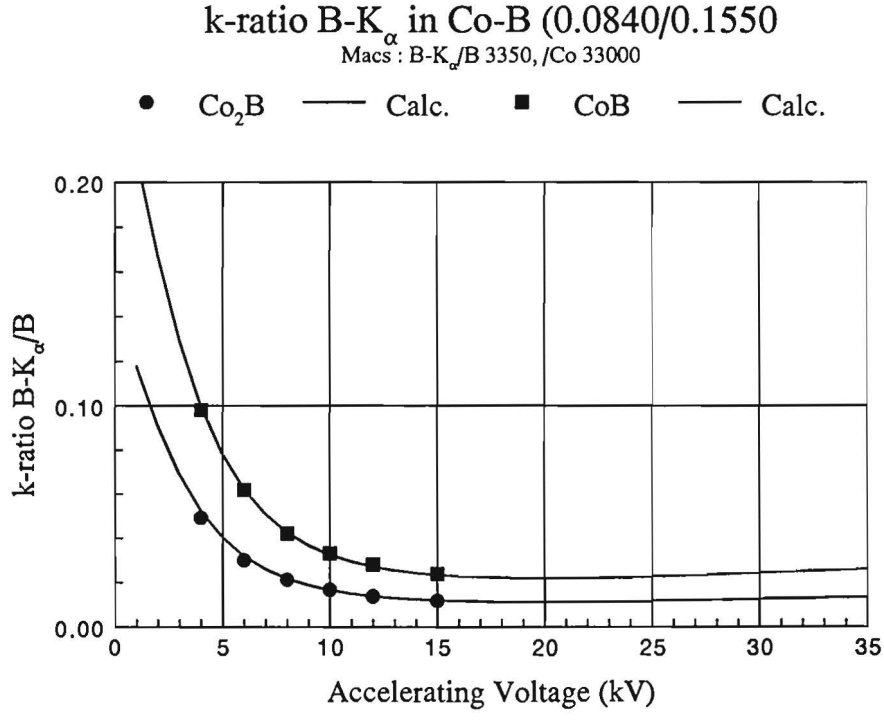

Fig. IV.4.g. Intensity ratios for Boron-K_α (integral) as a function of accelerating voltage for the two Fe-Borides (top) and Co-Borides (bottom). Dots represent our measurements and the curve the predictions of our PROZA96 correction program, using the mac's indicated.

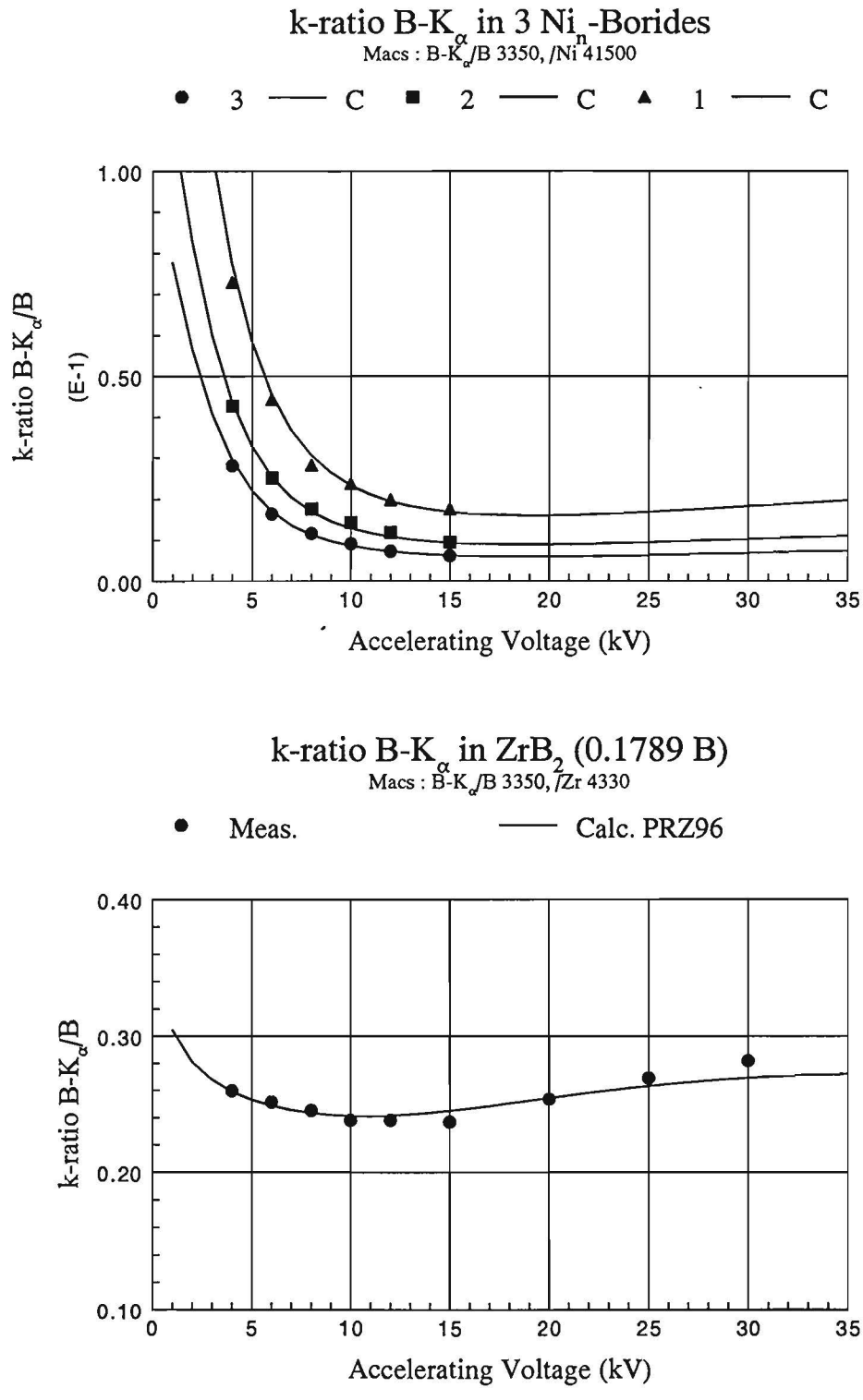

Fig. IV.4.h. Intensity ratios for Boron-K_α (integral) as a function of accelerating voltage for the three Ni-Borides (top) and ZrB_2 (bottom). Dots represent our measurements and the curve the predictions of our PROZA96 correction program, using the mac's indicated.

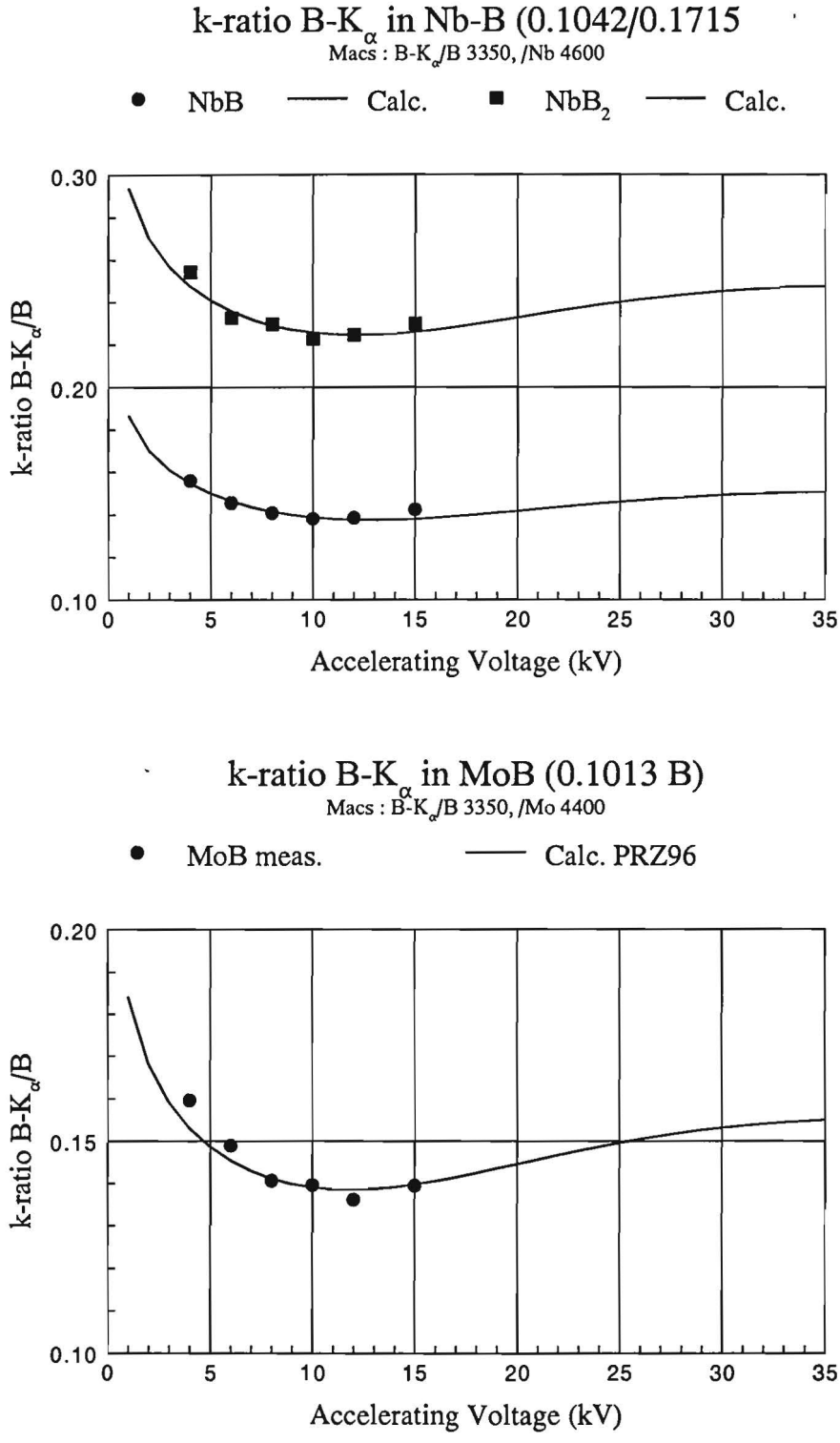

Fig. IV.4.i. Intensity ratios for Boron-K_α (integral) as a function of accelerating voltage for the two Nb-Borides (top) and MoB (bottom). Dots represent our measurements and the curve the predictions of our PROZA96 correction program, using the mac's indicated.

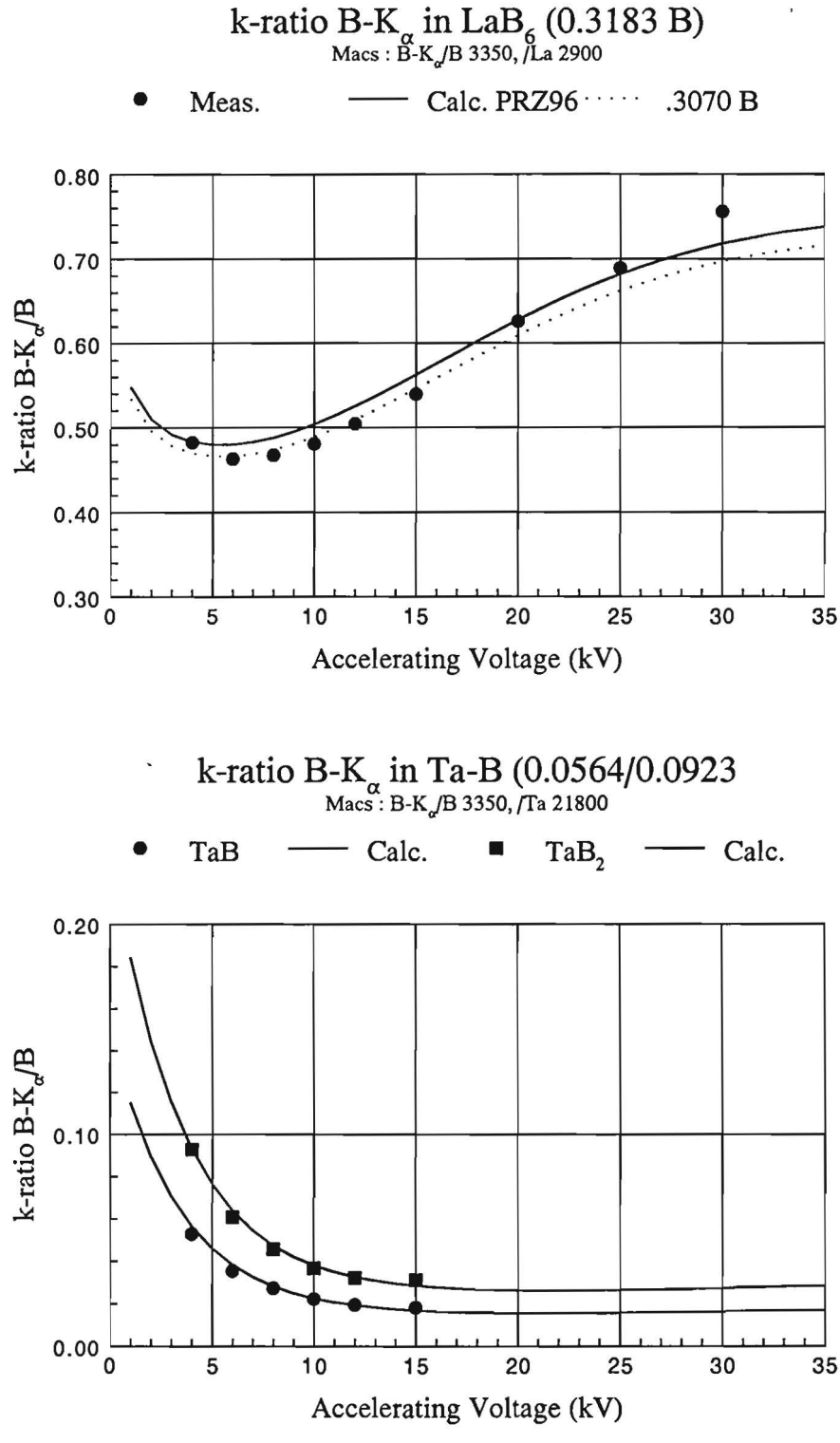

Fig. IV.4.j. Intensity ratios for Boron-K_α (integral) as a function of accelerating voltage for (stoichiometric) LaB_6 (top) and the two Ta-Borides (bottom). Dots represent our measurements and the curve the predictions of our PROZA96 correction program, using the mac's indicated. The dotted curve for LaB_6 shows the predictions for a 3 % (relative) lower boron content.

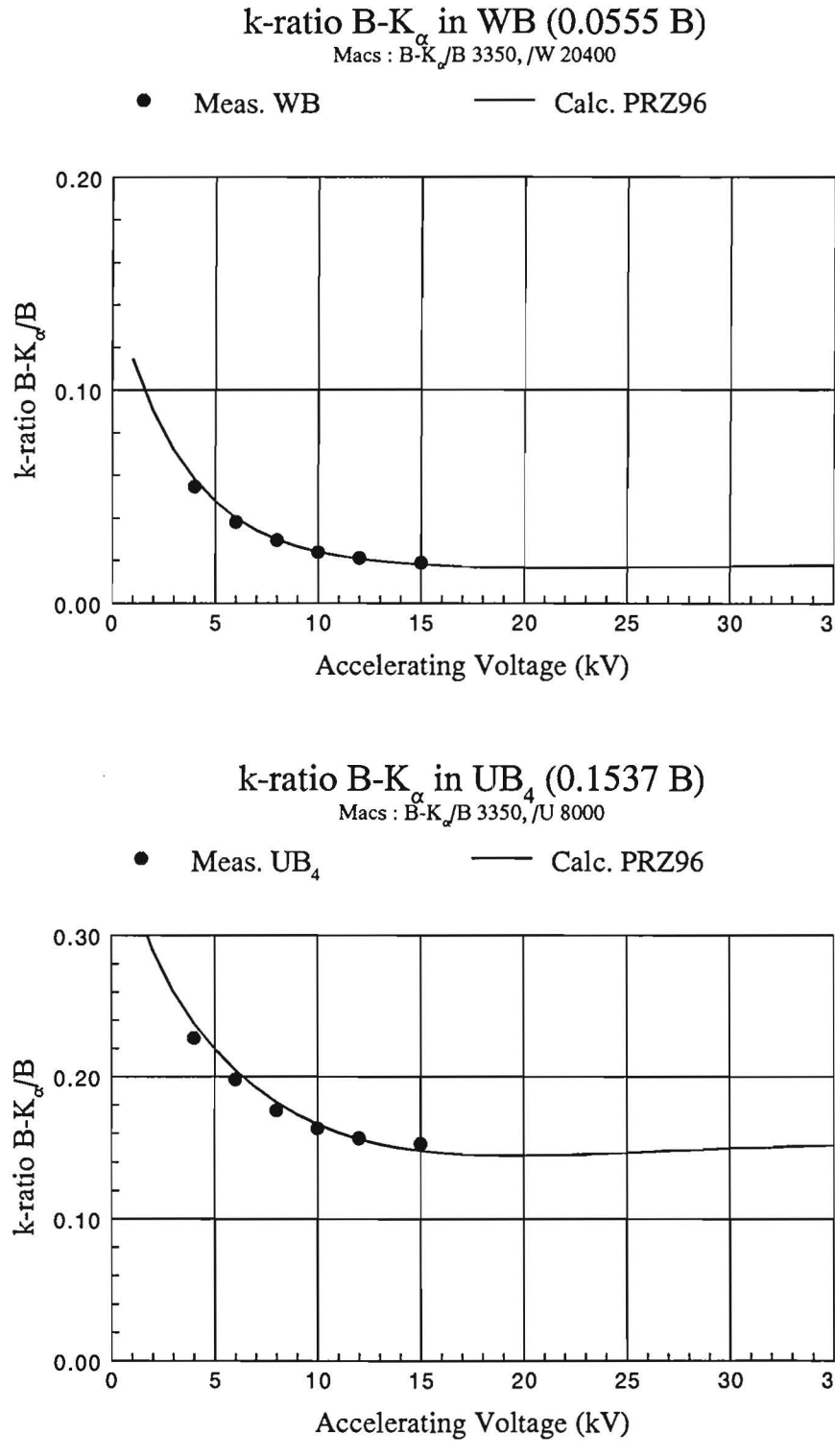

Fig. IV.4.k. Intensity ratios for Boron-K_α (integral) as a function of accelerating voltage for WB (top) and UB_4 (bottom). Dots represent our measurements and the curve the predictions of our PROZA96 correction program, using the mac's indicated.

IV.4 Relative emitted B-K_α intensities from the boride specimens as a function of accelerating voltage in relation to the mass absorption coefficients

Measurements of relative emitted x-ray intensities as a function of accelerating voltage can provide very valuable information about the functioning of a particular matrix correction model as well as on the correctness (or, perhaps rather, consistency) of the mass absorption coefficients used. As long ago as 1967, already, Andersen[17] showed empirically that there is a relationship between the accelerating voltage in the electron beam that produces the maximum emitted x-ray intensity of a specific x-ray line and the value of the mass absorption coefficient in a variety of elemental and compound targets used. This was then qualitatively explained by the counteraction of the increase in x-ray generation with increasing beam voltage and the increasing absorption in the specimen. This will eventually lead to a maximum in the emitted intensity at a very specific voltage which depends strongly on the value of the mac in the compound for the x-ray line in question.

This idea was later picked up by Kyser[18] and used, in a quantitative way, to determine experimentally the mac's for self absorption of V-L_α, Fe-L_α, Cu-L_α, and Zn-L_α.

The same idea has been used quite extensively by Pouchou and Pichoir[5] in conjunction with their "Double Parabolic" $\varphi(\rho z)$ correction model "PAP". It has been pointed out by these authors that when the absorption of a particular x-ray line in a compound is weak the variation of the calculated (and measured) emitted intensity is mainly governed by the variation of the integral of $\varphi(\rho z)$ and the variation of the x-ray ionization cross-section with overvoltage ratio U (E/E_c). (It should be kept in mind that $\varphi(\rho z)$ is always defined relative to the intensity emitted by an infinitely thin reference film free in space; hence the cross-section at U_o (E_o/E_c) plays a crucial role). For cases of weak absorption the actual shape of $\varphi(\rho z)$ does not play a vital role. In cases of stronger absorption, on the other hand, the shape of $\varphi(\rho z)$ starts to play an increasingly important role indeed. Ultimately, in the cases of heaviest absorption, the emitted intensity depends entirely upon the variation of the surface ionization value $\varphi(o)$ with voltage.

It is evident that the study of emitted intensity as a function of voltage provides valuable information about a number of physical parameters, not in the last place about the magnitude of the mac's.

Unfortunately, Pouchou and Pichoir[5] also pointed out that the measurements of emitted intensities are of a painstaking nature. The utmost care has to be exercised to monitor the stability of the instrument used, the beam current has to be known with high accuracy, as well as the accelerating voltage. Besides, the specimens should be plane and perfectly polished, carbon contamination has to be avoided, and the angle of incidence of the electron beam, as well as the x-ray take-off angle should be accurately known. Only under these (near-ideal) conditions are smooth and consistent measurements as a function of voltage possible.

An additional advantage of this approach is that the relative emitted intensities are relatively insensitive to the actual composition, contrary to the calculated k-ratios, which are very sensitive indeed to variations in the composition. In the ideal case the calculated k-ratio for the given composition should agree closely with the measured one over a wide range in accelerating voltage, using a single value of the mac. At the same time the measurements and calculations of the emitted intensities should agree closely using the same mac value.

In the present work we measured the absolute emitted intensities for B-K_α in a complicated (through APF's) and indirect way, i.e., through measurements of k-ratios relative to elemental boron. Therefore, it cannot be expected right-away that the data are sufficiently smooth and

consistent enough to be used for an inspection of the consistency of mac's in combination with the performance of a particular correction program. The data are bound to contain too much scatter for that purpose. However, we found a way to improve the measured data very much, in that we started out to generate a "best set" of relative B-K_α intensities emitted from pure Boron, using the best sets of measurements of B-K_α in the pure elemental Boron standards, which had been performed quite a number of times during the k-ratio measurements. This best set is represented in Fig. IV.5. which shows that very good agreement is obtained between the measurements and the predictions of our latest correction program "PROZA96" (See Chapter V) with a mac for B-K_α in B of 3350 (See Table II.1). Using the absolute emitted intensities from this "best set" the absolute emitted intensities from all boride specimens as a function of voltage have been recalculated using the measured integral k-ratios. As a result, much smoother and more consistent plots of relative intensities could be produced. In those cases, where our measurements covered the full range up to 30 kV, the results are given in Fig.s. IV.6.a-d.

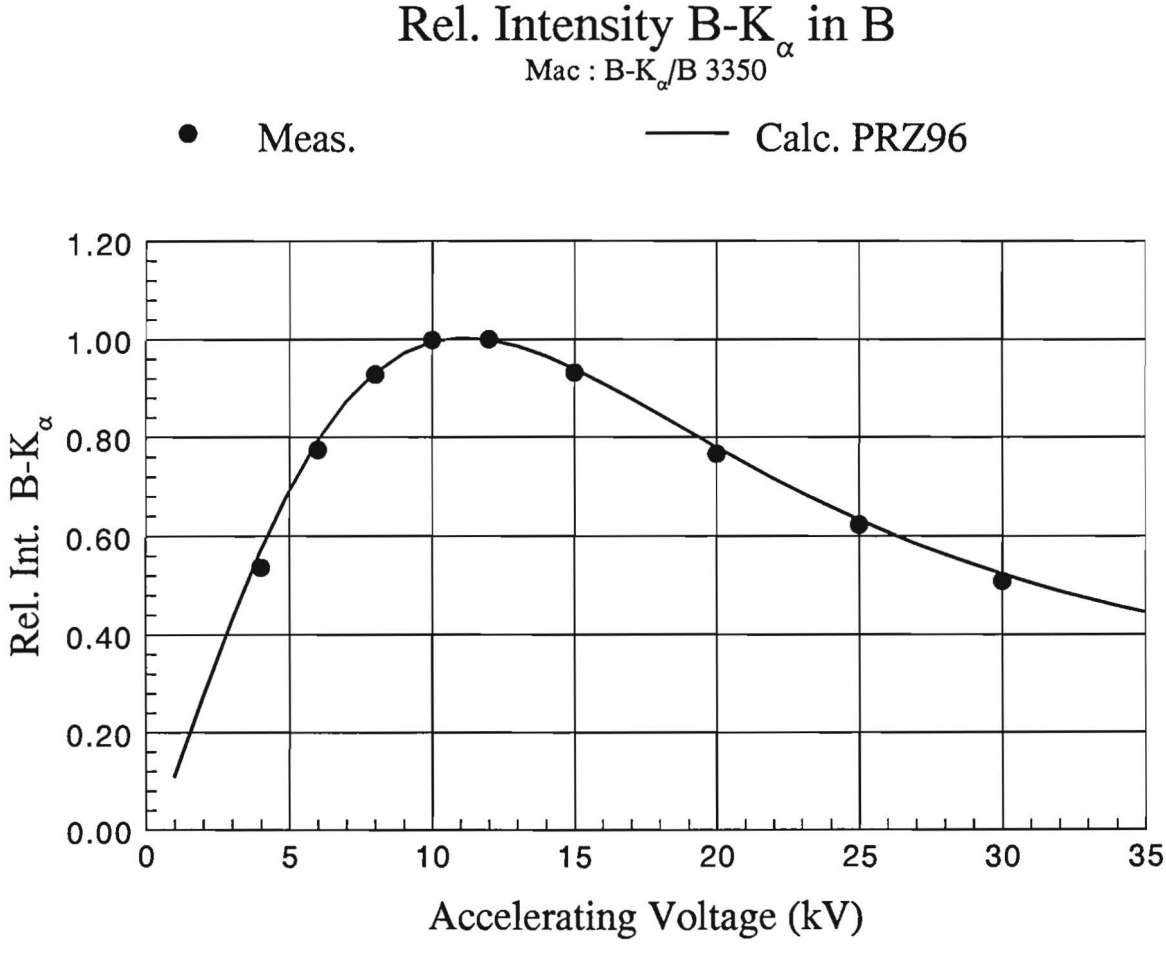

Fig. IV.5. Relative Emitted Intensity for Boron-K_α from pure Boron as a function of accelerating voltage. Dots represent our measurements and the curve the predictions of our PROZA96 correction program, using the mac indicated.

In all other cases (up to 15 kV) the results are represented in Fig. IV.7.a-e. Fig. IV.6 shows that excellent agreement is obtained in all cases with the mac's we propose in Table II.1. Obviously, optimum consistency is obtained between the model used and the magnitude of the mac's we propose. The situation is somewhat different in some of the remaining cases. Good agreement is again obtained in compounds such as AlB_2, SiB_3, SiB_6, VB_2, CrB, CrB_2, NbB, NbB_2,and MoB, as far as can be judged in this limited range of accelerating voltage. However, significant discrepancies are observed in the borides of Fe, Co, and Ni as well as in the Ta, W, and U-borides. Without exception, a much better agreement is obtained with significantly lower mac's than the ones we propose in Table II.1. The higher values are necessary to reproduce the correct (supposedly known) compositions in the data file, while the lower values are much more consistent with the measured relative intensities. Or, to put it in other words : with the lower mac values too low concentrations are calculated by the program; however, in that case they are virtually independent of accelerating voltage and very constant. Examples of the latter calculations are given for the three Ni-borides in Table IV.3, which actually represent the worst cases of discrepancies. It is clear that amazingly constant and very consistent concentrations are found for the three Ni-borides, taking into account the extreme absorption and the low Boron content in these compounds. Unfortunately, the Boron contents are only 80 % of what they are supposed to be. Since at present at least Ni_3B and Ni_2B are supposed to be stoichiometric line-compounds according to the latest phase diagrams, it must be assumed that the answers in Table IV.3 are not correct. Because the answers we could obtain in both lighter (Al, Si, Ti, V, Cr) as well as in heavier (Zr, Nb, Mo) borides are correct it is highly unlikely that the program produces such systematic errors, either as a result of the atomic number or of the absorption correction. At the moment we have the feeling that the most plausible explanation lies in systematic anomalies in the x-ray fluorescence yield for B-K_α in Nickel (and some other) compounds. Similar effects were observed (to a much lesser extent) in the Fe and Co borides. In case of the heavy borides of Ta, W, and U the observed discrepancies could very well be explained by lower Boron contents than we presently assume, as Table IV.4 shows. This suspicion is corroborated by the observation that the analytic totals in the analyses (in which the M_α lines of the metal partners were used) usually came out rather close to 100 %.

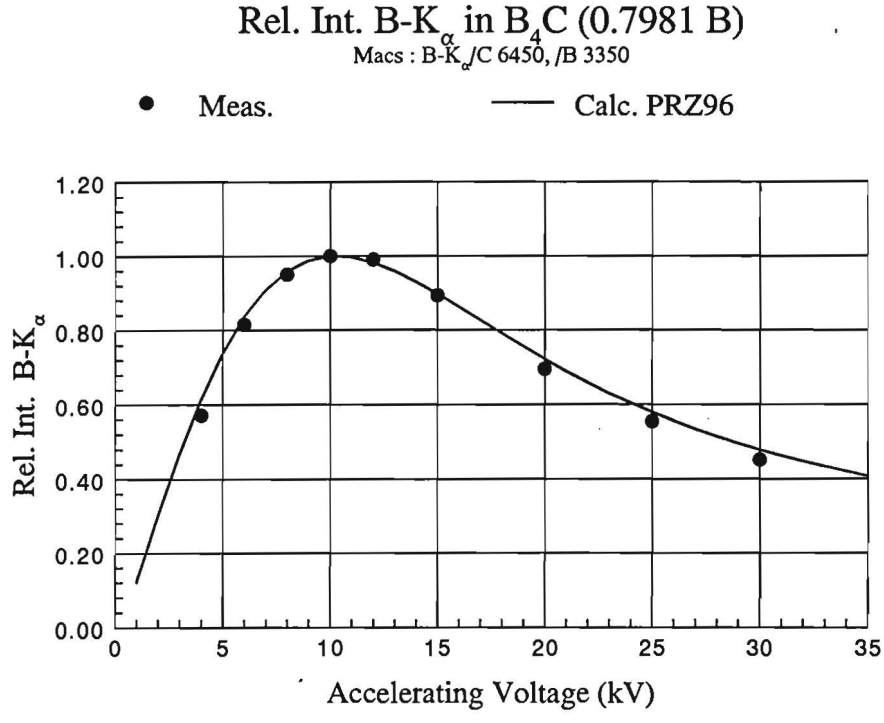

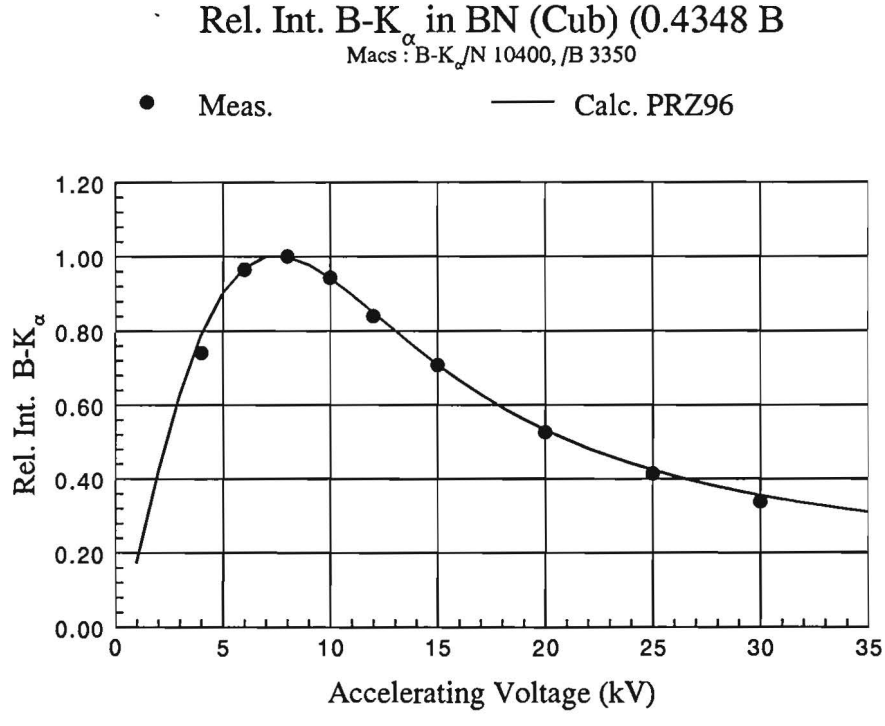

Fig. IV.6.a. Relative Emitted Intensity for B-K_α from B_4C (top) and cubic BN (bottom) as a function of accelerating voltage. Dots represent our measurements and the curve the predictions of our PROZA96 correction program, using the mac's indicated.

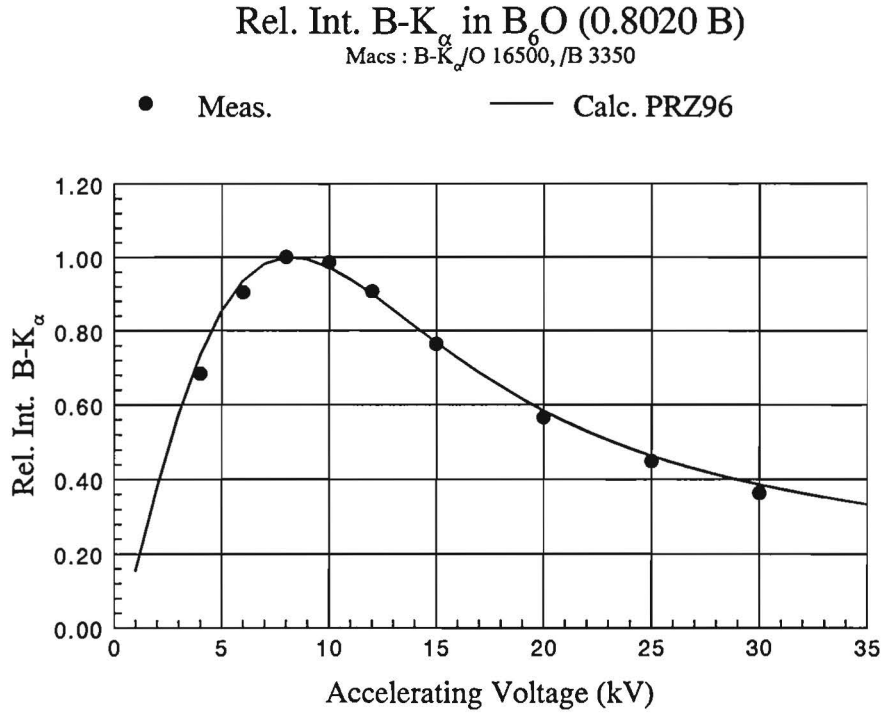

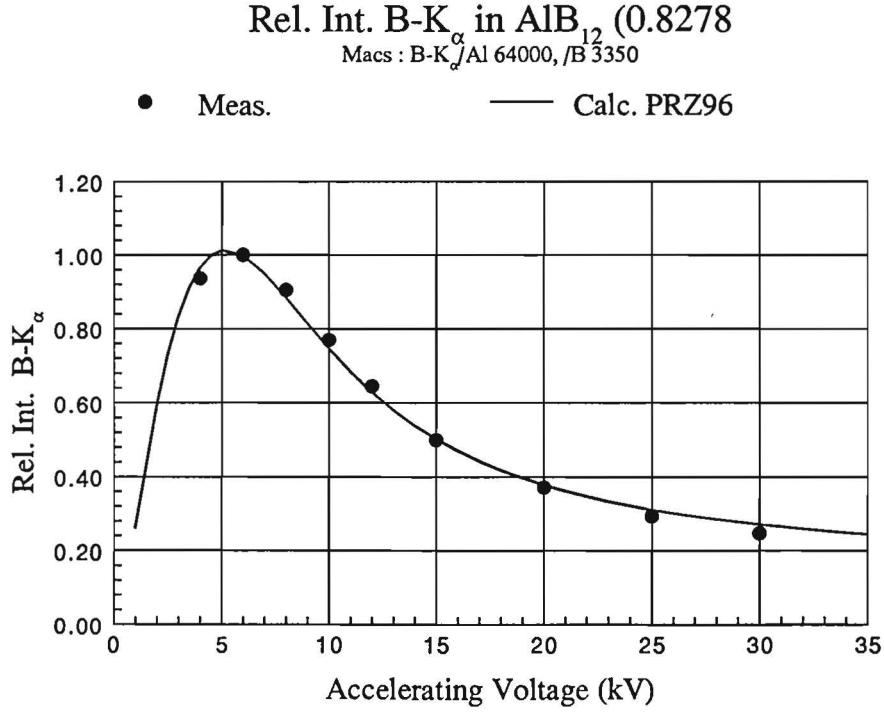

Fig. IV.6.b. Relative Emitted Intensity for B-K_α from B_6O (top) and AlB_{12} (bottom) as a function of accelerating voltage. Dots represent our measurements and the curve the predictions of our PROZA96 correction program, using the mac's indicated

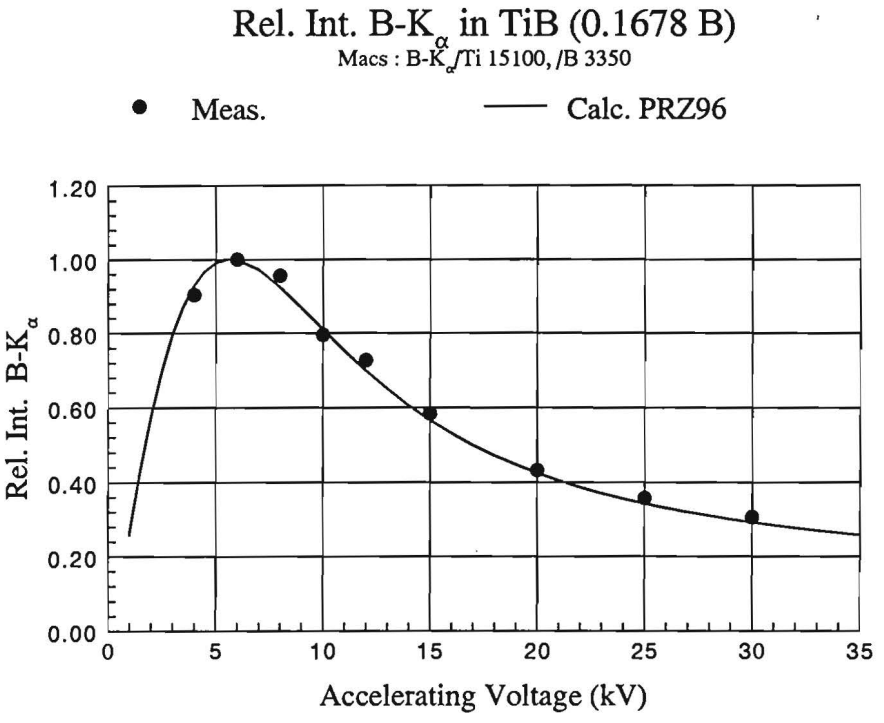

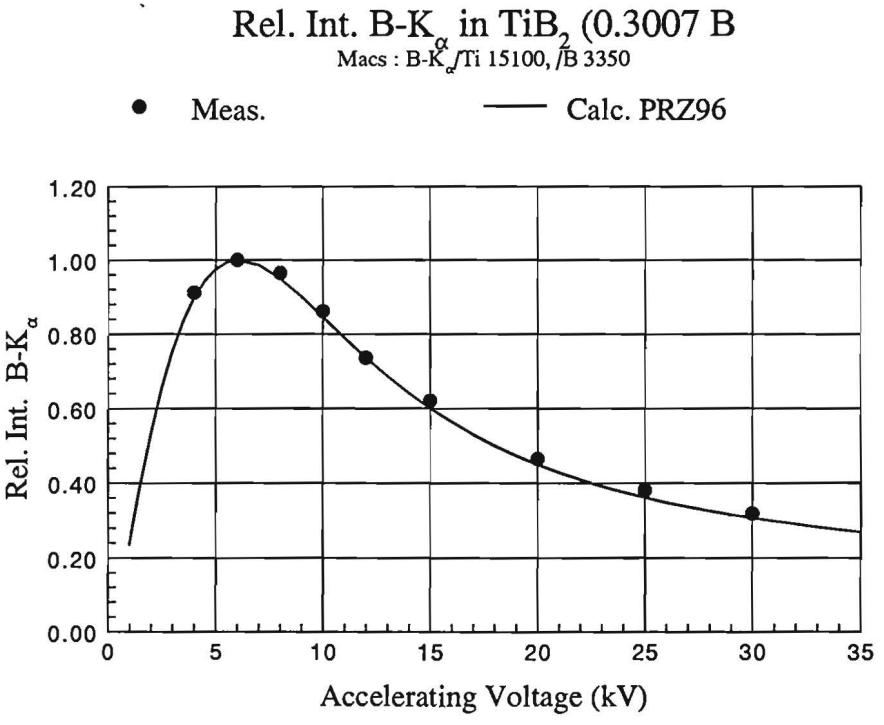

Fig. IV.6.c. Relative Emitted Intensity for B-K_α from TiB (top) and TiB_2 (bottom) as a function of accelerating voltage. Dots represent our measurements and the curve the predictions of our PROZA96 correction program, using the mac's indicated

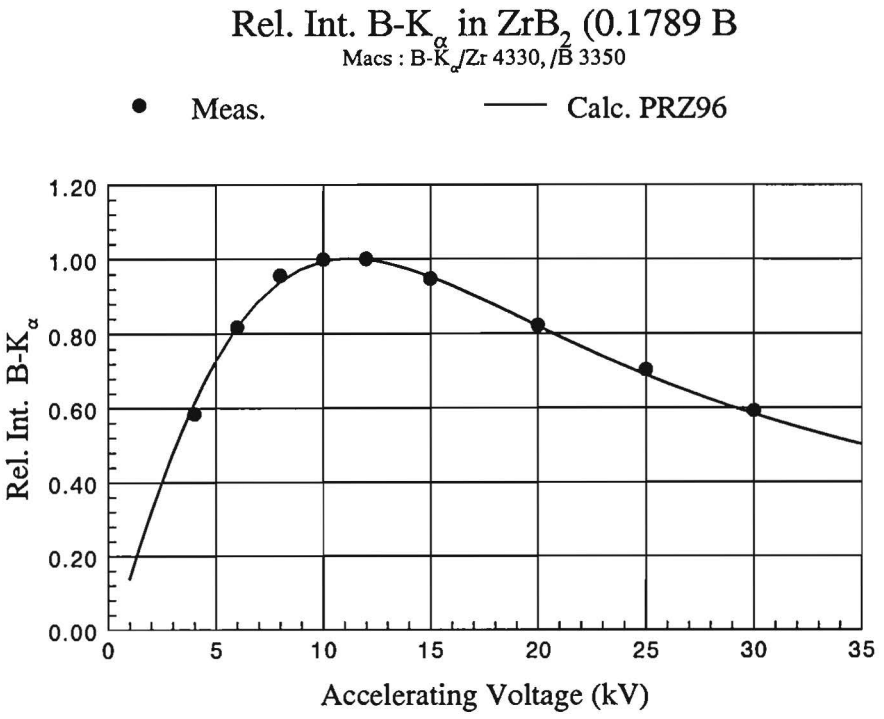

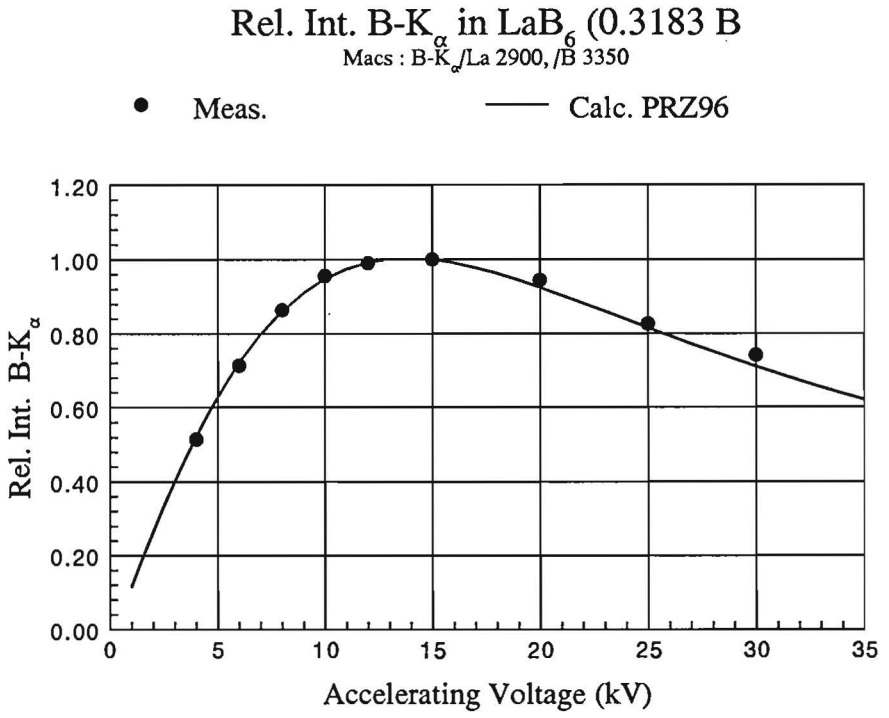

Fig. IV.6.d. Relative Emitted Intensity for B-K_α from ZrB_2 (top) and LaB_6 (bottom) as a function of accelerating voltage. Dots represent our measurements and the curve the predictions of our PROZA96 correction program, using the mac's indicated

Table IV.3

Examples of calculations with the PROZA96 program for the three Ni-borides using the lower mac value for B-K_α in Ni of 33,000, (consistent with the measured relative emitted intensities), rather than 41,500 (Table II.1)

	Ni_3B (5.78 wt. % B)		Ni_2B (8.43 wt. % B)		NiB (14.40 wt. % B)	
kV	**wt %**	**at.% B**	**wt. %**	**at. % B**	**wt. %**	**at. % B**
4	4.59	20.72	6.91	28.72	11.55	41.49
6	4.40	20.00	6.63	27.84	11.32	40.94
8	4.55	20.57	6.78	28.32	10.54	39.02
10	4.67	21.01	7.18	29.59	11.48	41.31
12	4.49	20.32	7.10	29.32	11.48	41.31
15	4.43	20.09	6.66	27.92	11.83	42.15
Mean :	**4.52**	**20.44**	**6.88**	**28.70**	**11.37**	**41.04**
Result :	**"Ni_4B"**		**"Ni_5B_2"**		**"Ni_3B_2"**	

Table IV.4

Examples of calculations with the PROZA96 program for TaB, WB, and UB_4 using the lower mac values for B-K_α in Ta, W, and U, of 20,000, 16,000 and 6,500 (more consistent with the measured relative emitted intensities), rather than the values proposed in Table II.1

	TaB (5.64 wt. % B)		WB (5.55 wt. % B)		UB_4 (15.37 wt. % B)	
kV	**wt %**	**at.% B**	**wt. %**	**at. % B**	**wt. %**	**at. % B**
4	4.98	46.88	4.55	45.91	13.85	77.96
6	4.84	46.19	4.36	44.73	13.60	77.60
8	5.00	46.96	4.36	44.61	13.24	77.06
10	5.05	47.21	4.28	44.04	13.13	76.89
12	5.14	47.65	4.33	44.26	13.15	76.93
15	5.48	49.29	4.41	44.58	13.25	77.08
Mean :	**5.08**	**47.25**	**4.38**	**44.65**	**13.37**	**77.26**
Result :	**"Substoich."**		**"W_5B_4"**		**"Substoich."**	

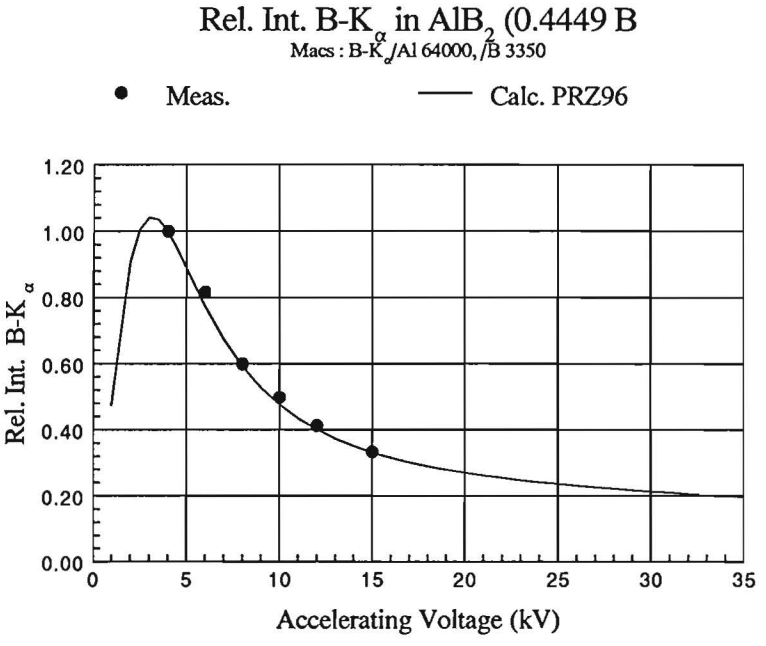

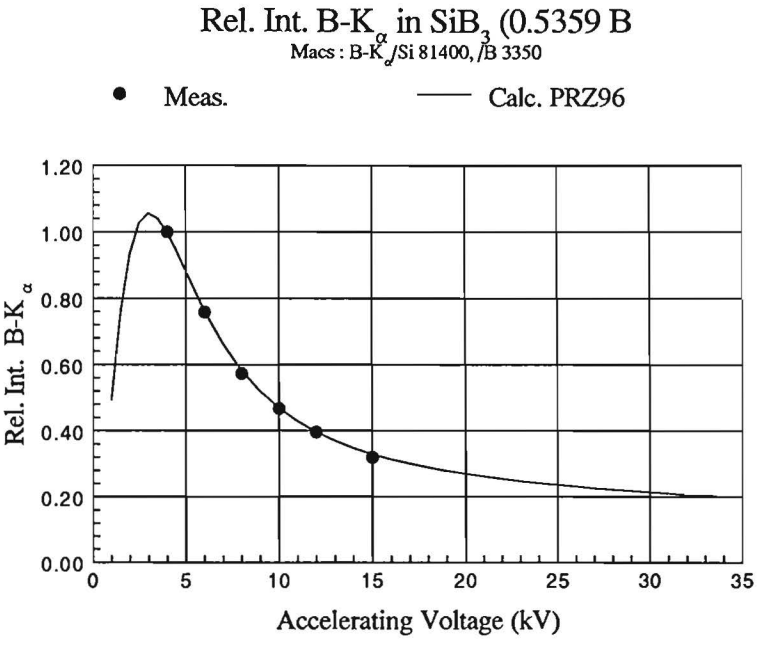

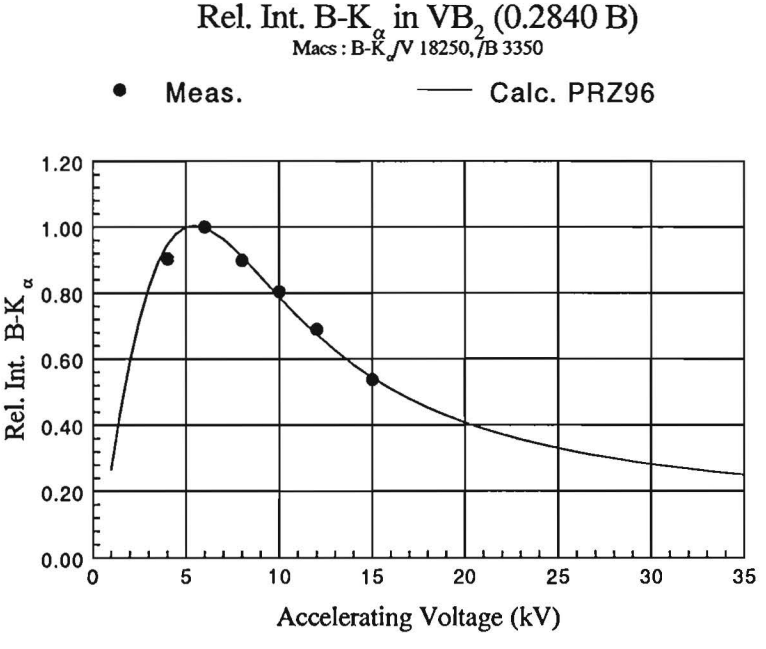

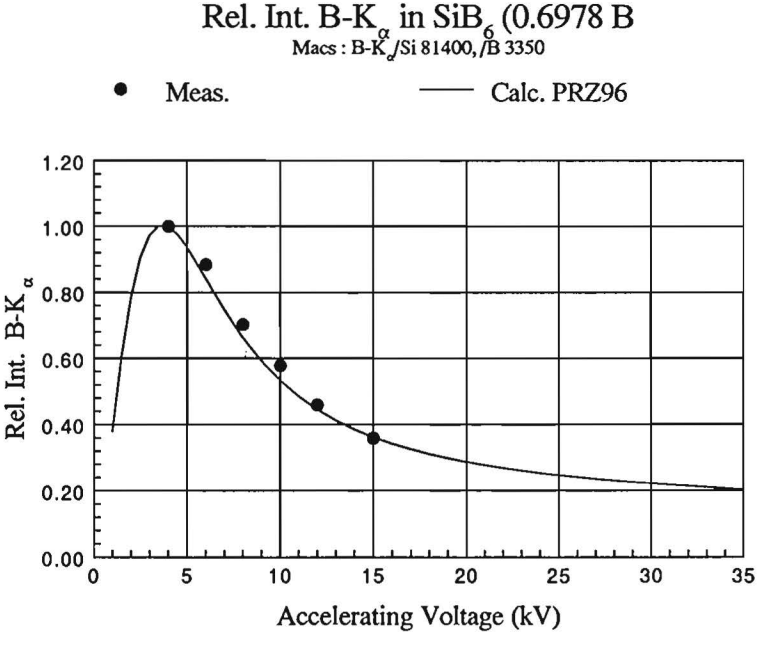

Fig. IV.7.a. Relative Emitted Intensity for B-K$_\alpha$ from AlB$_2$ and SiB$_3$ (top), and VB$_2$ and SiB$_6$ (bottom) as a function of accelerating voltage. Dots represent our measurements and the curve the predictions of our PROZA96 correction program, using the mac's indicated.

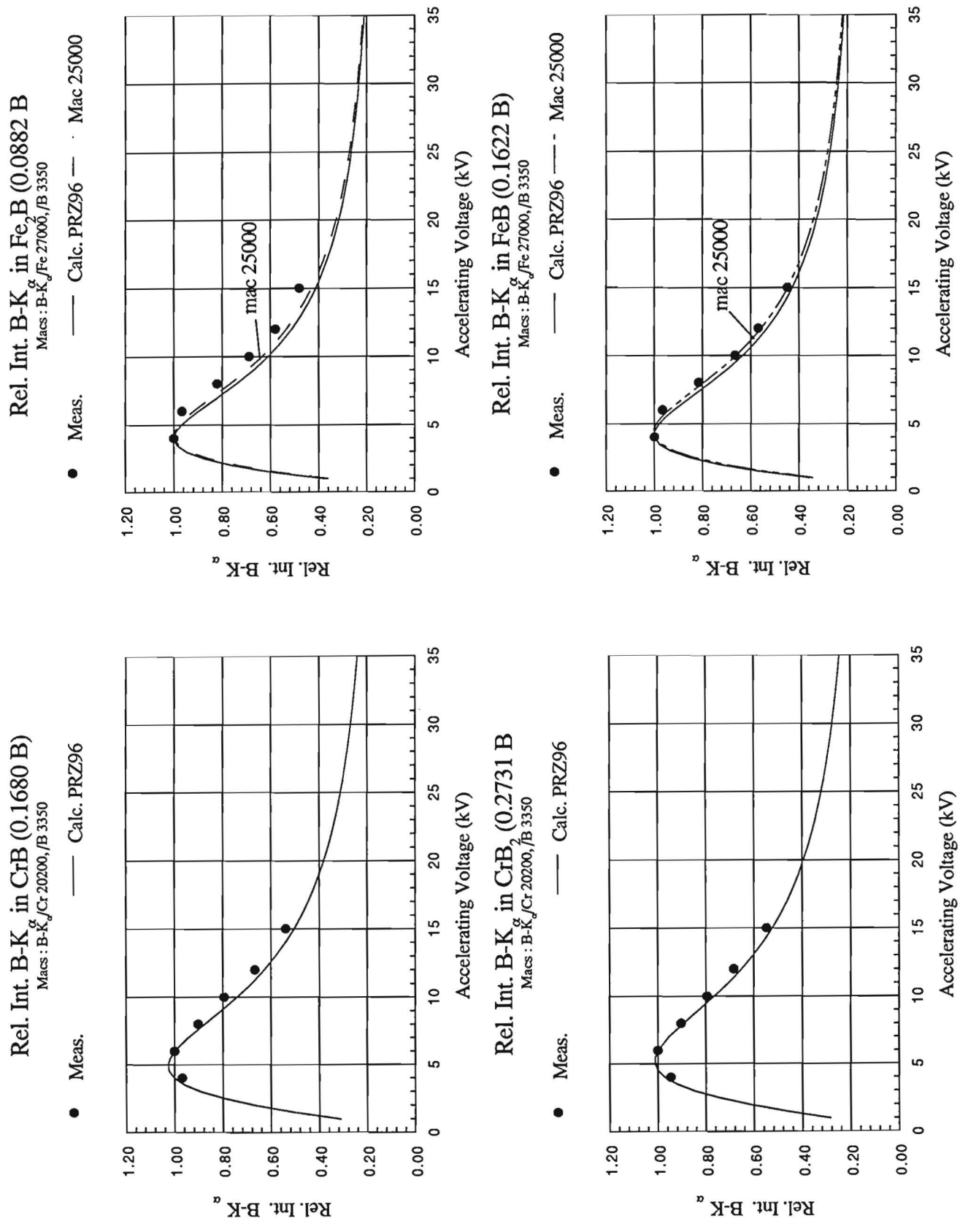

Fig. IV.7.b. Relative Emitted Intensity for B-K_α from CrB and Fe_2B (top), and CrB_2 and FeB (bottom) as a function of accelerating voltage. Dots represent our measurements and the curve the predictions of our PROZA96 correction program, using the mac's indicated.

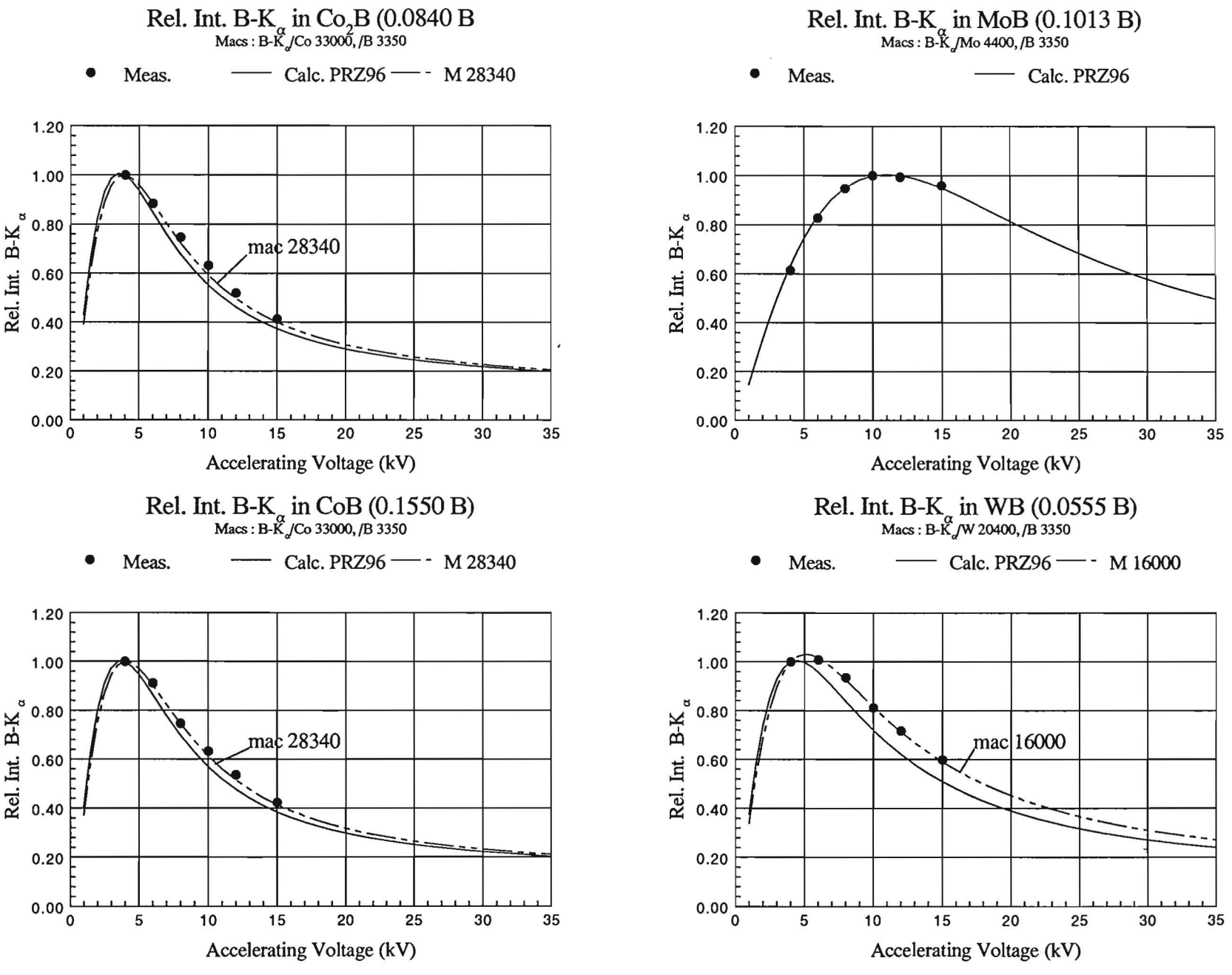

Fig. IV.7.c. Relative Emitted Intensity for B-K$_\alpha$ from Co_2B and MoB (top), and CoB and WB (bottom) as a function of accelerating voltage. Dots represent our measurements and the curve the predictions of our PROZA96 correction program, using the mac's indicated.

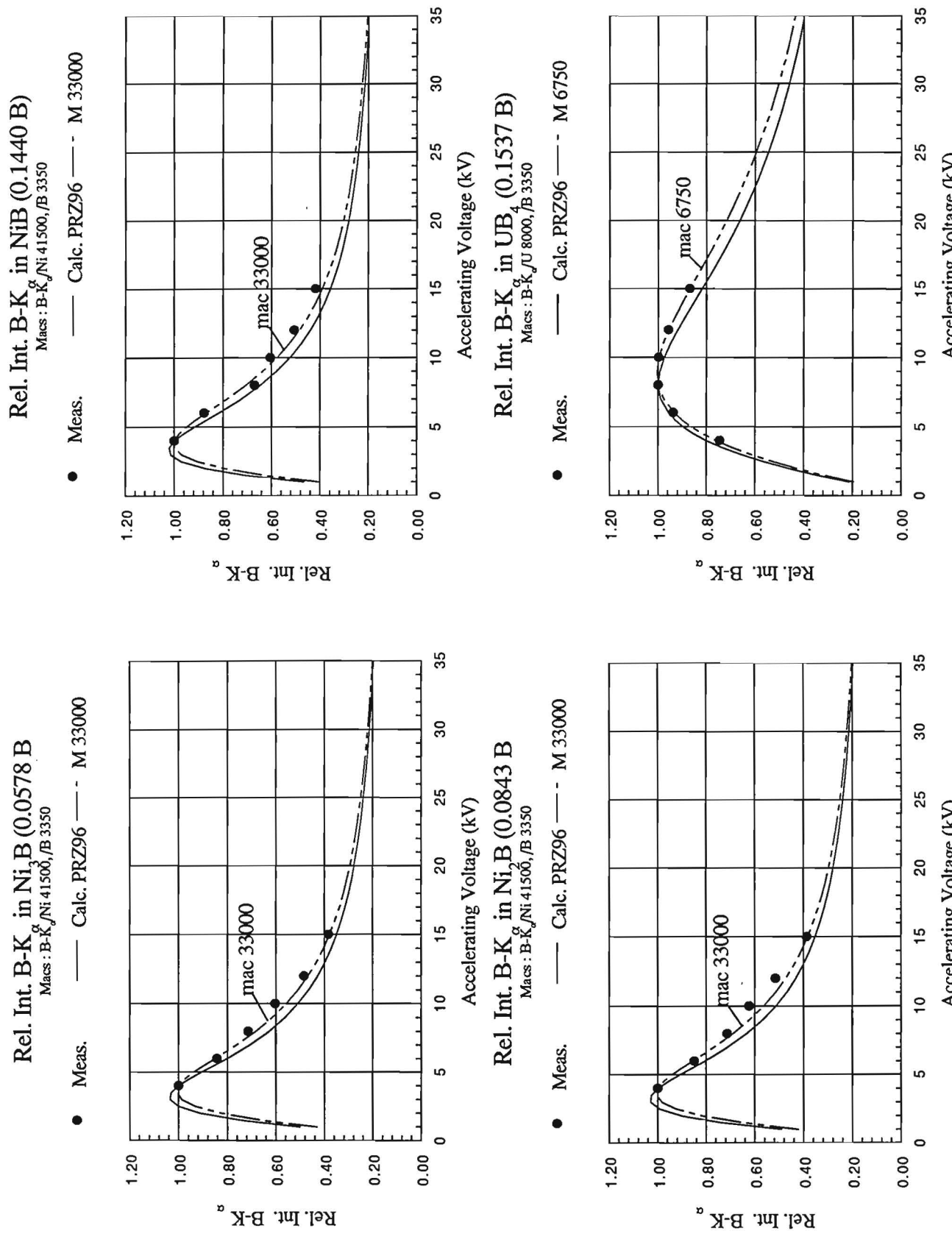

Fig. IV.7.d. Relative Emitted Intensity for B-K_α from Ni_3B and NiB (top), and Ni_2B and UB_4 (bottom) as a function of accelerating voltage. Dots represent our measurements and the curve the predictions of our PROZA96 correction program, using the mac's indicated.

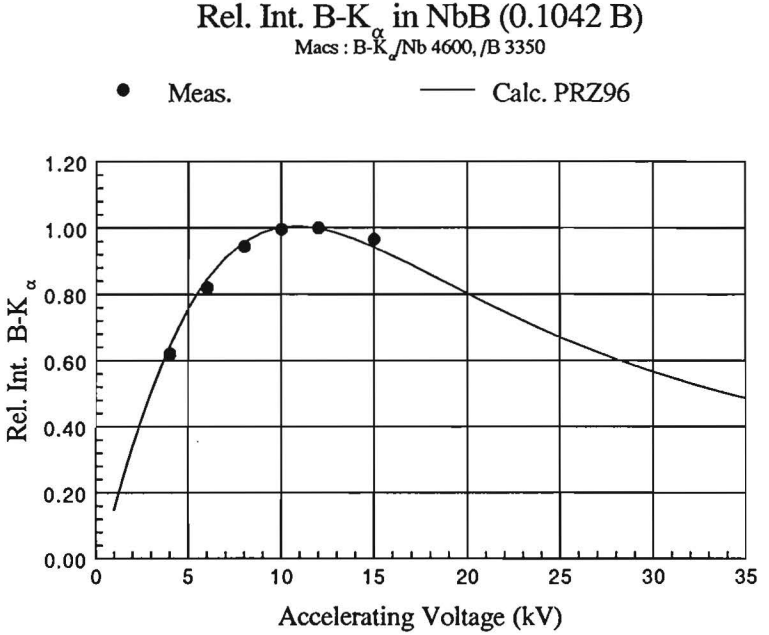

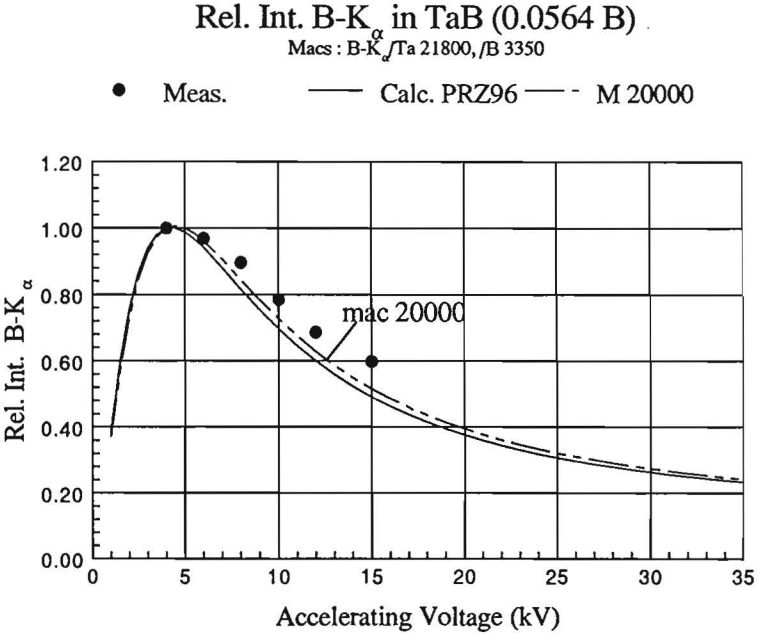

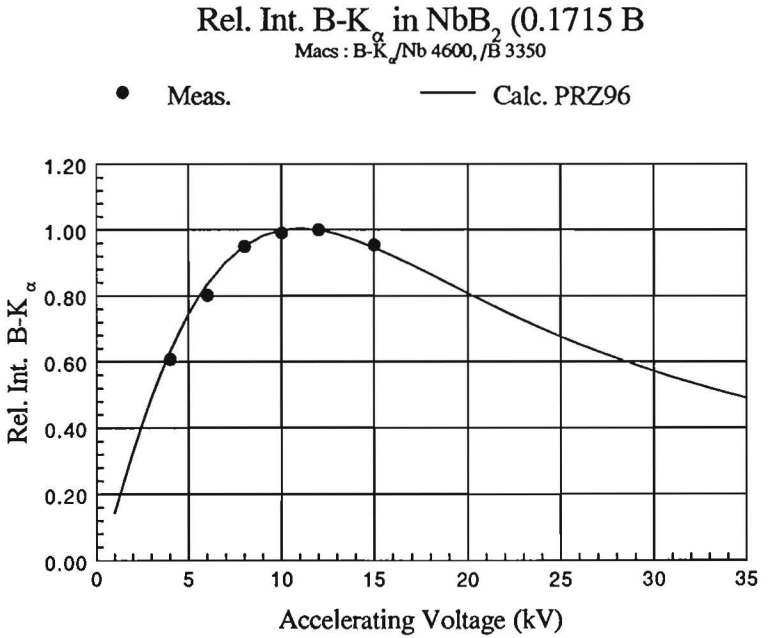

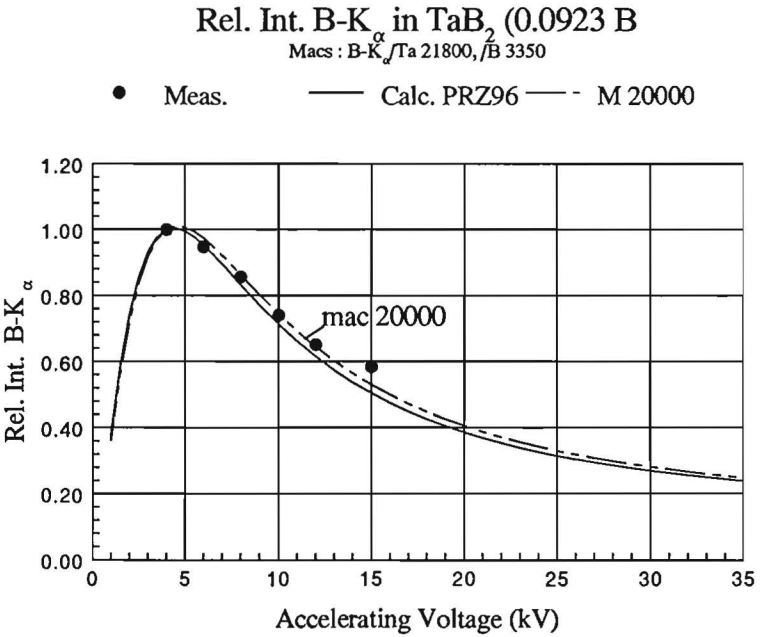

Fig. IV.7.e. Relative Emitted Intensity for B-K$_\alpha$ from NbB and TaB (top), and NbB_2 and TaB_2 (bottom) as a function of accelerating voltage. Dots represent our measurements and the curve the predictions of our PROZA96 correction program, using the mac's indicated.

V DATA REDUCTION AND COMPARISON OF CORRECTION PROGRAMS

The last step in the whole procedure is the conversion of measured k-ratios into the correct concentration units. To achieve this a number of correction programs which are currently in use, could be considered. In one of our previous publications[1] a number of these older programs have been discussed in detail. Since then, a number of new programs have emerged and/or existing programs modified. We mention the "PAP"[5,19] (Double Parabolic $\varphi(\rho z)$ approach), our own "PROZA"[20] (Surface-centered Gaussian $\varphi(\rho z)$ approach), Pouchou and Pichoir's "XPP"[21] model, and, most recently, the Merlet model[22] (based on a double Gaussian $\varphi(\rho z)$ approach). Besides, a new version of the Love and Scott program has been introduced[23]. This modification is based on an improved absorption correction (so-called "quadrilateral" model) which was claimed to perform particularly well for light element analysis. This last correction program, which was originally put forward in 1985[6], will henceforth be referred to as SELOS85. Much later this version of the quadrilateral model was modified[23], using our data bases for Boron and Carbon analyses in order to improve the absorption correction, and deficiencies in the atomic number correction were repaired. This last version will be called SELOS91. For the sake of completeness and in order to show the enormous progress, which has been achieved in matrix correction procedures in the last decade, we will include in the present work also some much older programs, such as ZAF (Duncumb-Reed atomic number correction and simplified Philibert-Heinrich absorption correction), RUSTE[4] (full Philibert absorption correction), and LOSCO851[6] (Love and Scott program, based on Love and Scott atomic number correction and Bishop's square absorption correction model[24])

With an exception for the Merlet program we were able to program all these correction programs and to achieve the performance claimed by the authors on the data bases they used. In spite of several efforts we have, most unfortunately, never been able to produce a Merlet program with the performance claimed by the author.

The performance of all the other correction programs mentioned will be compared to that of our PROZA96 program[25]. This last program, which is our own latest $\varphi(\rho z)$ program based on a double Gaussian procedure, the principles of which were originally introduced by Merlet[22], has been shown to be very successful, both for the analysis of ultra-light as well as for medium-to-high Z ($Z>11$) elements. This particular $\varphi(\rho z)$ approach will now be discussed in some more detail and compared to our previous "PROZA" program.

V.1 Description of our latest $\varphi(\rho z)$ program "PROZA96"

INTRODUCTION

The current "PROZA" $\varphi(\rho z)$ correction program[20] has been used since about 1986, for the vast majority of applications (including ultra-light element analyses[26,27] and thin-film applications[28]) with great success indeed. As far as the φ (ρz) modeling is concerned it was based on the "Surface-Centered Gaussian" model originally introduced by Packwood and

Brown[11] . This model is based on the assumption that the φ(ρz) curve starts at a fictitious height γ at the specimen surface as a Gaussian with a decay rate α (Fig. V.1) :

$$\gamma * \exp\left[-\alpha^2 * (\rho z)^2\right] \tag{1}$$

in which ρz is the mass thickness (product of density and linear thickness). According to Packwood and Brown the original surface-centered Gaussian is modified in the near-surface regions by the influence of an additional parameter β which ensures that the final φ(ρz) curve starts at the surface with the appropriate surface ionization value $\varphi(o)$ and that the actual φ(ρz) curve reaches its maximum somewhat deeper in the specimen. The final analytical description for φ(ρz) then becomes :

$$\varphi(\rho z) = \gamma * \exp\left[-\alpha^2 * (\rho z)^2\right] * \left[1 - \left(\frac{\gamma - \varphi(o)}{\gamma}\right) * \exp(-\beta \rho z)\right] \tag{2}$$

The major draw-back of this analytical approach is its inherent lack of mathematical flexibility. This is mainly caused by the use of the parameter γ, which imposes a kind of "ceiling" upon the final φ(ρz) curve[10]. Furthermore, with this model it is not immediately obvious where the position (ρz_m) of the maximum in φ(ρz) will be, nor how high this maximum (φ_m) will be. As long as the vital parameters α, β, γ and $\varphi(o)$ are calculated as independent parameters (as originally proposed by Packwood and Brown) then the position of the maximum and its height, as well as the integral of φ(ρz) (area under the φ(ρz) curve) happen to be the complex result of the cooperation between these four independent basic parameters.

Our own experience shows that with such an approach it is very difficult to get an atomic number correction (integral of φ(ρz)) with a smooth and reliable variation with accelerating voltage, especially at low overvoltage ratios. Therefore, in the current PROZA program we partially abandoned the original Packwood/Brown approach and we selected α, γ, and $\varphi(o)$ as 3 out of the 4 necessary basic parameters. The fourth parameter was *FI* (integral of φ(ρz)), which was obtained from an independent atomic number correction (by Pouchou and Pichoir[19]). We developed an iterative mathematical procedure which calculates β for a given set of α, γ, $\varphi(o)$ and a prespecified value of *FI*. The resulting PROZA program most probably performs very reliably as far as the atomic number correction is concerned. However, the model still lacks flexibility in a sense that it is very difficult to manipulate peak position and peak height in a straight-forward manner. The fundamental limitation is still the parameter γ which places a "ceiling" over the final φ(ρz) curve and narrows down the region in which the maximum can occur . The locus of peak position and peak height (Fig. V.1) is always a rather narrow and steep vertical loop which starts at $\varphi(o)$ (for β=0) and ends at γ (for β=∞). It follows that for a fixed set of α, γ, and $\varphi(o)$ values a prespecified value of *FI* can only be found (by varying the height of the peak) for one particular and fixed peak position. Unfortunately, as long as realistic values of α are to be used, the range in which this position can be controlled by variations in γ is too limited in a number of cases. In general this presents no problem for medium-to-high Z matrix elements where the position of the maximum is usually rather close to the specimen surface. However, it can definitely become a

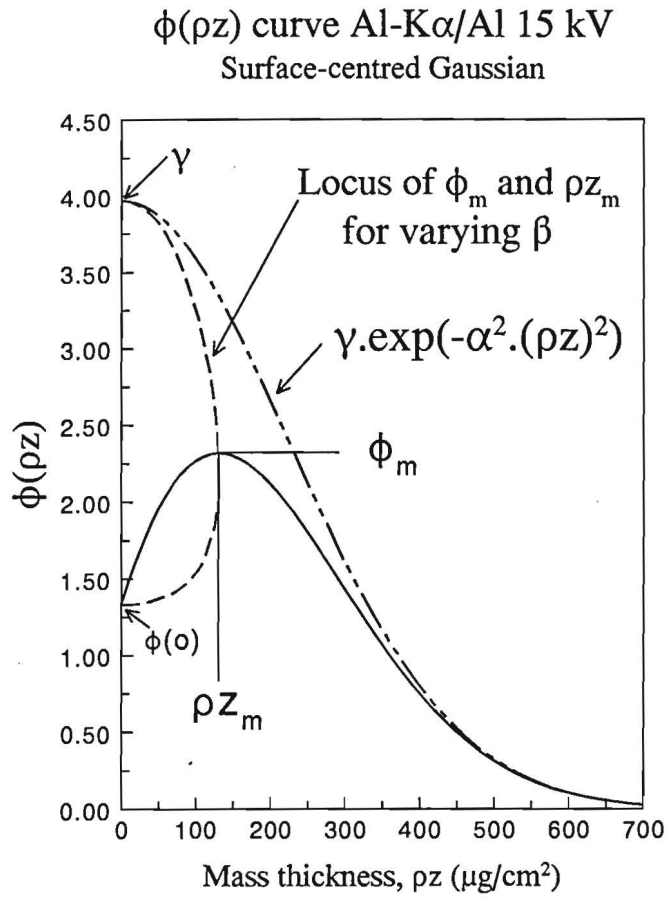

Fig. V.1. Functional behavior of parameters in the Surface-centred Gaussian φ(ρz) approach. Upper dashed curve shows the original surface-centred Gaussian, which begins at the surface with a starting value γ. The near-surface regions are modified by a transient function governed by β, with as a result that the real φ(ρz) curve (solid curve) starts at φ(o). The vertical dashed loop shows the locus of peak position and peak height when β is varied between zero (bottom) and infinity (top).

problem for ultra-light matrices where the maximum in φ(ρz) for very high overvoltage ratios can occur very deep in the specimen indeed. Although this would probably not cause serious problems for bulk applications, not even for ultra-light element radiations as long as the conditions are not too extreme, it could give rise to problems in thin-film applications where the position and height of the maximum are crucial.

It is possible (unpublished work) to impose a prespecified peak position, in addition to a prespecified value of *FI*, upon the surface-centered Gaussian procedure. We developed some PROZA versions which can operate with the independent parameters $\varphi(o)$, α, peak position (ρz_m), and *FI*. The appropriate values for γ and β are then calculated simultaneously through a complex iterative mathematical procedure. Even then, however, purely mathematical restrictions, again caused by the use of the parameter γ, prevent that the peak in φ(ρz) can be laid deep enough in ultra-light matrices (Be, B, C) under extreme conditions.

As a result of all this we decided to abandon the "surface-centred" Gaussian approach altogether and to look for a new model with more mathematical flexibility.

BASIC REQUIREMENTS FOR OUR NEW MODEL

Our starting point in the selection of a new model was that it should be built on parameters with a clear physical meaning and which can easily be recognized and preferably be measured. Since all evidence from the past decade points to the fact that the decay in φ(ρz), somewhere beyond the maximum, is Gaussian in nature we strongly prefer our new model to be Gaussian too. The list with additional requirements for the new model can be summarized as follows :

1. The model should produce a peak in φ(ρz) at a prespecified peak position ρz_m .
2. The integral of φ(ρz) should meet a prespecified value *FI*, resulting from an independent atomic number correction.
3. The new model should be completely modular in structure. This means that it should remain possible to change any of the vital independent input parameters at any time in the future (if better expressions should become available). Yet, we demand that the mathematics inside the model will produce at all times a Gaussian φ(ρz) curve with the required specified peak position and specified integral of φ(ρz). If a model can be conceived that satisfies all these requirements then it follows that whatever variation is introduced in the input in terms of e.g., $\varphi(o)$, α, or *FI* the resulting φ(ρz) curve adapts itself merely by adjusting the height of the maximum at the specified fixed peak position.

CHOICE of NEW MODEL

A very suitable candidate model for our purpose is the one recently introduced by Merlet[22] . It is based on the assumption that a φ(ρz) curve can be described by two Gaussian branches which are smoothly connected at the maximum φ_m in φ(ρz) (Fig. 2). Although from a fundamental point of view it is not immediately obvious why the left hand branch should also be Gaussian it is true that our Monte-Carlo simulations with the MC5 program[12] show that this is a quite reasonable assumption which leads to accurate φ(ρz) descriptions. The analytical descriptions of the two Gaussian branches φ (left) and φ (right) can be given as follows :

$$\varphi_l(\rho z) = \varphi_m * \exp\left[-\beta^2 * \left(\rho z - \rho z_m\right)^2\right] \qquad \text{for : } 0 \le \rho z \le \rho z_m \qquad (3)$$

$$\varphi_r(\rho z) = \varphi_m * \exp\left[-\alpha^2 * \left(\rho z - \rho z_m\right)^2\right] \qquad \text{for : } \rho z_m \le \rho z < \infty \qquad (4)$$

Notes :

1. $\varphi_m = \varphi(o) \,.\, \exp\left(\beta^2 . \rho z_m^2\right)$
2. β now has a different meaning than in the surface-centered Gaussian PROZA model.
3. We have chosen for a slightly different formulation of the Double Gaussian model than Merlet because we aim to use different independent input parameters.

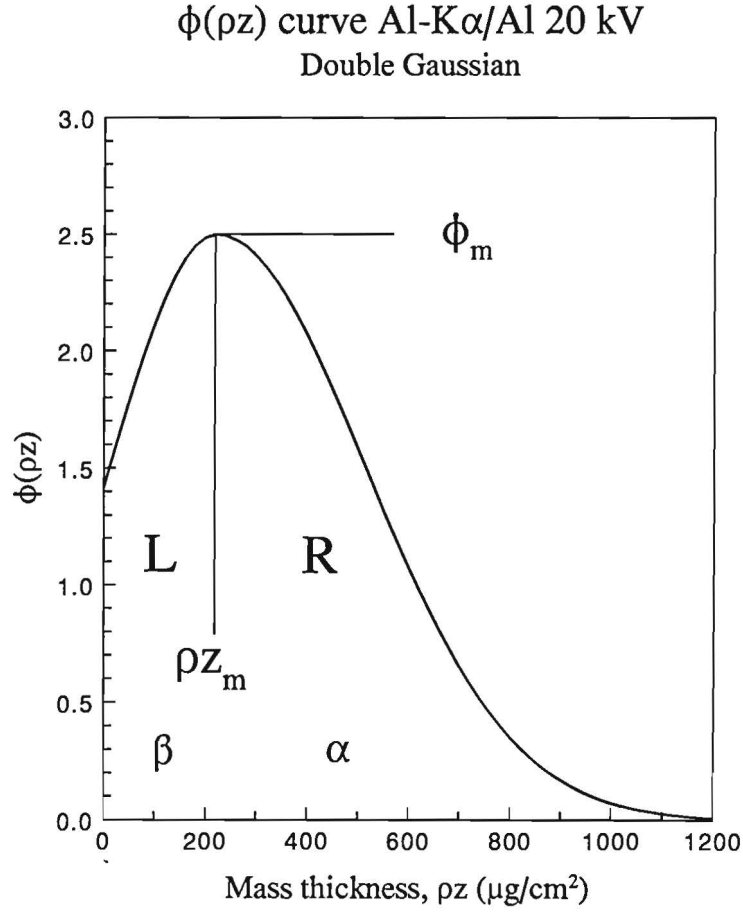

Fig. V.2. Schematic representation of the Double-Gaussian φ(ρz) model. The left-hand branch, with Gaussian increase rate β, is connected at the top (coordinates ρz_m , φ_m) to the right-hand branch with Gaussian decay rate α.

CALCULATION OF GENERATED AND EMITTED INTENSITIES FOR BULK APPLICATIONS

Generated Intensity

The total intensity generated in the specimen is nothing else than the integral of φ(ρz) (FI) which can simply be obtained by integration of φ(ρz) between the ρz limits of zero and infinity. It can be shown that :

$$FI = \frac{\varphi(o) * \sqrt{\pi}}{2} * \exp(\beta^2 * \rho z_m^2) * \left[\frac{erf(\beta * \rho z_m)}{\beta} + \frac{1}{\alpha} \right] \qquad (5)$$

A sufficiently accurate approximation for the error function erf(x) is the following [29] :

$$\mathrm{Erf}(x) = 1 - (a_1 t + a_2 t^2 + a_3 t^3 + a_4 t^4 + a_5 t^5) \,.\, \exp(-x^2) + \varepsilon(x) \qquad (6)$$

in which : $t = 1/(1 + .3275911 \,.\, x)$, and $|\varepsilon(x)| \leq 1.5 \,.\, 10^{-7}$.
The coefficients a are : $a_1 = .254829592$, $a_2 = -.284496736$, $a_3 = 1.421413741$, $a_4 = -1.453152027$, and $a_5 = 1.061405429$. If the 5th degree polynomial is denoted by P_5 it follows that :

$$\mathrm{Erf}(x) = 1 - P_5 \,.\, \exp(-x^2)$$

Emitted Intensity

In order to find the total emitted intensity we have to multiply each point in the $\varphi(\rho z)$ curve with the absorption factor $\exp(-\chi.\rho z)$, in which $\chi = \mu/\rho \,.\, \mathrm{cosec}\theta$ (μ/ρ is the mass absorption coefficient and θ is the X-ray take-off angle) and once again the integration has to be carried out over the ρz limits between zero and infinity.
For the left hand branch we finally arrive at :

$$I_{E,l} = \frac{\varphi_m * \sqrt{\pi}}{2\beta} * \exp\left[\left(\frac{\chi}{2\beta}\right)^2 - \chi * \rho z_m\right] * \left[erf\left(\beta * \rho z_m - \frac{\chi}{2\beta}\right) + erf\left(\frac{\chi}{2\beta}\right)\right] \qquad (7)$$

Likewise, we find for the right hand branch :

$$I_{E,r} = \frac{\varphi_m * \sqrt{\pi}}{2\alpha} * \exp\left[\left(\frac{\chi}{2\alpha}\right)^2 - \chi * \rho z_m\right] * \left[1 - erf\left(\frac{\chi}{2\alpha}\right)\right] \qquad (8)$$

The total emitted intensity I is then given by : $I = I_{E,l} + I_{E,r}$
Note that the indefinite integral (important when partial integration has to be applied, e.g. in thin-film applications) in the integration procedure is :

$$\frac{\varphi_m * \sqrt{\pi}}{2\gamma} * \exp\left[\left(\frac{\chi}{2\gamma}\right)^2 - \chi * \rho z_m\right] * \left[erf\left(\gamma * \rho z + \frac{\chi - 2\gamma^2 * \rho z_m}{2\gamma}\right)\right] + C$$

in which C represents a constant. The variable γ can be read either as α or β, whichever is appropriate.

BASIC STRATEGY FOLLOWED IN THE NEW MODEL

Since we prefer our new model to be based on recognizable and measurable parameters with a clear physical origin we selected as our independent input parameters the quantities $\varphi(o)$, ρz_m , *FI*, and α. It is our intention that each of these parameters is calculated through independent expressions which appear most appropriate at the moment. However, as mentioned before, it should remain possible at all times to change any of these formulations without any consequences to the mathematical functioning of the model (modular structure). It is clear, though, that if we want to calculate the generated and emitted intensities from our standards and specimen we definitely need to know β too. It follows that we have to find a way to determine the dependent parameter β by using the 4 independent parameters $\varphi(o)$, ρz_m , *FI, and* α. This must be done in such a way that the position of the maximum (ρz_m) in $\varphi(\rho z)$ remains at the prespecified position at all times. At the same time we demand that the integral of $\varphi(\rho z)$ (*FI*) takes the prespecified value and that the $\varphi(\rho z)$ curve starts at the selected surface ionization value $\varphi(o)$. Finally, we want to keep the decay rate α in the right hand Gaussian branch fixed. It is obvious that all these conditions can only be satisfied by varying β (increase rate in the left hand Gaussian branch), thereby varying the height of the maximum in $\varphi(\rho z)$ until the specified value of *FI* is found (for fixed $\varphi(o)$, ρz_m , and α). A useful relationship between the dependent parameter β and the other 4 independent parameters is already given in eqn. (5). Rearranging this equation and using the approximation given in eqn. (6) we can write :

$$\frac{\exp\left(\beta^2 * \rho z_m^2\right) - P_5}{\beta} + \frac{\exp\left(\beta^2 * \rho z_m^2\right)}{\alpha} - \frac{2 * FI}{\varphi(o) * \sqrt{\pi}} = 0 \qquad (9)$$

Note that β is also present in the input argument $\beta.\rho z_m$ for P_5 . It is clear that the last equation cannot be used to find a direct analytical solution for β. The only way towards a solution appears to be an iterative approach in which the function (*FCN*) :

$$FCN = \frac{\exp\left(\beta^2 * \rho z_m^2\right) - P_5}{\beta} + \frac{\exp\left(\beta^2 * \rho z_m^2\right)}{\alpha} - \frac{2 * FI}{\varphi(o) * \sqrt{\pi}} \qquad (10)$$

is minimized, i.e. brought as close as possible to zero by varying β. If the function *FCN* is investigated in detail as a function of β for a set of fixed $\varphi(o)$, ρz_m , *FI*, and α parameters it follows (Fig. V.3) that *FCN* varies in a monotonic way, starting at negative *FCN* values for small β, slowly increasing initially until *FCN* is zero, which is followed by a more rapid increase for larger β values. The iteration procedure we devised is simply based on a straight line approach :

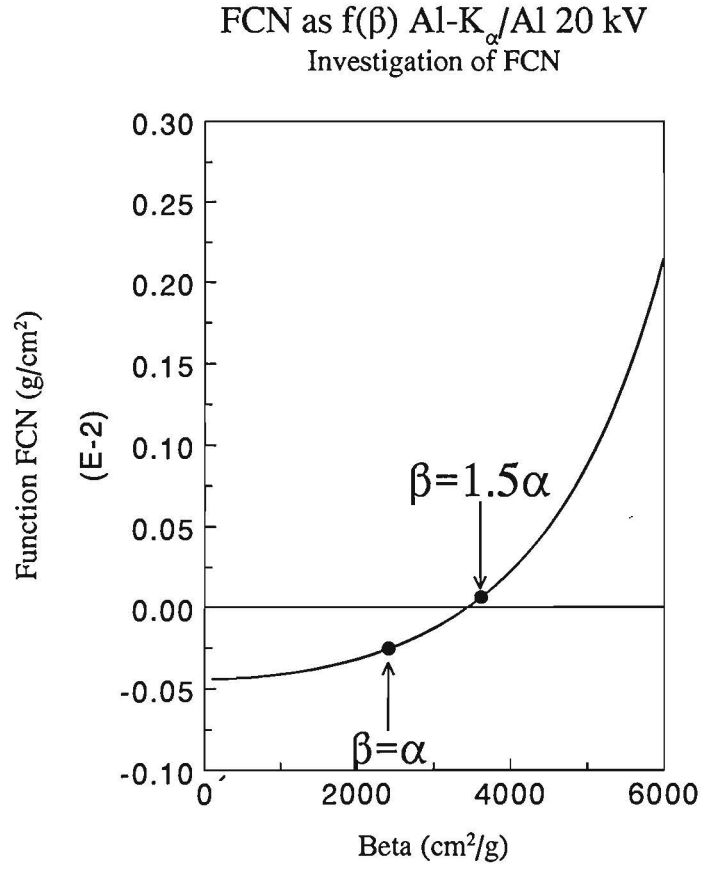

Fig. V.3. Variation in FCN (eq. 10) as a function of β for fixed values of α, $\varphi(o)$, ρz_m, and *FI*. The arrows show the initial estimates for β with which the iteration procedure, aimed at minimizing FCN, is started.

1. Start with two initial estimates for β : $\beta(0) = \alpha$ and $\beta(1) = 1.5 \, . \, \alpha$
2. Using eqn. (10) calculate the corresponding FCN values *FCN(0)* and *FCN(1)*.
3. Calculate the tangent and intersect of the straight line connecting $\{\beta(0),FCN(0)\}$ and $\{\beta(1),FCN(1)\}$, and determine subsequently where this straight line intersects the FCN=0 line.
4. For this particular value of β ($\beta(2)$) calculate the corresponding FCN value (*FCN(2)*).

Note : If $\beta(2)<0$ (this can happen for low overvoltage ratios) then α has to be increased in small increments of e.g. 1 % until a solution is found with $\beta(2)>0$. If a positive $\beta(2)$ value is found the procedure can be continued.

5. Calculate the integral using this $\beta(2)$ value. This will produce a value *F*, which will, in general, be different from the prespecified value *FI*.
6. Check the magnitude of the deviation between the prespecified *FI* and the calculated *F* values.
7. If $|(F - FI)/FI| < 10^{-5}$ (arbitrary threshold) the procedure can be stopped.
8. If the latter criterion is not met the procedure has to be continued at step 2 with new estimates for β :

$$\beta(1) = [\beta(0) + \beta(1)]_{old} /2 \text{ and } \beta(0) = \beta(2) \, .$$

ORIGIN OF INDEPENDENT INPUT PARAMETERS

Once the mathematical framework of the new model is understood it remains to explain how the four independent parameters α (decay rate in the right-hand Gaussian), ρz_m (position of the maximum in $\varphi(\rho z)$), FI (Integral of $\varphi(\rho z)$), and $\varphi(o)$ (surface ionization value) are obtained.

Decay rate α

The expression we currently use for α was obtained through fits to numerous $\varphi(\rho z)$ curves simulated with the MC5 Monte-Carlo program . The α-values were extracted from plots displaying $\ln(\varphi)$ vs. $(\rho z - \rho z_m)^2$ for a large range in wavelengths and in a variety of matrices: Be, Al, Cu, Ag, Au, and U. After the introduction of a parameter Q, defined by :

$$Q = \sqrt{\frac{Z/A * \ln\left(1.166 * E_o/J\right)}{E_o^{\,2} - E_c^{\,2}}}$$

in which Z, A, and J stand for the atomic number, atomic weight and ionization potential, respectively, of the matrix element in question and E_O and E_C are the accelerating voltage and critical excitation voltage of the X-ray line examined, it was observed that straight lines could be obtained when $\ln(\alpha/Q)$ was plotted vs. $\ln(E_O)$. For the various matrix elements the following data in terms of intercept (I) and slope (T) were obtained :

Matrix	I	T
Be	12.976021	0.8924
Al	12.840074	0.8313
Cu	12.912265	0.8455
Ag	12.655390	0.7500
Au	12.699802	0.7404
U	12.638304	0.7258

For each matrix element we can express : $\ln(\alpha/Q) = I - T \,.\, \ln(E_O)$
The intercept I could be fitted as :

$$I = 12.93774 - 0.003426515 \,.\, Z\,,$$

and the slope T as :

$$T = 1/(1.139231 + 0.002775625 \,.\, Z)$$

Hence, it follows that α can finally be expressed as :

$$\alpha = \frac{\exp(12.93774 - 0.003426515 * Z)}{E_o^{[1/(1.139231+0.002775625*Z)]}} * \sqrt{\frac{Z/A * \ln\left(1.166 * E_o/J\right)}{E_o^{\,2} - E_c^{\,2}}}$$

Notes :

1) In case of a compound target a matrix is calculated of α_i^n values representing α values for each element n-radiation in interaction with each element i in the target. The value of α for element n-radiation in the compound is then composed as follows :

$$1/\alpha^{n}_{Comp} = [\ \sum_i C_i * Z_i/A_i * (\ 1/\alpha_i^{n}\ )\ ] \Big/ [\ \sum_i C_i * Z_i/A_i\ ]$$

in which C_i represents the weight fraction of element i.

2) Originally, the fits were made with the expression of Zeller[30] for the ionization potential J. Later on Sternheimer's[31] equation was adopted. This produces small changes in α for ultra-light element matrices. However, for atomic numbers beyond 11 the differences are negligible. In the MC5 Monte-Carlo program, by the way, also Sternheimer's expression is used.

Position of the peak (ρz_m) in $\varphi(\rho z)$

Since it is very difficult to parameterize the peak position in absolute terms in a straight-forward manner it is advisable to try relating it so some other physical parameter which already contains a lot of the characteristics of the energy loss of the electrons and the associated production of x-ray photons in the matrix element in question. The most suitable choice is to link the peak position (henceforth denoted shortly by P) to the "Ionization range", which is nothing else than the total path length the electron travels between E_o and E_c. This ionization range (henceforth denoted by Ro) can be found by integrating an energy loss equation ($\partial E/\partial \rho s$, in which E is energy and s is path length) over the range ($E_o \rightarrow E_c$) in energy which can be used to excite a particular x-ray line. Following Pouchou and Pichoir[5,19] , and before them Love et al[24] , we use the modified slowing-down expression :

$$\partial E/\partial \rho s = -\frac{1}{J_c} * \sum_i \frac{C_i * Z_i}{A_i} * \frac{1}{f(V)}$$

with $V = E/J$ (E is voltage and J is ionization potential. For a compound target the ionization potential J_C is calculated according to :

$$\ln J_c = \left[\sum_i \frac{C_i * Z_i}{A_i} * \ln J_i \right] \Big/ \left[\sum_i \frac{C_i * Z_i}{A_i} \right]$$

The function f(V) is written as the sum of three terms[5,19] :

$$f(V) = \sum_{k=1}^{3} D_k * V^{P_k}$$

with : $D_1 = 6.6 \,.\, 10^{-6}$, $D_2 = 1.12 \,.\, 10^{-5} \,.\, (1.35 - 0.45\, J^2)$, and $D_3 = 2.2 \,.\, 10^{-6} / J$
and : $P_1 = 0.78$, $P_2 = 0.1$, and $P_3 = -\,(0.5 - 0.25 \,.\, J)$
After integration it follows that :

$$Ro = \frac{1}{\sum_i \frac{C_i * Z_i}{A_i}} * \sum_{k=1}^{3} J^{1-P_k} * D_k * \left(E_o^{1+P_k} - E_c^{1+P_k} \right) \Big/ \left(1 + P_k \right)$$

Pouchou and Pichoir used this Ro value for the calculation of their R_x parameter ("end" of the $\varphi(\rho z)$ curve). Their calculation of the peak position ρz_m (henceforth denoted shortly by P) takes place (using R_x) according to complex equations with many different parameters. We observed that essentially the same peak positions can be found by linking P directly to Ro, using an expression of the type :

$$\frac{P}{Ro} = a + b * \frac{\ln U}{U} + \frac{c}{U} \qquad (11)$$

in which U denotes the overvoltage ratio (E_O/E_C). The constant a could be parameterized as follows :

$$a = \exp\left[-0.6801 + 2.254 * 10^{-3} * Z * \sqrt{Z} - 0.09457 * \sqrt{Z} * \ln(Z) \right]$$

in which Z represents the atomic number of the matrix element. The constant b was fitted as :

$$b = -0.02887 - \frac{2.035}{\left(Z * \sqrt{Z} \right)} + 3.87 * \exp(-Z)$$

The constant c, finally, could be expressed by :

$$\frac{1}{c} = 27.78 - 6.123 * \sqrt{Z} - 52.96 * \frac{\ln(Z)}{Z}$$

In case of a compound matrix we use the weight fraction averaged atomic number Z_C defined by :

$$Z_c = \sum_i C_i * Z_i$$

When comparing the peak positions predicted by eqn. (11) with those in either measured or simulated (MC5-program) $\varphi(\rho z)$ curves we came across some peculiar discrepancies. While the agreement between the results of Monte-Carlo simulations and those of eqn. (11) was most satisfactory for both very low (< 6) as well as medium-to-high atomic numbers (>29) appreciable differences were observed for atomic numbers between 11 (Na) and 16 (S).
The maximum deviations we found correspond to Al at an overvoltage ratio U around 8 and were slightly over 15 % in the sense that the Monte-Carlo simulations yielded $\varphi(\rho z)$ curves with peaks much closer to the specimen surface. Unfortunately, the experimental evidence in this area is conflicting too. While Pouchou and Pichoir's[19] parameterization, and also eqn. (11), are in close agreement with the $\varphi(\rho z)$ measurements by Castaing and Henoc[32] (Mg tracer in Al matrix, a combination which gives rise to characteristic fluorescence in the tracer) they are partially in conflict with more recent determinations of Sewell et al[6] (Si tracer in Al). The latter results agree very well with the Monte-Carlo simulations at 10 kV and with eqn. (11) at 20 kV. At 15 kV, however, the results are intermediate between the two procedures. Since the experimental evidence is not conclusive and our new correction procedure is meant to be modular in structure, which makes it easy to switch from one parameterization to another, we decided to make a separate parameterization which follows the Monte-Carlo simulations more closely. Again, we linked the peak position P directly to Ro, this time according to the expression :

$$\frac{Ro}{P} = a + \frac{b}{\sqrt{U}} + \frac{c}{\left(U * \sqrt{U}\right)} \qquad (12)$$

in which a is :

$$a = 2.1040483 + 0.044934014 * Z * \sqrt{Z} - 5.518453 * 10^{-4} * Z^2 * \sqrt{Z} + 2.46257718 * 10^{-5} * Z^3$$

and b can be described by:

$$\ln(b) = 2.6219621 - \frac{2.5091694}{\sqrt{Z}} - \frac{4.6725352}{Z}$$

Finally, c can be expressed as:

$$\sqrt{c} = \frac{\left(3.2561755 - 0.060134019 * Z + 1.2310844 * 10^{-3} * Z^2\right)}{\left(1 - 1.7374036 * 10^{-2} * Z + 2.524835 * 10^{-4} * Z^2\right)}$$

For the time being we have selected eqn. (12) as the standard setting for the peak position in the PROZA96 program.

Integral of φ(ρz) (*FI*)

Essentially the atomic number correction of Pouchou and Pichoir[4] is being used as the basis for the calculation of *FI* in this new model (as in its predecessor "PROZA"). In spite of numerous attempts we have not seen, so far, an atomic number correction giving better results on the data bases we use for testing correction programs. The calculation of backscatter and stopping power corrections, in order to find the primary intensity (*PI*) generated in the specimen, proceeds, therefore, along the lines described earlier[5,19]. We did make two alterations, however, :

1) We replaced Zeller's[30] expression for the ionization potential J by Sternheimer's[31] formulation. This was done because significantly better results were obtained with the new program on our data bases of ultra-light element measurements when the latter equation was used.

2) We made some modifications in the coefficient m used in the expression for the ionization cross-section :

$$Q(U) \propto \frac{\ln(U)}{U^m * E_c^2}$$

Contrary to Pouchou and Pichoir we use the value of 0.9 for m in case of K-lines, with an exception for the ultra-light element radiations C-Kα (m=0.888), N-Kα (m=0.86), and O-Kα (m=0.89). The latter values were deduced from our own measurements of relative emitted intensities as a function of accelerating voltage. For L- and M-lines the values of 0.82 and 0.78, proposed by Pouchou and Pichoir, are still being used.

After the calculation of the backscatter factor R and the stopping power factor $1/S$ the primary intensity generated in the specimen can be calculated according to :

$$PI = R * 1/S$$

By definition :

$$PI \propto Q(U_0) * FI \qquad \text{with} \qquad FI = \int_0^\infty \varphi(\rho z) d(\rho z)$$

The use of *PI* as a basic parameter ensures that the integral *FI* represents correctly the the primary intensity generated by the incoming electrons, **independent** of the shape parameters of the φ(ρz) curve.

Surface ionization value *φ(o)*

In 1988 Rehbach and Karduck[33] proposed an expression for *φ(o)* which was partially based on experimental *φ(o)* values (for soft X-rays) and partially on Monte-Carlo simulations (for the full range of X-rays used in EPMA) :

$$\varphi(o) = 1 + \left(1 - 1/\sqrt{U_0}\right)^a * b \tag{13}$$

with $$a = \left(1 + 0.005 * Z/E_c\right) * \left(0.68 + 3.7/Z\right)$$

and

$$b = \left(1 + 0.05/E_c\right) * \left(-0.01 + 0.04805 * Z - 0.51599 * 10^{-3} * Z^2 + 0.20802 * 10^{-5} * Z^3\right)$$

A noticeable feature of this equation is that it contains E_C (the critical excitation threshold of the X-ray line in question) in an explicite form, which is not common in most *φ(o)* expressions.

We have fitted our own expression for *φ(o)*, in which our extensive experimental data from thin-film measurements on supported and unsupported Al- and Pd -films (Bastin et al[34]) have been used in addition to some data (for ultra-light element radiations) generated by the Rehbach and Karduck[33] expression. We arrived at an expression with the same U_O dependence as Rehbach and Karduck (eqn. 13), however, without the necessity to introduce an explicite E_C dependence into the parameters *a* and *b*. Our parameters are only dependent on the atomic number *Z* of the matrix element :

$$a = 0.61747243 + 1.0991805 * 10^{-3} * Z + 1.224221/\sqrt{Z}$$

$$b = -0.21964478 + 0.11332964 * Z - 2.0638629 * 10^{-2} * Z * \ln Z$$

In the case of a compound matrix we calculate $\varphi(o)$ by using the weight fraction averaged atomic number.

There are other, simple[35] or very complex[36], expressions for $\varphi(o)$ which we will not discuss here in detail. Fig V.4 shows the importance of the value of the surface ionization in the case of a heavily absorbing matrix.

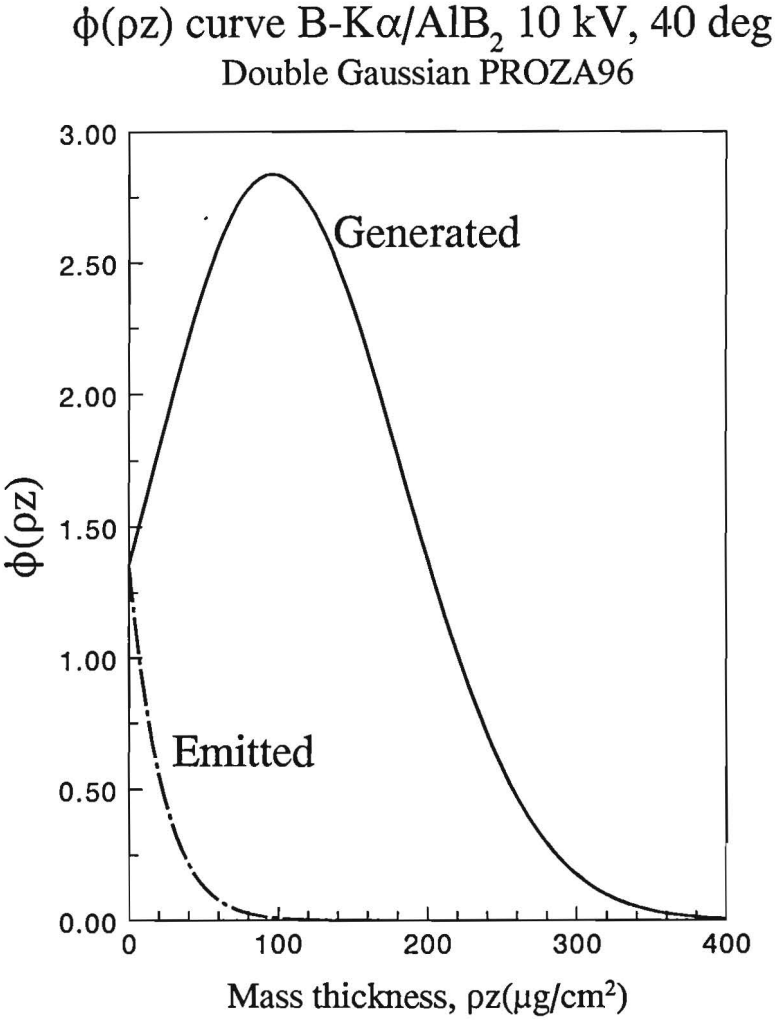

Fig. V.4. Example of a φ(ρz) curve for B-K_α radiation in an extremely highly absorbing system, e.g., in AlB_2 at 10 kV. The solid curve represent the generated intensity; the broken curve the emitted intensity. Note that the emitted intensity is almost exclusively due to the surface ionisation $\varphi(o)$ and the very first part of the φ(ρz) curve. X-ray take-off angle 40 deg.; mass absorption coefficients for B-K_α : in Al 64,000, in B 3,350.

V.2 PERFORMANCE OF THE NEW MODEL

On the grounds discussed in the introduction the increased flexibility of the new model in terms of manipulation of peak position is expected to pay off most in ultra-light matrices and at high overvoltage ratios, conditions where the peak in $\varphi(\rho z)$ has to move to very large depths in the specimen. In general, this will be the case in analyses of ultra-light element radiations, at least as far as the pure (light) element standard is concerned. We can, therefore, expect improvements particularly in the present case of Boron analyses. Nevertheless, we will concern ourselves first with an assessment of the performance of the new model on previous data.

V.2.1 Medium-to-heavy element analyses

The composition of the original data base and the origin of the measurements contained in it have been discussed in detail in Ref. 10. In the past decade this data base has been considerably expanded and at the same time some notorious flyers have been removed. At present it contains 1113 carefully selected and consistent measurements.

In assessing matrix correction programs it is standard practice to calculate the expected k-ratio (k') with a particular program using the (supposedly) known composition and accelerating voltage for each entry in the data base. This k' value is then compared to the measured one (k) and the results are finally displayed in a histogram, displaying the number of analyses vs. k'/k. The narrowness of the histogram, expressed in terms of the relative root-mean-square deviation (in %), together with the mean k'/k value, are then regarded as a measure of success.

The results obtained on this data base (using Heinrich's[37] mac's with a few exceptions) with 9 current correction programs are graphically displayed in Figs. V.5 and V.6 as histograms representing the number of analyses vs. the ratio between calculated and measured k-ratios. The relative root-mean-square values (r.m.s., in %) and the mean k'/k values are given in Table V.1. It is clear that our newest program (PROZA96) offers such a good performance that it can be ranked among the very best programs currently available.
Note that for the double parabolic PAP program 25 analyses have been removed from the results because we did not program all the necessary routines for proper functioning of the program at extremely low overvoltage ratios.
The ZAF and RUSTE programs develop a very long tail towards higher k'/k ratios, which is entirely due to the very poor performance on Al and Si measurements in highly absorbing matrices (Ni, Fe) at higher voltages. This is a demonstration of the failure of the absorption correction ("simplified" and "full" Philibert correction, respectively) of these programs. To a slightly lesser extent the LOSCO851 program, with Bishop's "square" absorption correction model, shows the same trend. It is noticeable that the "quadrilateral" absorption correction scheme in the SELOS85 and SELOS91 programs produces a genuine improvement in performance in terms of r.m.s. values, although a slight bias in mean k'/k value now becomes visible. The improvement in the parameterization for the quadrilateral model in SELOS91 only leads to a minor improvement in r.m.s. on this data base.

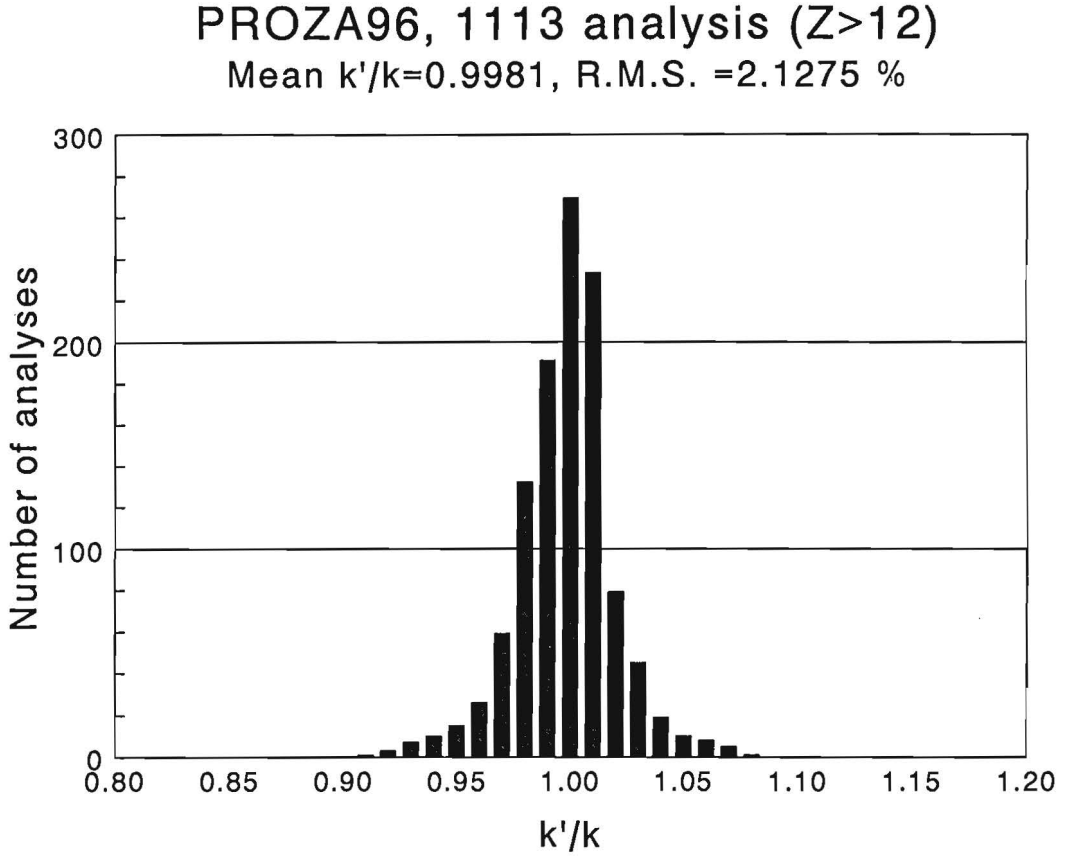

Fig V.5. Performance of our new PROZA96 matrix correction program on a database containing 1113 analyses of medium to heavy elements (Z > 11). The number of analyses have been plotted vs. the ratio between the calculated (k') and the measured k-ratio (k) for the given composition and accelerating voltage in the data base.

Table V.1

Relative root-mean square values and averages obtained with nine current correction programs on 1113 medium-to-heavy element (Z>11) analyses. The calculated k-ratio (k') is compared to the measured one (k).

Program	Mean k'/k	r.m.s.(%)
PROZA96	0.9981	2.1275
PROZA	0.9926	2.1063
PAP (DP)	0.9957	2.2566
XPP	0.9971	2.0110
LOSCO851	0.9962	3.2916
SELOS85	0.9899	2.5747
SELOS91	0.9873	2.4298
ZAF	1.0104	4.1848
RUSTE	1.0120	5.4986

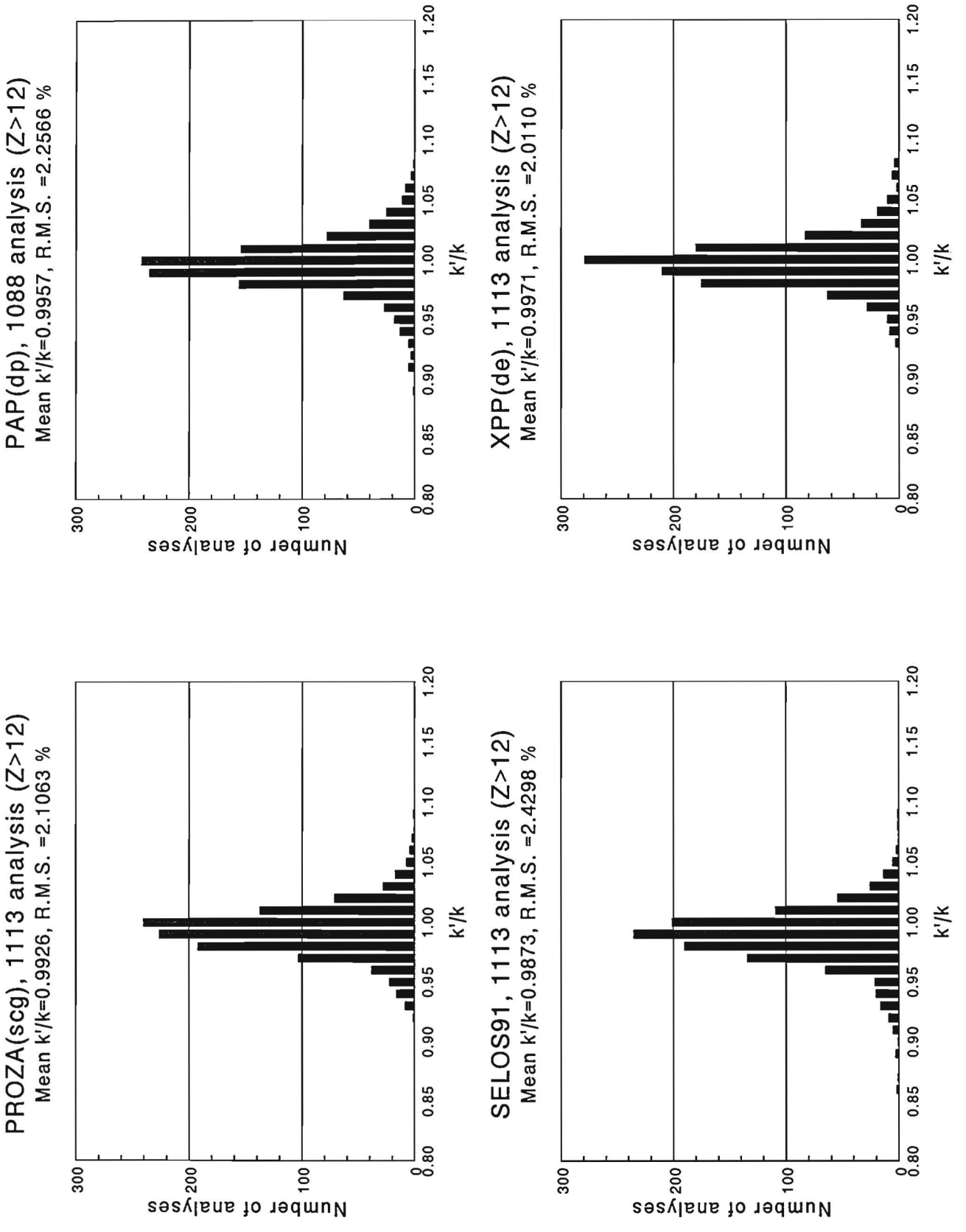

Fig V.6.a. Performance of PROZA, PAP, XPP, and SELOS91 matrix correction programs on a database containing 1113 analyses of medium to heavy elements (Z > 11). The number of analyses have been plotted vs. the ratio between the calculated and the measured k-ratio for the given composition and accelerating voltage in the data base.

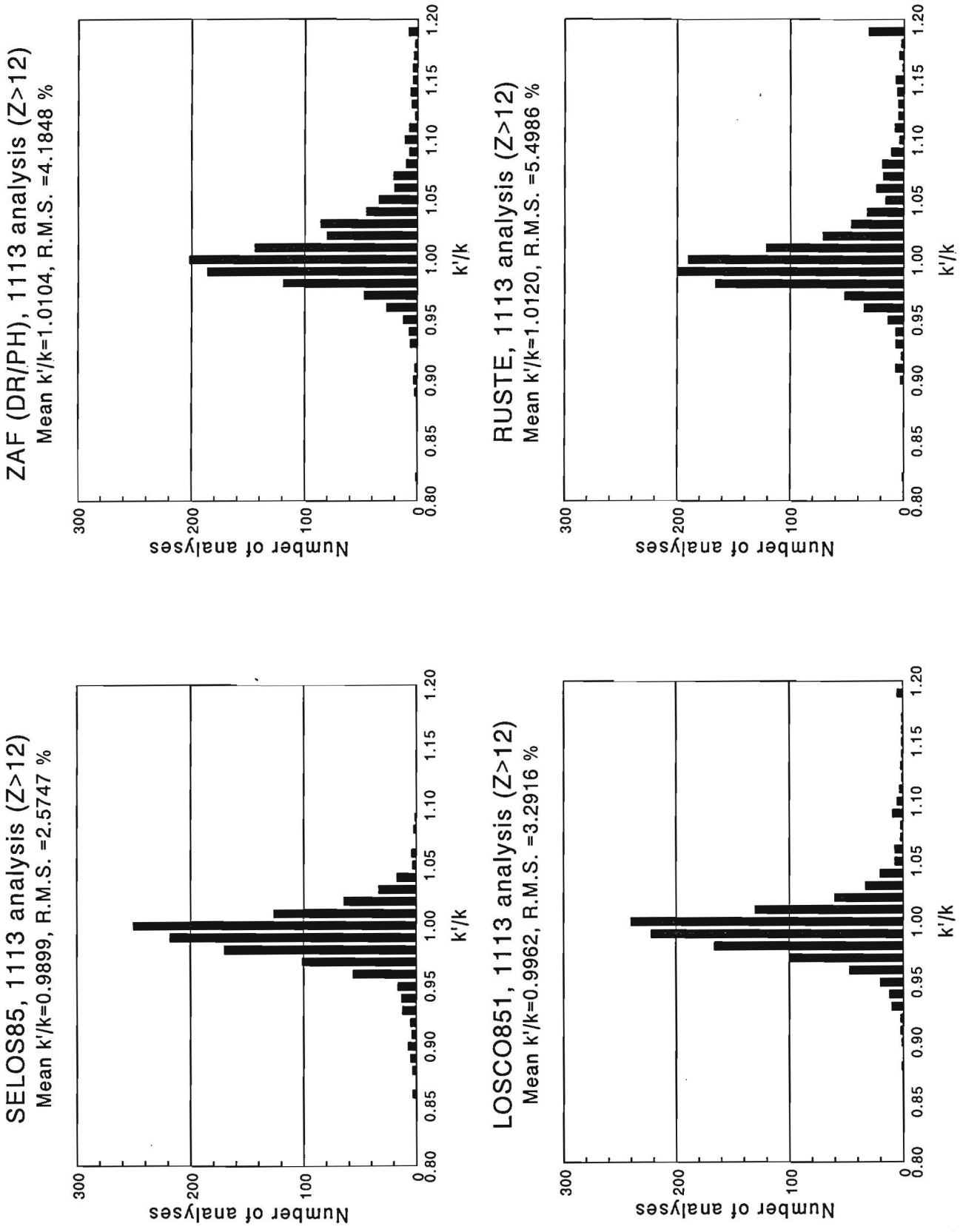

Fig V.6.b. Performance of SELOS85, LOSCO851, ZAF, and RUSTE matrix correction programs on a database containing 1113 analyses of medium to heavy elements (Z > 11). The number of analyses have been plotted vs. the ratio between the calculated and the measured k-ratio for the given composition and accelerating voltage in the data base.

V.3 Results from the present work

V.3.1 Metal analyses in binary borides

In this case the data base consists of 196 analyses (smoothed k-ratios, 4-30 kV). The results obtained with nine correction programs are graphically represented in Figs. V.7 and V.8, while the averages and r.m.s. values are given in Table V.2. Most programs have a tendency to develop a second "peak" or tail in their histograms, which can be either on the right or the left hand side of the mean k'/k value. In all cases this is due to relatively large errors for the Al- and/or the Si-borides. Apparently all atomic number corrections have great difficulties in dealing with these particular cases, particular in the sense that these compounds contain very large amounts of Boron on a weight fraction basis. The observed deviations may entirely be due to the fact that the interaction between the Al-K_α line and Boron as a matrix element is not properly described in most programs. The choice of an expression for the Ionization potential (J) is crucial, in this respect. Due to the large weight fraction of Boron in these compounds a fairly large proportion of this interaction will be revealed in the process of composing the interactions on a weight fraction basis. Such discrepancies would completely be obscured in heavy-metal borides due to the much smaller Boron content. It is interesting to point out the differences between the histograms of the PROZA96 and PROZA programs. In the former program we only replaced Zeller's J by Sternheimer's, with, as a result, the disappearance of the additional separated distribution between k'/k values of .92 and .95 in the PROZA histogram, which were entirely due to the Si-borides. In the histograms of the PAP and XPP programs, with identical atomic number corrections as PROZA, and the same Ionization potential of Zeller, the additional peak at low k'/k values is due to the Si-borides. In the LOSCO851, SELOS85, and SELOS91 programs, all with the same atomic number correction and Ionization potential (Bloch[38]), the same effect shows up, and again it is produced by the Si-borides. When using the ZAF and RUSTE programs the additional distribution is found on the high side of the mean k'/k value, and this time it is caused by the Al-borides. A possible explanation could be, of course, that the compositions of these compounds (which are supposed to be line compounds in the case of Al) are not what the latest phase diagrams suggest. It remains peculiar, however, that the results produced by the various programs on the same set of measurements in the same class of compounds (Al or Si borides) can end up either in the high or the low end of the histogram, merely by selecting a different atomic number correction. Therefore, as long as there is nothing else to go on, and, until new evidence is produced, we have to assume that the programs do not function well. The top 4 programs in Table V.2 perform best on the metal-boride data base. It is rather peculiar that the ZAF program is the worst, considering the fact that it performs best on analyses of metal lines in carbides[1]. This probably underlines the problems in making definite statements on the performance of correction programs because the results may to some extent be dependent on the particular type of data base used and it is very difficult to arrive at general conclusions. The differences in performance between carbides and borides must probably be attributed to the differences in average carbon content as compared to boron content and, hence, also to the different ways that interaction parameters are composed in the various programs. It is interesting to note that SiC (very high carbon content) in the carbide data base used to present a difficult problem for the metal X-ray line in most correction programs. In the present case AlB_2 and AlB_{12} ,also containing large amounts of the ultra-light element, present problems for most correction programs and again, the origin of these problems is difficult to understand.

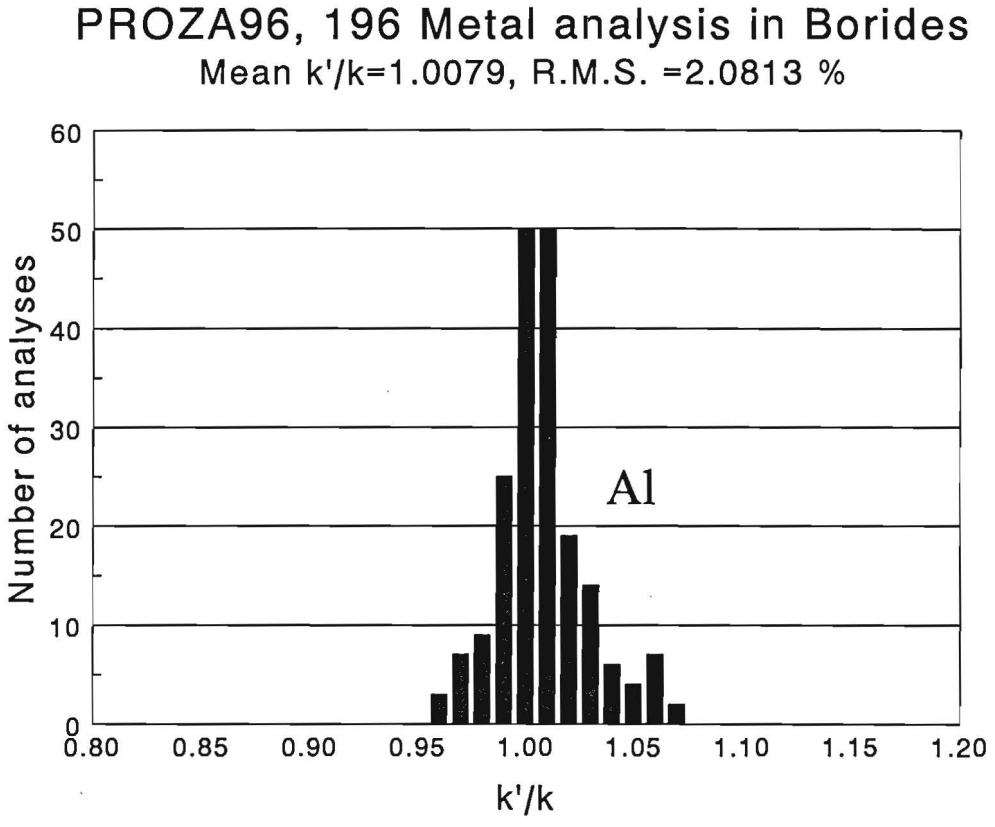

Fig V.7. Performance of our new PROZA96 matrix correction program on a database containing 196 metal analyses in binary borides. The number of analyses have been plotted vs. the ratio between the calculated and the measured k-ratio for the given composition and accelerating voltage in the data base.

Table V.2

Relative r.m.s. values and averages obtained with 9 current correction programs on 196 metal analyses in binary borides. The calculated k-ratio is compared to the measured one.

Program	Mean k'/k	r.m.s.(%)
PROZA96	1.0079	2.0813
PROZA	0.9896	2.2754
PAP(DP)	0.9923	2.2655
XPP	0.9949	2.2666
LOSCO851	0.9905	2.3228
SELOS85	0.9904	2.3098
SELOS91	0.9865	2.3131
ZAF	1.0078	2.7382
RUSTE	0.9964	2.3444

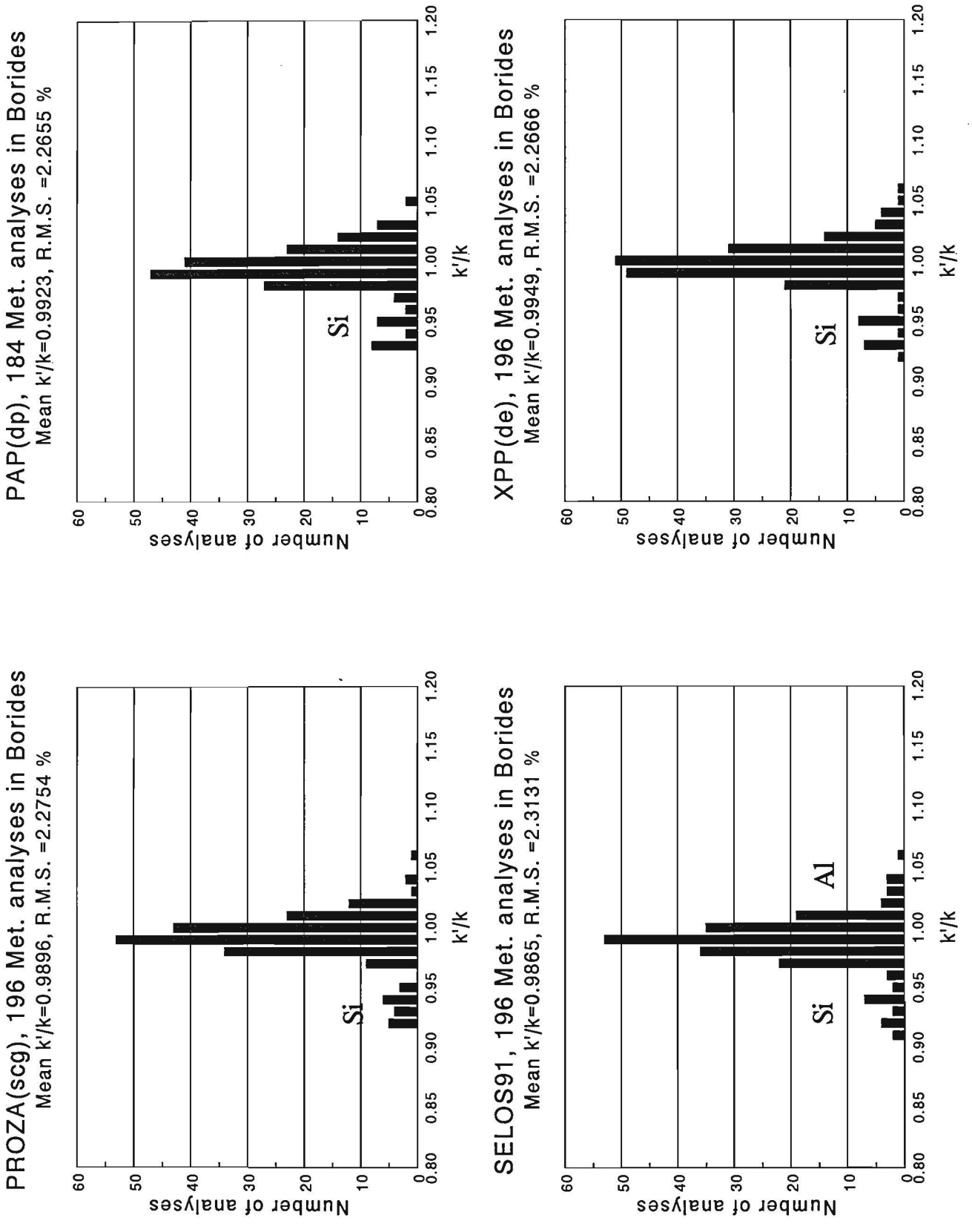

Fig V.8.a. Performance of PROZA, PAP, XPP, and SELOS91 matrix correction programs on a database containing 196 metal analyses in binary borides. The number of analyses have been plotted vs. the ratio between the calculated and the measured k-ratio for the given composition and accelerating voltage in the data base.

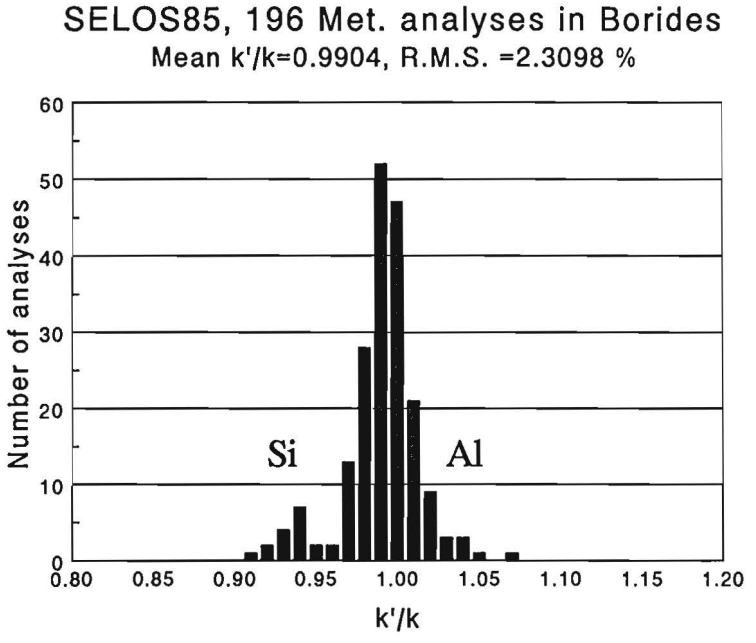

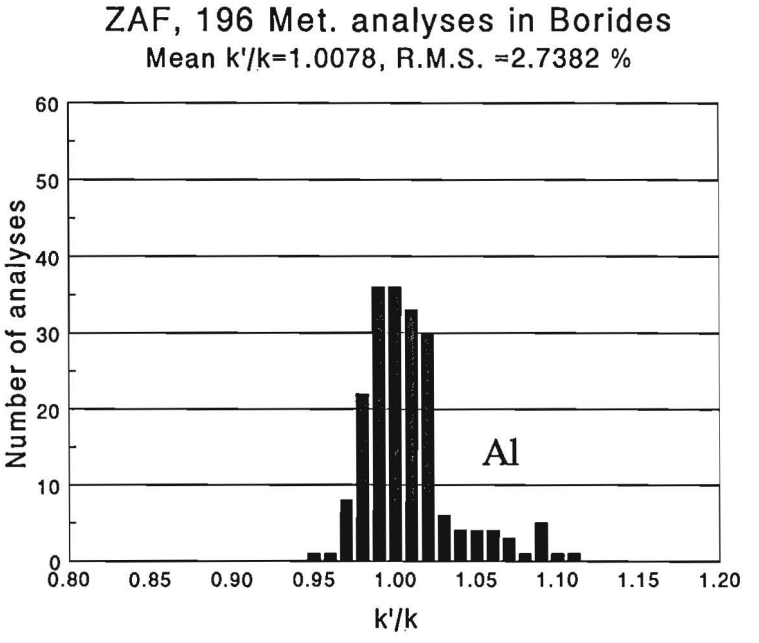

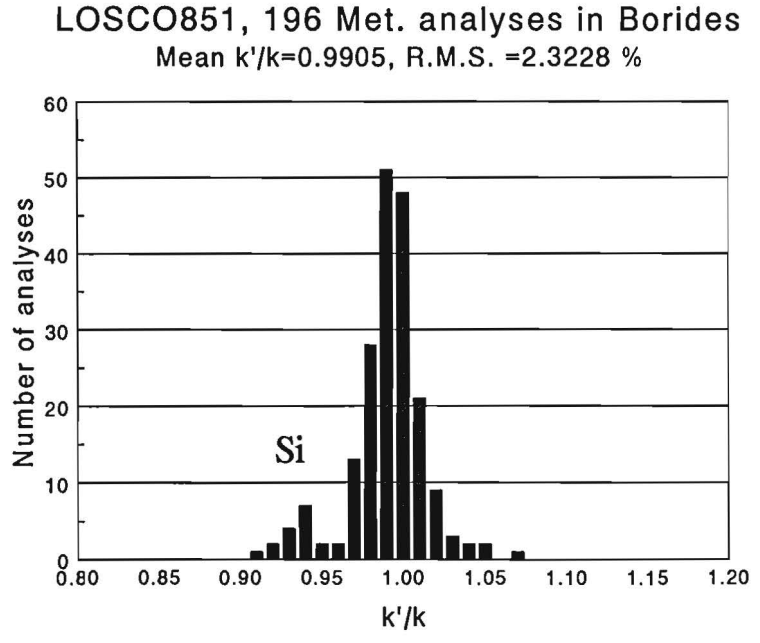

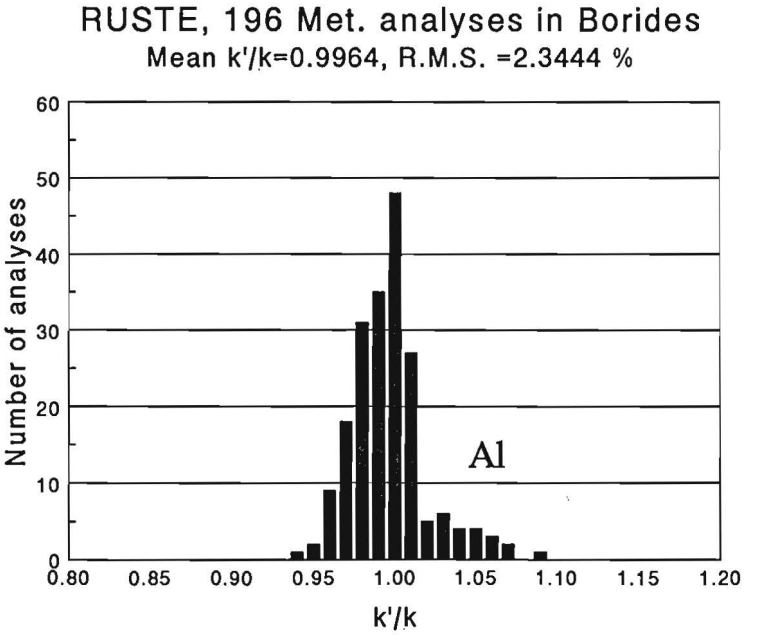

Fig V.8.b. Performance of SELOS85, LOSCO851, ZAF, and RUSTE matrix correction programs on a database containing 196 metal analyses in binary borides. The number of analyses have been plotted vs. the ratio between the calculated and the measured k-ratio for the given composition and accelerating voltage in the data base.

From a general point of view it must be concluded that none of the existing programs really performs well enough to let them be used in an analysis "by difference" as huge errors in the boron-content are likely to be the result.
Measuring ultra-light elements "by difference", is by the way, a procedure which we would not recommend in general, because small errors in the metal content will enlarge to 5 or 10 times this error in the boron (or carbon) content. Instead, it is much more advisable to measure the light element directly and take the metal "by difference". Best of all, of course, is it to measure both.

V.3.2 Boron Analysis

Finally we arrive at the main subject of the present work which is Boron analysis, of course. As we have already pointed out in chapter I and II matrix correction in ultra-light element work is just as much a question of the correction program as of the mass absorption coefficients which are probably not available with sufficient accuracy (< 1%). In the case of Carbon analysis[1-3] we have shown that there are several discrepancies in the available m.a.c.'s, especially in cases close to the M5 absorption edge (Zr, Nb, Mo). The observed discrepancies between calculations with a particular program and the measurements in a sequence of neighboring element borides or carbides cannot be attributed to a malfunctioning of the particular correction program, simply because the measurements were carried out relative to a complex standard (Fe_3C) and any program based on an adequate absorption correction should be able to deal with such cases. This is substantiated by the observation that the improved absorption correction in the SELOS programs, when our set of m.a.c.'s are being used, gives markedly improved results on the Carbon data base as compared to the inadequate square model used before (LOSCO851).

Similar experiences were made on the Boron data base. The use of Henke's sets of m.a.c.'s for B-K_α (Table II.1) led to r.m.s. values well beyond 20% for all 9 correction programs and this was entirely caused by erroneous values for Zr, Nb, Mo and La; i.e. again in cases close to absorption edges. Especially in ZrB_2 and LaB_6 the corrected concentrations exceeded the nominal values by 100% already beyond 20 kV, thus indicating that the m.a.c.'s in these metals are markedly too high. Henke's values for the transition elements, on the other hand, led to quite satisfactory results in the majority of cases for those programs with adequate absorption corrections. A series of calculations finally led us to adopt the set of m.a.c.'s given in Table II.1 and these values were used in the final comparison of the various programs. The resulting histograms are given in Figs. V.9 and V.10 and the averages and r.m.s. values in Table V.3. The results indicate that unexpectedly good results can be obtained for an ultra-light element like Boron. In fact, the results for the PROZA96 program are substantially better even than the rms value of 3.31% suggests. The results for each individual compound frequently have an rms value well below 3.31% as Table V.4 indicates. The good results in terms of individual rms values are largely spoiled by the fact that systematic anomalies occur in the Ni-borides and, to a lesser extent, in the Co-borides, resulting in what appears to be an abnormally low emission of B-K_α X-rays from these compounds (See also paragraph on relative emitted intensities). The very low rms values that can be obtained in these cases with mac's substantially lower than those reported in Table II.1 (lower than 33,000 for Ni) rule out the possibility of any malfunctioning of the correction program. Nevertheless, all tested programs, however bad their absorption correction may be, will show a pronounced dip in the calculated concentrations for

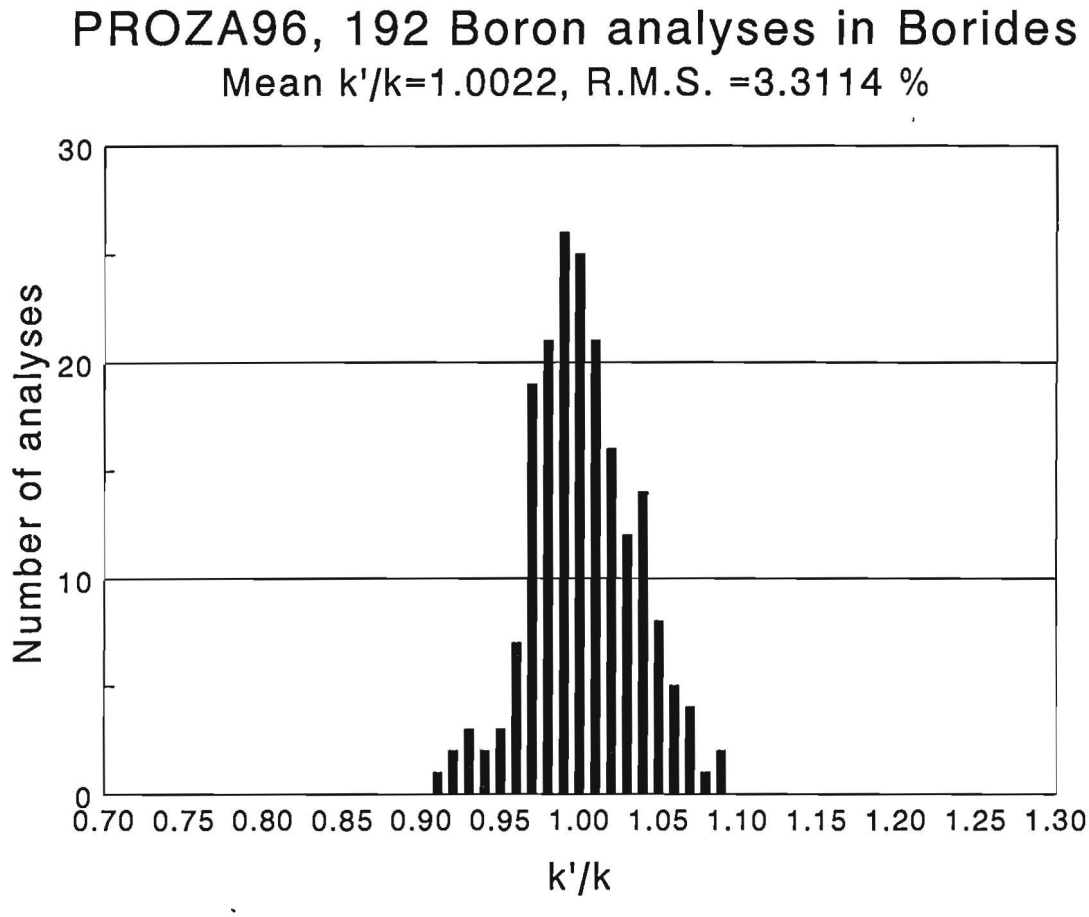

Fig V.9. Performance of our new PROZA96 matrix correction program on a database containing 192 boron analyses in binary borides. The number of analyses have been plotted vs. the ratio between the calculated and the measured k-ratio for the given composition and accelerating voltage in the data base.

Table V.3

Relative r.m.s. values and averages obtained with 9 current correction programs on 192 Boron analyses in binary borides.

Program	Mean k'/k	r.m.s.(%)
PROZA96	1.0022	3.3114
PROZA	1.0009	5.8646
PAP(DP)	0.9998	4.3744
XPP	0.9987	4.6991
LOSCO851	1.0781	14.6202
SELOS85	1.0045	12.8686
SELOS91	0.9814	4.9950
ZAF	1.0019	12.8484
RUSTE	0.9821	9.6091

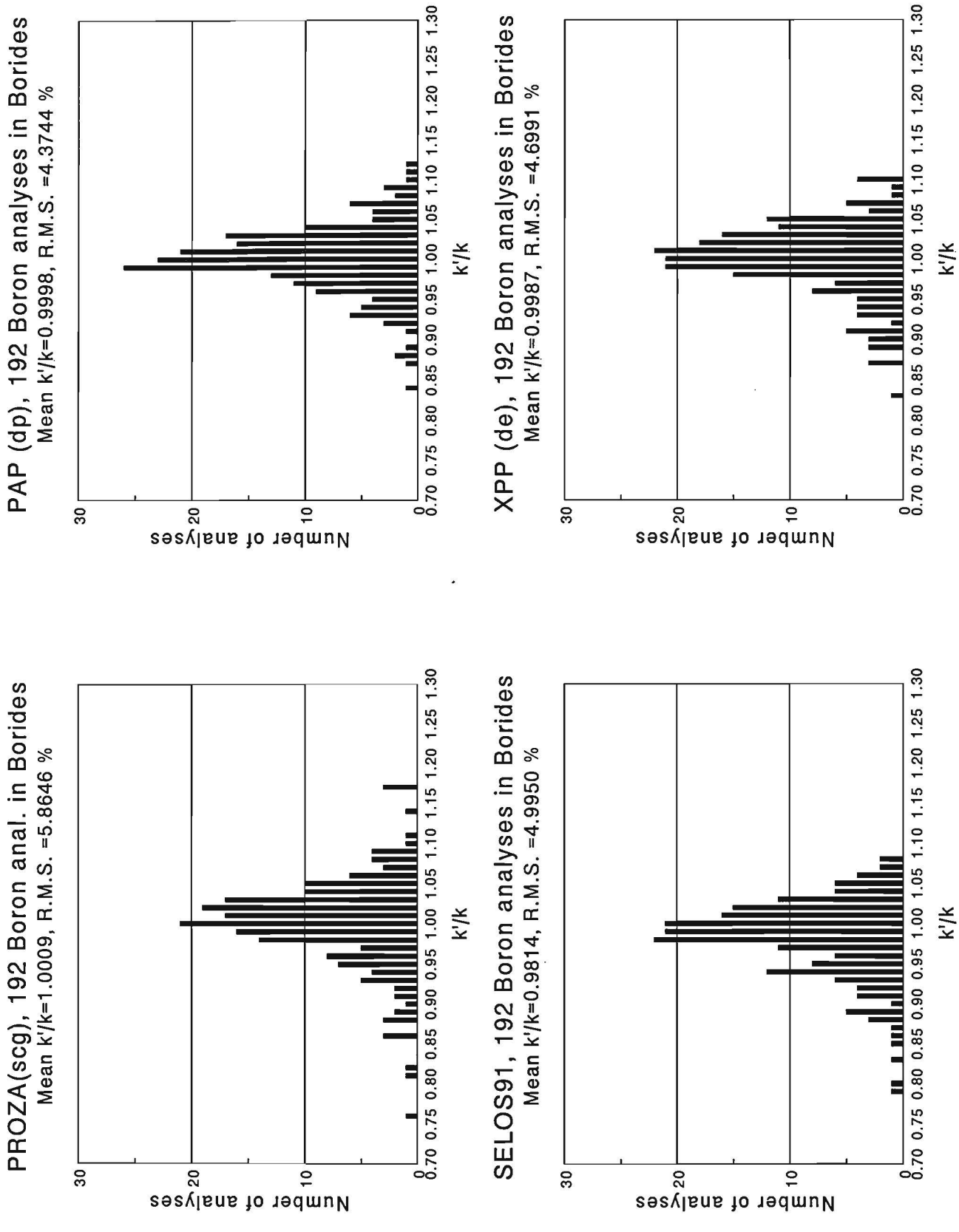

Fig V.10.a. Performance of PROZA, PAP, XPP, and SELOS91 matrix correction programs on a database containing 192 boron analyses in binary borides. The number of analyses have been plotted vs. the ratio between the calculated and the measured k-ratio for the given composition and accelerating voltage in the data base.

Fig V.10.b. Performance of SELOS85, LOSCO851, ZAF, and RUSTE matrix correction programs on a database containing 192 boron analyses in binary borides. The number of analyses have been plotted vs. the ratio between the calculated and the measured k-ratio for the given composition and accelerating voltage in the data base.

Table V.4

Results obtained with the PROZA96 program in the Boron analysis of individual borides

Compound	Mean k'/k	r.m.s.(%)
B_4C	0.9967	1.1547
BN(Cub.)	1.0000	0.8165
B_6O	0.9867	1.2472
AlB_2	0.9967	4.2295
AlB_{12}	0.9922	3.3259
SiB_3	0.9967	3.9016
SiB_6	1.0050	3.0957
TiB	0.9689	1.4487
TiB_2	1.0067	2.5820
VB_2	0.9983	1.9508
CrB	1.0000	1.7321
CrB_2	1.0200	1.2910
Fe_2B	0.9767	3.0368
FeB	1.0433	0.9428
Co_2B	1.0350	2.6300
CoB	0.9950	1.8930
Ni_3B	1.0083	3.6705
Ni_2B	0.9717	4.4127
NiB	1.0200	4.7610
ZrB_2	0.9967	1.8856
NbB	0.9967	1.4907
NbB_2	0.9950	1.5000
MoB	0.9933	1.8856
LaB_6	1.0178	3.2584
TaB	1.0267	5.3437
TaB_2	1.0117	4.3748
WB	1.0150	3.6401
UB_4	1.0183	2.6719

the Ni-borides if such low mac's are used. It is interesting to point out that similar anomalies have been reported[39] for the emission and absorption characteristics of the Ni-L_α X-ray line in Ni-compounds. In that case it has been suggested that the transition probabilities and the absorption properties of Ni are strongly influenced by the structure of the valence band and this may very well apply here too. Most likely the X-ray fluorescence yield for B-K_α in Ni compounds may be structurally lower than expected; this would manifest itself in an increased Auger yield which can perhaps be measured. From a chemical point of view these effects are quite exciting because they may reveal a lot of valuable information on the nature of the chemical bond in these compounds. A cooperation with experts in this field in order to clarify the nature of the observed discrepancies has not been successful.

A final remark must be made on the measurements in hexagonal BN. In this particular case 4 efforts have been done to measure the B-K_α k-ratio over the full range of 4-30 kV. In spite of all efforts, however, no consistent measurements were found possible below 10-12 kV, due to the very low electrical conductivity of the specimen. Much later, we were able to repeat the measurements on Cubic BN, which obviously has sufficient electrical conductivity to carry out meaningful and consistent EPMA measurements without any conductive coating. The latter data have been used in the present work.

The use of a conductive Carbon coating can, sometimes, produce acceptable results. However, there will always remain some doubts because, in our opinion, the application of a coating merely prevents surface charging without altering anything in the intrinsic conductivity in the specimen[40]. Hence, it seems unlikely that the real $\varphi(\rho z)$ curves in such specimens are in agreement with the calculated ones. It is more likely that the space charge, produced by the high-energy electrons inside a non-conducting specimen, will lead to a distortion of the expected $\varphi(\rho z)$ curve. Such a distortion will be very difficult to model and, at present, we do not know about any matrix correction program that can take such effects into account.

As far as the results of the LOSCO851, ZAF and RUSTE programs are concerned we can be rather brief: The obtained rms values indicate and confirm what was to be expected, namely that the absorption corrections in these programs are totally inadequate. They may, however, occasionally produce good results in cases like the lighter borides (B_4C, AlB_{12} etc.). They show a complete break-down in cases of really heavy absorption (AlB_2, SiB_3 etc.) at higher voltages and in compounds like ZrB_2 (LOSCO851, with calculated concentrations almost 1.5 times the nominal one) or LaB_6 (LOSCO851 : 2.2 times the nominal composition at 30 kV; RUSTE: 1.28 times and ZAF: 1.53 times). Needless to say that such pronounced deviations ruin the corresponding histograms (Fig. V.10.b).

The absorption correction scheme in the SELOS85 program (quadrilateral model), which was supposed to bring major improvements, does not raise much the level of performance in terms of r.m.s., compared to LOSCO851. It only produces an improved distribution around k'/k values of 1. This must mainly be attributed to a better performance in the lighter borides at not too high voltages. From Ti onward, however, it becomes evident that the new model may occasionally perform much worse than the original model used in LOSCO851 and this is especially noticeable at higher voltages (from 12 kV on) in heavier matrices (from TiB on). In such cases significant overcorrection for absorption takes place leading to calculated concentrations of approx. 1.5 times the nominal ones in TiB, 1.3 in TiB_2, 1.65 in ZrB_2 and even 1.91 in LaB_6. It should be noted that in many cases this effect is obscured because its onset at 12-15 kV almost coincides with the end of the measured range in accelerating voltages.

The malfunctioning of the absorption correction is enhanced by peculiarities in the atomic number correction (in both LOSCO851 and SELOS85), which we have pointed out before[10] . In TiB and heavier borides the Z-factor, which by definition represents the ratio between the intensities generated in elemental Boron and the boride specimen, has a tendency to increase at an ever increasing rate beyond 15 kV ($U_0 > 80$). While the increase between 4 and 6 kV in e.g., ZrB_2 is of the order of 1-1.5%, which seems reasonable, it suddenly becomes of the order of 10% between 15 and 20 kV; finally yielding Z-factors well exceeding 1 at 30 keV. It seems highly unlikely that at 30 kV more intensity is generated in the standard than in the boride. Hence, it follows that there must be something wrong in the atomic number correction for ultralight elements at high overvoltage ratios. Actually, it is a polynomial expression, used in the parameterization for one of the components in the backscatter factor R, which runs out of control at high overvoltage ratios in heavy matrices (1986). Apart from that it would appear that the parameterization for the quadrilateral absorption correction model needs reexamining at high overvoltages in heavy matrices as its performance in such cases is definitely unsatisfactory. As a matter of fact, this is exactly what the authors have done in the meantime. They have repaired the error in the atomic number correction and they undertook an optimization exercise for their main parameter ρz(mean) in the quadrilateral model, in which they made extensive use of our Boron and Carbon data files. The resulting SELOS91 program indeed performs remarkably much better now, although, at present there seems to be a slight bias in the mean k'/k value. A similar bias was already found on the medium-to-high Z data base, as well as on the metal analyses in the borides.

As far as the mass absorption coefficients are concerned the values we propose (Table II.1) are compared to those provided by Henke in Fig. V.11. It is evident that in general our values agree fairly well with those of Henke. Significant deviations are only apparent close to the absorption edges (Zr, Nb, Mo, La). It must be remarked that, although the absolute values of the m.a.c.'s we propose may be slightly dependent on the particular program used, the general trends should be correct. A similar experience was made in the case of Carbon where all realistic absorption corrections have been found to perform best with the set of m.a.c.'s we proposed.

VI CONCLUSIONS

As a general conclusion of the present work it seems to be justified to state that:

1. Accurate intensity measurements for Boron-K_α are possible, provided that the important variations in the shapes of the emitted B-K_α profiles are properly taken into account. The effects of peak shape alterations are less severe when a Synthetic Multilayer rather than a conventional Pb-stearate analyzer crystal is used. Even then, however, they cannot be ignored.
2. Accurate matrix correction for Boron is possible, in spite of the very extreme conditions encountered. The accuracy which can be achieved, nowadays, with several current correction programs, is almost comparable with that in the analysis of much heavier elements.

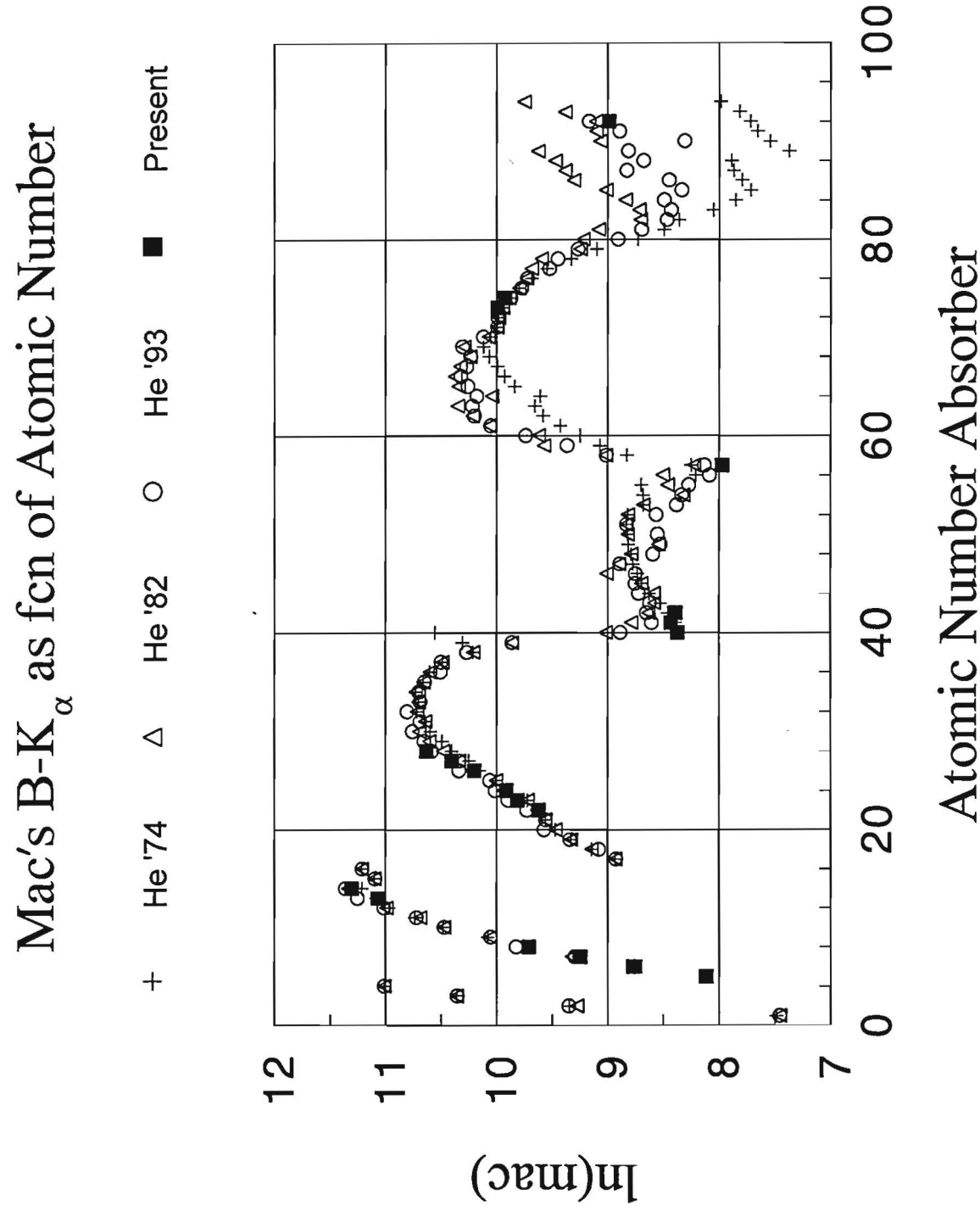

Fig. V.11. Variation of the mass absorption coefficient for B-K_α (logarithmic scale) with atomic number of the absorber. The mac values proposed in the present work (solid squares) are compared to those of Henke et al.[7-9].

REFERENCES

1. G.F. Bastin and H.J.M. Heijligers, "Quantitative Electron Probe Microanalysis of Carbon in binary Carbides", Internal Report, University of Technology, Eindhoven (1984), ISBN 90-6819-002-4.
2. G.F. Bastin and H.J.M. Heijligers, "Quantitative Electron Probe Microanalysis of Carbon in binary Carbides", Microbeam Analysis 291 (1984).
3. G.F. Bastin and H.J.M. Heijligers. "Quantitative Electron Probe Microanalysis of Carbon in binary Carbides", Part I and II, X-ray Spec., **15**, 135-150 (1986).
4. J. Ruste, "Principes généraux de la microanalyse quantitative appliquées aux éléments très légers", J. Microsc. Spectrosc. Electron., **4**, 123 (1979).
5. J.L. Pouchou and F. Pichoir, "A new model for quantitative X-ray microanalysis", Part I and II, Rech. Aerosp. 1984-3, 13 and 1984-5, 349.
6. D.A. Sewell, G. Love and V.D. Scott, "Universal correction procedure for electron-probe microanalysis", J.Phys.D.: Appl. Phys., Part I, II and III, **18**, 1233 (1985).
7. B.L. Henke and E. Ebisu, "Low energy X-ray and Electron Absorption within Solids", Advance in X-ray analysis, **17**, 150-213 (1974).
8. B.L. Henke et al., "Low-energy X-ray interaction coefficients: Photo-absorption, scattering, and reflection, Atomic Data and Nuclear Data Tables, **27**, 1-144 (1982).
9. B.L. Henke , E.M. Gullikson and J.C. Davies., "X-ray interactions : Photoabsorption, scattering, transmission and reflection at E=50-30,000 eV, Z=1-92". Atomic Data and Nuclear Data Tables, **54**, 181-342 (1993).
10. G.F. Bastin, H.J.M. Heijligers and F.J.J. van Loo, "A further improvement in the Gaussian $\varphi(\rho z)$ approach for matrix correction in quantitative electron probe microanalysis", Scanning, **8**, 45-67 (1986).
11. R.H. Packwood and J.D. Brown, "A Gaussian expression to describe $\varphi(\rho z)$ curves for quantitative electron probe microanalysis", X-ray Spec., **10**, 138 (1981).
12. N. Ammann, "Monte-Carlo Simulation der Röntgenstrahlungs-Erzeugung durch Elektronenbeschuß in Schicht-Substrat-Systemen", M.S. Thesis, R.W.T.H. Aachen, Germany (1989).
13. O. Brümmer, G. Dräger and K. Machlitt, in V.V. Nemoshkalenko, Ed., Proc. Intern. Symp. X-ray Spectra and Electronic Structure of Matter, Kiev: Inst. Met. Phys., Acad. Sci. Ukr. SSR. (1969), 300.
14. G. Dräger and O. Brümmer, "Polarized x-ray emission spectra of single crystals", Phys. Stat. Sol., **B124**, 11 (1984).
15. G. Wiech, "X-ray emission spectroscopy", Nato Adv. Study Inst., P. Day Ed., Emission and Scattering Techniques Ser. C, (1981), 103-151.
16. W.G. Moffatt, "The Handbook of binary phase diagrams", Genium Publ. Corp., New York, USA (1983-on).
17. C.A. Andersen, Brit. J. Appl. Phys., **18**, 1033 (1967).
18. D.F. Kyser, "Experimental determination of mass absorption coefficients for soft x-rays", I.B.M. research Report #RJ 911, 7 Sept. 1971.
19. J.L. Pouchou and F. Pichoir, in Proc. of the 11th Intern. Congress on X-ray Optics and Microanalysis, Ed. by J.D. Brown and R.H. Packwood, Graphic Services, U.W.O, London, Canada, 249 (1986).

20. G.F. Bastin and H.J.M. Heijligers, in Electron Probe Quantitation, Workshop at the Natonal Bureau of Standards, Gaithersburg, Maryland 1988, edited by K.F.J. Heinrich and D.E. Newbury, 145-161, Plenum Press, New York (1991).
21. J.L. Pouchou, F. Pichoir, and D. Boivin, in Proc. of the 12th Intern. Congress on X-ray Optics and Microanalysis, Cracow (Poland) (1989), Ed. by S. Jasienska.
Also available as ONERA report #TP. 1989-157.
22. C. Merlet, Inst. Phys. Conf. Ser. No 130 : Chapter 2, 123-126 (1992).
23. V.D.Scott and G. Love, in Electron Probe Quantitation, Workshop at the Natonal Bureau of Standards, Gaithersburg, Maryland 1988, edited by K.F.J. Heinrich and D.E. Newbury, 19-30, Plenum Press, New York (1991).
24. G. Love, M.G.C. Cox and V.D. Scott, J. Phys. D: Appl. Phys., **11**, 7-21 (1978).
25. G.F. Bastin, J.M. Dijkstra and H.J.M. Heijligers, accepted for publication in X-ray Spec., (January 1997).
26. G.F. Bastin and H.J.M. Heijligers, Scanning, **13**, 325-342 (1991).
27. G.F. Bastin and H.J.M. Heijligers, Mikrochim. Acta, **Suppl. 12**, 19-36, (1992).
28. G.F. Bastin, J.M. Dijkstra, H.J.M. Heijligers, and D. Klepper, Microbeam Analysis, **2**, 29-43 (1993).
29. M. Abramowitz and I.A. Stegun, "Handbook of Mathematical Functions", Dover Publications, Inc., New York, (1965).
30. C. Zeller, cited by J. Ruste and M. Gantois, J. Phys. D : Appl. Phys., **8**, 872 (1975).
31. R.M. Sternheimer, quoted in : M.J. Berger and S.M. Seltzer, Report number NASA SP-3012, Washington, DC, (1964).
32. R. Castaing and J. Henoc, in X-Ray Optics and Microanalysis, Hermann, Paris, 120 (1966).
33. W. Rehbach and P. Karduck, Microbeam Analysis 1988, 285 (1988).
34. G.F. Bastin, J.M. Dijkstra and H.J.M. Heijligers, to be published.
35. W. Reuter , Proc. 6th Int. Conf. on X-Ray Optics and Microanalysis 1971, University of Tokyo Press, 121 (1972).
36. C. Merlet, X-Ray Spec., **21**, 229-238 (1992).
37. K.F.J. Heinrich, in Proc. of the 11th Intern. Congress on X-ray Optics and Microanalysis, Ed. by J.D. Brown and R.H. Packwood, Graphic Services, U.W.O, London, Canada, 67 (1986).
38. F. Bloch, Zeit. Phys., **81**, 363 (1933).
39. J.L. Pouchou and F. Pichoir, "Emission and absorption anomalies of the Nickel L_a line", J. Microsc. Spectrosc. Electron, **10**, 291 (1985)
40. G.F. Bastin and H.J.M. Heijligers, in Electron Probe Quantitation, Workshop at the Natonal Bureau of Standards, Gaithersburg, Maryland 1988, edited by K.F.J. Heinrich and D.E. Newbury, 163-175, Plenum Press, New York (1991).

APPENDIX A.1

Area/Peak Factors on STE as a function of detected Peak Position for the boride specimens

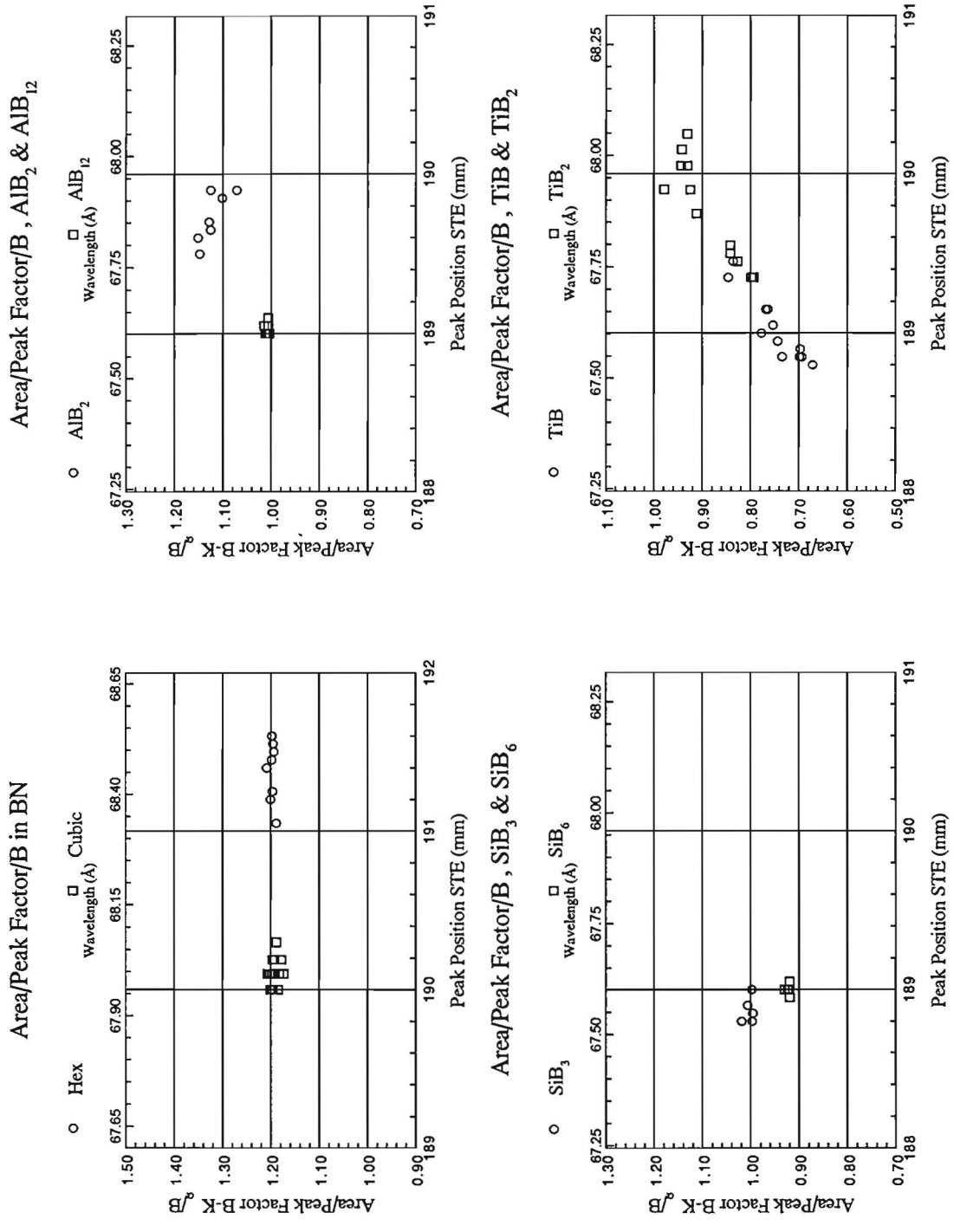

APPENDIX A.2

Area/Peak Factors on STE as a function of detected Peak Position for the boride specimens

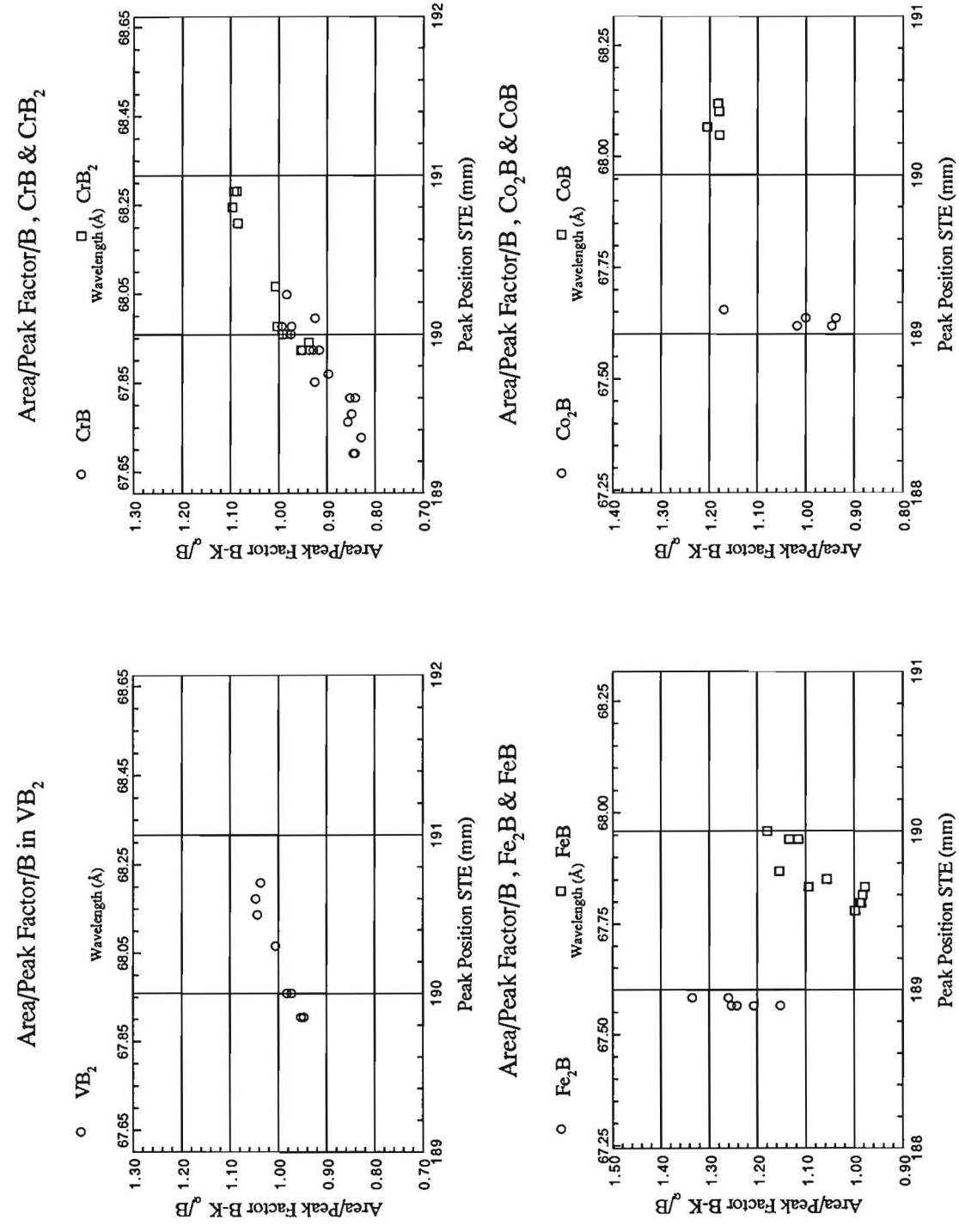

APPENDIX A.3

Area/Peak Factors on STE as a function of detected Peak Position for the boride specimens

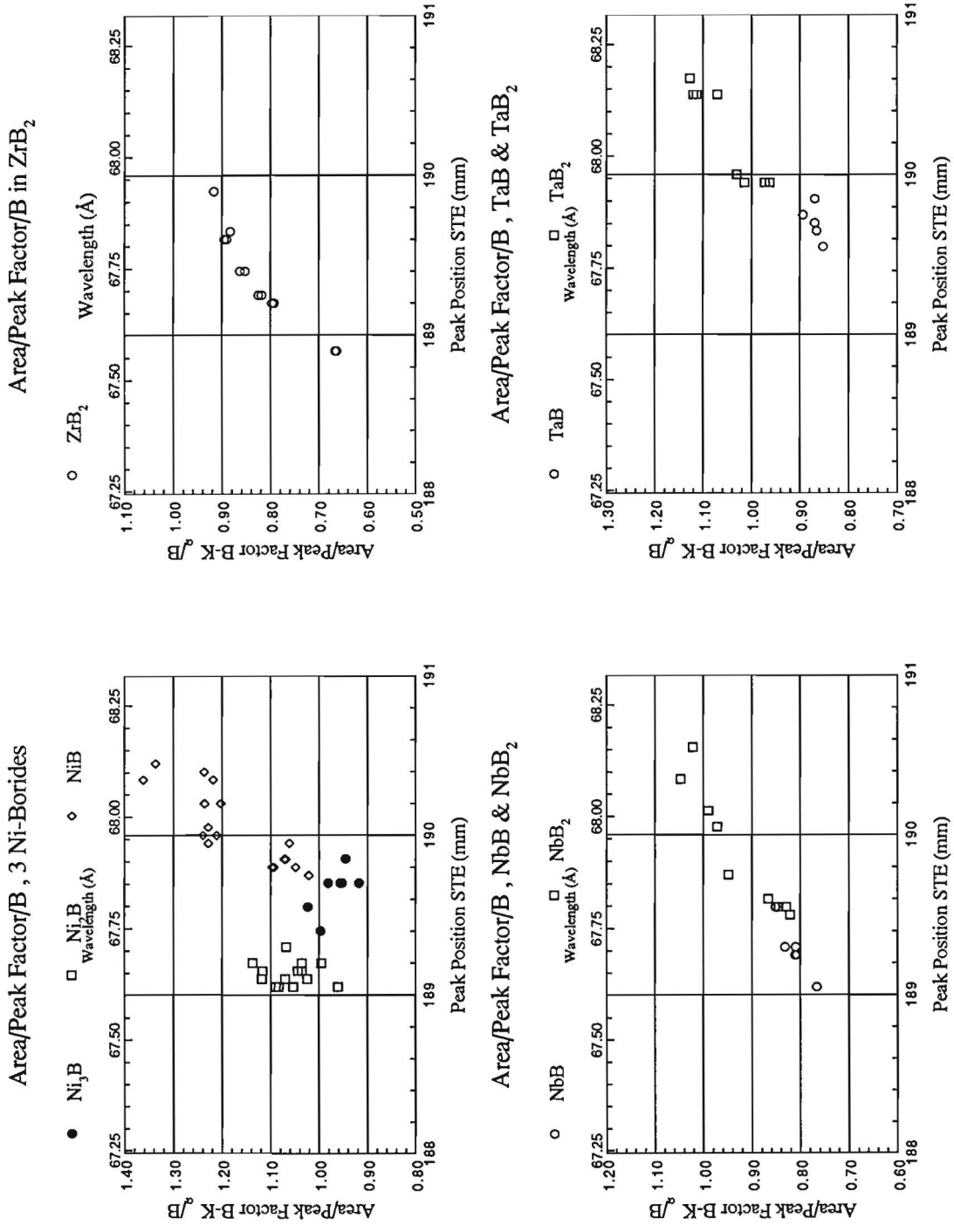

Boride: B_4C (79.81 w/o Boron)

B: 300884

kV	Beam Current (nA)	Gross Intensities (cps/nA)			Backgrounds (cps/nA)			k-ratios
		B-K_α		B-K_α (Area)		B-K_α		B-K_α
				B	Boride	B	Boride	Area
4		300		13.57	10.540	0.13	0.10	0.7768
6		200		19.37	15.020	0.18	0.14	0.7754
8		180		23.45	17.515	0.22	0.16	0.7471
10		165		25.21	18.435	0.22	0.17	0.7309
12		160		25.58	18.237	0.22	0.15	0.7132
15		175		23.97	16.433	0.18	0.13	0.6853
20		220		19.57	12.808	0.15	0.10	0.6544
25		270		15.66	10.206	0.12	0.08	0.6516
30		300		12.64	8.301	0.09	0.07	0.6574

Background for B-K_α measured at ± 25 mm
B-K_α on STE
Pulse Height Analyzer setting : B-K_α : Counter 1700 V, Lower Level 0.6 V, Window 2.8 V, Gain 64 * 8

Boride: BN (Cubic) (43.48 w/o Boron)

B: 080787

kV	Beam Current (nA)		Gross Intensities (cps/nA)				Backgrounds (cps/nA)				k-ratios	
		$B\text{-}K_\alpha$			$B\text{-}K_\alpha$ (Area)				$B\text{-}K_\alpha$			$B\text{-}K_\alpha$
					B	Boride			B	Boride		Area
4		300			9.24	3.469			0.09	0.04		0.3747
6		300			13.59	4.518			0.12	0.05		0.3317
8		300			16.34	4.680			0.13	0.05		0.2856
10		300			17.33	4.415			0.14	0.05		0.2539
12		300			16.93	3.921			0.13	0.03		0.2316
15		300			16.11	3.306			0.12	0.03		0.2049
20		300			13.45	2.454			0.10	0.02		0.1823
25		300			10.71	1.935			0.07	0.02		0.1800
30		300			8.60	1.586			0.06	0.02		0.1834

Background for $B\text{-}K_\alpha$ measured at ± 25 mm
$B\text{-}K_\alpha$ on STE
Pulse Height Analyzer setting : $B\text{-}K_\alpha$: Counter 1700 V, Lower Level 0.5 V, Window 3.0 V, Gain 64 * 5.5

Boride: B_6O (80.20 w/o Boron)

B: 170688

kV	Beam Current (nA)	Gross Intensities (cps/nA)			Backgrounds (cps/nA)			k-ratios	
		$B\text{-}K_\alpha$		$B\text{-}K_\alpha$ (Area)			$B\text{-}K_\alpha$		$B\text{-}K_\alpha$
				B	Boride		B	Boride	Area
4		300		8.83	6.447		0.09	0.04	0.7376
6		300		13.19	8.872		0.12	0.05	0.6750
8		300		15.85	9.840		0.14	0.05	0.6232
10		300		16.56	9.436		0.13	0.05	0.5713
12		300		16.98	8.861		0.14	0.03	0.5244
15		300		15.99	7.557		0.12	0.03	0.4743
20		300		13.30	5.652		0.11	0.02	0.4270
25		300		10.66	4.430		0.08	0.02	0.4168
30		300		8.68	3.584		0.06	0.02	0.4135

Background for $B\text{-}K_\alpha$ measured at ± 25 mm
$B\text{-}K_\alpha$ on STE
Pulse Height Analyzer setting : $B\text{-}K_\alpha$: Counter 1700 V, Lower Level 0.5 V, Window 3.5 V, Gain 64 * 5

Boride: AlB_2 (44.49 w/o Boron)

B: 041084 Al: 060684

kV	Beam Current (nA)		Gross Intensities (cps/nA)				Backgrounds (cps/nA)				k-ratios	
	Al-K_α	B-K_α	Al-K_α (Peak)		B-K_α (Area)		Al-K_α		B-K_α		Al-K_α	B-K_α
			Al	Boride	B	Boride	Al	Boride	B	Boride	Peak	Area
4	30	300	148.79	84.42	14.43	2.716	0.40	0.25	0.13	0.04	0.5672	0.1872
5	30	---	287.36	142.61	-----	-----	0.58	0.42	---	---	0.4958	------
6	10	300	412.27	218.39	21.20	2.251	0.93	0.58	0.19	0.03	0.5295	0.1057
8	3	300	749.66	387.59	25.94	1.696	1.65	0.87	0.22	0.03	0.5170	0.0648
10	3	150	1084.07	552.44	27.32	1.378	1.72	0.87	0.22	0.02	0.5096	0.0501
12	3	300	1426.58	742.25	28.13	1.124	2.14	1.33	0.21	0.02	0.5202	0.0396
15	1	300	1950.72	1015.16	26.23	0.911	3.09	1.81	0.20	0.02	0.5240	0.0342
20	1	----	2762.46	1400.08	-----	-----	3.60	2.22	----	----	0.5067	-------
25	1	----	3361.32	1706.33	-----	-----	3.81	4.04	----	----	0.5070	-------
30	1	----	3809.73	1919.74	-----	-----	6.10	4.04	----	----	0.5037	-------

Background for B-K_α measured at ± 25 mm , that of Al-K_α at ± 5 mm on either side of the peak and interpolated.
Al-K_α on TAP, B-K_α on STE
Pulse Height Analyzer settings : Al-K_α : Counter 1600 V, Lower Level 0.6 V, Window open, Gain 32 * 5.5
B-K_α : Counter 1700 V, Lower Level 0.5 V, Window 3.4 V, Gain 64 * 8

Boride: AlB_{12} (82.78 w/o Boron)

B: 140984 Al: 060684

kV	Beam Current (nA)		Gross Intensities (cps/nA)				Backgrounds (cps/nA)				k-ratios	
	$Al\text{-}K_\alpha$	$B\text{-}K_\alpha$	$Al\text{-}K_\alpha$ (Peak)		$B\text{-}K_\alpha$ (Area)		$Al\text{-}K_\alpha$		$B\text{-}K_\alpha$		$Al\text{-}K_\alpha$	$B\text{-}K_\alpha$
			Al	Boride	B	Boride	Al	Boride	B	Boride	Peak	Area
4	30	300	148.79	24.01	14.78	8.995	0.40	0.11	0.39	0.25	0.1611	0.6077
5	30	---	287.36	42.09	-----	-----	0.58	0.16	---	---	0.1462	------
6	10	300	412.27	63.21	21.62	9.833	0.93	0.27	0.42	0.31	0.1530	0.4492
8	3	300	749.66	112.20	26.19	9.035	1.65	0.60	0.46	0.31	0.1492	0.3391
10	3	300	1085.07	158.96	28.31	7.769	1.72	0.50	0.73	0.38	0.1464	0.2679
12	3	300	1426.58	214.83	28.72	6.691	2.14	0.77	0.68	0.40	0.1502	0.2244
15	1	300	1950.72	293.81	27.20	5.609	3.09	0.95	0.75	0.68	0.1504	0.1864
20	1	300	2762.46	410.53	22.42	4.166	3.60	0.51	0.77	0.52	0.1486	0.1684
25	1	300	3361.32	494.48	17.95	3.522	3.81	2.20	0.78	0.71	0.1466	0.1638
30	1	300	3809.73	555.06	14.17	2.660	6.10	1.82	0.12	0.28	0.1455	0.1694

Background for $B\text{-}K_\alpha$ measured at ± 25 mm , that of $Al\text{-}K_\alpha$ at ± 5 mm on either side of the peak and interpolated.
$Al\text{-}K_\alpha$ on TAP, $B\text{-}K_\alpha$ on STE
Pulse Height Analyzer settings : $Al\text{-}K_\alpha$: Counter 1600 V, Lower Level 0.6 V, Window open, Gain 32 * 5.5
$B\text{-}K_\alpha$: Counter 1700 V, Lower Level 0.5 V, Window 3.4 V, Gain 64 * 8

Boride: SiB_3 (53.59 w/o Boron)

B: 111084 Si: 150584

kV	Beam Current (nA)		Gross Intensities (cps/nA)				Backgrounds (cps/nA)				k-ratios	
	Si-K_α	B-K_α	Si-K_α (Peak)		B-K_α (Area)		Si-K_α		B-K_α		Si-K_α	B-K_α
			Si	Boride	B	Boride	Si	Boride	B	Boride	Peak	Area
4	30	245	136.73	61.18	16.44	3.786	0.56	0.310	0.38	0.30	0.4470	0.2171
6	10	300	387.94	177.08	23.81	2.864	1.34	0.792	0.42	0.22	0.4560	0.1131
8	3	300	716.94	329.36	28.92	2.229	2.50	1.510	0.48	0.23	0.4589	0.0703
10	3	300	1052.51	483.93	30.36	1.858	2.93	1.233	0.43	0.23	0.4599	0.0544
12	3	300	1408.76	659.21	31.45	1.609	3.42	1.788	0.44	0.23	0.4678	0.0445
15	3	300	1988.05	928.49	29.44	1.333	4.82	2.326	0.43	0.22	0.4670	0.0384
20	1	----	2859.02	1355.98	-----	-----	8.30	3.030	----	----	0.4746	-------
25	1	----	3607.28	1711.75	-----	-----	8.63	4.550	----	----	0.4744	-------
30	1	----	4246.78	2000.12	-----	-----	10.45	6.500	----	----	0.4706	-------

Background for B-K_α measured at ± 25 mm , that of Si-K_α at ± 5 mm on either side of the peak and interpolated.
Si-K_α on TAP, B-K_α on STE
Pulse Height Analyzer settings : Si-K_α : Counter 1600 V, Lower Level 0.5 V, Window open, Gain 32 * 5
B-K_α : Counter 1700 V, Lower Level 0.5 V, Window 3.5 V, Gain 64 * 8

Boride: SiB_6 (69.78 w/o Boron)

B: 111084 Si: 150584

kV	Beam Current (nA)		Gross Intensities (cps/nA)				Backgrounds (cps/nA)				k-ratios	
	Si-K_α	B-K_α	Si-K_α (Peak)		B-K_α (Area)		Si-K_α		B-K_α		Si-K_α	B-K_α
			Si	Boride	B	Boride	Si	Boride	B	Boride	Peak	Area
4	30	254	136.73	39.99	16.44	5.832	0.56	0.233	0.38	0.29	0.2920	0.3451
6	10	300	387.94	114.78	23.81	5.173	1.34	0.582	0.42	0.23	0.2954	0.2113
8	3	300	716.94	213.96	28.92	4.205	2.50	0.770	0.48	0.22	0.2984	0.1401
10	3	300	1052.51	311.27	30.36	3.426	2.93	0.906	0.43	0.22	0.2957	0.1071
12	3	300	1408.76	429.55	31.45	2.866	3.42	1.623	0.44	0.23	0.3045	0.0850
15	3	300	1988.05	578.69	29.44	2.289	4.82	1.773	0.43	0.22	0.2909	0.0713
20	1	----	2859.02	898.68	-----	-----	8.30	2.630	----	----	0.3134	-------
25	1	----	3607.28	1139.15	-----	-----	8.63	3.780	----	----	0.3155	-------
30	1	----	4246.78	1334.98	-----	-----	10.45	6.040	----	----	0.3137	-------

Background for B-K_α measured at ± 25 mm , that of Si-K_α at ± 5 mm on either side of the peak and interpolated.
Si-K_α on TAP, B-K_α on STE
Pulse Height Analyzer settings : Si-K_α : Counter 1600 V, Lower Level 0.5 V, Window open, Gain 32 * 5
B-K_α : Counter 1700 V, Lower Level 0.5 V, Window 3.5 V, Gain 64 * 8

Boride: TiB (16.78 w/o Boron)

B: 260984 Ti: 160584

kV	Beam Current (nA)		Gross Intensities (cps/nA)				Backgrounds (cps/nA)				k-ratios	
	$Ti\text{-}K_\alpha$	$B\text{-}K_\alpha$	$Ti\text{-}K_\alpha$ (Peak)		$B\text{-}K_\alpha$ (Area)		$Ti\text{-}K_\alpha$		$B\text{-}K_\alpha$		$Ti\text{-}K_\alpha$	$B\text{-}K_\alpha$
			Ti	Boride	B	Boride	Ti	Boride	B	Boride	Peak	Area
4	---	300	-------	-----	14.99	2.480	-----	-----	0.14	0.07	-------	0.1623
6	100	300	22.00	17.82	21.65	2.724	0.25	0.22	0.20	0.06	0.8089	0.1242
8	30	300	131.52	103.75	25.96	2.606	0.93	0.62	0.25	0.06	0.7897	0.0990
10	15	300	289.93	231.56	28.04	2.389	1.23	1.06	0.38	0.19	0.7984	0.0795
12	10	300	501.86	396.73	28.40	1.986	1.75	1.49	0.70	0.05	0.7903	0.0699
15	10	300	881.23	700.14	26.16	1.607	2.65	2.49	0.35	0.05	0.7941	0.0603
20	3	300	1642.14	1317.53	21.51	1.350	5.13	4.65	0.28	0.20	0.8020	0.0542
25	3	300	2467.29	1983.22	17.63	1.082	6.35	6.10	0.38	0.13	0.8034	0.0552
30	1	300	3188.01	2578.37	14.58	0.914	9.84	12.63	0.50	0.10	0.8073	0.0578

Background for $B\text{-}K_\alpha$ measured at ± 25 mm , that of $Ti\text{-}K_\alpha$ at ± 5 mm on either side of the peak and interpolated.
$Ti\text{-}K_\alpha$ on PET, $B\text{-}K_\alpha$ on STE
Pulse Height Analyzer settings : $Ti\text{-}K_\alpha$: Counter 1600 V, Lower Level 0.6 V, Window open, Gain 64 * 6.5
$B\text{-}K_\alpha$: Counter 1700 V, Lower Level 0.6 V, Window 3.5 V, Gain 64 * 8

Boride: TiB_2 (30.07 w/o Boron)

B: 260984 Ti: 160584

kV	Beam Current (nA)		Gross Intensities (cps/nA)				Backgrounds (cps/nA)				k-ratios	
	$Ti\text{-}K_\alpha$	$B\text{-}K_\alpha$	$Ti\text{-}K_\alpha$ (Peak)		$B\text{-}K_\alpha$ (Area)		$Ti\text{-}K_\alpha$		$B\text{-}K_\alpha$		$Ti\text{-}K_\alpha$	$B\text{-}K_\alpha$
			Ti	Boride	B	Boride	Ti	Boride	B	Boride	Peak	Area
4	---	300	-------	-----	14.99	4.449	-----	-----	0.14	0.06	-------	0.2956
6	100	300	22.00	13.92	21.65	4.873	0.25	0.15	0.20	0.06	0.6329	0.2244
8	30	300	131.52	84.45	25.96	4.725	0.93	0.68	0.25	0.08	0.6415	0.1807
10	15	300	289.93	189.47	28.04	4.384	1.23	0.95	0.38	0.24	0.6530	0.1498
12	10	300	501.86	327.41	28.40	3.774	1.75	1.54	0.70	0.23	0.6516	0.1279
15	10	300	881.23	579.59	26.16	3.119	2.65	2.28	0.35	0.13	0.6571	0.1158
20	3	300	1642.14	1096.01	21.51	2.310	5.13	4.12	0.28	0.07	0.6669	0.1055
25	3	300	2467.29	1662.55	17.63	1.924	6.35	6.09	0.38	0.09	0.6731	0.1063
30	1	300	3188.01	2165.96	14.58	1.644	9.84	7.98	0.50	0.11	0.6790	0.1090

Background for $B\text{-}K_\alpha$ measured at ± 25 mm , that of $Ti\text{-}K_\alpha$ at ± 5 mm on either side of the peak and interpolated.
$Ti\text{-}K_\alpha$ on PET, $B\text{-}K_\alpha$ on STE
Pulse Height Analyzer settings : $Ti\text{-}K_\alpha$: Counter 1600 V, Lower Level 0.6 V, Window open, Gain 64 * 6.5
$B\text{-}K_\alpha$: Counter 1700 V, Lower Level 0.6 V, Window 3.5 V, Gain 64 * 8

Boride: VB_2 (28.40 w/o Boron)

B: 121084 V: 170584

kV	Beam Current (nA)		Gross Intensities (cps/nA)				Backgrounds (cps/nA)				k-ratios	
	$V\text{-}K_\alpha$	$B\text{-}K_\alpha$	$V\text{-}K_\alpha$ (Peak)		$B\text{-}K_\alpha$ (Area)		$V\text{-}K_\alpha$		$B\text{-}K_\alpha$		$V\text{-}K_\alpha$	$B\text{-}K_\alpha$
			V	Boride	B	Boride	V	Boride	B	Boride	Peak	Area
4	----	300	-----	-----	16.84	4.383	----	-----	0.18	0.08	-------	0.2583
6	200	300	1.03	0.657	24.64	4.999	0.04	0.03	0.35	0.19	0.6336	0.1980
8	30	300	128.97	84.086	29.57	4.601	1.08	0.83	0.45	0.28	0.6510	0.1484
10	15	300	315.21	208.47	31.77	4.063	1.91	1.32	0.41	0.19	0.6612	0.1235
12	10	300	574.82	384.64	31.97	3.427	2.75	2.15	0.43	0.09	0.6686	0.1058
15	10	300	1048.45	709.70	30.13	4.003	4.07	3.07	0.27	1.42	0.6766	0.0865
20	3	----	2014.79	1360.06	-----	-----	7.00	5.40	----	----	0.6747	-------
25	3	----	3028.30	2092.91	-----	-----	9.38	7.44	----	----	0.6908	-------
30	2	----	4114.87	2879.28	-----	-----	12.70	12.68	----	----	0.6988	-------

Background for $B\text{-}K_\alpha$ measured at ± 25 mm , that of $V\text{-}K_\alpha$ at ± 5 mm on either side of the peak and interpolated.
$V\text{-}K_\alpha$ on PET, $B\text{-}K_\alpha$ on STE
Pulse Height Analyzer settings : $V\text{-}K_\alpha$: Counter 1600 V, Lower Level 0.6 V, Window open, Gain 64 *6. 5
$B\text{-}K_\alpha$: Counter 1700 V, Lower Level 0.5 V, Window 3.5 V, Gain 64 * 8

Boride: CrB (16.80 w/o Boron)

B: 261084 Cr: 020784

kV	Beam Current (nA)		Gross Intensities (cps/nA)				Backgrounds (cps/nA)				k-ratios	
	$Cr\text{-}K_\alpha$	$B\text{-}K_\alpha$	$Cr\text{-}K_\alpha$ (Peak)		$B\text{-}K_\alpha$ (Area)		$Cr\text{-}K_\alpha$		$B\text{-}K_\alpha$		$Cr\text{-}K_\alpha$	$B\text{-}K_\alpha$
			Cr	Boride	B	Boride	Cr	Boride	B	Boride	Peak	Area
4	----	250	-----	-----	15.58	2.217	----	-----	0.17	0.08	-------	0.1387
6	----	300	-----	-----	24.53	2.477	----	-----	0.23	0.07	-------	0.0991
8	30	300	96.84	75.38	29.36	2.233	1.19	1.06	0.26	0.06	0.7770	0.0747
10	30	300	281.83	221.07	31.76	2.059	2.02	1.70	0.34	0.14	0.7840	0.0611
12	10	300	543.29	429.10	32.29	1.974	3.10	2.30	0.39	0.17	0.7901	0.0512
15	5	300	1039.45	831.46	30.12	1.511	4.15	3.32	0.38	1.19	0.7999	0.0444
20	1	----	2044.95	1646.38	-----	-----	7.47	7.80	----	----	0.8043	-------
25	1	----	3164.96	2566.96	-----	-----	9.97	10.40	----	----	0.8103	-------
30	1	----	4281.35	3487.28	-----	-----	13.32	11.52	----	----	0.8144	-------

Background for $B\text{-}K_\alpha$ measured at ± 25 mm , that of $Cr\text{-}K_\alpha$ at ± 5 mm on either side of the peak and interpolated.
$Cr\text{-}K_\alpha$ on PET, $B\text{-}K_\alpha$ on STE
Pulse Height Analyzer settings : $Cr\text{-}K_\alpha$: Counter 1600 V, Lower Level 0.6 V, Window open, Gain 64 *6
$B\text{-}K_\alpha$: Counter 1700 V, Lower Level 0.5 V, Window 3.5 V, Gain 64 * 8

Boride: CrB_2 (27.31 w/o Boron)

B: 120984 Cr: 020784

kV	Beam Current (nA)		Gross Intensities (cps/nA)				Backgrounds (cps/nA)				k-ratios	
	$Cr\text{-}K_\alpha$	$B\text{-}K_\alpha$	$Cr\text{-}K_\alpha$ (Peak)		$B\text{-}K_\alpha$ (Area)		$Cr\text{-}K_\alpha$		$B\text{-}K_\alpha$		$Cr\text{-}K_\alpha$	$B\text{-}K_\alpha$
			Cr	Boride	B	Boride	Cr	Boride	B	Boride	Peak	Area
4	----	250	-----	-----	15.58	3.616	----	-----	0.17	0.07	-------	0.2301
6	----	300	-----	-----	24.53	4.158	----	-----	0.23	0.07	-------	0.1682
8	30	300	96.84	60.29	29.36	3.750	1.19	0.81	0.26	0.06	0.6218	0.1268
10	30	300	281.83	180.12	31.76	3.409	2.02	1.41	0.34	0.15	0.6387	0.1037
12	10	300	543.29	353.74	32.29	2.992	3.10	2.40	0.39	0.15	0.6504	0.0891
15	5	300	1039.45	685.90	30.12	2.492	4.15	3.74	0.38	0.21	0.6589	0.0767
20	1	----	2044.95	1368.69	-----	-----	7.47	5.70	----	----	0.6689	-------
25	1	----	3164.96	2141.69	-----	-----	9.97	7.37	----	----	0.6765	-------
30	1	----	4281.35	2939.76	-----	-----	13.32	10.70	----	----	0.6863	-------

Background for $B\text{-}K_\alpha$ measured at ± 25 mm , that of $Cr\text{-}K_\alpha$ at ± 5 mm on either side of the peak and interpolated.
$Cr\text{-}K_\alpha$ on PET, $B\text{-}K_\alpha$ on STE
Pulse Height Analyzer settings : $Cr\text{-}K_\alpha$: Counter 1600 V, Lower Level 0.6 V, Window open, Gain 64 *6
$B\text{-}K_\alpha$: Counter 1700 V, Lower Level 0.5 V, Window 3.5 V, Gain 64 *8

Boride: Fe_2B (8.82 w/o Boron)

B: 291084 Fe: 030784

kV	Beam Current (nA)		Gross Intensities (cps/nA)				Backgrounds (cps/nA)				k-ratios	
	Fe-K_α	B-K_α	Fe-K_α (Peak)		B-K_α (Area)		Fe-K_α		B-K_α		Fe-K_α	B-K_α
			Fe	Boride	B	Boride	Fe	Boride	B	Boride	Peak	Area
4	----	300	-----	-----	16.26	1.178	----	-----	0.26	0.20	-------	0.0611
6	----	300	-----	-----	24.26	1.057	----	-----	0.39	0.08	-------	0.0409
8	300	300	6.44	5.62	29.18	0.898	0.11	0.11	0.29	0.06	0.8563	0.0290
10	100	300	38.36	33.65	31.58	0.760	0.18	0.20	0.27	0.06	0.8761	0.0226
12	50	300	92.95	81.68	31.79	0.649	0.32	0.37	0.26	0.05	0.8778	0.0190
15	30	300	202.10	178.47	29.97	0.580	0.63	0.54	0.29	0.08	0.8832	0.0169
20	15	----	440.11	389.83	-----	-----	0.94	0.86	----	----	0.8857	-------
25	15	----	729.48	649.94	-----	-----	1.56	1.29	----	----	0.8911	-------
30	10	----	1011.67	909.51	-----	-----	1.83	2.06	----	----	0.8986	-------

Background for B-K_α measured at ± 25 mm , that of Fe-K_α at ± 5 mm on either side of the peak and interpolated.
Fe-K_α on LiF, B-K_α on STE
Pulse Height Analyzer settings : Fe-K_α : Counter 1600 V, Lower Level 0.6 V, Window open, Gain 64 *4.7
B-K_α : Counter 1700 V, Lower Level 0.5 V, Window 3.5 V, Gain 64 * 8

Boride: FeB (16.22 w/o Boron)

B: 291084 Fe: 030784

kV	Beam Current (nA)		Gross Intensities (cps/nA)				Backgrounds (cps/nA)				k-ratios	
	Fe-K_α	B-K_α	Fe-K_α (Peak)		B-K_α (Area)		Fe-K_α		B-K_α		Fe-K_α	B-K_α
			Fe	Boride	B	Boride	Fe	Boride	B	Boride	Peak	Area
4	----	300	-----	-----	16.26	1.886	----	-----	0.26	0.11	-------	0.1131
6	----	300	-----	-----	24.26	1.887	----	-----	0.39	0.08	-------	0.0757
8	300	300	6.44	5.04	29.18	1.590	0.11	0.09	0.29	0.05	0.7827	0.0533
10	100	300	38.36	30.45	31.58	1.326	0.18	0.20	0.27	0.06	0.7923	0.0404
12	50	300	92.95	74.48	31.79	1.138	0.32	0.24	0.26	0.05	0.8015	0.0345
15	30	300	202.10	163.35	29.97	0.947	0.63	0.49	0.29	0.08	0.8084	0.0292
20	15	----	440.11	357.85	-----	-----	0.94	1.02	----	----	0.8125	-------
25	15	----	729.48	599.62	-----	-----	1.56	1.20	----	----	0.8221	-------
30	10	----	1011.67	848.43	-----	-----	1.83	1.74	----	----	0.8384	-------

Background for B-K_α measured at ± 25 mm , that of Fe-K_α at ± 5 mm on either side of the peak and interpolated.
Fe-K_α on LiF, B-K_α on STE
Pulse Height Analyzer settings : Fe-K_α : Counter 1600 V, Lower Level 0.6 V, Window open, Gain 64 *4.7
B-K_α : Counter 1700 V, Lower Level 0.5 V, Window 3.5 V, Gain 64 * 8

Boride: Co_2B (8.40 w/o Boron)

B: 121184 Co: 040784

kV	Beam Current (nA)		Gross Intensities (cps/nA)				Backgrounds (cps/nA)				k-ratios	
	$Co\text{-}K_\alpha$	$B\text{-}K_\alpha$	$Co\text{-}K_\alpha$ (Peak)		$B\text{-}K_\alpha$ (Area)		$Co\text{-}K_\alpha$		$B\text{-}K_\alpha$		$Co\text{-}K_\alpha$	$B\text{-}K_\alpha$
			Co	Boride	B	Boride	Co	Boride	B	Boride	Peak	Area
4	----	300	-----	-----	16.02	0.828	----	-----	0.20	0.05	-------	0.0492
6	----	300	-----	-----	23.49	0.741	----	-----	0.22	0.04	-------	0.0301
8	----	300	-----	-----	27.99	0.617	----	-----	0.26	0.03	-------	0.0212
10	300	300	31.57	27.37	29.85	0.523	0.27	0.27	0.25	0.03	0.8659	0.0167
12	50	300	88.21	77.66	30.13	0.439	0.45	0.39	0.25	0.03	0.8805	0.0137
15	30	300	211.19	190.02	28.36	0.359	0.79	0.69	0.23	0.03	0.8999	0.0117
20	15	----	484.77	444.56	-----	-----	1..31	1.35	----	----	0.9167	-------
25	10	----	809.41	736.49	-----	-----	1.85	2.01	----	----	0.9095	-------
30	5	----	1175.55	1068.03	-----	-----	2.75	2.38	----	----	0.9071	-------

Background for $B\text{-}K_\alpha$ measured at ± 25 mm , that of $Co\text{-}K_\alpha$ at ± 5 mm on either side of the peak and interpolated.
$Co\text{-}K_\alpha$ on LiF, $B\text{-}K_\alpha$ on STE
Pulse Height Analyzer settings : $Co\text{-}K_\alpha$: Counter 1600 V, Lower Level 0.6 V, Window open, Gain 32 *9.5
$B\text{-}K_\alpha$: Counter 1700 V, Lower Level 0.5 V, Window 3.5 V, Gain 64 * 8

Boride: CoB (15.50 w/o Boron)

B: 121184 Co: 040784

kV	Beam Current (nA)		Gross Intensities (cps/nA)				Backgrounds (cps/nA)				k-ratios	
	$Co\text{-}K_\alpha$	$B\text{-}K_\alpha$	$Co\text{-}K_\alpha$ (Peak)		$B\text{-}K_\alpha$ (Area)		$Co\text{-}K_\alpha$		$B\text{-}K_\alpha$		$Co\text{-}K_\alpha$	$B\text{-}K_\alpha$
			Co	Boride	B	Boride	Co	Boride	B	Boride	Peak	Area
4	----	300	-----	-----	16.02	1.603	----	-----	0.20	0.05	-------	0.0981
6	----	300	-----	-----	23.49	1.481	----	-----	0.22	0.04	-------	0.0619
8	----	300	-----	-----	27.99	1.214	----	-----	0.26	0.04	-------	0.0423
10	300	300	31.57	24.36	29.85	1.026	0.27	0.23	0.25	0.04	0.7710	0.0333
12	50	300	88.21	70.54	30.13	0.873	0.45	0.38	0.25	0.03	0.7994	0.0282
15	30	300	211.19	170.59	28.36	0.703	0.79	0.70	0.23	0.03	0.8075	0.0239
20	15	----	484.77	397.68	-----	-----	1..31	1.18	----	----	0.8201	-------
25	10	----	809.41	672.65	-----	-----	1.85	1.67	----	----	0.8309	-------
30	5	----	1175.55	973.61	-----	-----	2.75	2.14	----	----	0.8269	-------

Background for $B\text{-}K_\alpha$ measured at ± 25 mm , that of $Co\text{-}K_\alpha$ at ± 5 mm on either side of the peak and interpolated.
$Co\text{-}K_\alpha$ on LiF, $B\text{-}K_\alpha$ on STE
Pulse Height Analyzer settings : $Co\text{-}K_\alpha$: Counter 1600 V, Lower Level 0.6 V, Window open, Gain 32 *9.5
$B\text{-}K_\alpha$: Counter 1700 V, Lower Level 0.5 V, Window 3.5 V, Gain 64 * 8

Boride: Ni_3B (5.78 w/o Boron)

B: 021184 Ni: 040784

kV	Beam Current (nA)		Gross Intensities (cps/nA)				Backgrounds (cps/nA)				k-ratios	
	Ni-K_α	B-K_α	Ni-K_α (Peak)		B-K_α (Area)		Ni-K_α		B-K_α		Ni-K_α	B-K_α
			Ni	Boride	B	Boride	Ni	Boride	B	Boride	Peak	Area
4	----	300	-----	-----	15.18	0.462	----	-----	0.16	0.04	-------	0.0281
6	----	300	-----	-----	23.32	0.419	----	-----	0.21	0.04	-------	0.0164
8	----	300	-----	-----	27.95	0.352	----	-----	0.25	0.03	-------	0.0116
10	200	300	20.45	18.81	29.24	0.294	0.30	0.31	0.25	0.03	0.9181	0.0091
12	100	300	76.70	71.48	29.64	0.245	0.60	0.52	0.26	0.03	0.9325	0.0073
15	50	300	207.43	191.48	27.61	0.200	0.93	0.88	0.21	0.03	0.9230	0.0062
20	15	----	511.85	479.50	-----	-----	1.52	1.70	----	----	0.9363	-------
25	10	----	881.45	818.27	-----	-----	2.52	2.61	----	----	0.9280	-------
30	5	----	1283.45	1204.81	-----	-----	3.96	2.73	----	----	0.9395	-------

Background for B-K_α measured at ± 25 mm , that of Ni-K_α at ± 5 mm on either side of the peak and interpolated.
Ni-K_α on LiF, B-K_α on STE
Pulse Height Analyzer settings : Ni-K_α : Counter 1600 V, Lower Level 0.6 V, Window open, Gain 32 *6.5
B-K_α : Counter 1700 V, Lower Level 0.5 V, Window 3.5 V, Gain 64 * 8

Boride: Ni_2B (8.43 w/o Boron)

B: 021184 Ni: 040784

kV	Beam Current (nA)		Gross Intensities (cps/nA)				Backgrounds (cps/nA)				k-ratios	
	$Ni\text{-}K_\alpha$	$B\text{-}K_\alpha$	$Ni\text{-}K_\alpha$ (Peak)		$B\text{-}K_\alpha$ (Area)		$Ni\text{-}K_\alpha$		$B\text{-}K_\alpha$		$Ni\text{-}K_\alpha$	$B\text{-}K_\alpha$
			Ni	Boride	B	Boride	Ni	Boride	B	Boride	Peak	Area
4	----	300	-----	-----	15.18	0.691	----	-----	0.16	0.05	-------	0.0427
6	----	300	-----	-----	23.32	0.670	----	-----	0.21	0.09	-------	0.0251
8	----	300	-----	-----	27.95	0.517	----	-----	0.25	0.03	-------	0.0176
10	200	300	20.45	17.14	29.24	0.444	0.30	0.29	0.25	0.03	0.8817	0.0143
12	100	300	76.70	68.32	29.64	0.376	0.60	0.54	0.26	0.03	0.8906	0.0118
15	50	300	207.43	184.27	27.61	0.390	0.93	0.90	0.21	0.13	0.8880	0.0095
20	15	----	511.85	463.33	-----	-----	1.52	1.68	----	----	0.9046	-------
25	10	----	881.45	794.78	-----	-----	2.52	2.35	----	----	0.9016	-------
30	5	----	1283.45	1160.85	-----	-----	3.96	2.95	----	----	0.9050	-------

Background for $B\text{-}K_\alpha$ measured at ± 25 mm , that of $Ni\text{-}K_\alpha$ at ± 5 mm on either side of the peak and interpolated.
$Ni\text{-}K_\alpha$ on LiF, $B\text{-}K_\alpha$ on STE
Pulse Height Analyzer settings : $Ni\text{-}K_\alpha$: Counter 1600 V, Lower Level 0.6 V, Window open, Gain 32 *6.5
$B\text{-}K_\alpha$: Counter 1700 V, Lower Level 0.5 V, Window 3.5 V, Gain 64 * 8

Boride: NiB (14.40 w/o Boron)

B: 021184 Ni: 040784

kV	Beam Current (nA)		Gross Intensities (cps/nA)				Backgrounds (cps/nA)				k-ratios	
	$Ni\text{-}K_\alpha$	$B\text{-}K_\alpha$	$Ni\text{-}K_\alpha$ (Peak)		$B\text{-}K_\alpha$ (Area)		$Ni\text{-}K_\alpha$		$B\text{-}K_\alpha$		$Ni\text{-}K_\alpha$	$B\text{-}K_\alpha$
			Ni	Boride	B	Boride	Ni	Boride	B	Boride	Peak	Area
4	----	300	-----	-----	15.18	1.145	----	-----	0.16	0.05	-------	0.0729
6	----	300	-----	-----	23.32	1.064	----	-----	0.21	0.04	-------	0.0443
8	----	300	-----	-----	27.95	0.841	----	-----	0.25	0.06	-------	0.0282
10	200	300	20.45	16.56	29.24	0.716	0.30	0.26	0.25	0.03	0.8090	0.0237
12	100	300	76.70	63.12	29.64	0.611	0.60	0.51	0.26	0.03	0.8227	0.0198
15	50	300	207.43	171.63	27.61	0.502	0.93	0.82	0.21	0.02	0.8272	0.0176
20	15	----	511.85	431.04	-----	-----	1.52	1.56	----	----	0.8416	-------
25	10	----	881.45	738.61	-----	-----	2.52	2.08	----	----	0.8380	-------
30	5	----	1283.45	1083.24	-----	-----	3.96	3.25	----	----	0.8441	-------

Background for $B\text{-}K_\alpha$ measured at ± 25 mm , that of $Ni\text{-}K_\alpha$ at ± 5 mm on either side of the peak and interpolated.
$Ni\text{-}K_\alpha$ on LiF, $B\text{-}K_\alpha$ on STE
Pulse Height Analyzer settings : $Ni\text{-}K_\alpha$: Counter 1600 V, Lower Level 0.6 V, Window open, Gain 32 *6.5
$B\text{-}K_\alpha$: Counter 1700 V, Lower Level 0.5 V, Window 3.5 V, Gain 64 * 8

Boride: ZrB_2 (17.89 w/o Boron)

B: 100984 Zr: 050784

kV	Beam Current (nA)		Gross Intensities (cps/nA)				Backgrounds (cps/nA)				k-ratios	
	$Zr\text{-}L_\alpha$	$B\text{-}K_\alpha$	$Zr\text{-}L_\alpha$ (Peak)		$B\text{-}K_\alpha$ (Area)		$Zr\text{-}L_\alpha$		$B\text{-}K_\alpha$		$Zr\text{-}L_\alpha$	$B\text{-}K_\alpha$
			Zr	Boride	B	Boride	Zr	Boride	B	Boride	Peak	Area
4	100	300	6.69	5.06	15.21	4.068	0.04	0.03	0.16	0.16	0.7567	0.2597
6	100	300	20.50	15.71	21.53	5.590	0.08	0.06	0.20	0.23	0.7667	0.2513
8	100	300	36.92	28.76	25.51	6.453	0.14	0.10	0.21	0.25	0.7775	0.2452
10	100	300	53.20	41.75	27.66	6.820	0.19	0.14	0.21	0.28	0.7849	0.2382
12	100	300	70.49	55.55	29.21	7.197	0.25	0.16	0.25	0.30	0.7886	0.2382
15	100	300	94.82	75.65	27.80	6.805	0.31	0.24	0.21	0.27	0.7979	0.2369
20	30	300	128.33	104.14	22.53	5.933	0.48	0.45	0.16	0.26	0.8110	0.2536
25	50	300	153.92	127.12	17.84	4.996	0.65	0.53	0.13	0.23	0.8259	0.2691
30	50	300	169.58	140.70	14.36	4.207	0.79	0.67	0.11	0.19	0.8296	0.2819

Background for $B\text{-}K_\alpha$ measured at ± 25 mm , that of $Zr\text{-}L_\alpha$ at ± 5 mm on either side of the peak and interpolated.
$Zr\text{-}L_\alpha$ on PET, $B\text{-}K_\alpha$ on STE
Pulse Height Analyzer settings : $Zr\text{-}L_\alpha$: Counter 1600 V, Lower Level 0.6 V, Window open, Gain 128 * 7.4
$B\text{-}K_\alpha$: Counter 1700 V, Lower Level 0.6 V, Window 3.4 V, Gain 64 * 8

Boride: NbB (10.42 w/o Boron)

B: 181084 Nb: 160884

kV	Beam Current (nA)		Gross Intensities (cps/nA)				Backgrounds (cps/nA)				k-ratios	
	$Nb\text{-}L_\alpha$	$B\text{-}K_\alpha$	$Nb\text{-}L_\alpha$ (Peak)		$B\text{-}K_\alpha$ (Area)		$Nb\text{-}L_\alpha$		$B\text{-}K_\alpha$		$Nb\text{-}L_\alpha$	$B\text{-}K_\alpha$
			Nb	Boride	B	Boride	Nb	Boride	B	Boride	Peak	Area
4	150	300	7.07	6.13	15.76	2.656	0.04	0.03	0.19	0.23	0.8672	0.1558
6	200	300	23.39	20.20	22.27	3.448	0.10	0.08	0.20	0.24	0.8637	0.1454
8	150	300	43.41	37.72	26.50	3.944	0.15	0.16	0.25	0.25	0.8683	0.1407
10	100	300	61.93	54.44	28.23	4.110	0.21	0.20	0.25	0.25	0.8788	0.1380
12	50	300	82.06	72.72	28.50	4.193	0.30	0.21	0.23	0.28	0.8869	0.1384
15	30	300	110.68	98.63	26.77	4.048	0.44	0.38	0.23	0.27	0.8912	0.1423
20	20	----	152.34	137.37	-----	-----	0.65	0.50	----	----	0.9023	-------
25	20	----	182.08	166.33	-----	-----	0.79	0.74	----	----	0.9134	-------
30	20	----	202.24	185.51	-----	-----	1.00	0.91	----	----	0.9173	-------

Background for $B\text{-}K_\alpha$ measured at ± 25 mm , that of $Nb\text{-}L_\alpha$ at ± 5 mm on either side of the peak and interpolated.
$Nb\text{-}L_\alpha$ on PET, $B\text{-}K_\alpha$ on STE
Pulse Height Analyzer settings : $Nb\text{-}L_\alpha$: Counter 1600 V, Lower Level 0.6 V, Window open, Gain 128 *8
$B\text{-}K_\alpha$: Counter 1700 V, Lower Level 0.5 V, Window 3.5 V, Gain 64 * 8

Boride: NbB_2 (17.15 w/o Boron)

B: 181084 Nb: 160884

kV	Beam Current (nA)		Gross Intensities (cps/nA)				Backgrounds (cps/nA)				k-ratios	
	$Nb\text{-}L_\alpha$	$B\text{-}K_\alpha$	$Nb\text{-}L_\alpha$ (Peak)		$B\text{-}K_\alpha$ (Area)		$Nb\text{-}L_\alpha$		$B\text{-}K_\alpha$		$Nb\text{-}L_\alpha$	$B\text{-}K_\alpha$
			Nb	Boride	B	Boride	Nb	Boride	B	Boride	Peak	Area
4	150	300	7.07	5.31	15.76	4.160	0.04	0.03	0.19	0.20	0.7512	0.2543
6	200	300	23.39	17.88	22.27	5.410	0.10	0.09	0.20	0.28	0.7640	0.2325
8	150	300	43.41	33.63	26.50	6.258	0.15	0.13	0.25	0.23	0.7744	0.2296
10	100	300	61.93	48.89	28.23	6.478	0.21	0.15	0.25	0.25	0.7897	0.2226
12	50	300	82.06	65.61	28.50	6.617	0.30	0.21	0.23	0.27	0.7999	0.2245
15	30	300	110.68	89.11	26.77	6.328	0.44	0.38	0.23	0.23	0.8053	0.2298
20	20	----	152.34	124.87	-----	-----	0.65	0.52	----	----	0.8198	-------
25	20	----	182.08	152.18	-----	-----	0.79	0.76	----	----	0.8352	-------
30	20	----	202.24	171.18	-----	-----	1.00	0.79	----	----	0.8467	-------

Background for $B\text{-}K_\alpha$ measured at ± 25 mm , that of $Nb\text{-}L_\alpha$ at ± 5 mm on either side of the peak and interpolated.
$Nb\text{-}L_\alpha$ on PET, $B\text{-}K_\alpha$ on STE
Pulse Height Analyzer settings : $Nb\text{-}L_\alpha$: Counter 1600 V, Lower Level 0.6 V, Window open, Gain 128 *8
$B\text{-}K_\alpha$: Counter 1700 V, Lower Level 0.5 V, Window 3.5 V, Gain 64 * 8

Boride: MoB (10.13 w/o Boron)

B: 151084 Mo: 200884

kV	Beam Current (nA)		Gross Intensities (cps/nA)				Backgrounds (cps/nA)				k-ratios	
	Mo-L_α	B-K_α	Mo-L_α (Peak)		B-K_α (Area)		Mo-L_α		B-K_α		Mo-L_α	B-K_α
			Mo	Boride	B	Boride	Mo	Boride	B	Boride	Peak	Area
4	150	200	7.56	6.44	16.78	2.814	0.04	0.04	0.16	0.16	0.8505	0.1597
6	150	300	26.71	22.57	24.44	3.837	0.11	0.09	0.22	0.23	0.8451	0.1489
8	30	300	49.42	42.17	29.56	4.399	0.21	0.19	0.27	0.25	0.8531	0.1416
10	30	300	72.00	62.38	31.67	4.630	0.27	0.25	0.29	0.25	0.8662	0.1396
12	10	300	95.39	83.28	32.23	4.604	0.39	0.37	0.26	0.25	0.8727	0.1362
15	5	300	129.02	114.61	30.35	4.421	0.40	0.46	0.23	0.22	0.8875	0.1395
20	5	----	181.22	161.60	-----	-----	0.88	0.65	----	----	0.8925	-------
25	5	----	216.61	198.21	-----	-----	1.08	0.94	----	----	0.9153	-------
30	5	----	245.49	225.02	-----	-----	1.02	0.81	----	----	0.9171	-------

Background for B-K_α measured at ± 25 mm , that of Mo-L_α at ± 5 mm on either side of the peak and interpolated.
Mo-L_α on PET, B-K_α on STE
Pulse Height Analyzer settings : Mo-L_α : Counter 1600 V, Lower Level 0.1 V, Window open, Gain 128 *5
B-K_α : Counter 1700 V, Lower Level 0.5 V, Window 3.5 V, Gain 64 *8

Boride: LaB_6 (31.83 w/o Boron)

B: 120984

kV	Beam Current (nA)		Gross Intensities (cps/nA)				Backgrounds (cps/nA)				k-ratios	
		B-K_α			B-K_α (Area)				B-K_α			B-K_α
					B	Boride			B	Boride		Area
4		300			14.84	7.204			0.14	0.12		0.4822
6		300			22.11	10.276			0.20	0.14		0.4626
8		300			27.00	12.569			0.25	0.16		0.4673
10		300			29.44	14.182			0.27	0.16		0.4807
12		300			29.71	15.007			0.25	0.15		0.5043
15		300			28.04	15.144			0.21	0.14		0.5391
20		300			22.80	14.299			0.16	0.13		0.6259
25		300			18.28	12.516			0.12	0.12		0.6892
30		300			14.84	11.241			0.12	0.12		0.7555

Background for B-K_α measured at ± 25 mm
B-K_α on STE
Pulse Height Analyzer setting : B-K_α : Counter 1700 V, Lower Level 0.5 V, Window 3.4 V, Gain 64 * 8

Boride: TaB (5.64 w/o Boron)

B: 081184 Ta: 240884

kV	Beam Current (nA)		Gross Intensities (cps/nA)				Backgrounds (cps/nA)				k-ratios	
	$Ta\text{-}M_\alpha$	$B\text{-}K_\alpha$	$Ta\text{-}M_\alpha$ (Peak)		$B\text{-}K_\alpha$ (Area)		$Ta\text{-}M_\alpha$		$B\text{-}K_\alpha$		$Ta\text{-}M_\alpha$	$B\text{-}K_\alpha$
			Ta	Boride	B	Boride	Ta	Boride	B	Boride	Peak	Area
4	300	300	5.64	5.18	14.63	0.846	0.05	0.05	0.14	0.08	0.9166	0.0529
6	300	300	13.51	12.47	22.00	0.853	0.10	0.10	0.22	0.08	0.9226	0.0355
8	200	300	22.11	20.39	26.52	0.800	0.17	0.17	0.25	0.08	0.9216	0.0274
10	100	300	29.76	27.22	28.87	0.709	0.23	0.24	0.25	0.07	0.9136	0.0223
12	100	300	36.93	34.28	28.94	0.629	0.29	0.41	0.25	0.07	0.9245	0.0195
15	50	300	46.41	43.60	27.45	0.590	0.39	0.39	0.20	0.06	0.9390	0.0182
20	20	---	57.38	54.43	------	-----	0.50	0.52	----	----	0.9477	-------
25	20	---	64.62	60.70	------	-----	0.61	0.66	----	----	0.9378	-------
30	20	---	67.30	63.99	------	-----	0.77	0.72	----	----	0.9510	-------
	$Ta\text{-}L_\alpha$		$Ta\text{-}L_\alpha$ (Peak)				$Ta\text{-}L_\alpha$				$Ta\text{-}L_\alpha$	
12	100		22.49	20.57			1.66	1.52			0.9148	
15	50		88.89	81.74			2.82	2.55			0.9200	
20	20		245.02	226.95			4.69	4.27			0.9266	
25	10		422.49	388.43			6.78	6.06			0.9198	
30	5		611.17	565.01			8.26	7.80			0.9242	

Background for $B\text{-}K_\alpha$ measured at ± 12 mm (Interference !!); that of $Ta\text{-}M_\alpha$ and $Ta\text{-}L_\alpha$ at ± 5 mm on either side of the peak and interpolated.
$Ta\text{-}M_\alpha$ on PET, $Ta\text{-}L_\alpha$ on LiF, $B\text{-}K_\alpha$ on STE
Pulse Height Analyzer settings : $Ta\text{-}M_\alpha$: Counter 1600 V, Lower Level 0.6 V, Window open, Gain 128 * 8
$Ta\text{-}L_\alpha$: Counter 1600 V, Lower Level 0.6 V, Window open, Gain 32 * 5
$B\text{-}K_\alpha$: Counter 1700 V, Lower Level 0.5 V, Window 3.5 V, Gain 64 * 8

Boride: TaB_2 (9.23 w/o Boron)

B: 081184 Ta: 240884

kV	Beam Current (nA)		Gross Intensities (cps/nA)				Backgrounds (cps/nA)				k-ratios	
	Ta-M_α	B-K_α	Ta-M_α (Peak)		B-K_α (Area)		Ta-M_α		B-K_α		Ta-M_α	B-K_α
			Ta	Boride	B	Boride	Ta	Boride	B	Boride	Peak	Area
4	300	300	5.64	4.76	14.63	1.425	0.05	0.04	0.14	0.08	0.8435	0.0928
6	300	300	13.51	11.66	22.00	1.416	0.10	0.09	0.22	0.09	0.8629	0.0609
8	200	300	22.11	19.08	26.52	1.285	0.17	0.14	0.25	0.08	0.8631	0.0459
10	100	300	29.76	25.55	28.87	1.137	0.23	0.21	0.25	0.08	0.8581	0.0369
12	100	300	36.93	32.07	28.94	1.010	0.29	0.25	0.25	0.08	0.8686	0.0324
15	50	300	46.41	41.00	27.59	0.924	0.39	0.42	0.20	0.07	0.8818	0.0312
20	20	---	57.38	51.56	------	-----	0.50	0.50	----	----	0.8977	-------
25	20	---	64.62	56.18	------	-----	0.61	0.64	----	----	0.8876	-------
30	20	---	67.30	60.87	------	-----	0.77	0.62	----	----	0.9055	-------
	Ta-L_α		Ta-L_α (Peak)				Ta-L_α				Ta-L_α	
12	100		22.49	18.46			1.66	1.34			0.8218	
15	50		88.89	74.38			2.82	2.25			0.8381	
20	20		245.02	208.95			4.69	4.13			0.8522	
25	10		422.49	364.01			6.78	5.35			0.8628	
30	5		611.17	531.05			8.26	7.62			0.8682	

Background for B-K_α measured at ± 12 mm (Interference !!); that of Ta-M_α and Ta-L_α at ± 5 mm on either side of the peak and interpolated.
Ta-M_α on PET, Ta-L_α on LiF, B-K_α on STE
Pulse Height Analyzer settings : Ta-M_α : Counter 1600 V, Lower Level 0.6 V, Window open, Gain 128 * 8
Ta-L_α : Counter 1600 V, Lower Level 0.6 V, Window open, Gain 32 * 5
B-K_α : Counter 1700 V, Lower Level 0.5 V, Window 3.5 V, Gain 64 * 8

Boride: WB (5.55 w/o Boron)

B: 161084 W: 240884

kV	Beam Current (nA)		Gross Intensities (cps/nA)				Backgrounds (cps/nA)				k-ratios	
	$W\text{-}M_\alpha$	$B\text{-}K_\alpha$	$W\text{-}M_\alpha$ (Peak)		$B\text{-}K_\alpha$ (Area)		$W\text{-}M_\alpha$		$B\text{-}K_\alpha$		$W\text{-}M_\alpha$	$B\text{-}K_\alpha$
			W	Boride	B	Boride	W	Boride	B	Boride	Peak	Area
4	300	250	6.00	5.18	16.63	0.975	0.05	0.05	0.15	0.07	0.8626	0.0546
6	300	300	14.42	12.98	24.26	0.985	0.11	0.09	0.22	0.07	0.9007	0.0381
8	200	300	23.63	21.47	29.54	0.932	0.17	0.15	0.29	0.07	0.9050	0.0295
10	100	300	31.51	28.75	31.62	0.816	0.21	0.18	0.25	0.07	0.9129	0.0238
12	100	300	39.41	36.08	31.88	0.723	0.28	0.28	0.25	0.06	0.9150	0.0210
15	50	300	49.72	46.05	30.09	0.621	0.39	0.34	0.25	0.06	0.9266	0.0188
20	20	---	62.14	58.10	------	-----	0.44	0.57	----	----	0.9324	-------
25	20	---	68.33	65.40	------	-----	0.73	0.66	----	----	0.9543	-------
30	20	---	71.70	68.54	------	-----	0.66	0.80	----	----	0.9536	-------
	$W\text{-}L_\alpha$		$W\text{-}L_\alpha$ (Peak)				$W\text{-}L_\alpha$				$W\text{-}L_\alpha$	
12	100		18.50	16.51			1.84	1.63			0.8930	
15	50		84.58	75.98			2.97	2.80			0.8967	
20	20		243.70	221.67			4.91	4.70			0.9086	
25	10		425.73	392.57			7.67	7.70			0.9206	
30	5		617.83	571.45			9.72	9.16			0.9247	

Background for $B\text{-}K_\alpha$ measured at ± 12 mm (Interference !!); that of $W\text{-}M_\alpha$ and $W\text{-}L_\alpha$ at ± 5 mm on either side of the peak and interpolated.
$W\text{-}M_\alpha$ on PET, $W\text{-}L_\alpha$ on LiF, $B\text{-}K_\alpha$ on STE
Pulse Height Analyzer settings : $W\text{-}M_\alpha$: Counter 1600 V, Lower Level 0.6 V, Window open, Gain 128 * 8
$W\text{-}L_\alpha$: Counter 1600 V, Lower Level 0.6 V, Window open, Gain 32 * 5
$B\text{-}K_\alpha$: Counter 1700 V, Lower Level 0.5 V, Window 3.5 V, Gain 64 * 8

Boride: UB_4 (15.37 w/o Boron)

B: 151084

kV	Beam Current (nA)	Gross Intensities (cps/nA)			Backgrounds (cps/nA)			k-ratios
		$B\text{-}K_\alpha$	$B\text{-}K_\alpha$ (Area)		$B\text{-}K_\alpha$			$B\text{-}K_\alpha$
			B	Boride	B	Boride		Area
4		300	16.77	3.877	0.16	0.10		0.2274
6		300	24.23	4.878	0.25	0.13		0.1980
8		300	29.30	5.256	0.25	0.14		0.1761
10		300	31.57	5.245	0.27	0.13		0.1634
12		300	32.08	5.104	0.26	0.12		0.1566
15		300	30.11	4.659	0.23	0.10		0.1526

Background for $B\text{-}K_\alpha$ measured at ± 25 mm
$B\text{-}K_\alpha$ on STE
Pulse Height Analyzer setting : $B\text{-}K_\alpha$: Counter 1700 V, Lower Level 0.5 V, Window 3.4 V, Gain 64 * 8

Appendix C

Numerical details in the data base containing the k-ratios for B-K_α (integral) and the metal X-ray lines

Legend : 1 *Analysis number*
2,3 *Atomic numbers of metal and boron, respectively*
4,5 *Mass absorption coefficients for metal line in metal and boron*
6 *Critical excitation voltage of metal line*
7 *Weight fraction of metal*
8 *k-ratio of metal line, relative to elemental standard (smoothed !)*
9 *k-ratio for B-K_α (integral !), relative to elemental boron*
10 *Accelerating voltage (kV)*
11 *X-ray take-off angle (degr.)*
12 *Type of metal X-ray line (K=0, L=1, M=2)*

1	*2*	*3*	*4*	*5*	*6*	*7*	*8*	*9*	*10*	*11*	*12*
1	6	5	2373	35200	0.284	0.2019	0.0000	0.7768	4	40	0
2	6	5	2373	35200	0.284	0.2019	0.0000	0.7754	6	40	0
3	6	5	2373	35200	0.284	0.2019	0.0000	0.7471	8	40	0
4	6	5	2373	35200	0.284	0.2019	0.0000	0.7309	10	40	0
5	6	5	2373	35200	0.284	0.2019	0.0000	0.7132	12	40	0
6	6	5	2373	35200	0.284	0.2019	0.0000	0.6853	15	40	0
7	6	5	2373	35200	0.284	0.2019	0.0000	0.6544	20	40	0
8	6	5	2373	35200	0.284	0.2019	0.0000	0.6516	25	40	0
9	6	5	2373	35200	0.284	0.2019	0.0000	0.6574	30	40	0
10	7	5	1600	16000	0.400	0.5652	0.0000	0.3747	4	40	0
11	7	5	1600	16000	0.400	0.5652	0.0000	0.3317	6	40	0
12	7	5	1600	16000	0.400	0.5652	0.0000	0.2856	8	40	0
13	7	5	1600	16000	0.400	0.5652	0.0000	0.2539	10	40	0
14	7	5	1600	16000	0.400	0.5652	0.0000	0.2316	12	40	0
15	7	5	1600	16000	0.400	0.5652	0.0000	0.2049	15	40	0
16	7	5	1600	16000	0.400	0.5652	0.0000	0.1823	20	40	0
17	7	5	1600	16000	0.400	0.5652	0.0000	0.1800	25	40	0
18	7	5	1600	16000	0.400	0.5652	0.0000	0.1834	30	40	0
19	8	5	1200	8800	0.531	0.1980	0.0000	0.7376	4	40	0
20	8	5	1200	8800	0.531	0.1980	0.0000	0.6750	6	40	0
21	8	5	1200	8800	0.531	0.1980	0.0000	0.6232	8	40	0
22	8	5	1200	8800	0.531	0.1980	0.0000	0.5713	10	40	0
23	8	5	1200	8800	0.531	0.1980	0.0000	0.5244	12	40	0
24	8	5	1200	8800	0.531	0.1980	0.0000	0.4743	15	40	0
25	8	5	1200	8800	0.531	0.1980	0.0000	0.4270	20	40	0
26	8	5	1200	8800	0.531	0.1980	0.0000	0.4168	25	40	0
27	8	5	1200	8800	0.531	0.1980	0.0000	0.4135	30	40	0
28	13	5	398	399	1.559	0.5551	0.5150	0.1872	4	40	0
29	13	5	398	399	1.559	0.5551	0.5178	0.1057	6	40	0
30	13	5	398	399	1.559	0.5551	0.5188	0.0648	8	40	0
31	13	5	398	399	1.559	0.5551	0.5200	0.0501	10	40	0
32	13	5	398	399	1.559	0.5551	0.5198	0.0396	12	40	0
33	13	5	398	399	1.559	0.5551	0.5170	0.0342	15	40	0
34	13	5	398	399	1.559	0.5551	0.5130	0.0000	20	40	0

Appendix C (Continued)

Numerical details in the data base containing the k-ratios for B-K_α (integral) and the metal X-ray lines

1	*2*	*3*	*4*	*5*	*6*	*7*	*8*	*9*	*10*	*11*	*12*
35	13	5	398	399	1.559	0.5551	0.5080	0.0000	25	40	0
36	13	5	398	399	1.559	0.5551	0.5030	0.0000	30	40	0
37	13	5	398	399	1.559	0.1722	0.1500	0.6077	4	40	0
38	13	5	398	399	1.559	0.1722	0.1502	0.4492	6	40	0
39	13	5	398	399	1.559	0.1722	0.1503	0.3391	8	40	0
40	13	5	398	399	1.559	0.1722	0.1503	0.2679	10	40	0
41	13	5	398	399	1.559	0.1722	0.1503	0.2244	12	40	0
42	13	5	398	399	1.559	0.1722	0.1504	0.1864	15	40	0
43	13	5	398	399	1.559	0.1722	0.1495	0.1684	20	40	0
44	13	5	398	399	1.559	0.1722	0.1490	0.1638	25	40	0
45	13	5	398	399	1.559	0.1722	0.1455	0.1694	30	40	0
46	14	5	347	246	1.838	0.4641	0.4465	0.2171	4	40	0
47	14	5	347	246	1.838	0.4641	0.4528	0.1131	6	40	0
48	14	5	347	246	1.838	0.4641	0.4580	0.0703	8	40	0
49	14	5	347	246	1.838	0.4641	0.4622	0.0544	10	40	0
50	14	5	347	246	1.838	0.4641	0.4658	0.0445	12	40	0
51	14	5	347	246	1.838	0.4641	0.4696	0.0384	15	40	0
52	14	5	347	246	1.838	0.4641	0.4738	0.0000	20	40	0
53	14	5	347	246	1.838	0.4641	0.4758	0.0000	25	40	0
54	14	5	347	246	1.838	0.4641	0.4760	0.0000	30	40	0
55	14	5	347	246	1.838	0.3022	0.2900	0.3541	4	40	0
56	14	5	347	246	1.838	0.3022	0.2940	0.2113	6	40	0
57	14	5	347	246	1.838	0.3022	0.2978	0.1401	8	40	0
58	14	5	347	246	1.838	0.3022	0.3002	0.1071	10	40	0
59	14	5	347	246	1.838	0.3022	0.3036	0.0850	12	40	0
60	14	5	347	246	1.838	0.3022	0.3072	0.0713	15	40	0
61	14	5	347	246	1.838	0.3022	0.3120	0.0000	20	40	0
62	14	5	347	246	1.838	0.3022	0.3140	0.0000	25	40	0
63	14	5	347	246	1.838	0.3022	0.3156	0.0000	30	40	0
64	22	5	108	12	0.455	0.8322	0.0000	0.1623	4	40	1
65	22	5	108	12	4.965	0.8322	0.7922	0.1242	6	40	0
66	22	5	108	12	4.965	0.8322	0.7937	0.0990	8	40	0
67	22	5	108	12	4.965	0.8322	0.7942	0.0795	10	40	0
68	22	5	108	12	4.965	0.8322	0.7960	0.0699	12	40	0
69	22	5	108	12	4.965	0.8322	0.7978	0.0603	15	40	0
70	22	5	108	12	4.965	0.8322	0.8012	0.0542	20	40	0
71	22	5	108	12	4.965	0.8322	0.8042	0.0552	25	40	0
72	22	5	108	12	4.965	0.8322	0.8077	0.0578	30	40	0
73	22	5	108	12	4.965	0.6993	0.0000	0.2956	4	40	0
74	22	5	108	12	4.965	0.6993	0.6330	0.2244	6	40	0
75	22	5	108	12	4.965	0.6993	0.6400	0.1807	8	40	0
76	22	5	108	12	4.965	0.6993	0.6462	0.1498	10	40	0
77	22	5	108	12	4.965	0.6993	0.6513	0.1279	12	40	0
78	22	5	108	12	4.965	0.6993	0.6578	0.1158	15	40	0
79	22	5	108	12	4.965	0.6993	0.6662	0.1055	20	40	0
80	22	5	108	12	4.965	0.6993	0.6738	0.1063	25	40	0
81	22	5	108	12	4.965	0.6993	0.6782	0.1090	30	40	0
82	23	5	95	9	0.513	0.7160	0.0000	0.2583	4	40	0

Appendix C (Continued)

Numerical details in the data base containing the k-ratios for B-K_α (integral) and the metal X-ray lines

1	*2*	*3*	*4*	*5*	*6*	*7*	*8*	*9*	*10*	*11*	*12*
83	23	5	95	9	5.463	0.7160	0.6378	0.1980	6	40	0
84	23	5	95	9	5.463	0.7160	0.6500	0.1484	8	40	0
85	23	5	95	9	5.463	0.7160	0.6602	0.1235	10	40	0
86	23	5	95	9	5.463	0.7160	0.6681	0.1058	12	40	0
87	23	5	95	9	5.463	0.7160	0.6770	0.0865	15	40	0
88	23	5	95	9	5.463	0.7160	0.6878	0.0000	20	40	0
89	23	5	95	9	5.463	0.7160	0.6939	0.0000	25	40	0
90	23	5	95	9	5.463	0.7160	0.6977	0.0000	30	40	0
91	24	5	87	7	0.575	0.8320	0.0000	0.1387	4	40	1
92	24	5	87	7	0.575	0.8320	0.0000	0.0991	6	40	1
93	24	5	87	7	5.988	0.8320	0.7758	0.0747	8	40	0
94	24	5	87	7	5.988	0.8320	0.7840	0.0611	10	40	0
95	24	5	87	7	5.988	0.8320	0.7905	0.0512	12	40	0
96	24	5	87	7	5.988	0.8320	0.7981	0.0444	15	40	0
97	24	5	87	7	5.988	0.8320	0.8070	0.0000	20	40	0
98	24	5	87	7	5.988	0.8320	0.8122	0.0000	25	40	0
99	24	5	87	7	5.988	0.8320	0.8156	0.0000	30	40	0
100	24	5	87	7	0.575	0.7269	0.0000	0.2301	4	40	1
101	24	5	87	7	0.575	0.7269	0.0000	0.1682	6	40	1
102	24	5	87	7	5.988	0.7269	0.6230	0.1268	8	40	0
103	24	5	87	7	5.988	0.7269	0.6374	0.1037	10	40	0
104	24	5	87	7	5.988	0.7269	0.6480	0.0891	12	40	0
105	24	5	87	7	5.988	0.7269	0.6603	0.0767	15	40	0
106	24	5	87	7	5.988	0.7269	0.6738	0.0000	20	40	0
107	24	5	87	7	5.988	0.7269	0.6810	0.0000	25	40	0
108	24	5	87	7	5.988	0.7269	0.6850	0.0000	30	40	0
109	26	5	71	4	0.707	0.9118	0.0000	0.0611	4	40	1
110	26	5	71	4	0.707	0.9118	0.0000	0.0409	6	40	1
111	26	5	71	4	7.111	0.9118	0.8680	0.0290	8	40	0
112	26	5	71	4	7.111	0.9118	0.8730	0.0226	10	40	0
113	26	5	71	4	7.111	0.9118	0.8764	0.0190	12	40	0
114	26	5	71	4	7.111	0.9118	0.8821	0.0169	15	40	0
115	26	5	71	4	7.111	0.9118	0.8888	0.0000	20	40	0
116	26	5	71	4	7.111	0.9118	0.8940	0.0000	25	40	0
117	26	5	71	4	7.111	0.9118	0.8970	0.0000	30	40	0
118	26	5	71	4	0.707	0.8378	0.0000	0.1131	4	40	1
119	26	5	71	4	0.707	0.8378	0.0000	0.0757	6	40	1
120	26	5	71	4	7.111	0.8378	0.7823	0.0533	8	40	0
121	26	5	71	4	7.111	0.8378	0.7922	0.0404	10	40	0
122	26	5	71	4	7.111	0.8378	0.8002	0.0345	12	40	0
123	26	5	71	4	7.111	0.8378	0.8098	0.0292	15	40	0
124	26	5	71	4	7.111	0.8378	0.8203	0.0000	20	40	0
125	26	5	71	4	7.111	0.8378	0.8280	0.0000	25	40	0
126	26	5	71	4	7.111	0.8378	0.8330	0.0000	30	40	0
127	27	5	64	3	0.779	0.9160	0.0000	0.0492	4	40	1
128	27	5	64	3	0.779	0.9160	0.0000	0.0301	6	40	1
129	27	5	64	3	0.779	0.9160	0.0000	0.0212	8	40	1
130	27	5	64	3	7.709	0.9160	0.8660	0.0167	10	40	0

Appendix C (Continued)

Numerical details in the data base containing the k-ratios for B-K_α (integral) and the metal X-ray lines

1	*2*	*3*	*4*	*5*	*6*	*7*	*8*	*9*	*10*	*11*	*12*
131	27	5	64	3	7.709	0.9160	0.8832	0.0137	12	40	0
132	27	5	64	3	7.709	0.9160	0.8980	0.0117	15	40	0
133	27	5	64	3	7.709	0.9160	0.9101	0.0000	20	40	0
134	27	5	64	3	7.709	0.9160	0.9120	0.0000	25	40	0
135	27	5	64	3	7.709	0.9160	0.9078	0.0000	30	40	0
136	27	5	64	3	0.779	0.8450	0.0000	0.0981	4	40	1
137	27	5	64	3	0.779	0.8450	0.0000	0.0619	6	40	1
138	27	5	64	3	0.779	0.8450	0.0000	0.0423	8	40	1
139	27	5	64	3	7.709	0.8450	0.7823	0.0333	10	40	0
140	27	5	64	3	7.709	0.8450	0.7939	0.0282	12	40	0
141	27	5	64	3	7.709	0.8450	0.8058	0.0239	15	40	0
142	27	5	64	3	7.709	0.8450	0.8180	0.0000	20	40	0
143	27	5	64	3	7.709	0.8450	0.8244	0.0000	25	40	0
144	27	5	64	3	7.709	0.8450	0.8278	0.0000	30	40	0
145	28	5	60	3	0.853	0.9422	0.0000	0.0281	4	40	1
146	28	5	60	3	0.853	0.9422	0.0000	0.0164	6	40	1
147	28	5	60	3	0.853	0.9422	0.0000	0.0116	8	40	1
148	28	5	60	3	8.331	0.9422	0.9238	0.0091	10	40	0
149	28	5	60	3	8.331	0.9422	0.9262	0.0073	12	40	0
150	28	5	60	3	8.331	0.9422	0.9303	0.0062	15	40	0
151	28	5	60	3	8.331	0.9422	0.9358	0.0000	20	40	0
152	28	5	60	3	8.331	0.9422	0.9380	0.0000	25	40	0
153	28	5	60	3	8.331	0.9422	0.9382	0.0000	30	40	0
154	28	5	60	3	0.854	0.9157	0.0000	0.0427	4	40	1
155	28	5	60	3	0.854	0.9157	0.0000	0.0251	6	40	1
156	28	5	60	3	0.854	0.9157	0.0000	0.0176	8	40	1
157	28	5	60	3	8.331	0.9157	0.8858	0.0143	10	40	0
158	28	5	60	3	8.331	0.9157	0.8899	0.0118	12	40	0
159	28	5	60	3	8.331	0.9157	0.8950	0.0095	15	40	0
160	28	5	60	3	8.331	0.9157	0.9005	0.0000	20	40	0
161	28	5	60	3	8.331	0.9157	0.9040	0.0000	25	40	0
162	28	5	60	3	8.331	0.9157	0.9060	0.0000	30	40	0
163	28	5	60	3	0.854	0.8560	0.0000	0.0729	4	40	1
164	28	5	60	3	0.854	0.8560	0.0000	0.0443	6	40	1
165	28	5	60	3	0.854	0.8560	0.0000	0.0282	8	40	1
166	28	5	60	3	8.331	0.8560	0.8083	0.0237	10	40	0
167	28	5	60	3	8.331	0.8560	0.8180	0.0198	12	40	0
168	28	5	60	3	8.331	0.8560	0.8283	0.0176	15	40	0
169	28	5	60	3	8.331	0.8560	0.8388	0.0000	20	40	0
170	28	5	60	3	8.331	0.8560	0.8438	0.0000	25	40	0
171	28	5	60	3	8.331	0.8560	0.8450	0.0000	30	40	0
172	40	5	757	150	2.220	0.8211	0.7540	0.2597	4	40	1
173	40	5	757	150	2.220	0.8211	0.7662	0.2513	6	40	1
174	40	5	757	150	2.220	0.8212	0.7770	0.2452	8	40	1
175	40	5	757	150	2.220	0.8210	0.7855	0.2382	10	40	1
176	40	5	757	150	2.220	0.8211	0.7930	0.2382	12	40	1
177	40	5	757	150	2.220	0.8211	0.8024	0.2369	15	40	1
178	40	5	757	150	2.220	0.8211	0.8140	0.2536	20	40	1

Appendix C (Continued)

Numerical details in the data base containing the k-ratios for B-K_α (integral) and the metal X-ray lines

1	*2*	*3*	*4*	*5*	*6*	*7*	*8*	*9*	*10*	*11*	*12*
179	40	5	757	150	2.220	0.8211	0.8225	0.2691	25	40	1
180	40	5	757	150	2.220	0.8211	0.8290	0.2819	30	40	1
181	41	5	718	125	2.374	0.8958	0.8588	0.1558	4	40	1
182	41	5	718	125	2.374	0.8958	0.8680	0.1454	6	40	1
183	41	5	718	125	2.374	0.8958	0.8758	0.1407	8	40	1
184	41	5	718	125	2.374	0.8958	0.8820	0.1380	10	40	1
185	41	5	718	125	2.374	0.8958	0.8878	0.1384	12	40	1
186	41	5	718	125	2.374	0.8958	0.8942	0.1423	15	40	1
187	41	5	718	125	2.374	0.8958	0.9036	0.0000	20	40	1
188	41	5	718	125	2.374	0.8958	0.9100	0.0000	25	40	1
189	41	5	718	125	2.374	0.8958	0.9157	0.0000	30	40	1
190	41	5	718	125	2.374	0.8285	0.7502	0.2543	4	40	1
191	41	5	718	125	2.374	0.8285	0.7640	0.2325	6	40	1
192	41	5	718	125	2.374	0.8285	0.7760	0.2296	8	40	1
193	41	5	718	125	2.374	0.8285	0.7862	0.2226	10	40	1
194	41	5	718	125	2.374	0.8285	0.7950	0.2245	12	40	1
195	41	5	718	125	2.374	0.8285	0.8060	0.2298	15	40	1
196	41	5	718	125	2.374	0.8285	0.8210	0.0000	20	40	1
197	41	5	718	125	2.374	0.8285	0.8338	0.0000	25	40	1
198	41	5	718	125	2.374	0.8285	0.8442	0.0000	30	40	1
199	42	5	673	105	2.523	0.8987	0.8401	0.1597	4	40	1
200	42	5	673	105	2.523	0.8987	0.8500	0.1489	6	40	1
201	42	5	673	105	2.523	0.8987	0.8580	0.1416	8	40	1
202	42	5	673	105	2.523	0.8987	0.8660	0.1396	10	40	1
203	42	5	673	105	2.523	0.8987	0.8731	0.1362	12	40	1
204	42	5	673	105	2.523	0.8987	0.8828	0.1395	15	40	1
205	42	5	673	105	2.523	0.8987	0.8978	0.0000	20	40	1
206	42	5	673	105	2.523	0.8987	0.9100	0.0000	25	40	1
207	42	5	673	105	2.523	0.8987	0.9202	0.0000	30	40	1
208	57	5	2744	2189	0.832	0.6817	0.0000	0.4822	4	40	2
209	57	5	2744	2189	0.832	0.6817	0.0000	0.4626	6	40	2
210	57	5	2744	2189	0.832	0.6817	0.0000	0.4673	8	40	2
211	57	5	2744	2189	0.832	0.6817	0.0000	0.4807	10	40	2
212	57	5	2744	2189	0.832	0.6817	0.0000	0.5043	12	40	2
213	57	5	2744	2189	0.832	0.6817	0.0000	0.5391	15	40	2
214	57	5	2744	2189	0.832	0.6817	0.0000	0.6259	20	40	2
215	57	5	2744	2189	0.832	0.6817	0.0000	0.6892	25	40	2
216	57	5	2744	2189	0.832	0.6817	0.0000	0.7555	30	40	2
217	73	5	1256	260	1.743	0.9436	0.9160	0.0529	4	40	2
218	73	5	1256	260	1.743	0.9436	0.9208	0.0355	6	40	2
219	73	5	1256	260	1.743	0.9436	0.9258	0.0274	8	40	2
220	73	5	1256	260	1.743	0.9436	0.9295	0.0223	10	40	2
221	73	5	1256	260	1.743	0.9436	0.9324	0.0195	12	40	2
222	73	5	1256	260	1.743	0.9436	0.9365	0.0182	15	40	2
223	73	5	1256	260	1.743	0.9436	0.9430	0.0000	20	40	2
224	73	5	1256	260	1.743	0.9436	0.9462	0.0000	25	40	2
225	73	5	1256	260	1.743	0.9436	0.9482	0.0000	30	40	2
226	73	5	161	2	9.877	0.9436	0.9158	0.0000	12	40	1

Appendix C (Continued)

Numerical details in the data base containing the k-ratios for B-K_α (integral) and the metal X-ray lines

1	*2*	*3*	*4*	*5*	*6*	*7*	*8*	*9*	*10*	*11*	*12*
227	73	5	161	2	9.877	0.9436	0.9193	0.0000	15	40	1
228	73	5	161	2	9.877	0.9436	0.9230	0.0000	20	40	1
229	73	5	161	2	9.877	0.9436	0.9258	0.0000	25	40	1
230	73	5	161	2	9.877	0.9436	0.9260	0.0000	30	40	1
231	73	5	1256	260	1.743	0.9077	0.8478	0.0928	4	40	2
232	73	5	1256	260	1.743	0.9077	0.8560	0.0609	6	40	2
233	73	5	1256	260	1.743	0.9077	0.8625	0.0459	8	40	2
234	73	5	1256	260	1.743	0.9077	0.8690	0.0369	10	40	2
235	73	5	1256	260	1.743	0.9077	0.8740	0.0324	12	40	2
236	73	5	1256	260	1.743	0.9077	0.8803	0.0312	15	40	2
237	73	5	1256	260	1.743	0.9077	0.8895	0.0000	20	40	2
238	73	5	1256	260	1.743	0.9077	0.8960	0.0000	25	40	2
239	73	5	1256	260	1.743	0.9077	0.9002	0.0000	30	40	2
240	73	5	161	2	9.877	0.9077	0.8230	0.0000	12	40	1
241	73	5	161	2	9.877	0.9077	0.8365	0.0000	15	40	1
242	73	5	161	2	9.877	0.9077	0.8525	0.0000	20	40	1
243	73	5	161	2	9.877	0.9077	0.8622	0.0000	25	40	1
244	73	5	161	2	9.877	0.9077	0.8690	0.0000	30	40	1
245	74	5	1215	232	1.814	0.9445	0.8850	0.0546	4	40	2
246	74	5	1215	232	1.814	0.9445	0.8950	0.0381	6	40	2
247	74	5	1215	232	1.814	0.9445	0.9038	0.0295	8	40	2
248	74	5	1215	232	1.814	0.9445	0.9105	0.0238	10	40	2
249	74	5	1215	232	1.814	0.9445	0.9178	0.0210	12	40	2
250	74	5	1215	232	1.814	0.9445	0.9258	0.0188	15	40	2
251	74	5	1215	232	1.814	0.9445	0.9375	0.0000	20	40	2
252	74	5	1215	232	1.814	0.9445	0.9463	0.0000	25	40	2
253	74	5	1215	232	1.814	0.9445	0.9530	0.0000	30	40	2
254	74	5	154	2	10.200	0.9445	0.8918	0.0000	12	40	0
255	74	5	154	2	10.200	0.9445	0.8990	0.0000	15	40	0
256	74	5	154	2	10.200	0.9445	0.9103	0.0000	20	40	0
257	74	5	154	2	10.200	0.9445	0.9198	0.0000	25	40	0
258	74	5	154	2	10.200	0.8463	0.9264	0.0000	30	40	0
259	92	5	721	38	3.720	0.8463	0.0000	0.2274	4	40	2
260	92	5	721	38	3.720	0.8463	0.0000	0.1980	6	40	2
261	92	5	721	38	3.720	0.8463	0.0000	0.1761	8	40	2
262	92	5	721	38	3.720	0.8463	0.0000	0.1634	10	40	2
263	92	5	721	38	3.720	0.8463	0.0000	0.1566	12	40	2
264	92	5	721	38	3.720	0.8463	0.0000	0.1526	15	40	2